

# TURKISH JOURNAL OF PHARMACEUTICAL SCIENCES



# TURKISH JOURNAL OF PHARMACEUTICAL SCIENCES



## Editor-in-Chief

Feyyaz ONUR, Prof. Dr.

Lokman Hekim University, Ankara, Turkey,

E-mail: onur@pharmacy.ankara.edu.tr

ORCID ID: orcid.org/0000-0001-9172-1126

## Vice Editor

Gülgün KILCIĞIL, Prof. Dr.

Ankara University, Ankara, Turkey

E-mail: Gulgun.A.Kilcigil@pharmacy.ankara.edu.tr

ORCID ID: orcid.org/0000-0001-5626-6922

## Associate Editors

Rob VERPOORTE, Prof. Dr.

Leiden University, Leiden, Netherlands

E-mail: verpoort@chem.LeidenUniv.NL

Bezhan CHANKVETADZE, Prof. Dr.

Ivane Javakishvili Tbilisi State University,

Tbilisi, Georgia

E-mail: jpba\_bezhan@yahoo.com

Ülkü ÜNDEĞER-BUCURGAT, Prof. Dr.

Hacettepe University, Ankara, Turkey

E-mail: uundeger@hacettepe.edu.tr

ORCID ID: orcid.org/0000-0002-6692-0366

Luciano SASO, Prof. Dr.

Sapienza University, Rome, Italy

E-mail: luciano.saso@uniroma1.it

Müge KILIÇARSLAN, Assoc. Prof. Dr.

Ankara University, Ankara, Turkey

E-mail: muge.kilicarслан@pharmacy.ankara.edu.tr

ORCID ID: orcid.org/0000-0003-3710-7445

Fernanda BORGES, Prof. Dr.

Porto University, Porto, Portugal

E-mail: fborges@fc.up.pt

Tayfun UZBAY, Prof. Dr.

Üsküdar University, İstanbul, Turkey

E-mail: uzbayt@yahoo.com

İpek SUNTAR, Assoc. Prof. Dr.

Gazi University, Ankara, Türkiye

E-mail: ipesin@gazi.edu.tr

ORCID ID: orcid.org/0000-0003-4201-1325

## Advisory Board

Ali H. MERİÇLİ, Prof. Dr.

Near East University, Nicosia, Cypruss

Ahmet BAŞARAN, Prof. Dr.

Hacettepe University, Ankara, Turkey

Berrin ÖZÇELİK, Prof. Dr.

Gazi University, Ankara, Turkey

Betül DORTUNÇ, Prof. Dr.

Marmara University, İstanbul, Turkey

Christine LAFFORGUE, Prof. Dr.

Paris-Sud University, Paris, France

Cihat ŞAFAK, Prof. Dr.

Hacettepe University, Ankara, Turkey

Fethi ŞAHİN, Prof. Dr.

Eastern Mediterranean University, Famagusta,

Cyprus

Filiz ÖNER, Prof. Dr.

Hacettepe University, Ankara, Turkey

Gülten ÖTÜK, Prof. Dr.

İstanbul University, İstanbul, Turkey

Hermann BOLT, Prof. Dr.

Dortmund University, Dortmund, Germany

Hilbert WAGNER, Prof. Dr.

Ludwig-Maximilians University, Munich, Germany

Jean-Alain FEHRENTZ, Prof. Dr.

Montpellier University, Montpellier, France

Joerg KREUTER, Prof. Dr.

Johann Wolfgang Goethe University, Frankfurt, Germany

Makbule AŞIKOĞLU, Prof. Dr.

Ege University, İzmir, Turkey

Meral KEYER UYSAL, Prof. Dr.

Marmara University, İstanbul, Turkey

Meral TORUN, Prof. Dr.

Gazi University, Ankara, Turkey

Mümtaz İŞCAN, Prof. Dr.

Ankara University, Ankara, Turkey

Robert RAPOPORT, Prof. Dr.

Cincinnati University, Cincinnati, USA

Sema BURGAZ, Prof. Dr.

Gazi University, Ankara, Turkey

Uğur ATİK, Prof. Dr.

Mersin University, Mersin, Türkiye

Wolfgang SADEE, Prof. Dr.

Ohio State University, Ohio, USA

Yasemin YAZAN, Prof. Dr.

Anadolu University, Eskişehir, Turkey

Yılmaz ÇAPAN, Prof. Dr.

Hacettepe University, Ankara, Turkey

Yusuf ÖZTÜRK, Prof. Dr.

Anadolu University, Eskişehir, Turkey

Yücel KADIOĞLU, Prof. Dr.

Atatürk University, Erzurum, Turkey

Zühre ŞENTÜRK, Prof. Dr.

Yüzüncü Yıl University, Van, Turkey

# TÜRK ECZACILIK BİLİMLERİ DERGİSİ



## Baş Editör

Feyyaz ONUR, Prof. Dr.

Lokman Hekim Üniversitesi, Ankara, Türkiye

E-posta: onur@pharmacy.ankara.edu.tr

ORCID ID: orcid.org/0000-0001-9172-1126

## İkinci Editör

Gülgün KILCIGİL, Prof. Dr.

Ankara Üniversitesi, Ankara, Türkiye

E-posta: kilcigil@pharmacy.ankara.edu.tr

ORCID ID: orcid.org/0000-0001-5626-6922

## Yardımcı Editörler

Rob VERPOORTE, Prof. Dr.

Leiden Üniversitesi, Leiden, Amsterdam

E-posta: verpoort@chem.LeidenUniv.NL

Bezhan CHANKVETADZE, Prof. Dr.

Ivane Javakhishvili Tbilisi Devlet Üniversitesi, Tbilisi, Gürcistan

E-posta: jpba\_bezhan@yahoo.com

Ükü ÜNDEĞER-BUCURGAT, Prof. Dr.

Hacettepe Üniversitesi, Ankara, Türkiye

E-posta: uundeger@hacettepe.edu.tr

ORCID ID: orcid.org/0000-0002-6692-0366

Luciano SASO, Prof. Dr.

Sapienze Üniversitesi, Roma, İtalya

E-posta: luciano.saso@uniroma1.it

Müge KILIÇARSLAN, Assoc. Prof. Dr.

Ankara Üniversitesi, Ankara, Türkiye

E-posta: muge.kilicarслан@pharmacy.ankara.edu.tr

ORCID ID: orcid.org/0000-0003-3710-7445

Fernanda BORGES, Prof. Dr.

Porto Üniversitesi, Porto, Portekiz

E-posta: fborges@fc.up.pt

Tayfun UZBAY, Prof. Dr.

Üsküdar Üniversitesi, İstanbul, Türkiye

E-posta: uzbayt@yahoo.com

İpek SUNTAR, Assoc. Prof. Dr.

Gazi Üniversitesi, Ankara, Türkiye

E-posta: ipesin@gazi.edu.tr

ORCID ID: orcid.org/0000-0003-4201-1325

## Danışma Kurulu

Ali H. MERİÇLİ, Prof. Dr.

Near East Üniversitesi, Lefkoşa, Kıbrıs

Ahmet BAŞARAN, Prof. Dr.

Hacettepe Üniversitesi, Ankara, Türkiye

Berrin ÖZÇELİK, Prof. Dr.

Gazi Üniversitesi, Ankara, Türkiye

Betül DORTUNÇ, Prof. Dr.

Marmara Üniversitesi, İstanbul, Türkiye

Christine LAFFORGUE, Prof. Dr.

Paris-Sud Üniversitesi, Paris

Cihat ŞAFAK, Prof. Dr.

Hacettepe Üniversitesi, Ankara, Türkiye

Fethi ŞAHİN, Prof. Dr.

Doğu Akdeniz Üniversitesi, Gazimağusa, Kıbrıs

Filiz ÖNER, Prof. Dr.

Hacettepe Üniversitesi, Ankara, Türkiye

Gülten ÖTÜK, Prof. Dr.

İstanbul Üniversitesi, İstanbul, Türkiye

Hermann BOLT, Prof. Dr.

Dortmund Üniversitesi, Dortmund, Almanya

Hilbert WAGNER, Prof. Dr.

Ludwig-Maximilians Üniversitesi, Münih, Almanya

Jean-Alain FEHRENTZ, Prof. Dr.

Montpellier Üniversitesi, Montpellier, Fransa

Joerg KREUTER, Prof. Dr.

Johann Wolfgang Goethe Üniversitesi, Frankfurt, Almanya

Makbule AŞIKOĞLU, Prof. Dr.

Ege Üniversitesi, İzmir, Türkiye

Meral KEYER UYSAL, Prof. Dr.

Marmara Üniversitesi, İstanbul, Türkiye

Meral TORUN, Prof. Dr.

Gazi Üniversitesi, Ankara, Türkiye

Mümtaz İŞCAN, Prof. Dr.

Ankara Üniversitesi, Ankara, Türkiye

Robert RAPOPORT, Prof. Dr.

Cincinnati Üniversitesi, Cincinnati, Amerika

Sema BURGAZ, Prof. Dr.

Gazi Üniversitesi, Ankara, Türkiye

Uğur ATİK, Prof. Dr.

Mersin Üniversitesi, Mersin, Türkiye

Wolfgang SADEE, Prof. Dr.

Ohio State Üniversitesi, Ohio, Amerika

Yasemin YAZAN, Prof. Dr.

Anadolu Üniversitesi, Eskişehir, Türkiye

Yılmaz ÇAPAN, Prof. Dr.

Hacettepe Üniversitesi, Ankara, Türkiye

Yusuf ÖZTÜRK, Prof. Dr.

Anadolu Üniversitesi, Eskişehir, Türkiye

Yücel KADIOĞLU, Prof. Dr.

Atatürk Üniversitesi, Erzurum, Türkiye

Zühre ŞENTÜRK, Prof. Dr.

Yüzüncü Yıl Üniversitesi, Van, Türkiye

# TURKISH JOURNAL OF PHARMACEUTICAL SCIENCES

## AIMS AND SCOPE

The Turkish Journal of Pharmaceutical Sciences is the only scientific periodical publication of the Turkish Pharmacists' Association and has been published since April 2004.

Turkish Journal of Pharmaceutical Sciences is an independent international open access periodical journal based on double-blind peer-review principles. The journal is regularly published 3 times a year and the publication language is English. The issuing body of the journal is Galenos Yayınevi/Publishing House.

The aim of Turkish Journal of Pharmaceutical Sciences is to publish original research papers of the highest scientific and clinical value at an international level.

The target audience includes specialists and physicians in all fields of pharmaceutical sciences.

The editorial policies are based on the "Recommendations for the Conduct, Reporting, Editing, and Publication of Scholarly Work in Medical Journals (ICMJE Recommendations)" by the International Committee of Medical Journal Editors (2016, archived at <http://www.icmje.org/>) rules.

### Editorial Independence

Turkish Journal of Pharmaceutical Sciences is an independent journal with independent editors and principles and has no commercial relationship with the commercial product, drug or pharmaceutical company regarding decisions and review processes upon articles.

### ABSTRACTED/INDEXED IN

Web of Science-Emerging Sources Citation Index (ESCI)

SCOPUS SJR

Directory of Open Access Journals (DOAJ)

ProQuest

Chemical Abstracts Service (CAS)

EBSCO

EMBASE

Analytical Abstracts

International Pharmaceutical Abstracts (IPA)

Medicinal & Aromatic Plants Abstracts (MAPA)

TÜBİTAK/ULAKBİM TR Dizin

Türkiye Atıf Dizini

UDL-EDGE

### OPEN ACCESS POLICY

This journal provides immediate open access to its content on the principle that making research freely available to the public supports a greater global exchange of knowledge.

Open Access Policy is based on the rules of the Budapest Open Access Initiative (BOAI) <http://www.budapestopenaccessinitiative.org/>. By "open access" to peer-reviewed research literature, we mean its free availability on the public internet, permitting any users to read, download, copy, distribute, print, search, or link to the full texts of these articles, crawl them for indexing, pass them as data to software, or use them for any other lawful purpose, without financial, legal, or technical barriers other than those inseparable from gaining access to the internet itself. The only constraint on reproduction and distribution, and the only role for copyright in this domain, should be to give authors control over the integrity of their work and the right to be properly acknowledged and cited.

### CORRESPONDENCE ADDRESS

Editor-in-Chief, Feyyaz ONUR, Prof.Dr.

Address: Lokman Hekim University, Faculty of Pharmacy, Department of Analytical Chemistry, 06100 Tandoğan-Ankara, TURKEY

E-mail: [onur@pharmacy.ankara.edu.tr](mailto:onur@pharmacy.ankara.edu.tr)

### PERMISSION

Requests for permission to reproduce published material should be sent to the editorial office. Editor-in-Chief, Prof. Dr. Feyyaz ONUR

### ISSUING BODY CORRESPONDING ADDRESS

Issuing Body : Galenos Yayınevi

Address: Molla Gürani Mah. Kaçamak Sk. No: 21/1, 34093 İstanbul, TURKEY

Phone: +90 212 621 99 25 Fax: +90 212 621 99 27

E-mail: [info@galenos.com.tr](mailto:info@galenos.com.tr)

### INSTRUCTIONS FOR AUTHORS

Instructions for authors are published in the journal and on the website <http://turkjps.org>

### MATERIAL DISCLAIMER

The author(s) is (are) responsible for the articles published in the JOURNAL.

The editor, editorial board and publisher do not accept any responsibility for the articles.

This work is licensed under a Creative Commons Attribution-NonCommercial-NoDerivatives 4.0 International License.



Galenos Publishing House  
Owner and Publisher  
Erkan Mor

Publication Coordinator  
Burak Sever

Web Coordinators  
Turgay Akpınar

Graphics Department  
Ayda Alaca  
Çiğdem Birinci  
Gülşah Özgül

Project Coordinators  
Eda Kolukısa  
Hatice Balta  
Lütfiye Ayhan İrtem  
Sedanur Sert  
Zeynep Altındağ

Project Assistants  
Gamze Aksoy  
Nurcan Acarçağ

Finance Coordinator  
Sevinç Çakmak

Research&Development  
Kerim Sancar Ölmez  
Mert Can Köse

### Publisher Contact

Address: Molla Gürani Mah. Kaçamak Sk. No: 21/1  
34093 İstanbul, Turkey

Phone: +90 (212) 621 99 25 Fax: +90 (212) 621 99 27

E-mail: [info@galenos.com.tr](mailto:info@galenos.com.tr) | [yayin@galenos.com.tr](mailto:yayin@galenos.com.tr)

Web: [www.galenos.com.tr](http://www.galenos.com.tr) | Publisher Certificate Number: 14521

Printing at: Üniform Basım San. ve Turizm Ltd. Şti.  
Matbaacılar Sanayi Sitesi 1. Cad. No: 114 34204 Bağcılar, İstanbul, Turkey

Phone: +90 (212) 429 10 00 | Certificate Number: 42419

Printing Date: March 2019

ISSN: 1304-530X

International scientific journal published quarterly.

# TURKISH JOURNAL OF PHARMACEUTICAL SCIENCES

## INSTRUCTIONS TO AUTHORS

Turkish Journal of Pharmaceutical Sciences is the official double peer-reviewed publication of The Turkish Pharmacists' Association. This journal is published every 4 months (3 issues per year; April, August, December) and publishes the following articles:

- Research articles
- Reviews (only upon the request or consent of the Editorial Board)
- Preliminary results/Short communications/Technical notes/Letters to the Editor in every field or pharmaceutical sciences.

The publication language of the journal is English.

The Turkish Journal of Pharmaceutical Sciences does not charge any article submission or processing charges.

A manuscript will be considered only with the understanding that it is an original contribution that has not been published elsewhere.

The Journal should be abbreviated as "Turk J Pharm Sci" when referenced.

The scientific and ethical liability of the manuscripts belongs to the authors and the copyright of the manuscripts belongs to the Journal. Authors are responsible for the contents of the manuscript and accuracy of the references. All manuscripts submitted for publication must be accompanied by the Copyright Transfer Form [copyright transfer]. Once this form, signed by all the authors, has been submitted, it is understood that neither the manuscript nor the data it contains have been submitted elsewhere or previously published and authors declare the statement of scientific contributions and responsibilities of all authors.

Experimental, clinical and drug studies requiring approval by an ethics committee must be submitted to the JOURNAL with an ethics committee approval report including approval number confirming that the study was conducted in accordance with international agreements and the Declaration of Helsinki (revised 2013) (<http://www.wma.net/en/30publications/10policies/b3/>). The approval of the ethics committee and the fact that informed consent was given by the patients should be indicated in the Materials and Methods section. In experimental animal studies, the authors should indicate that the procedures followed were in accordance with animal rights as per the Guide for the Care and Use of Laboratory Animals (<http://oacu.od.nih.gov/regs/guide/guide.pdf>) and they should obtain animal ethics committee approval.

Authors must provide disclosure/acknowledgment of financial or material support, if any was received, for the current study.

If the article includes any direct or indirect commercial links or if any institution provided material support to the study, authors must state in the cover letter that they have no relationship with the commercial product, drug, pharmaceutical company, etc. concerned; or specify the type of relationship (consultant, other agreements), if any.

Authors must provide a statement on the absence of conflicts of interest among the authors and provide authorship contributions.

All manuscripts submitted to the journal are screened for plagiarism using the 'iThenticate' software. Results indicating plagiarism may result in manuscripts being returned or rejected.

### The Review Process

This is an independent international journal based on double-blind peer-review principles. The manuscript is assigned to the Editor-in-Chief, who reviews the manuscript and makes an initial decision based

on manuscript quality and editorial priorities. Manuscripts that pass initial evaluation are sent for external peer review, and the Editor-in-Chief assigns an Associate Editor. The Associate Editor sends the manuscript to at least two reviewers (internal and/or external reviewers). The reviewers must review the manuscript within 21 days. The Associate Editor recommends a decision based on the reviewers' recommendations and returns the manuscript to the Editor-in-Chief. The Editor-in-Chief makes a final decision based on editorial priorities, manuscript quality, and reviewer recommendations. If there are any conflicting recommendations from reviewers, the Editor-in-Chief can assign a new reviewer.

The scientific board guiding the selection of the papers to be published in the Journal consists of elected experts of the Journal and if necessary, selected from national and international authorities. The Editor-in-Chief, Associate Editors may make minor corrections to accepted manuscripts that do not change the main text of the paper.

In case of any suspicion or claim regarding scientific shortcomings or ethical infringement, the Journal reserves the right to submit the manuscript to the supporting institutions or other authorities for investigation. The Journal accepts the responsibility of initiating action but does not undertake any responsibility for an actual investigation or any power of decision.

The Editorial Policies and General Guidelines for manuscript preparation specified below are based on "Recommendations for the Conduct, Reporting, Editing, and Publication of Scholarly Work in Medical Journals (ICMJE Recommendations)" by the International Committee of Medical Journal Editors (2016, archived at <http://www.icmje.org/>).

Preparation of research articles, systematic reviews and meta-analyses must comply with study design guidelines:

CONSORT statement for randomized controlled trials (Moher D, Schultz KF, Altman D, for the CONSORT Group. The CONSORT statement revised recommendations for improving the quality of reports of parallel group randomized trials. *JAMA* 2001; 285: 1987-91) (<http://www.consort-statement.org/>);

PRISMA statement of preferred reporting items for systematic reviews and meta-analyses (Moher D, Liberati A, Tetzlaff J, Altman DG, The PRISMA Group. Preferred Reporting Items for Systematic Reviews and Meta-Analyses: The PRISMA Statement. *PLoS Med* 2009; 6(7): e1000097.) (<http://www.prisma-statement.org/>);

STARD checklist for the reporting of studies of diagnostic accuracy (Bossuyt PM, Reitsma JB, Bruns DE, Gatsonis CA, Glasziou PP, Irwig LM, et al., for the STARD Group. Towards complete and accurate reporting of studies of diagnostic accuracy: the STARD initiative. *Ann Intern Med* 2003;138:40-4.) (<http://www.stard-statement.org/>);

STROBE statement, a checklist of items that should be included in reports of observational studies (<http://www.strobe-statement.org/>);

MOOSE guidelines for meta-analysis and systemic reviews of observational studies (Stroup DF, Berlin JA, Morton SC, et al. Meta-analysis of observational studies in epidemiology: a proposal for reporting Meta-analysis of observational Studies in Epidemiology (MOOSE) group. *JAMA* 2000; 283: 2008-12).

### Authorship

Each author should have participated sufficiently in the work to assume public responsibility for the content. Any portion of a manuscript that

---

# TURKISH JOURNAL OF PHARMACEUTICAL SCIENCES

---

## INSTRUCTIONS TO AUTHORS

is critical to its main conclusions must be the responsibility of at least 1 author.

### GENERAL GUIDELINES

Manuscripts can only be submitted electronically through the Journal Agent website (<http://journalagent.com/tjps/>) after creating an account. This system allows online submission and review.

The manuscripts are archived according to ICMJE, Web of Science-Emerging Sources Citation Index (ESCI), SCOPUS, Chemical Abstracts, EBSCO, EMBASE, Analytical Abstracts, International Pharmaceutical Abstracts, MAPA (Medicinal & Aromatic Plants Abstracts), Tübitak/Ulakbim Turkish Medical Database, Türkiye Citation Index Rules.

**Format:** Manuscripts should be prepared using Microsoft Word, size A4 with 2.5 cm margins on all sides, 12 pt Arial font and 1.5 line spacing.

**Abbreviations:** Abbreviations should be defined at first mention and used consistently thereafter. Internationally accepted abbreviations should be used; refer to scientific writing guides as necessary.

**Cover letter:** The cover letter should include statements about manuscript type, single-Journal submission affirmation, conflict of interest statement, sources of outside funding, equipment (if applicable), for original research articles.

The ORCID (Open Researcher and Contributor ID) number of the all authors should be provided while sending the manuscript. A free registration can be done at <http://orcid.org>.

### REFERENCES

Authors are solely responsible for the accuracy of all references.

**In-text citations:** References should be indicated as a superscript immediately after the period/full stop of the relevant sentence. If the author(s) of a reference is/are indicated at the beginning of the sentence, this reference should be written as a superscript immediately after the author's name. If relevant research has been conducted in Turkey or by Turkish investigators, these studies should be given priority while citing the literature.

Presentations presented in congresses, unpublished manuscripts, theses, Internet addresses, and personal interviews or experiences should not be indicated as references. If such references are used, they should be indicated in parentheses at the end of the relevant sentence in the text, without reference number and written in full, in order to clarify their nature.

**References section:** References should be numbered consecutively in the order in which they are first mentioned in the text. All authors should be listed regardless of number. The titles of Journals should be abbreviated according to the style used in the Index Medicus.

#### Reference Format

**Journal:** Last name(s) of the author(s) and initials, article title, publication title and its original abbreviation, publication date, volume, the inclusive page numbers. Example: Collin JR, Rathbun JE. Involuntal entropion: a review with evaluation of a procedure. Arch Ophthalmol. 1978;96:1058-1064.

**Book:** Last name(s) of the author(s) and initials, book title, edition, place of publication, date of publication and inclusive page numbers of the extract cited.

**Example:** Herbert L. The Infectious Diseases (1st ed). Philadelphia; Mosby Harcourt; 1999:11;1-8.

**Book Chapter:** Last name(s) of the author(s) and initials, chapter title, book editors, book title, edition, place of publication, date of publication and inclusive page numbers of the cited piece.

**Example:** O'Brien TP, Green WR. Periocular Infections. In: Feigin RD, Cherry JD, eds. Textbook of Pediatric Infectious Diseases (4th ed). Philadelphia; W.B. Saunders Company; 1998:1273-1278.

Books in which the editor and author are the same person: Last name(s) of the author(s) and initials, chapter title, book editors, book title, edition, place of publication, date of publication and inclusive page numbers of the cited piece. Example: Solcia E, Capella C, Kloppel G. Tumors of the exocrine pancreas. In: Solcia E, Capella C, Kloppel G, eds. Tumors of the Pancreas. 2nd ed. Washington: Armed Forces Institute of Pathology; 1997:145-210.

### TABLES, GRAPHICS, FIGURES, AND IMAGES

All visual materials together with their legends should be located on separate pages that follow the main text.

**Images:** Images (pictures) should be numbered and include a brief title. Permission to reproduce pictures that were published elsewhere must be included. All pictures should be of the highest quality possible, in JPEG format, and at a minimum resolution of 300 dpi.

**Tables, Graphics, Figures:** All tables, graphics or figures should be enumerated according to their sequence within the text and a brief descriptive caption should be written. Any abbreviations used should be defined in the accompanying legend. Tables in particular should be explanatory and facilitate readers' understanding of the manuscript, and should not repeat data presented in the main text.

### MANUSCRIPT TYPES

#### Original Articles

Clinical research should comprise clinical observation, new techniques or laboratories studies. Original research articles should include title, structured abstract, key words relevant to the content of the article, introduction, materials and methods, results, discussion, study limitations, conclusion references, tables/figures/images and acknowledgement sections. Title, abstract and key words should be written in both Turkish and English. The manuscript should be formatted in accordance with the above-mentioned guidelines and should not exceed 16 A4 pages.

**Title Page:** This page should include the title of the manuscript, short title, name(s) of the authors and author information. The following descriptions should be stated in the given order:

1. Title of the manuscript (Turkish and English), as concise and explanatory as possible, including no abbreviations, up to 135 characters
2. Short title (Turkish and English), up to 60 characters
3. Name(s) and surname(s) of the author(s) (without abbreviations and academic titles) and affiliations
4. Name, address, e-mail, phone and fax number of the corresponding author
5. The place and date of scientific meeting in which the manuscript was presented and its abstract published in the abstract book, if applicable

# TURKISH

---

# JOURNAL OF PHARMACEUTICAL SCIENCES

---

## INSTRUCTIONS TO AUTHORS

**Abstract:** A summary of the manuscript should be written in both Turkish and English. References should not be cited in the abstract. Use of abbreviations should be avoided as much as possible; if any abbreviations are used, they must be taken into consideration independently of the abbreviations used in the text. For original articles, the structured abstract should include the following sub-headings:

**Objectives:** The aim of the study should be clearly stated.

**Materials and Methods:** The study and standard criteria used should be defined; it should also be indicated whether the study is randomized or not, whether it is retrospective or prospective, and the statistical methods applied should be indicated, if applicable.

**Results:** The detailed results of the study should be given and the statistical significance level should be indicated.

**Conclusion:** Should summarize the results of the study, the clinical applicability of the results should be defined, and the favorable and unfavorable aspects should be declared.

**Keywords:** A list of minimum 3, but no more than 5 key words must follow the abstract. Key words in English should be consistent with "Medical Subject Headings (MESH)" ([www.nlm.nih.gov/mesh/MBrowser.html](http://www.nlm.nih.gov/mesh/MBrowser.html)). Turkish key words should be direct translations of the terms in MESH.

**Original research articles should have the following sections:**

**Introduction:** Should consist of a brief explanation of the topic and indicate the objective of the study, supported by information from the literature.

**Materials and Methods:** The study plan should be clearly described, indicating whether the study is randomized or not, whether it is retrospective or prospective, the number of trials, the characteristics, and the statistical methods used.

**Results:** The results of the study should be stated, with tables/figures given in numerical order; the results should be evaluated according to the statistical analysis methods applied. See General Guidelines for details about the preparation of visual material.

**Discussion:** The study results should be discussed in terms of their favorable and unfavorable aspects and they should be compared with the literature. The conclusion of the study should be highlighted.

**Study Limitations:** Limitations of the study should be discussed. In addition, an evaluation of the implications of the obtained findings/results for future research should be outlined.

**Conclusion:** The conclusion of the study should be highlighted.

**Acknowledgements:** Any technical or financial support or editorial contributions (statistical analysis, English/Turkish evaluation) towards the study should appear at the end of the article.

**References:** Authors are responsible for the accuracy of the references. See General Guidelines for details about the usage and formatting required.

### Review Articles

Review articles can address any aspect of clinical or laboratory pharmaceuticals. Review articles must provide critical analyses of contemporary evidence and provide directions of or future research. Most review articles are commissioned, but other review submissions are also welcome. Before sending a review, discussion with the editor is recommended.

Reviews articles analyze topics in depth, independently and objectively. The first chapter should include the title in Turkish and English, an unstructured summary and key words. Source of all citations should be indicated. The entire text should not exceed 25 pages (A4, formatted as specified above).

### CORRESPONDENCE

All correspondence should be directed to the Turkish Journal of Pharmaceutical Sciences editorial board;

Post: Turkish Pharmacists' Association

Address: Willy Brandt Sok. No: 9 06690 Ankara, TURKEY

Phone: +90 312 409 8136

Fax: +90 312 409 8132

Web Page: <http://turkjps.org/home/>

E-mail: [onur@pharmacy.ankara.edu.tr](mailto:onur@pharmacy.ankara.edu.tr)

# TURKISH JOURNAL OF PHARMACEUTICAL SCIENCES

## CONTENTS

- 119 A Comprehensive Study on Thiadiazole-Based Anticancer Agents Inducing Cell Cycle Arrest and Apoptosis/ Necrosis Through Suppression of Akt Activity in Lung Adenocarcinoma and Glioma Cells  
*Akciğer Adenokarsinom ve Glioma Hücrelerinde Akt Aktivitesinin Bastırılması Yoluyla Hücre Döngüsü Arrestini ve Apoptozu İndükleyen Tiyadiazol Türevi Antikanser Ajanlar Üzerine Kapsamlı Bir Çalışma*  
Gülşen AKALIN ÇİFTÇİ, Belgin SEVER, Mehlika Dilek ALTINTOP
- 132 Preparation and Biopharmaceutical Evaluation of Novel Polymeric Nanoparticles Containing Etoposide for Targeting Cancer Cells  
*Kanser Hücrelerini Hedefleyen Etoposid İçeren Yeni Polimerik Nanopartiküllerin Hazırlanması ve Biyofarmasötik Değerlendirmesi*  
Ayyappan THIYAGARAJAN, Shanmugam SARAVANABHAVAN, Vetrichelvan THANGARASU
- 141 Quantitative Structure–Activity Relationship Analysis of Selective Rho Kinase Inhibitors as Neuro-regenerator Agents  
*Nöro-rejeneratör Ajan Olarak Seçici Rho Kinaz İnhibitörlerinin Kantitatif Yapı-Etkinlik İlişki Analizi*  
Seema KESAR, Sarvesh K. PALIWAL, Pooja MISHRA, Monika CHAUHAN
- 155 Investigation of the Polyphenol Composition, Biological Activities, and Detoxification Properties of Some Medicinal Mushrooms from Turkey  
*Türkiye'deki Bazı Tıbbi Mantarların Polifenol Bileşiminin, Biyolojik Aktivitelerinin ve Detoksifikasyon Özelliklerinin Araştırılması*  
Naznoosh SHOMALI, Okan ONAR, Tuğçe ALKAN, Nergiz DEMİRTAŞ, İlğaz AKATA, Özlem YILDIRIM
- 161 Study of the Tableting Properties of MCR, a Newly Coprocessed Cellulose-based Direct Compression Excipient  
*Yeni Koproses Selüloz Bazlı Doğrudan Basım Yardımcı Maddesi Olan MCR'nin Tabletleme Özelliklerinin İncelenmesi*  
Salah ALY
- 169 Decreased Protein Kinase C Expression in the Cochlear Fibroblasts of Diabetic Rat Models Induced by Curcumin  
*Kurkumin Tarafından İndüklenen Diyabetik Sıçan Modellerinin Koklear Fibroblastlarındaki Azalmış Protein Kinaz C Ekspresyonları*  
Tengku Siti Hajar HARYUNA, Farhat FARHAT, Siska INDRIANY
- 175 Investigation of the Antioxidant,  $\alpha$ -Glucosidase Inhibitory, Anti-inflammatory, and DNA Protective Properties of *Vaccinium arctostaphylos* L.  
*Vaccinium arctostaphylos L.'nin Antioksidan,  $\alpha$ -Glukozidazi İnhibe Edici, Anti-inflamatuvar ve DNA Koruyucu Özelliklerinin İncelenmesi*  
Burak BARUT, Elif Nur BARUT, Seçkin ENĞİN, Arzu ÖZEL, Feride Sena SEZEN
- 184 Electroanalytical Determination of the Anti-inflammatory Drug Tenoxicam in Pharmaceutical Dosage Forms  
*Anti-enflamatuvar İlaç Tenoksikamin Farmasötik Dozaj Formlarından Elektroanalitik Miktar Tayini*  
Fatma AĞIN, Sena ATAL
- 191 Flavonoid Glycosides from *Heracleum pastinaca* Fenzl  
*Heracleum pastinaca Fenzl'in Flavonoit Glikozitleri*  
Perihan GÜRBÜZ
- 196 Optimization of Thiazolidone Scaffolds Using Pocket Modeling for Development of Potential Secretory System Inhibitors of *Mycobacterium tuberculosis*  
*Mycobacterium tuberculosis'in Potansiyel Sekreter Sistem İnhibitörleri Olarak Thiazolidone İskelelerinin Optimizasyonu*  
Shivratna V. KHARE, Sujata P. CHOUDHARI, Siddharth P. PHALLE, Santosh S. KUMBHAR, Prafulla B. CHOUDHARI, Sambhaji R. MASAL, Aakash K. PATIL, Rakesh P. DHAVALA, Durgacharan A. BHAGWAT, Atul M. KADAM
- 206 Optimization of Immobilized Aldose Reductase Isolated from Bovine Liver  
*Sığır Karaciğerinden İzole Edilen İmmobilize Aldoz Redüktazın Optimizasyonu*  
Marya Vakıl NASLIYAN, Sidar BEREKETOĞLU, Özlem YILDIRIM
- 211 Screening of Sacrificial Excipients for Arresting Devitrification of Itraconazole from Solid Dispersion  
*İtrakonazolün Katı Dispersiyondan Devitrifikasyonunu Önlemek için Amaca Yönelik Yardımcı Maddelerin Taranması*  
Bhargavi M. PATEL, Mukesh C. GOHEL, Vaishali T. THAKKAR, Lalji H. BALDANIYA, Ruby R. CHRISTIAN, Tejal R. GANDHI



# TURKISH

---

# JOURNAL OF PHARMACEUTICAL SCIENCES

---

## CONTENTS

- 220 Essential Oil and Fatty Acid Composition of Endemic *Gypsophila laricina* Schreb. from Turkey  
*Türkiye’de Yetişen Endemik Gypsophila laricina Schreb. Türünün Uçucu Yağ ve Yağ Asidi Bileşimi*  
Hüseyin SERVİ, Betül Eren KESKİN, Sezgin ÇELİK, Ümit BUDAK, Büşra KABABIYIK
- 227 Simultaneous Estimation of Saxagliptin and Dapagliflozin in Human Plasma by Validated High Performance Liquid Chromatography - Ultraviolet Method  
*Saxagliptin ve Dapagliflozin Tarafından Doğrulanmış HPLC-UV Yöntemi İnsan Plazma Eş Zamanlı Tahmin*  
Sharmila DONEPUDI, Suneetha ACHANTA
- 234 Identification, Quantification, and Antioxidant Activity of Hydroalcoholic Extract of *Artemisia campestris* from Algeria  
*Cezayir’de Yetişen Artemisia campestris’in Sulu Alkollü Ekstresinin Tanımlanması, Kantitasyonu ve Antioksidan Aktivitesi*  
Boulanouar BAKCHICHE, Abdelaziz GHERIB, Maria Rosário BRONZE, Mosad A. GHAREEB
- 240 Antimicrobial and Anti-Inflammatory Activity of Some *Lathyrus* L. (Fabaceae) Species Growing in Turkey  
*Türkiye’de Yetişen Bazı Lathyrus L. (Fabaceae) Türlerinin Antimikrobiyal ve Antiinflamatuvar Aktivite Değerlendirilmesi*  
Hajar HEYDARI, Gülçin SALTAN İŞCAN, Müjde ERYILMAZ, Özlem BAHADIR ACIKARA, Sezen YILMAZ SARIALTIN, Mehmet TEKİN, Tülay ÇOBAN
- 246 Phytotherapy as a Complementary Medicine for Multiple Sclerosis  
*Multipl Sklerozda Tamamlayıcı Tedavi Olarak Fitoterapi*  
Zahra RABIEI

<b>PUBLICATION NAME</b>	Turkish Journal of Pharmaceutical Sciences
<b>TYPE OF PUBLICATION</b>	Vernacular Publication
<b>PERIOD AND LANGUAGE</b>	Quarterly- English
<b>OWNER</b>	Erdoğan ÇOLAK on behalf of the Turkish Pharmacists' Association
<b>EDITOR-IN-CHIEF</b>	Feyyaz ONUR
<b>ADDRESS OF PUBLICATION</b>	Cinnah Mah. Willy Brandt Sok. No: 9 Çankaya-Ankara/TURKEY

# TURKISH JOURNAL OF PHARMACEUTICAL SCIENCES

Volume: 16, No: 2, Year: 2019

## CONTENTS

### Original articles

- A Comprehensive Study on Thiazazole-Based Anticancer Agents Inducing Cell Cycle Arrest and Apoptosis/Necrosis Through Suppression of Akt Activity in Lung Adenocarcinoma and Glioma Cells  
Gülşen AKALIN ÇİFTÇİ, Belgin SEVER, Mehlika Dilek ALTINTOP .....119
- Preparation and Biopharmaceutical Evaluation of Novel Polymeric Nanoparticles Containing Etoposide for Targeting Cancer Cells  
Ayyappan THIYAGARAJAN, Shanmugam SARAVANABHAVAN, Vetrichelvan THANGARASU ..... 132
- Quantitative Structure–Activity Relationship Analysis of Selective Rho Kinase Inhibitors as Neuro-regenerator Agents  
Seema KESAR, Sarvesh K. PALIWAL, Pooja MISHRA, Monika CHAUHAN .....141
- Investigation of the Polyphenol Composition, Biological Activities, and Detoxification Properties of Some Medicinal Mushrooms from Turkey  
Naznoosh SHOMALI, Okan ONAR, Tuğçe ALKAN, Nergiz DEMİRTAŞ, İlgaz AKATA, Özlem YILDIRIM ..... 155
- Study of the Tableting Properties of MCR, a Newly Coprocessed Cellulose-based Direct Compression Excipient  
Salah ALY .....161
- Decreased Protein Kinase C Expression in the Cochlear Fibroblasts of Diabetic Rat Models Induced by Curcumin  
Tengku Siti Hajar HARYUNA, Farhat FARHAT, Siska INDRIANY ..... 169
- Investigation of the Antioxidant,  $\alpha$ -Glucosidase Inhibitory, Anti-inflammatory, and DNA Protective Properties of *Vaccinium arctostaphylos* L.  
Burak BARUT, Elif Nur BARUT, Seçkin ENGİN, Arzu ÖZEL, Feride Sena SEZEN ..... 175
- Electroanalytical Determination of the Anti-inflammatory Drug Tenoxicam in Pharmaceutical Dosage Forms  
Fatma AĞIN, Sena ATAL ..... 184
- Flavonoid Glycosides from *Heracleum pastinaca* Fenzl  
Perihan GÜRBÜZ .....191
- Optimization of Thiazolidone Scaffolds Using Pocket Modeling for Development of Potential Secretory System Inhibitors of *Mycobacterium tuberculosis*  
Shivratna V. KHARE, Sujata P. CHOUDHARI, Siddharth P. PHALLE, Santosh S. KUMBHAR, Prafulla B. CHOUDHARI, Sambhaji R. MASAL, Aakash K. PATIL, Rakesh P. DHAVALE, Durgacharan A. BHAGWAT, Atul M. KADAM ..... 196
- Optimization of Immobilized Aldose Reductase Isolated from Bovine Liver  
Marya Wakil NASLIYAN, Sidar BEREKETOĞLU, Özlem YILDIRIM ..... 206
- Screening of Sacrificial Excipients for Arresting Devitrification of Itraconazole from Solid Dispersion  
Bhargavi M. PATEL, Mukesh C. GOHEL, Vaishali T. THAKKAR, Lalji H. BALDANIYA, Ruby R. CHRISTIAN, Tejal R. GANDHI ..... 211
- Essential Oil and Fatty Acid Composition of Endemic *Gypsophila larcina* Schreb. from Turkey  
Hüseyin SERVİ, Betül Eren KESKİN, Sezgin ÇELİK, Ümit BUDAK, Büşra KABABIYIK ..... 220
- Simultaneous Estimation of Saxagliptin and Dapagliflozin in Human Plasma by Validated High Performance Liquid Chromatography - Ultraviolet Method  
Sharmila DONEPUDI, SUNEETHA ACHANTA .....227
- Identification, Quantification, and Antioxidant Activity of Hydroalcoholic Extract of *Artemisia campestris* from Algeria  
Boulanouar BAKCHICHE, Abdelaziz GHERIB, Maria Rosário BRONZE, Mosad A. GHAREEB ..... 234
- Antimicrobial and Anti-Inflammatory Activity of Some *Lathyrus* L. (Fabaceae) Species Growing in Turkey  
Hajar HEYDARI, Gülçin SALTAN İŞCAN, Müjde ERYILMAZ, Özlem BAHADIR ACIKARA, Sezen YILMAZ SARIALTIN, Mehmet TEKİN, Tülay ÇOBAN ..... 240

### Review

- Phytotherapy as a Complementary Medicine for Multiple Sclerosis  
Zahra RABIEI .....246



# A Comprehensive Study on Thiadiazole-Based Anticancer Agents Inducing Cell Cycle Arrest and Apoptosis/Necrosis Through Suppression of Akt Activity in Lung Adenocarcinoma and Glioma Cells

Akciğer Adenokarsinom ve Glioma Hücrelerinde Akt Aktivitesinin Bastırılması Yoluyla Hücre Döngüsü Arrestini ve Apoptozu İndükleyen Tiyadiazol Türevi Antikanser Ajanlar Üzerine Kapsamlı Bir Çalışma

© Gülşen AKALIN ÇİFTÇİ<sup>1</sup>, © Belgin SEVER<sup>2</sup>, © Mehlika Dilek ALTINTOP<sup>2\*</sup>

<sup>1</sup>Anadolu University, Faculty of Pharmacy, Department of Biochemistry, Eskişehir, Turkey

<sup>2</sup>Anadolu University, Faculty of Pharmacy, Department of Pharmaceutical Chemistry, Eskişehir, Turkey

## ABSTRACT

**Objectives:** Akt is considered as an attractive target for anticancer drug discovery and development and therefore extensive efforts have been devoted to the discovery of new potent anticancer agents targeting Akt.

**Materials and Methods:** Due to the importance of thiadiazoles for anticancer drug discovery, herein eight 1,3,4-thiadiazole derivatives were investigated for their cytotoxic effects on C6 rat glioma and A549 human lung adenocarcinoma cell lines using the MTT assay. The effects of the most promising anticancer agents on apoptosis, caspase-3 activation, mitochondrial membrane potential, and cell cycle arrest were determined on a BD FACSAria (I) flow cytometer. Akt activity was measured in the C6 and A549 cell lines using an ELISA colorimetric method. Schrödinger's Maestro molecular modeling package was used to explore the possible binding modes of compounds **3** and **8** in the active site of Akt enzyme (PDB code: 3OW4).

**Results:** *N*-(4-Chlorophenyl)-2-[(5-((4-nitrophenyl)amino)-1,3,4-thiadiazol-2-yl)thio]acetamide (**3**) and *N*-(6-nitrobenzothiazol-2-yl)-2-[(5-((4-nitrophenyl)amino)-1,3,4-thiadiazol-2-yl)thio]acetamide (**8**) induced apoptosis and cell cycle arrest in the C6 cell line through inhibition of Akt activity (92.36% and 86.52%, respectively). The docking results of compounds **3** and **8** indicated that  $\pi$ - $\pi$  interactions, H bonds, and salt-bridge formation were responsible for the observed Akt inhibitory activity.

**Conclusion:** According to *in vitro* and docking studies, compounds **3** and **8** stand out as promising anti-glioma agents.

**Key words:** Apoptosis, Akt activity, cancer, molecular docking, thiadiazole

## ÖZ

**Amaç:** Akt, antikanser ilaç keşfinde ve gelişiminde önemli bir hedef olarak düşünülmektedir ve bu nedenle Akt enzimini hedefleyen yeni potent antikanser ajanların keşfi için yoğun çaba harcanmıştır.

**Gereç ve Yöntemler:** Tiyadiazollerin antikanser ilaç keşfindeki önemine bağlı olarak, bu çalışmada sekiz adet 1,3,4-tiyadiazol türevinin C6 sıçan glioma ve A549 insan akciğer adenokarsinoma hücre dizileri üzerindeki sitotoksik etkileri MTT deneyi kullanılarak araştırılmıştır. En etkili antikanser ajanların apoptoz, kaspaz-3 aktivasyonu, mitokondriyal membran potansiyeli, hücre döngüsü arresti üzerindeki etkileri BD FACSAria (I) akış sitometrisi ile belirlenmiştir. Akt aktivite, C6 ve A549 hücre dizilerinde ELISA kolorimetrik yöntem kullanılarak ölçülmüştür. **3** ve **8** no'lu bileşiklerin Akt enziminin (PDB kod: 3OW4) aktif bölgesindeki olası bağlanma biçimlerini araştırmak için Schrödinger's Maestro moleküler modelleme programı kullanılmıştır.

**Bulgular:** *N*-(4-Klorofenil)-2-[(5-((4-nitrofenil)amino)-1,3,4-tiyadiazol-2-il)tiyo]asetamit (**3**) ve *N*-(6-nitrobenzotiyazol-2-il)-2-[(5-((4-nitrofenil)amino)-1,3,4-tiyadiazol-2-il)tiyo]asetamit (**8**), C6 hücre dizisinde apoptozu ve hücre döngüsü tutuklanmasını Akt aktivitesi inhibisyonu aracılığıyla

\*Correspondence: E-mail: mdaltintop@anadolu.edu.tr, Phone: +90 535 258 67 35 ORCID-ID: orcid.org/0000-0002-8159-663X

Received: 10.11.2017, Accepted: 25.01.2018

©Turk J Pharm Sci, Published by Galenos Publishing House.

(sırasıyla %92.36 ve %86.52) indüklemişlerdir. Bu bileşiklerin docking sonuçları, gözlemlenen Akt inhibitör aktiviteden  $\pi$ - $\pi$  etkileşimleri, hidrojen bağları ve tuz köprüsü oluşumunun sorumlu olduğunu belirtmektedir.

**Sonuç:** *In vitro* ve docking çalışmalarına göre, **3** ve **8** no'lu bileşikler umut vadeden anti glioma ajanlar olarak dikkat çekmektedirler.

**Anahtar kelimeler:** Apoptoz, Akt aktivite, kanser, moleküler docking, tiyadiazol

## INTRODUCTION

Targeted cancer therapies, which are used to inhibit tumor growth, progression, and metastasis by interfering with specific molecular targets, have emerged as a promising therapeutic approach for the management of cancer.<sup>1</sup>

Akt, also known as protein kinase B, is overexpressed or activated in a variety of human cancers, including gliomas and lung, breast, ovarian, gastric, and pancreatic cancers.<sup>1,2</sup> Inhibition of Akt signaling results in induction of apoptosis and inhibition of tumor growth and therefore Akt has attracted a great deal of attention as a promising target for anticancer drug discovery and development.<sup>1-6</sup>

Thiadiazole has been studied extensively for more than one hundred years due to its outstanding therapeutic applications. The sulfur atom of the thiadiazole ring imparts improved liposolubility and the mesoionic nature of thiadiazoles also allows these compounds to cross cellular membranes and interact with biological targets with distinct affinities. 1,3,4-Thiadiazoles display a wide spectrum of biological activities including anticancer, antimicrobial, antiviral, antiepileptic, antidiabetic, analgesic, and anti-inflammatory activities.<sup>7-14</sup> In particular, recent studies have pointed out the significance of the 1,3,4-thiadiazole scaffold in the field of current cancer research. Thiadiazole-based anticancer agents exert potent antitumor activity against a variety of human cancer cell lines through the inhibition of diverse molecular targets including histone deacetylase, Abl tyrosine kinase, focal adhesion kinase, Akt, and tubulin polymerization.<sup>7-22</sup>

Prompted by the aforementioned findings, herein we focused on the *in vitro* antiproliferative effects of a series of 1,3,4-thiadiazoles on A549 human lung adenocarcinoma and C6 rat glioma cell lines. Further *in vitro* and *in silico* studies were also carried out to determine the mechanism of antitumor action of the most potent anticancer agents in this series.

## MATERIALS AND METHODS

### Chemistry

5-(4-Nitrophenyl)amino-1,3,4-thiadiazole-2(3H)-thione was synthesized via the ring closure reaction of 4-(4-nitrophenyl) thiosemicarbazide with carbon disulfide in the presence of potassium hydroxide. Finally, the reaction of 5-(4-nitrophenyl) amino-1,3,4-thiadiazole-2(3H)-thione with *N*-(alkyl/aryl)-2-chloroacetamide/4-(chloroacetyl)morpholine in the presence of potassium carbonate afforded compounds **1-8**. The synthetic procedure and the spectral data of compounds **1-8** were reported previously by our research group.<sup>23</sup> The chemical structures of the test compounds are given in Table 1.

### Biochemistry

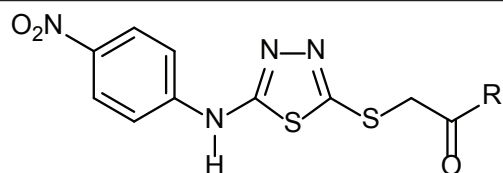
#### Cell culture and drug treatment

C6 rat glioma and NIH/3T3 mouse embryonic fibroblast cells were incubated in Dulbecco's Modified Eagle's Medium (Sigma, Deisenhofen, Germany) supplemented with 10% fetal calf serum (Gibco, Paisley, Scotland). A549 human lung adenocarcinoma cells were incubated in 90% RPMI supplemented with 10% fetal bovine serum (Gibco, Paisley, Scotland). All media were supplemented with 100 IU/mL penicillin-streptomycin (Gibco, Paisley, Scotland) and the cells were incubated at 37°C in a humidified atmosphere of 95% air and 5% CO<sub>2</sub>. Exponentially growing cells were plated at 2×10<sup>4</sup> cells/mL into 96-well microtiter tissue culture plates (Nunc, Denmark) and incubated for 24 h before the addition of the drugs (the optimum cell number for cytotoxicity assays was determined in preliminary experiments). The stock solutions of the compounds were prepared in dimethyl sulfoxide (DMSO; Sigma Aldrich, Poole, UK) and further dilutions were made with fresh culture medium (the concentration of DMSO in the final culture medium was <0.1%, which had no effect on cell viability).

#### MTT assay

The level of cellular 3-(4,5-dimethylthiazol-2-yl)-2,5-diphenyltetrazolium bromide (MTT) (Sigma) reduction was quantified as previously described in the literature<sup>24,25</sup> with small modifications.<sup>26</sup> Compounds **1-8** were investigated for their anticancer activity against A549 human lung adenocarcinoma and C6 rat glioma cell lines. NIH/3T3 mouse embryonic fibroblast cells were used to evaluate the selectivity of the compounds.

Table 1. The chemical structures of compounds 1-8



Compound	R
1	Diethylamino
2	(3-Chlorophenyl)amino
3	(4-Chlorophenyl)amino
4	(4-Nitrophenyl)amino
5	(1,3-Benzodioxol-5-ylmethyl)amino
6	Morpholin-4-yl
7	(Benzothiazol-2-yl)amino
8	(6-Nitrobenzothiazol-2-yl)amino

After 24 h of preincubation, compounds **1-8** and cisplatin (positive control) were added to give a final concentration in the range 3.9-500  $\mu\text{g}/\text{mL}$  and the cells were incubated for 24 h. This concentration range was chosen based on our previous studies.<sup>26</sup> At the end of this period, MTT was added to a final concentration of 0.5 mg/mL and the cells were incubated for 4 h at 37°C. After the medium was removed, the formazan crystals formed by MTT metabolism were solubilized by addition of 200  $\mu\text{L}$  of DMSO to each well and absorbance was read at 540 nm with a microtiter plate spectrophotometer (Bio-Tek plate reader, Winooski, VT, USA). Every concentration was repeated in three wells. The half maximal inhibitory concentration ( $\text{IC}_{50}$ ) values were defined as the drug concentrations that reduced absorbance to 50% of control values.

#### *Flow cytometric analyses of apoptosis*

After the cells were incubated with compounds **1, 2, 3, 4, 5, 8**, and cisplatin at  $\text{IC}_{50}$  concentrations, phosphatidylserine externalization, which indicates early apoptosis, was measured by Annexin V-propidium iodide (PI) (BD Pharmingen, San Jose, CA, USA) on a BD FACSAria flow cytometer for 24 h. The Annexin V staining protocol was applied according to the manufacturer's instructions (BD Pharmingen, San Jose, CA, USA). The cells were then briefly washed with cold phosphate buffer saline (PBS) and suspended in a binding buffer at a concentration of  $1 \times 10^6$  cells/mL. Then 100  $\mu\text{L}$  of this solution containing  $1 \times 10^5$  cells was transferred to a 5 mL test tube. After addition of 5  $\mu\text{L}$  of Annexin-V and PI, the cells were incubated for 15 min at room temperature (RT) in the dark. Then 400  $\mu\text{L}$  of 1X binding buffer was added to each tube and the cells were processed for data acquisition, and analyzed on a Becton Dickinson FACSAria flow cytometer using BD FACSDiva software version 6.1.1 (BD Biosciences, San Jose, CA, USA).<sup>26</sup>

#### *Flow cytometric analyses of caspase-3*

After C6 cells were incubated with compounds **1, 2, 3, 4, 5, 8**, and cisplatin at  $\text{IC}_{50}$  concentrations for 24 h, the caspase-3 activity measurement protocol was applied according to the manufacturer's instructions (BD Pharmingen, San Jose, CA, USA). In brief, the cells were washed with cold PBS 1X cells and incubated with 0.5 mL of perm lyse solution for 30 min at RT in the dark. The pellets were washed twice with 0.5 mL of perm wash buffer. The cells were resuspended in 100  $\mu\text{L}$  of perm wash buffer and 10  $\mu\text{L}$  of caspase-3 antibody was added over 20 min at RT in the dark. At least 10,000 cells were counted for each sample and the cells were analyzed by BD FACSAria flow cytometry using BD FACSDiva software version 6.1.1 (BD Biosciences, San Jose, CA, USA).

#### *Analysis of mitochondrial membrane potential (MMP) by flow cytometry*

The cells were seeded in six-well plates at a density of  $10^5$  cells/mL, and the  $\text{IC}_{50}$  doses of compounds **1, 2, 3, 4, 5, 8**, and cisplatin were added to cells. The cells were incubated in 5%  $\text{CO}_2$  air-conditioned atmosphere at 37°C. After 48 h of incubation, the cells were trypsinized, washed with PBS, and centrifuged at  $400 \times g$  for 5 min. 5,5',6,6'-Tetrachloro-1,1',3,3'-tetraethylbenz

imidazolylcarbocyanine iodide (JC-1) dye solution (1X assay buffer + JC-1 stock solution) was added to the cells. The stock solution was prepared by dissolving DMSO. Then the samples were incubated at 37°C for 10-15 min. After incubation, the cells were washed twice with an assay buffer and analyzed by BD FACSAria flow cytometry using BD FACSDiva software version 6.1.1 (BD Biosciences, San Jose, CA, USA). The cells showing mitochondrial membrane potential disruption were determined as a percentage of all cells.<sup>26</sup>

#### *Cell cycle analysis*

After C6 and A549 cells were incubated with  $\text{IC}_{50}$  concentrations of the compounds for 24 h, the cell cycle analysis measurement protocol was applied according to the manufacturer's instructions (BD Biosciences, San Jose, CA, USA). The cells were briefly suspended in citrate buffer. The cells were then centrifuged at  $400 \times g$  for 5 min at RT. The supernatant was decanted and 250  $\mu\text{L}$  of solution A was added to the pellet and kept at RT for 10 min. Then 200  $\mu\text{L}$  of solution B was added and the resulting mixture was gently mixed and kept at RT for 10 min. Then 200  $\mu\text{L}$  of solution C was added. After being gently mixed, it was kept in the dark at 4°C for 10 min and then analyzed on a BD FACSAria flow cytometer using BD Bioscience's ModFit software.<sup>27</sup>

#### *Inhibition of Akt enzyme*

After 10,000 cells/well were incubated with compounds **1, 2, 3, 4, 5, 8**, and cisplatin at  $\text{IC}_{50}$  concentrations for 24 h, the in-cell ELISA colorimetric Akt activity protocol was applied according to the manufacturer's instructions (Thermo Fisher Scientific, Rockford, IL, USA). Briefly, the medium was removed and 100  $\mu\text{L}$  of 4% formaldehyde was added to each well. The plate was incubated in a fume hood at RT for 15 min. Formaldehyde was removed and the plate was washed twice with 100  $\mu\text{L}$ /well of 1X TBS. The 1X TBS was removed and 100  $\mu\text{L}$ /well of 1X permeabilization buffer was added, followed by incubation for 15 min at RT. Permeabilization buffer was removed and the plate was washed once with 100  $\mu\text{L}$ /well of 1X TBS. The 1X TBS was removed and 100  $\mu\text{L}$ /well quenching solution was added, followed by incubation at RT for 20 min. The quenching solution was removed and the plate was washed once with 100  $\mu\text{L}$ /well of 1X TBS. The 1X TBS was removed and 100  $\mu\text{L}$ /well of blocking buffer was added, followed by incubation at RT for 30 min. After the blocking buffer was removed, 50  $\mu\text{L}$ /well of primary antibody was added. A plate sealer was applied and incubation was conducted overnight at 4°C. The primary antibody solution was removed and the plate was washed three times with 100  $\mu\text{L}$ /well of 1X wash buffer. After the wash buffer was removed, 100  $\mu\text{L}$ /well of diluted horseradish peroxidase conjugate was added, followed by incubation for 30 min at RT. The wash buffer was removed and 100  $\mu\text{L}$ /well of 3,3',5,5'-tetramethylbenzidine substrate was added. Then the plate was incubated at RT, protected from light. Next, 100  $\mu\text{L}$ /well of 3,3',5,5'-tetramethylbenzidine stop solution was added and the absorbance was measured at 450 nm within 30 min of stopping the reaction. The experiment was performed in triplicate wells. The values of blank wells were subtracted from

each well of treated and control cells. Percent Akt activity was defined as the relative absorbance of treated versus untreated control cells.

#### Statistical analysis

Statistical Package for the Social Sciences (SPSS) (Chicago, IL, USA) for Windows 15.0 was used for statistical analysis. The data were expressed as mean  $\pm$  standard deviation. Comparisons were performed by one-way analysis of variance for normally distributed continuous variables and post-hoc analyses of group differences were expressed by the Tukey test. Probability values less than 0.05 ( $p < 0.05$ ) were regarded as significant.

#### Molecular docking studies

Compounds **3** and **8** were docked to the active site of Akt enzyme. Ligands were set to the physiological pH (pH= 7.4) at the protonation step and the crystal structure of Akt enzyme was retrieved from the Protein Data Bank server (PDB code: 3OW4). The structures of compounds **3** and **8** were submitted to the protein preparation module of Schrödinger's Maestro molecular modeling package (Schrödinger Release 2016-2: Schrödinger, LLC, New York, NY, USA). In molecular docking simulations, Glide/XP docking protocols were applied for prediction of the topologies of compounds **3** and **8** in the active site of the target structure.<sup>28</sup>

## RESULTS AND DISCUSSION

The MTT assay was carried out to determine the anticancer effects of the compounds on A549 human lung adenocarcinoma and C6 rat glioma cell lines (Table 2).

Compounds **3** and **4** were more effective on the C6 cell line than cisplatin ( $IC_{50} = 24.33 \pm 0.58 \mu\text{g/mL}$ ). Compounds **3** and **4** showed antiproliferative effects on the C6 cell line with  $IC_{50}$  values of  $22.00 \pm 3.00 \mu\text{g/mL}$  and  $18.50 \pm 4.95 \mu\text{g/mL}$ , respectively. This outcome clearly indicated that *p*-chloro and *p*-nitro substituents significantly enhanced anticancer activity against the C6 cell line. Compounds **1**, **2**, **5**, and **8** exhibited notable cytotoxic activity against the C6 cell line with  $IC_{50}$  values of  $50.66 \pm 12.50$ ,

$42.33 \pm 2.52$ ,  $46.67 \pm 2.89$ , and  $42.67 \pm 2.08 \mu\text{g/mL}$ , respectively. These results showed the importance of the alkyl and aryl groups attached to the acetamido moiety for anticancer activity against C6 cells.

Compound **3** was found to be the most promising anticancer agent against the A549 cell line with an  $IC_{50}$  value of  $21.00 \pm 1.15 \mu\text{g/mL}$  when compared with cisplatin ( $IC_{50} = 13.50 \pm 2.12 \mu\text{g/mL}$ ). Compounds **1**, **5**, and **8** also showed anticancer activity against the A549 cell line with  $IC_{50}$  values of  $46.33 \pm 2.31$ ,  $42.67 \pm 2.52$ , and  $41.33 \pm 1.15 \mu\text{g/mL}$ , respectively. Interestingly, compound **4**, the most potent anticancer agent against the C6 cell line, did not show any inhibitory activity against the A549 cell line ( $IC_{50} > 500 \mu\text{g/mL}$ ). This outcome indicated that *p*-nitro substituent significantly decreased anticancer activity against the A549 cell line.

Toxicity to host cells is an important characteristic to assess the safety of drug candidates early in the drug discovery process. In order to evaluate whether the compounds were toxic or nontoxic to healthy cells, the cytotoxic effects of compounds **1-8** on NIH/3T3 mouse embryonic fibroblast cells were investigated using the MTT assay (Table 2). Generally, the most potent anticancer agents in this series showed low cytotoxicity against the NIH/3T3 cell line with  $IC_{50}$  values higher than their effective  $IC_{50}$  values.

After the 24 h incubation period, the apoptotic effects of compounds **1**, **2**, **3**, **4**, **5**, and **8** were analyzed based on Annexin V-PI binding capacities in flow cytometry. Following flow cytometric analyses, the early and late apoptotic effects of compounds **1**, **2**, **3**, **4**, **5**, and **8** (for  $IC_{50}$  doses) on the C6 cell line were determined as 25.7%, 23.8%, 22.7%, 13.6%, 17.4%, and 10.0%, respectively (Table 3, Figure 1). On the other hand, the early and late apoptotic effects of compounds **1**, **3**, **5**, and **8** (for  $IC_{50}$  doses) on the A549 cell line were very low (1.5%, 0.3%, 0.2%, and 2.3%, respectively). However, their necrotic cell percentages were very high (60.2%, 25.5%, 81.1%, and 54.0%,

**Table 3. Percentages of typical quadrant analysis of Annexin V FITC/PI flow cytometry of C6 cells treated with compounds 1, 2, 3, 4, 5, 8, and cisplatin**

Groups	Early apoptotic cells %	Late apoptotic cells %	Viable cells %	Necrotic cells %
Control (untreated)	5.2	4.3	87.0	3.1
Compound 1 treated cells	9.7	16.0	66.1	8.2
Compound 2 treated cells	12.2	11.6	63.5	12.8
Compound 3 treated cells	12.8	9.9	21.8	21.8
Compound 4 treated cells	9.6	4.0	78.7	7.6
Compound 5 treated cells	11.1	6.3	74.6	8.0
Compound 8 treated cells	4.7	5.3	71.7	18.3
Cisplatin treated cells	3.4	15.4	55.5	25.7

C6 cells were cultured for 24 h in medium with compounds **1**, **2**, **3**, **4**, **5**, **8**, and cisplatin at  $IC_{50}$  values. At least 10,000 cells were analyzed per sample and quadrant analysis was performed; PI: Propidium iodide

**Table 2.  $IC_{50}$  values of the compounds against A549, C6, and NIH/3T3 cells for 24 h**

Compound	C6 cell line	A549 cell line	NIH/3T3 cell line
1	$50.66 \pm 12.50$	$46.33 \pm 2.31$	>500
2	$42.33 \pm 2.52$	$160.00 \pm 34.64$	$175.00 \pm 35.35$
3	$22.00 \pm 3.00$	$21.00 \pm 1.15$	$91.67 \pm 7.64$
4	$18.50 \pm 4.95$	>500	$275.00 \pm 35.36$
5	$46.67 \pm 2.89$	$42.67 \pm 2.52$	$450.00 \pm 70.71$
6	$135.00 \pm 21.21$	$91.67 \pm 2.89$	>500
7	$76.67 \pm 2.89$	$88.33 \pm 7.64$	$480.00 \pm 26.46$
8	$42.67 \pm 2.08$	$41.33 \pm 1.15$	$125.00 \pm 35.36$
Cisplatin	$24.33 \pm 0.58$	$13.50 \pm 2.12$	nt

nt: Not tested; Values are given as mean  $\pm$  standard deviation

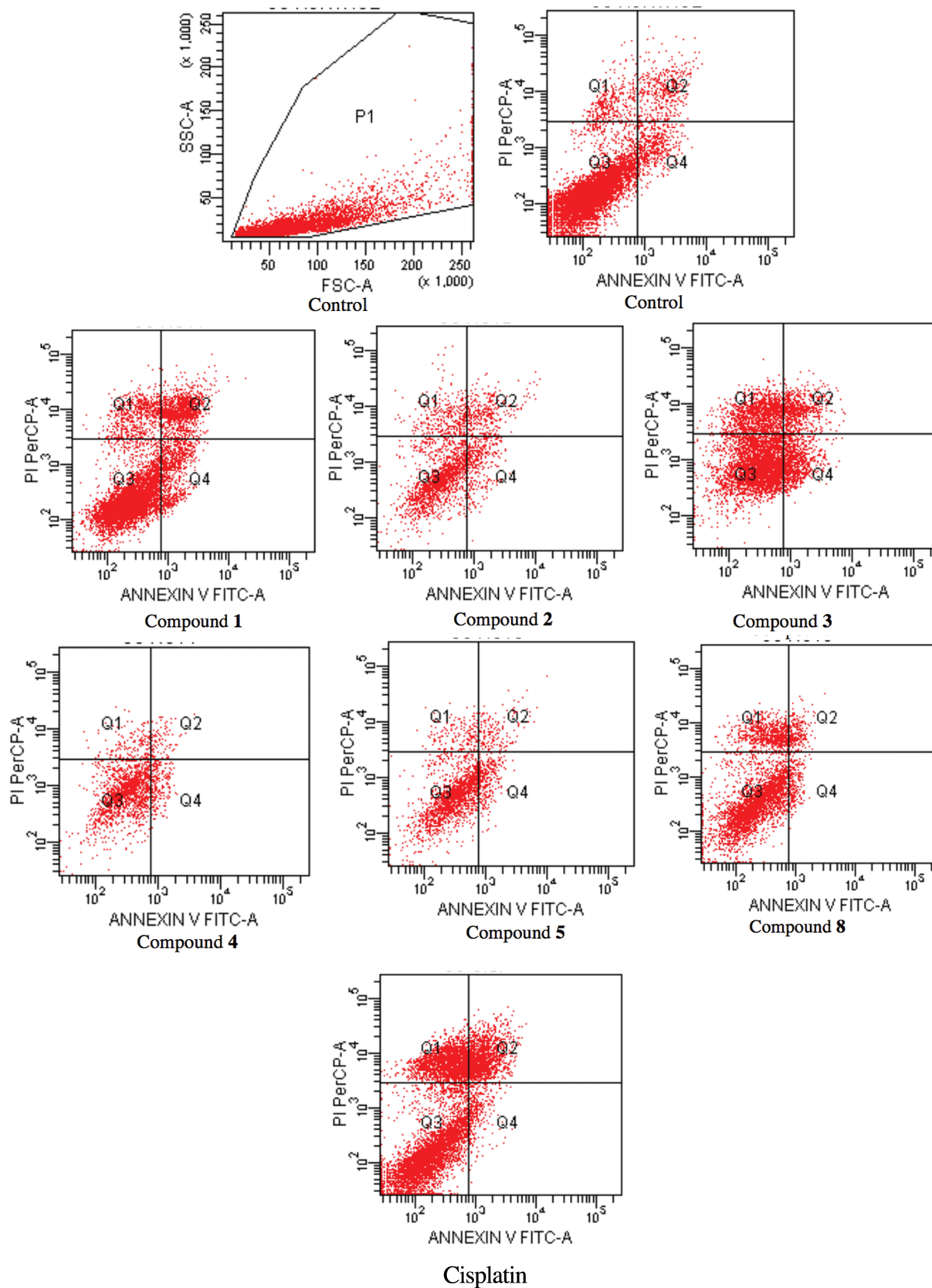


**Figure 1.** Typical quadrant analysis of Annexin V-FITC/PI flow cytometry of C6 cells treated with compounds 1, 2, 3, 4, 5, 8, and cisplatin. At least 10,000 cells were analyzed per sample and quadrant analysis was performed. The portion (%) of cell number is shown in each quadrant. Q1, necrotic cells; Q2, late apoptotic cells; Q3, viable cells; Q4, early apoptotic cells. C6 cells were cultured for 24 h in medium with  $IC_{50}$  concentrations of the compounds, cisplatin, and untreated control cells



respectively) (Table 4, Figure 2). According to these findings, compounds **1**, **2**, and **3** (25.7%, 23.8%, and 22.7%) showed more apoptotic activity than cisplatin (18.8%) against C6 cells. On the other hand, compounds **1**, **3**, **5**, and **8** caused necrotic cell death in A549 cells.

Due to the key role of caspase-3 activation in the initiation of cellular events during the early apoptotic process,<sup>29</sup> the effects of compounds **1**, **2**, **3**, **4**, **5**, and **8** on caspase-3 activation in the C6 cell line were determined. Caspase-3 positive cell percentages of compounds **1**, **3**, and cisplatin (for IC<sub>50</sub> doses) were determined as 18.6%, 49.7%, and 14.9%, respectively (Table 5, Figure 3). On the other hand, caspase-3 negative cell percentages of these compounds and cisplatin (for IC<sub>50</sub> doses) were determined as 80.4%, 49.5%, and 85.0%, respectively. These findings indicated that compound **3** was the most effective compound on caspase-3 activation in the C6 cell line.

In order to investigate the effects of compounds **1**, **2**, **3**, **4**, **5**, and **8** on the MMP of C6 and A549 cells, the cells were incubated with IC<sub>50</sub> concentrations of these compounds for 24

h. Compounds **3** and **8** caused higher disturbance to MMP than cisplatin in both cell line. Mitochondrial membrane depolarized cell percentages of compounds **3**, **8** and cisplatin (for IC<sub>50</sub> doses) were determined as 27.6, 27.9, and 16.9 in the C6 cell line (Table 6, Figure 4), while mitochondrial membrane depolarized cell percentages of these compounds and cisplatin (for IC<sub>50</sub> doses) were determined as 44.7, 28.2, and 24.1, respectively, in the A549 cell line (Table 6, Figure 5).

Due to the importance of cell cycle checkpoints for the progression of cell proliferation,<sup>30</sup> the compounds were analyzed for their effects on the cell cycle in A549 and C6 cells (Table 7, Figure 6). Compounds **2**, **3**, **4**, **5**, and **8** induced G1/S phase arrest in C6 cells. Among them, compound **3** caused more

**Table 4.** Percentages of typical quadrant analysis of Annexin V FITC/PI flow cytometry of A549 cells treated with compounds **1**, **3**, **5**, **8**, and cisplatin

Groups	Early apoptotic cells %	Late apoptotic cells %	Viable cells %	Necrotic cells %
Control (untreated)	3.6	2.5	91.7	2.2
Compound <b>1</b> treated cells	0.3	1.2	38.2	60.2
Compound <b>3</b> treated cells	0.1	0.2	74.2	25.5
Compound <b>5</b> treated cells	0.0	0.2	18.7	81.1
Compound <b>8</b> treated cells	0.7	1.6	43.6	54.0
Cisplatin treated cells	0.0	0.8	30.5	68.7

A549 cells were cultured for 24 h in medium with compounds **1**, **3**, **5**, **8**, and cisplatin at IC<sub>50</sub> values. At least 10,000 cells were analyzed per sample and quadrant analysis was performed; PI: Propidium iodide

**Table 5.** Percentages of quadrant analysis of active caspase-3 phycoerythrin staining by flow cytometry of C6 cells treated with IC<sub>50</sub> concentrations of compounds **1**, **2**, **3**, **4**, **5**, **8**, and cisplatin

Groups	Caspase-3 (-) cells %	Caspase-3 (+) cells %
Control (untreated)	96.3	3.1
Compound <b>1</b> treated cells	80.4	18.6
Compound <b>2</b> treated cells	88.6	11.1
Compound <b>3</b> treated cells	49.5	49.7
Compound <b>4</b> treated cells	87.7	12.7
Compound <b>5</b> treated cells	89.4	10.1
Compound <b>8</b> treated cells	97.4	2.0
Cisplatin treated cells	85.0	14.9

C6 cells were cultured for 24 h in medium with compounds **1**, **2**, **3**, **4**, **5**, **8**, and cisplatin at IC<sub>50</sub> concentrations. At least 10,000 cells were analyzed per sample and quadrant analysis was performed

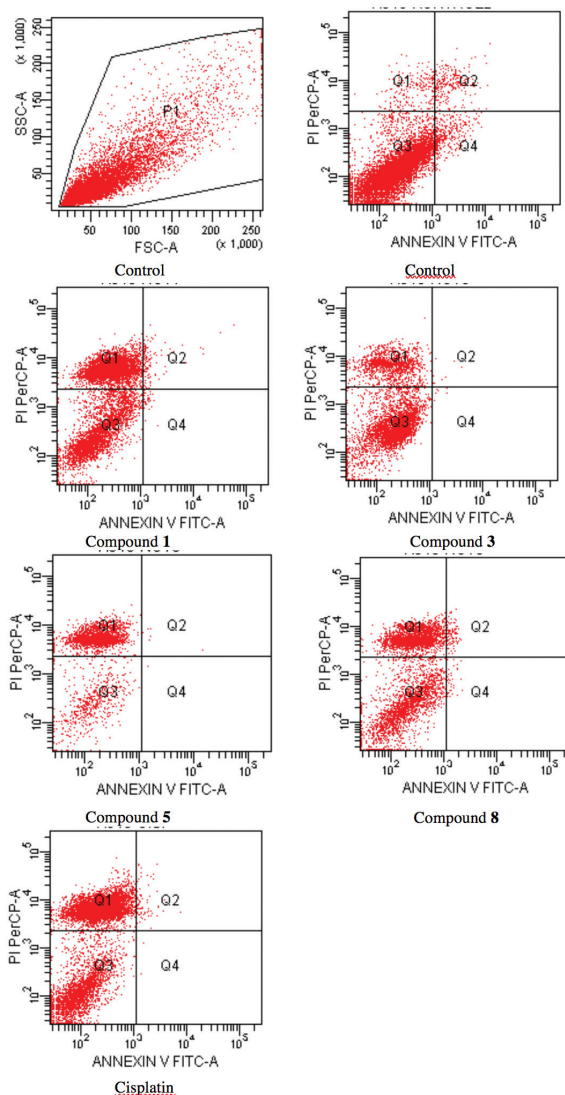


**Figure 2.** Typical quadrant analysis of Annexin V-FITC/PI flow cytometry of A549 cells treated with compounds **1**, **3**, **5**, **8**, and cisplatin. At least 10,000 cells were analyzed per sample and quadrant analysis was performed. The portion (%) of cell number is shown in each quadrant. Q1, necrotic cells; Q2, late apoptotic cells; Q3, viable cells; Q4, early apoptotic cells. A549 cells were cultured for 24 h in medium with IC<sub>50</sub> concentrations of the compounds, cisplatin, and untreated control cells

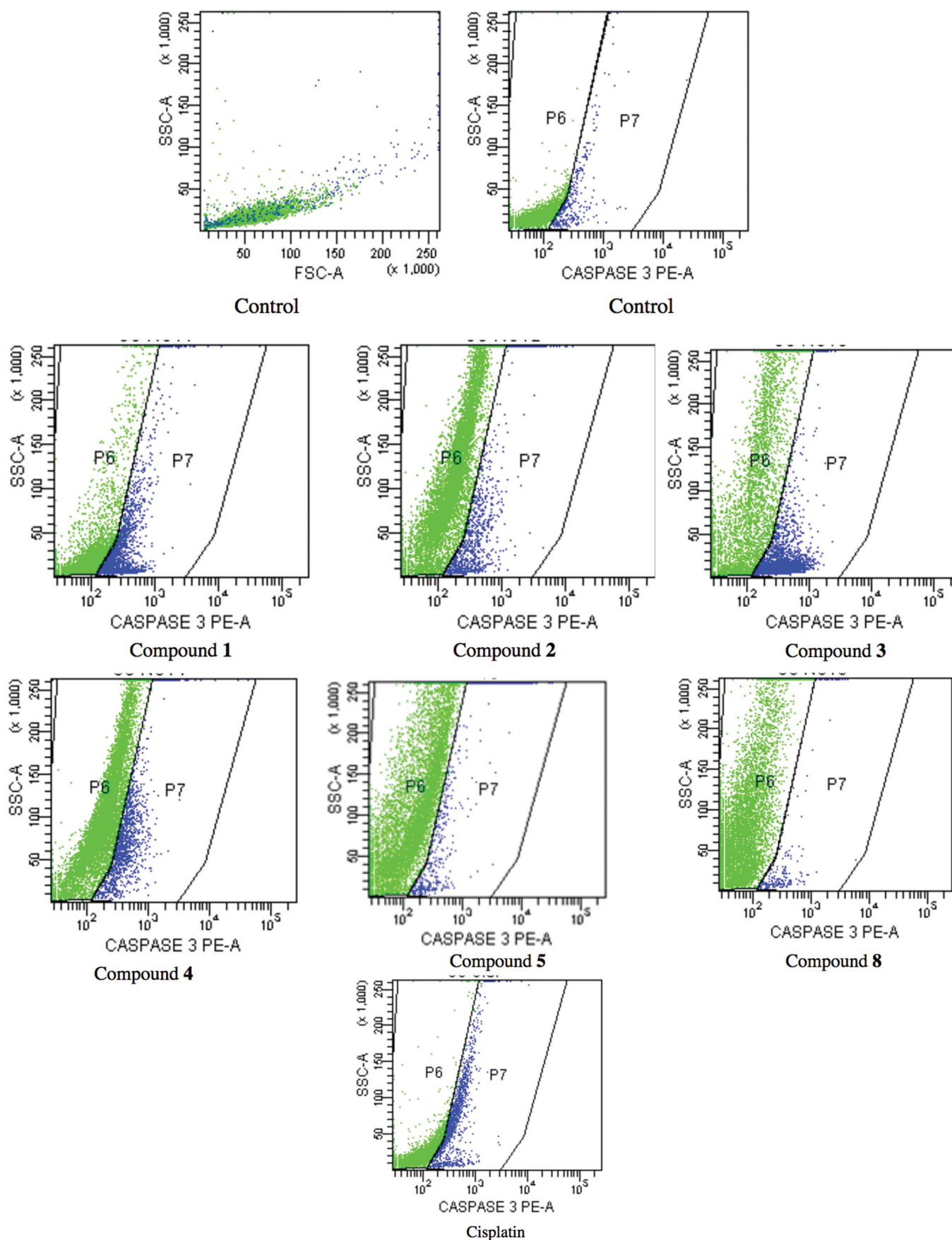
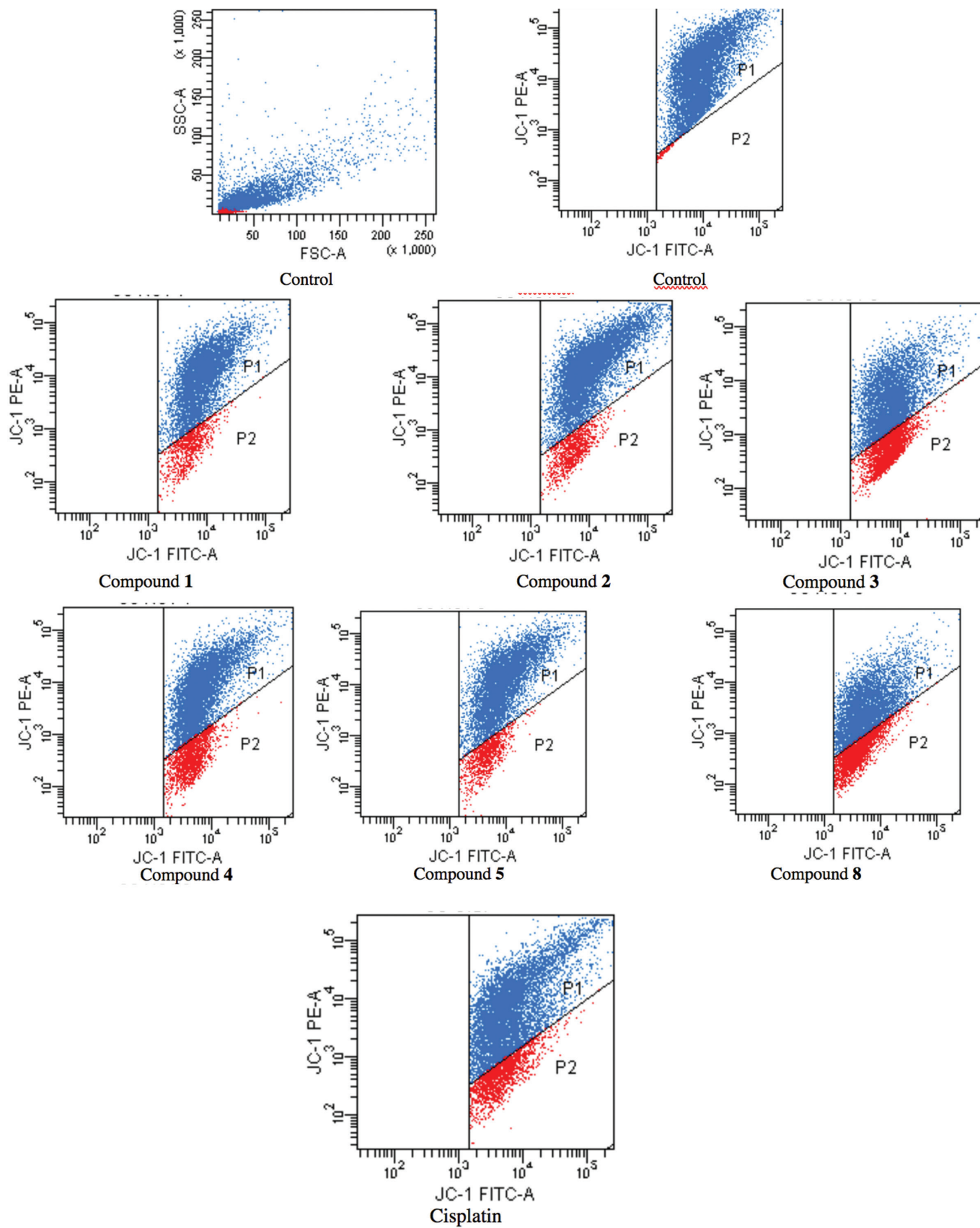
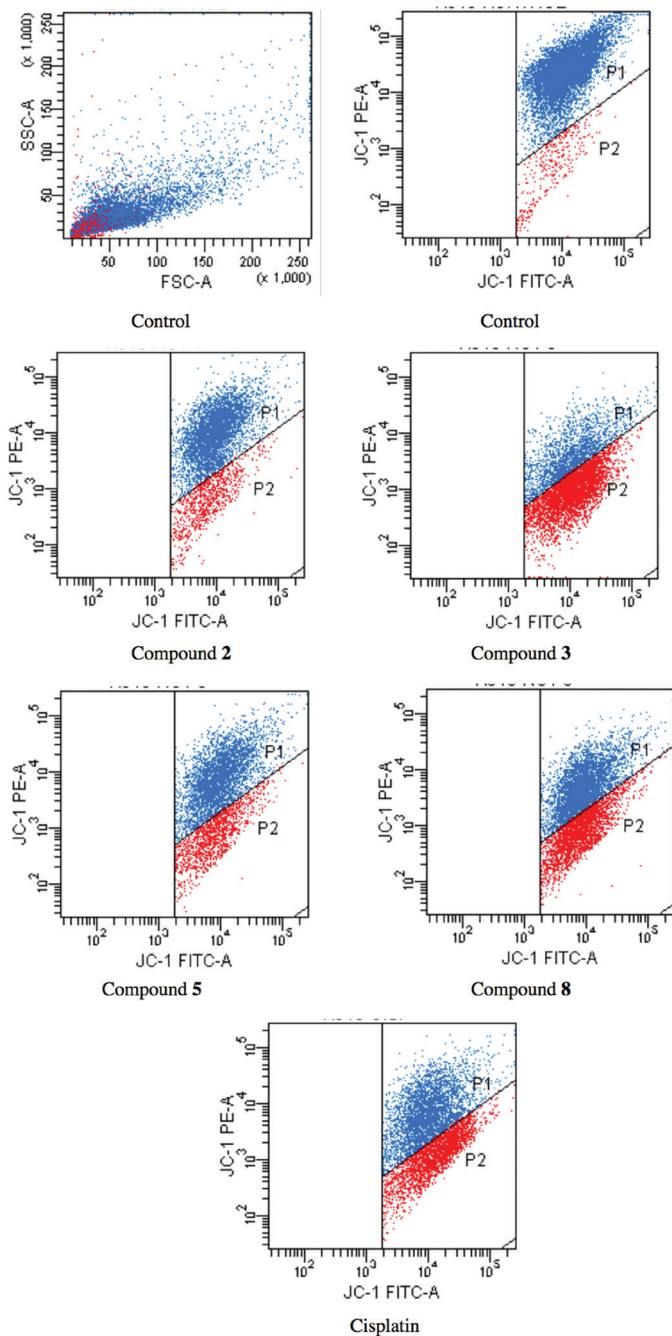


Figure 3. Caspase 3 activity of C6 cells treated with IC<sub>50</sub> concentrations of compounds 1, 3, 5, 8, and cisplatin



**Figure 4.** The reduction in the MMP in the C6 cell line by the compounds. The cells treated or untreated with IC<sub>50</sub> doses of the compounds for 24 h were stained with mitochondrial-selective JC-1 dye and analyzed by flow cytometry. P1: mitochondrial membrane polarized cells, P2: mitochondrial membrane depolarized cells



**Figure 5.** The reduction in the MMP in the A549 cell line by the compounds. The cells treated or untreated with  $IC_{50}$  doses of the compounds for 24 h were stained with the mitochondrial-selective JC-1 dye and analyzed by flow cytometry. P1: mitochondrial membrane polarized cells, P2: mitochondrial membrane depolarized cells

G1/S phase arrest (67.21%) than cisplatin (62.57%). Compounds 1, 2, 3, 4, 5, and 8 arrested the G2/M cell cycle in C6 cells. On the other hand, compounds 1, 5, and 8 caused G2/M cell cycle arrest in A549 cells (Table 7, Figure 7). Only compound 8 caused G1/S cell cycle phase arrest in A549 cells. The effects of compound 8 on G1/S arrest were more significant in A549 cells than in C6 cells.

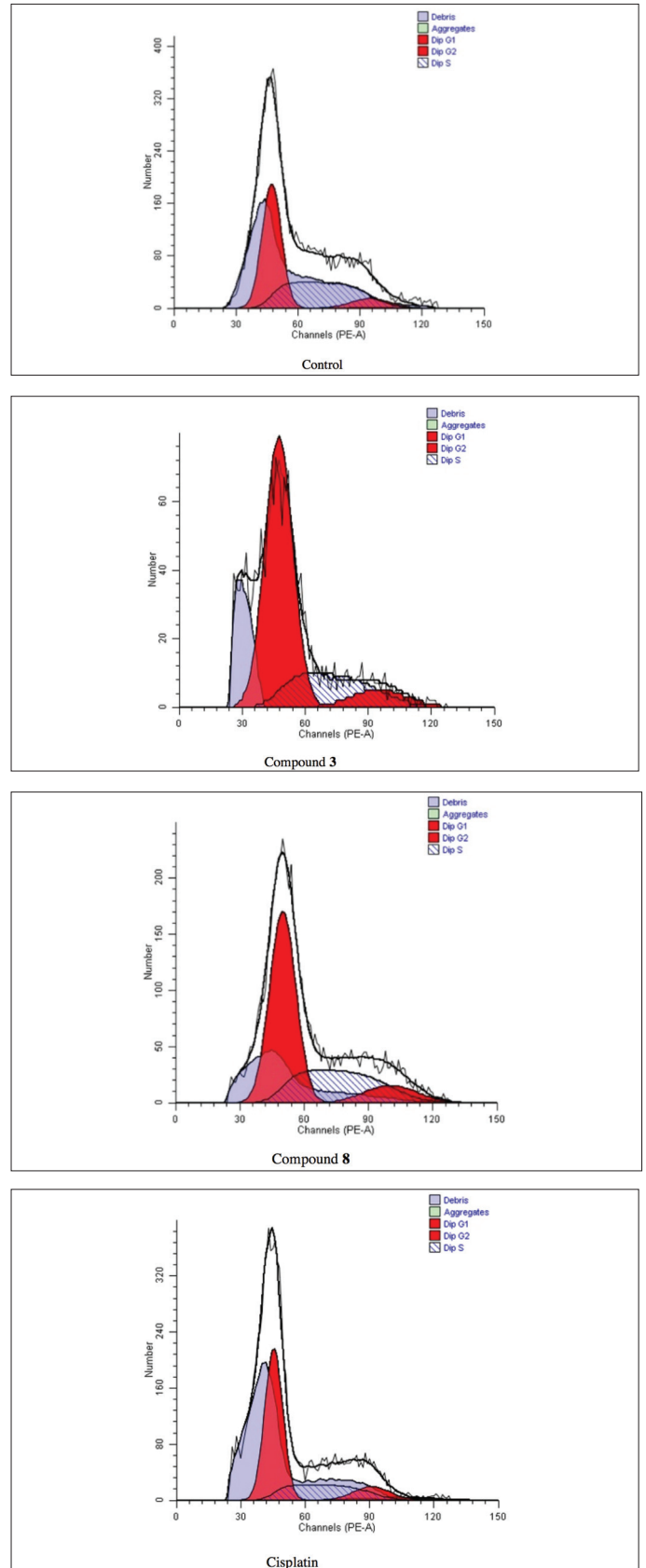


**Figure 6.** Cell cycle distribution of C6 cells treated with  $IC_{50}$  concentrations of the compounds for 24 h. At least 10,000 cells were analyzed per sample. Blue color shows debris, green color shows aggregates, and red color shows cells in G1 and G2 phases

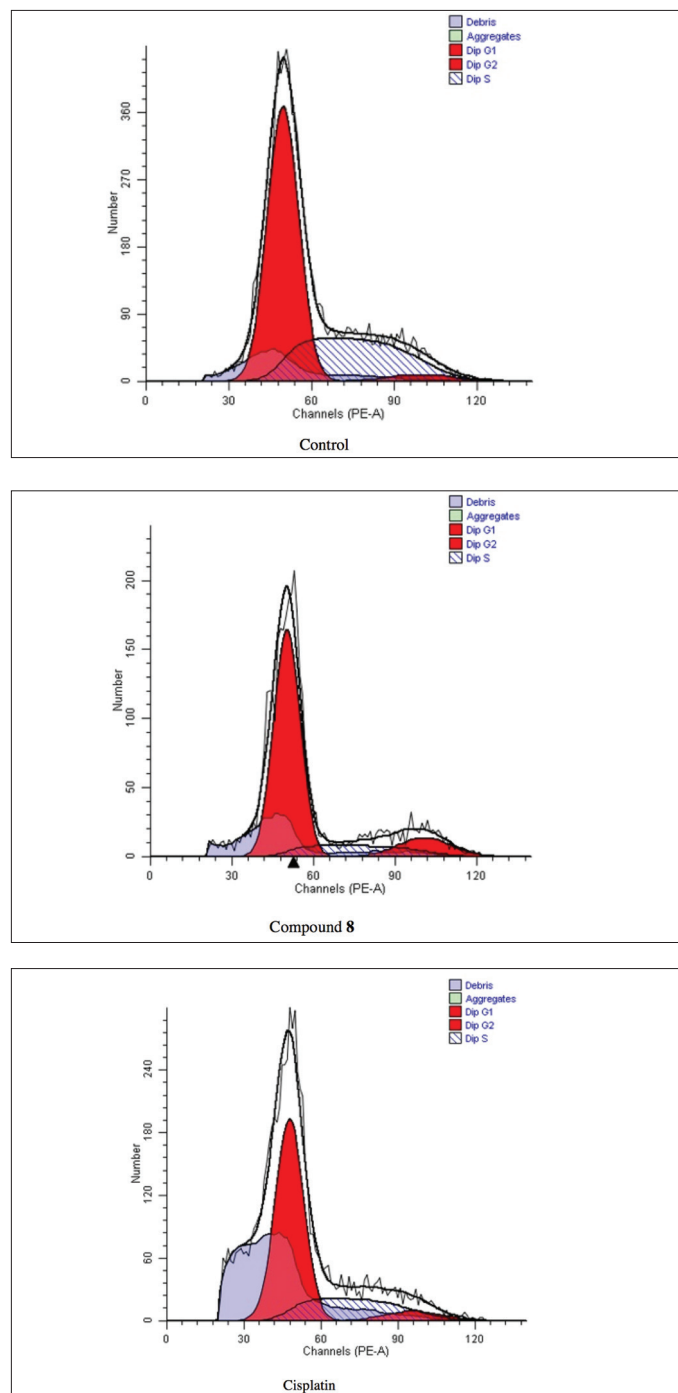


**Figure 7.** Cell cycle distribution of A549 cells treated with  $IC_{50}$  concentration of compound **8** and cisplatin for 24 h. At least 10,000 cells were analyzed per sample. Blue color shows debris, green color shows aggregates, and red color shows cells in G1 and G2 phases

As a consequence of the pivotal role of Akt in regulating diverse cellular functions including cell growth, proliferation, and survival,<sup>1-6</sup> the most potent anticancer agents were investigated for their inhibitory effects on Akt activity (Table 8). Compounds **3** ( $92.36 \pm 0.70\%$  and  $91.22 \pm 0.16\%$  for C6 and A549 cells, respectively) and **8** ( $86.52 \pm 0.37\%$  and  $70.48 \pm 13.28\%$  for C6 and A549 cells, respectively) were the most potent Akt inhibitors in this series compared to control cells ( $p < 0.001$ ).

**Table 6.** Reduction in the MMP in C6 and A549 cells by  $IC_{50}$  concentrations of the compounds and cisplatin

Groups	Mitochondrial membrane polarized (P1) cells (%)		Mitochondrial membrane depolarized cells (P2) (%)	
	C6 cells	A549 cells	C6 cells	A549 cells
Control (untreated)	96.0	92.5	1.3	3.3
Compound <b>1</b> treated cells	61.7	9.0	45.4	8.3
Compound <b>2</b> treated cells	87.2	-	10.8	-
Compound <b>3</b> treated cells	58.1	19.9	27.6	44.7
Compound <b>4</b> treated cells	78.5	-	20.1	-
Compound <b>5</b> treated cells	75.5	37.1	11.6	12.9
Compound <b>8</b> treated cells	63.0	44.8	27.9	28.2
Cisplatin treated cells	77.0	38.8	16.9	24.1

P1: Mitochondrial membrane polarized cells, P2: Mitochondrial membrane depolarized cells; Cells treated or untreated with  $IC_{50}$  concentrations of the compounds and cisplatin for 24 h were stained with mitochondrial-selective JC-1 dye and analyzed by flow cytometry

**Table 7.** C6 and A549 cell percentages on G1/S and G2/M cell cycle phases

Compounds	A549 cell line		C6 cell line	
	G1/S phase	G2/M phase	G1/S phase	G2/M phase
Control	62.9	2.85	49.99	7.69
Compound <b>1</b> treated cells	58.05	5.51	49.26	10.91
Compound <b>2</b> treated cells	-	-	51.13	8.42
Compound <b>3</b> treated cells	-	-	67.21	8.59
Compound <b>4</b> treated cells	-	-	56.99	11.48
Compound <b>5</b> treated cells	61.84	4.64	57.71	7.96
Compound <b>8</b> treated cells	73.86	11.87	57.53	10.35
Cisplatin	68.22	6.27	62.57	11.21

Molecular docking simulations were performed to elucidate the possible binding modes of compounds **3** and **8** in the active site of Akt enzyme (PDB code: 3OW4). The docking results of compounds **3** and **8** indicated that  $\pi$ - $\pi$  interactions, H bonds, and salt-bridge formation were responsible for the observed affinity (Figure 8). The nitrophenyl and chlorophenyl groups and acetamido moiety of compound **3** formed  $\pi$ - $\pi$  interactions and H-bonds with Ala230, Lys179, and Asp292 residues, respectively. However, the nitrophenylamino group and acetamido moiety of compound **8** presented  $\pi$ - $\pi$  interactions, H-bonds, and salt-bridge formation with Asp439, Glu234, Arg4, and Lys158 and 276, Phe442, and Ser7 residues, respectively. Nitro substitution on the benzothiazole ring was engaged in  $\pi$ - $\pi$  interactions with Phe161. Docking scores were  $-5.55$  kcal/mol

Table 8. Akt inhibitory effects of compounds 1, 2, 3, 4, 5, 8, and cisplatin

Compound	Inhibition %	
	C6 cell line	A549 cell line
1	38.68±0.75*	43.39±5.86*
2	66.37±2.47**	-
3	92.36±0.70***	91.22±0.16***
4	43.30±32.03*	-
5	68.84±20.82**	66.57±8.75**
8	86.52±0.37***	70.48±13.28***
Cisplatin	23.64±5.09*	54.18±28.50**

Significant differences versus control values, \*p<0.05, \*\*p<0.01, \*\*\*p<0.001. Values are given as mean ± standard deviation

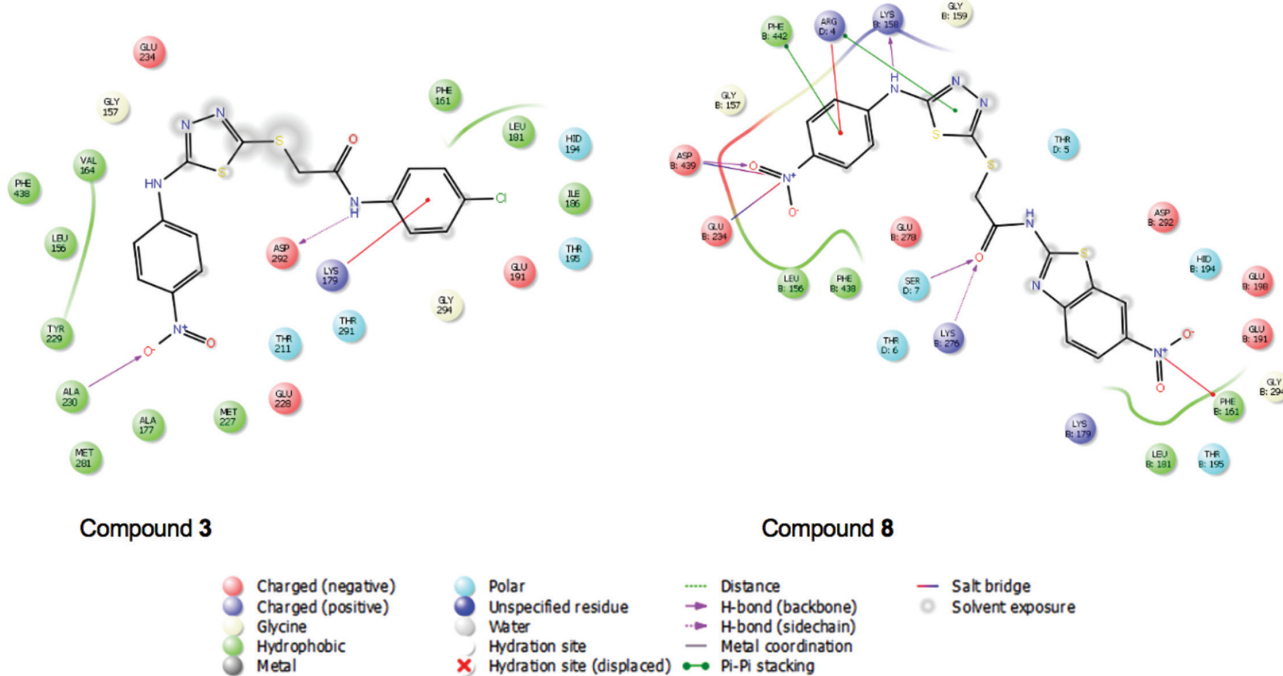
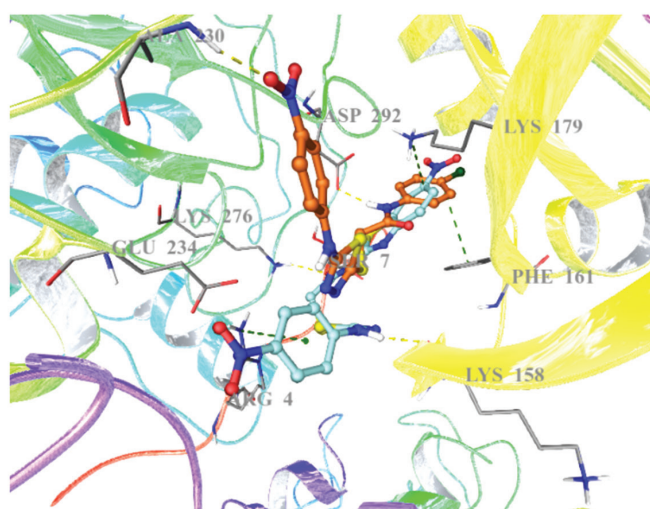


Figure 8. Docking positions and interactions of compounds 3 and 8 in the active site of Akt enzyme, respectively (Ligand custom carbons are colored orange for compound 3 and turquoise for compound 8)

for compound **3** and -5.33 kcal/mol for compound **8** in the active site of Akt enzyme.

## CONCLUSIONS

In the current work, *in vitro* and *in silico* studies were carried out to determine the mechanism of antitumor action of thiadiazole-based anticancer agents. Compounds **3** and **8** induced apoptosis and cell cycle arrest in G1/S and G2/M phases in the C6 cell line through inhibition of Akt activity. Docking studies also confirmed that compounds **3** and **8** demonstrated high affinity to the active site of Akt enzyme by forming  $\pi$ - $\pi$  interactions, hydrogen bonds, and salt-bridge formation with appropriate residues. According to *in vitro* and docking studies, compounds **3** and **8** stand out as promising antiglioma agents for further *in vitro* and *in vivo* studies.

## ACKNOWLEDGEMENTS

We thank Anadolu University Medicinal Plants, Drugs and Scientific Research Center for the equipment used in the cytotoxicity assays.

*Conflict of Interest:* No conflict of interest was declared by the authors.

## REFERENCES

- Nitulescu GM, Margina D, Juzenas P, Peng Q, Olaru OT, Saloustris E, Fenga C, Spandidos D, Libra M, Tsatsakis AM. Akt inhibitors in cancer treatment: The long journey from drug discovery to clinical use (Review). *Int J Oncol*. 2016;48:869-885.
- McDowell KA, Riggins GJ, Gallia GL. Targeting the AKT Pathway in Glioblastoma. *Curr Pharm Des*. 2011;17:2411-2420.
- Morrow JK, Du-Cuny L, Chen L, Meuillet EJ, Mash EA, Powis G, Zhang S. Recent Development of Anticancer Therapeutics Targeting Akt. *Recent Pat Anti-Cancer Drug Discov*. 2011;6:146-159.
- Cassinelli G, Zuco V, Gatti L, Lanzi C, Zaffaroni N, Colombo D, Perego P. Targeting the Akt Kinase to Modulate Survival, Invasiveness and Drug Resistance of Cancer Cells. *Curr Med Chem*. 2013;20:1923-1945.
- Brown JS, Banerji U. Maximising the potential of AKT inhibitors as anti-cancer treatments. *Pharmacol Ther*. 2017;172:101-115.
- Roy NK, Bordoloi D, Monisha J, Padmavathi G, Kotoky J, Golla R, Kunnumakkara AB. Specific Targeting of Akt Kinase Isoforms: Taking the Precise Path for Prevention and Treatment of Cancer. *Curr Drug Targets*. 2017;18:421-435.
- Jain AK, Sharma S, Vaidya A, Ravichandran V, Agrawal RK. 1,3,4-Thiadiazole and Its Derivatives: A Review on Recent Progress in Biological Activities. *Chem Biol Drug Des*. 2013;81:557-576.
- Li Y, Geng J, Liu Y, Yu S, Zhao G. Thiadiazole-A Promising Structure in Medicinal Chemistry. *Chem Med Chem*. 2013;8:27-41.
- Hu Y, Li CY, Wang XM, Yang YH, Zhu HL. 1,3,4-Thiadiazole: Synthesis, Reactions, and Applications in Medicinal, Agricultural, and Materials Chemistry. *Chem Rev*. 2014;114:5572-5610.
- Matysiak J. Biological and Pharmacological Activities of 1,3,4-Thiadiazole Based Compounds. *Mini-Rev Med Chem*. 2015;15:762-775.
- Haider S, Alam MS, Hamid H. 1,3,4-Thiadiazoles: A Potent Multi Targeted Pharmacological Scaffold. *Eur J Med Chem*. 2015;92:156-177.
- Aliabadi A. 1,3,4-Thiadiazole Based Anticancer Agents. *Anti-Cancer Agents Med Chem*. 2016;16:1301-1314.
- Dawood KM, Farghaly TA. Thiadiazole Inhibitors: A Patent Review. *Expert Opin Ther Pat*. 2017;27:477-505.
- Raj V, Rai A, Saha S. Human Cancer Cell Line Based Approach of 1,3,4-thiadiazole and its Fused Ring: A Comprehensive Review. *Anti-Cancer Agents Med Chem*. 2017;17:500-523.
- Chou JY, Lai SY, Pan SL, Jow GM, Chern JW, Guh JH. Investigation of anticancer mechanism of thiadiazole-based compound in human non-small cell lung cancer A549 cells. *Biochem Pharmacol*. 2003;66:115-124.
- Radi M, Crespan E, Botta G, Falchi F, Maga G, Manetti F, Corradi V, Mancini M, Santucci MA, Schenone S, Botta M. Discovery and SAR of 1,3,4-Thiadiazole Derivatives as Potent Abl Tyrosine Kinase Inhibitors and Cytodifferentiating Agents. *Bioorg Med Chem Lett*. 2008;18:1207-1211.
- Sun J, Yang YS, Li W, Zhang YB, Wang XL, Tang JF, Zhu HL. Synthesis, Biological Evaluation and Molecular Docking Studies of 1,3,4-Thiadiazole Derivatives Containing 1,4-Benzodioxan as Potential Antitumor Agents. *Bioorg Med Chem Lett*. 2011;21:6116-6121.
- Juszczak M, Matysiak J, Szeliga M, Pozarowski P, Niewiadomy A, Albrecht J, Rzeski W. 2-Amino-1,3,4-thiadiazole Derivative (FABT) Inhibits the Extracellular Signal-Regulated Kinase Pathway and Induces Cell Cycle Arrest in Human Non-Small Lung Carcinoma Cells. *Bioorg Med Chem Lett*. 2012;22:5466-5469.
- Guan P, Sun F, Hou X, Wang F, Yi F, Xu W, Fang H. Design, Synthesis and Preliminary Bioactivity Studies of 1,3,4-Thiadiazole Hydroxamic Acid Derivatives as Novel Histone Deacetylase Inhibitors. *Bioorg Med Chem*. 2012;20:3865-3872.
- Li YJ, Qin YJ, Makawana JA, Wang YT, Zhang YQ, Zhang YL, Yang MR, Jiang AQ, Zhu HL. Synthesis, Biological Evaluation and Molecular Modeling of 1,3,4-Thiadiazol-2-amide Derivatives as Novel Antitubulin Agents. *Bioorg Med Chem*. 2014;22:4312-4322.
- Hosseinzadeh L, Khorand A, Aliabadi A. Discovery of 2-Phenyl-N-(5-(trifluoromethyl)-1,3,4-thiadiazol-2-yl) acetamide Derivatives as Apoptosis Inducers via the Caspase Pathway with Potential Anticancer Activity. *Arch Pharm Chem (Weinheim)*. 2013;346:812-818.
- Guan P, Wang L, Hou X, Wan Y, Xu W, Tang W, Fang H. Improved Antiproliferative Activity of 1,3,4-Thiadiazole-Containing Histone Deacetylase (HDAC) Inhibitors by Introduction of the Heteroaromatic Surface Recognition Motif. *Bioorg Med Chem*. 2014;22:5766-5775.
- Altıntop MD, Can ÖD, Demir Özkay Ü, Kaplancıklı ZA. Synthesis and Evaluation of New 1,3,4-Thiadiazole Derivatives as Antinociceptive Agents. *Molecules*. 2016;21.
- Mosmann T. Rapid colorimetric assay for cellular growth and survival: application to proliferation and cytotoxicity assays. *J Immunol Methods*. 1983;65:55-63.
- Keiser K, Johnson CC, Tipton DA. Cytotoxicity of mineral trioxide aggregate using human periodontal ligament fibroblasts. *J Endod*. 2000;26:288-291.
- Altıntop MD, Temel HE, Sever B, Akalın Çiftçi G, Kaplancıklı ZA. Synthesis and Evaluation of New Benzodioxole-Based Thiosemicarbazone Derivatives as Potential Antitumor Agents. *Molecules*. 2016;21.

27. Çiftçi GA, Işcan A, Kutlu M. Escin reduces cell proliferation and induces apoptosis on glioma and lung adenocarcinoma cell lines. *Cytotechnology*. 2015;67:893-904.
28. Bencsik JR, Xiao D, Blake JF, Kallan NC, Mitchell IS, Spencer KL, Xu R, Gloor SL, Martinson M, Risom T, Woessner RD, Dizon F, Wu WI, Vigers GP, Brandhuber BJ, Skelton NJ, Prior WW, Murray LJ. Discovery of dihydrothieno- and dihydrofuropyrimidines as potent pan Akt inhibitors. *Bioorg Med Chem Lett*. 2010;20:7037-7041.
29. Porter AG, Jänicke RU. Emerging roles of caspase-3 in apoptosis. *Cell Death Differ*. 1999;6:99-104.
30. Williams GH, Stoeber K. The cell cycle and cancer. *J Pathol*. 2012;226:352-364.





# Preparation and Biopharmaceutical Evaluation of Novel Polymeric Nanoparticles Containing Etoposide for Targeting Cancer Cells

## Kanser Hücrelerini Hedefleyen Etopozit İçeren Yeni Polimerik Nanopartiküllerin Hazırlanması ve Biyofarmasötik Değerlendirmesi

© Ayyappan THIYAGARAJAN<sup>1,2\*</sup>, © Shanmugam SARAVANABHAVAN<sup>1</sup>, © Vetrichelvan THANGARASU<sup>3</sup>

<sup>1</sup>Adhiparasakthi College of Pharmacy, Department of Pharmaceutics, Tamil Nadu, India

<sup>2</sup>Research Scholar, The Tamil Nadu Dr. M.G.R. Medical University, Chennai, India

<sup>3</sup>Adhiparasakthi College of Pharmacy, Department of Pharmaceutical Analysis, Tamil Nadu, India

### ABSTRACT

**Objectives:** Polymeric nanoparticles are a promising novel drug delivery system and have advantages in cancer therapy. Etoposide is an anticancer agent that is used in the treatment of a variety of malignancies. The aim of the present study was to prepare and evaluate novel polymeric nanoparticles containing etoposide.

**Materials and Methods:** A 3<sup>2</sup> full factorial design was used to study the effect of Eudragit EPO and Pluronic F-68 on the characterization of nanoparticle suspensions. The polymeric nanoparticles were prepared by nanoprecipitation technique. The prepared nanoparticles were evaluated by percentage yield, drug polymer compatibility using fourier transform infrared (FTIR) spectroscopy and differential scanning calorimetric (DSC) analysis, drug content, entrapment efficiency, zeta potential, particle size, scanning electron microscopy, X-ray diffraction, *in vitro* drug release studies, kinetic modeling, stability studies, and *in vivo* animal studies. Response surface plots were studied, which were generated using PCP dissolution software.

**Results:** Scanning electron microscopic studies confirmed their porous structure with a number of nanochannels. The FTIR spectra showed the stable character of etoposide in a mixture of polymers and revealed the absence of drug-polymer interactions. The DSC study revealed that the drug was involved in complexation with nanoparticles. The average particle size of etoposide nanoparticles was in the range of 114.4 nm to 136.7 nm. The zeta potential values were attained to ensure good stability of nanosuspensions. *In vitro* release of the drug from nanoparticles follows the Peppas model and showed controlled release behavior for a period of 24 h. The optimized nanoparticles were subjected to stability studies at 4°C in a refrigerator and the most suitable temperature for storage of etoposide nanoparticles found. The average targeting efficiency of drug-loaded nanoparticles was 41.88±0.030% of the injected dose in the liver, 25.66±0.320% in the spleen 13.82±0.090% in the lungs, 4.52±0.300% in the kidney, and 4.18±0.490% in the brain.

**Conclusion:** Etoposide loaded nanoparticles was found to be effective in sustained release.

**Key words:** Etoposide, Eudragit EPO, pluronic F-68, 3<sup>2</sup> full factorial design, nanoparticles

### ÖZ

**Amaç:** Polimerik nanopartiküller kanser tedavisinde avantajlı ve gelecek vaat eden yeni ilaç salım sistemidir. Etopozid, çeşitli malignitelerin tedavisinde kullanılan bir antikanser ajanıdır. Bu çalışmanın amacı, etopozit içeren yeni polimerik nanopartiküllerin hazırlanması ve değerlendirilmesidir.

**Gereç ve Yöntemler:** Eudragit EPO ve Pluronic F-68'in nanopartikül süspansiyonunun karakterizasyonu üzerindeki etkisini incelemek için 3<sup>2</sup> tam faktöriyel tasarım kullanılmıştır. Polimerik nanopartiküller nano presipitasyon tekniği ile hazırlanmıştır. Hazırlanan nanopartiküller, yüzde verim, fourier dönüşümü kızılötesi (FTIR) spektroskopisi ve diferansiyel taramalı kalorimetrik (DSC) analizi kullanılarak ilaç polimer uyumluluğu, etkin madde içeriği, yükleme kapasitesi, zeta potansiyeli, partikül boyutu, taramalı elektron mikroskobu, X-ışını difraksiyon, *in vitro* etkin madde salım

\*Correspondence: E-mail: tayyaps@yahoo.co.in, Phone: 919894567170

Received: 08.12.2017, Accepted: 25.01.2018

©Turk J Pharm Sci, Published by Galenos Publishing House.

çalışmaları, kinetik modelleme, stabilite çalışmaları ve *in vivo* hayvan çalışması ile değerlendirilmiştir. PCP çözünme yazılımı kullanılarak oluşturulan tepki yüzey grafikleri incelenmiştir.

**Bulgular:** Taramalı elektron mikroskopisi çalışmaları çok sayıda nano-kanal içeren gözenekli yapılarını doğrulamıştır. FTIR spektrumları, polimer karışımında etopozitin stabil olduğunu ve ilaç polimer etkileşimlerinin olmadığını ortaya çıkartmıştır. DSC çalışması, etkin maddenin komplikasyon ile nanopartiküllere yüklendiğini ortaya koymuştur. Etopozid nanopartiküllerin ortalama partikül büyüklüğünün 114.4 nm ile 136.7 nm arasında olduğu bulunmuştur. Zeta potansiyel değerlerinden elde edilen sonuç nanosüspansiyonların iyi bir stabilitede olmasını sağlamıştır. Nano-partiküllerden etkin maddenin *in vitro* salımı Peppas'a uyumlu olup, 24 saatlik bir süre boyunca kontrollü salım göstermiştir. Optimiz edilmiş nanopartiküller, 4°C'de buzdolabında stabilite çalışmalarına tabi tutulmuş ve Etopozid nanopartiküllerinin depolanması için en uygun sıcaklık olarak bulunmuştur. Etkin madde yüklü nanopartiküllerin ortalama hedefleme etkinliği, karaciğerde enjekte edilen dozun %41.88±0.030'u, dalakta %25.66±0.320'si, akciğerlerde %13.82±0.090'ı, böbreklerde %4.52±0.300'ü ve beyinde %4.18±0.490'ı olarak bulunmuştur.

**Sonuç:** Etopozit yüklü nanopartiküllerin sürekli salımda etkili olduğu sonucuna varılmıştır.

**Anahtar kelimeler:** Etopozit, Eudragit EPO, pluronic F-68, 32 tam faktöriyel tasarım, nanopartiküller

## INTRODUCTION

Cancer is a major public health problem around the world. There were 14.1 million new cancer cases and 8.2 million cancer deaths in 2012 worldwide. If these rates do not change, the global cancer burden is expected to nearly double to 21.4 million cases and 13.5 million deaths by 2030. Breast cancer is the most common cancer among women worldwide, with nearly 1.7 million new cases diagnosed in 2012 (the second most common cancer). This represents about 12% of all new cancer cases and 25% of all cancers in women. Cancer is the second leading cause of death worldwide, and was responsible for 8.8 million deaths in 2015. According to the WHO, nearly 1 in 6 deaths is due to cancer.

A typical example of topoisomerase inhibitors is etoposide and it is a first-line chemotherapeutic agent used in the treatment of many types of cancer. The mechanism of action of etoposide is by forming a ternary complex with topoisomerase II and DNA, causing DNA breaks and cell death.<sup>1</sup> However, there are many side effects related to the drug,<sup>2-4</sup> and the administration of etoposide is rate limited by its low solubility in aqueous solutions.<sup>5,6</sup> Therefore, finding an effective approach to facilitate the transport of drugs and to improve the bioavailability of therapeutics is necessary.

The drug candidate etoposide has variable oral bioavailability ranging from 24% to 74% and has a terminal half-life of 1.5 h by intravenous route and 0.44 h by oral route. Conventional oral therapy has the drawback of low bioavailability and parenteral therapy causes inconvenience and pain to the patients as it has to be given through a continuous IV infusion over 24-34 h.

Hence, the aim of the present study was to prepare and evaluate formulations of Eudragit EPO-based nanoparticles. A nanoparticle suspension was prepared by nanoprecipitation technique using Eudragit EPO. Eudragit EPO is a cationic nonbiodegradable synthetic polymer that is used for the design of controlled drug delivery systems. Moreover, 3<sup>2</sup> factorial designs are widely used to study the effect of Eudragit EPO and Pluronic F-68 on the characterization of nanoparticle suspensions. The optimized formulation was subjected to lyophilization. The prepared nanoparticles were characterized with respect to particle size and surface morphology, surface charge-zeta potential, drug content, entrapment efficiency, *in vitro* drug release studies, kinetic modeling, stability studies, and animal study like biodistribution studies.

## MATERIALS AND METHODS

### Materials

Etoposide was a gift sample from Biocon Limited, Bangalore, India; Eudragit® EPO and HPMC K-15 were gifts from Cipla Pharmaceuticals, Mumbai, India. Pluronic® F-68 was gifted by Alembic Pharmaceuticals, Mumbai, India. Synthetic cellulose membrane (mol. cut-off value 12,000) was procured from Himedia Labs, Mumbai, India. All other reagents and chemicals used in this study were of analytical grade.

### Solubility study

The solubility profile of etoposide was established by different solvent systems such as methanol and purified water as per the standard procedure.

### Preparation of Eudragit EPO-based nanoparticle suspension

Nanoparticle suspensions were prepared by nanoprecipitation. First 50 mg of the drug and a specific amount of Eudragit®-EPO were dissolved in 15 mL of methanol. The organic solution was quickly injected into 40 mL of aqueous solution containing Pluronic® F-68 under stirring at 2000 rpm. Stirring was continued for 2 h at 40°C for the evaporation of methanol. The volume was adjusted up to 40 mL with aqueous solution of 200 mg of HPMC K-15 to obtain a nanoparticle suspension. The optimized nanoparticle suspension was lyophilized at -42°C for 72 h and also redispersed in water to get an aqueous nanoparticle suspension.<sup>7</sup> Blank nanoparticles were prepared under the same conditions without the drug.

### Formulation design by 3<sup>2</sup> factorial design techniques

Prior knowledge and understanding of the process and the variable under investigation led to preliminary experiments. Based on the preliminary data, a 3<sup>2</sup> factorial design was used to optimize the amount of Eudragit®-EPO (X1) and Pluronic® F-68 (X2) and identify the independent variable affecting the drug content and the percentage drug encapsulation efficiency (dependent variable). The response surfaces of the obtained results were plotted. The coded and the actual values of the experimental design are given in Table 1. The data obtained from various batches for drug content and entrapment efficiency were subjected to multiple regression analysis using PCP dissolution software, and the equation fitted was;

$$\text{Response } Y = \beta_0 + \beta_1 X_1 + \beta_2 X_2 + \beta_{11} X_1^2 + \beta_{22} X_2^2 + \beta_{12} X_1 X_2 \dots (1)$$

Where  $y$  is the measured response,  $X$  is the level of factors, and  $\beta$  is the coefficient computed from the responses of the formulations (quadratic form).

Physical mixtures of the drugs, Eudragit EPO, Pluronic F-68, and HPMC K-15, were prepared by dry blending using the same ratios as used for the preparation of the optimized batch of nanoparticle suspension.<sup>7</sup>

### Characterization of nanoparticles

#### Practical yield

Percentage practical yield<sup>8</sup> is calculated to know about the efficiency of the method. Thus it helps in selection of an appropriate method of production. Practical yield was calculated as the weight of nanoparticles recovered from each and every batch in relation to the sum of the starting material. The percentage yield of prepared nanoparticles was calculated by practical yield/theoretical yield  $\times$  100.

#### Compatibility studies

##### a) Fourier transform infrared spectroscopy

The fourier transform infrared (FTIR) spectra of the drug<sup>9</sup> and lyophilized nanoparticles were determined using a Shimadzu FTIR-801 spectrophotometer. The pellets were prepared by gently mixing a 10 mg sample with 200 mg of potassium bromide at high compaction pressure. Baseline correction was performed using dried potassium bromide and the spectra of a dried mixture of drug and polymers were recorded. The prepared pellets were scanned at a resolution from 4000  $\text{cm}^{-1}$  to 400  $\text{cm}^{-1}$ .

##### b) Differential scanning calorimetry

Differential scanning calorimetry (DSC) studies were performed using a differential scanning calorimeter (Shimadzu W70 thermal analyzer) to determine the thermal behavior of the drug and lyophilized nanoparticles. Then 5 mg samples were weighed into aluminum pans and heated in these hermetically sealed pans in the temperature range of 100-300°C at a heating rate of 10°C/min under nitrogen flow of 30 mL/min.<sup>10</sup>

#### Estimation of drug content

Accurately weighed amounts equivalent to 10 mg of each batch of polymeric nanoparticles were dissolved in methanol. The solution was filtered using a 0.45  $\mu\text{m}$  Millipore filter as per the reported method. The drug content was estimated using a UV-visible spectrophotometer (Shimadzu UV-1700) at 286 nm against a blank solvent system containing the same concentration of drug in the formulation.<sup>11</sup>

$$\% \text{ drug content} = \frac{\text{Amount of drug found}}{\text{Label claim}} \times 100$$

#### Estimation of entrapment efficiency

The entrapment efficiency of the prepared formulation was determined by measuring the concentration of free drug in the dispersion medium. The entrapped drug was determined by adding 1 mL of nanosuspension to 9 mL of methanol in order to dissolve the entrapped drug. The nanoparticle suspension

needed to be centrifuged for 2 h at 14,000 rpm. The supernatant liquid was separated and filtered through a 0.45  $\mu\text{m}$  Millipore filter. The filtrate was diluted with the solvent system and measured spectrophotometrically (Shimadzu UV-1700). Entrapment efficiency was calculated using the following equation:<sup>12</sup>

$$\% \text{ drug entrapment efficiency} = \frac{W \text{ initial drug} - W \text{ free drug}}{W \text{ initial drug}} \times 100$$

#### Particle size analysis

Particle size analysis of nanoparticles was performed by photon correlation spectroscopy. This technique yields the mean particle diameter and particle size distribution.<sup>13</sup> Lyophilized nanoparticles were analyzed using a Mastersizer 2000 (Malvern Instruments, Malvern, UK).

#### Scanning electron microscopy analysis

The shape and surface morphology of nanoparticles was studied using scanning electron microscopy (SEM). SEM analysis was used to determine particle shape, surface topography, and texture and to examine the morphology of the fractured structure. A small volume of nanoparticle suspension was mounted on metal stubs using double-sided tape and coated with gold under a vacuum. The stub was visualized under a scanning electron microscope.<sup>14</sup>

#### Zeta potential measurement

The surface of particles in suspension develops a charge due to adsorption of ions or ionization of surface groups and the charge is correspondingly dependent on both the surface chemistry and environment of the particles. The zeta potential was determined by zeta potentiometer. A sample was placed into the cell; an electrode inserted was placed under the microscope and connected to the zeta meter. The electrode was energized and the colloids were watched to move across a grid in the microscope's eye piece. A colloid is tracked by simply pressing the track button and holding it down while the colloid traverses the grid. When the track button is released, the zeta meter instantly calculates and displays the colloid's zeta potential (Zetasizer, Malvern, UK).<sup>13</sup>

#### X-ray diffractometry analysis

The X-ray diffraction pattern of the drug and lyophilized nanoparticles was recorded using a Philips X-ray diffractometer with copper target. The conditions were as follows: voltage 30 kV; current 30 mA; scanning speed -1°/min; temperature of acquisition: room temperature; detector: scintillation counter detector; sample holder: nonrotating holder.<sup>7</sup>

#### In vitro drug release study

The *in vitro* drug release of the drug, physical mixture, and lyophilized nanoparticles was determined using the dialysis membrane method.<sup>15</sup> The formulation equivalent to 50 mg of drug was poured into dialysis bags (with a cut-off of 12,000 Da, Sigma). The dialysis bag was suspended in a beaker containing 100 mL of phosphate buffer at pH 7.4 on a magnetic stirrer at 100 rpm, with temperature adjusted to 37 $\pm$ 0.5°C at

a selected time interval. A 5 mL sample was removed and replaced with fresh medium. The sample was filtered through a 0.45 µm Millipore filter. The samples were analyzed for drug release by measuring absorbance at 286 nm using a UV-visible spectrophotometer (Shimadzu UV-1700). The rate of etoposide release was obtained using the standard curve.

#### *Kinetics of in vitro drug release*

PCP dissolution software was used to study the mechanism and kinetics of drug release from etoposide nanoparticles. The data obtained from the *in vitro* release study were entered into PCP dissolution software to study the various kinetic equations like zero order (% cumulative drug release vs time), first order (log% cumulative drug remaining vs time), and Higuchi matrix (% cumulative drug release vs square root of time). In order to define a model that will represent a better fit for the formulation, the drug release data were further analyzed by the Peppas equation. The value of *n* indicates a measure of the primary mechanism of drug release. *R*<sup>2</sup> values were calculated for the linear curves obtained by regression analysis.

#### *Statistical analysis*

Prior knowledge and understanding of the process and the variable under investigation led to preliminary experiments. Based on the preliminary data, the 3<sup>2</sup> factorial design was adopted to optimize the amount of Eudragit®-EPO (X1) and Pluronic® F-68 (X2) and identify the independent variable affecting the drug content and the percentage drug encapsulation efficiency (dependent variable). The response surfaces of the obtained results were plotted. The values obtained from various batches for drug content and encapsulation efficiency were subjected to multiple regression analysis using PCP dissolution software and the equation fitted was;

$$Y: \beta_0 + \beta_1 X_1 + \beta_2 X_2 + \beta_{11} X_{12} + \beta_{22} X_2 + \beta_{12} X_1 X_2 \dots 1$$

Where Y is the measured response, X is the level of factors, and β is the coefficient computed from the responses of the formulations.

#### *Stability studies*

The stability studies of the optimized nanoparticles were evaluated<sup>16</sup> by storing the formulation at 4±1°C in a refrigerator as per ICH guidelines. The nanoparticles were stored in screw capped amber-glass bottles. Physical instability like change in appearance and settling behavior was also observed. The sample was withdrawn and analyzed for its drug content, drug entrapment efficiency, and *in vitro* drug release profile.

#### *In vivo drug targeting studies*

The experimental protocol was approved by the institutional Animal Ethical Committee (APCP/IAEC/409/01) prior to the start of the animal studies. The experiments were performed in accordance with the current guidelines of the CPCSEA.

Healthy rats weighing 200–250 g were selected. A constant day and night cycle was maintained and they were fasted for 12 h. The animals are divided into 3 groups, each containing 6 rats.

Group I rats were treated as controls (received orally 0.5% CMC dispersion only);

Group II rats received 9 mg/kg etoposide given orally after redispersal in 0.5% CMC dispersion;

Group III rats received nanoparticles equivalent to 9 mg/kg of etoposide given orally after redispersal in 0.5% CMC dispersion; optimized formulation (F6) was selected for the study.

After 24 h the rats were sacrificed and their liver, lungs, spleen, kidney, heart, and brain were isolated. Individual organs of each rat were homogenized separately using a tissue homogenizer. The tissue homogenate was made using methanol, and 1.2 mL of tert-butyl methyl ether was mixed with a 0.1 mL aliquot of the tissue sample in a 2.0 mL polypropylene microtube. Then the homogenate was centrifuged at 15,000 rpm for 30 min. The supernatant liquid was collected and filtered through 0.22 µm filters and samples were analyzed by HPLC system.

## RESULTS AND DISCUSSION

Spectral data of etoposide sample and standard etoposide confirmed the identity of the compound as etoposide. The solubility of etoposide in 10 mg/10 mL solvent was tested and it revealed that it was freely soluble in methanol and poorly soluble in water (less than mg/mL) at 37°C. Nanoprecipitation technology was selected for the production of submicron particles complying with the low aqueous solubility of etoposide. On the basis of drug solubility and miscibility in the aqueous phase, methanol was selected as the solvent. The rapid diffusion of methanol from dispersed droplets into the aqueous phase with subsequent evaporation leads to fast precipitation of dissolved drug and polymer in the form of nanoparticles.<sup>17</sup>

The drug content and encapsulation efficiency of the nanoparticle suspensions were in the range of 61% to 89% and 48% to 94%, respectively (Tables 1 and 1a), which were mainly influenced by polymer concentration. A curvilinear relation was observed between the drug content and encapsulation efficiency with Eudragit® EPO concentration. It can be explained on the basis of the lipophilic–lipophilic interaction between etoposide and Eudragit® EPO. Consequently, with an increase in the Eudragit® EPO amount, etoposide gets preferentially dispersed in the internal organic phase.<sup>18</sup> Pluronic® F-68 also displayed a similar trend and an increase in encapsulation efficiency, which can be due to the formation of an interpenetrated network chain between the hydrophobic portions of Pluronic® F-68 with Eudragit® EPO during precipitation (synergistic effect evidenced from a positive coefficient value for the X1X2 interaction term).<sup>19</sup> It is confirmed by the positive regression values of the X1X2 term as shown in Table 1a. Particle size also showed similar effects. The influence of polymer–polymer interaction as compared to polymer–pluronic interaction signifies the stabilizing effect of the latter by minimizing the dispersion and distribution of drug outside the matrix. In this research, two responses were evaluated, and each response was plotted in relation to the modified factor. Both the experimental design and the linearity and response surface plots for drug content and encapsulation efficiency are shown in Figures 1a and 1b.

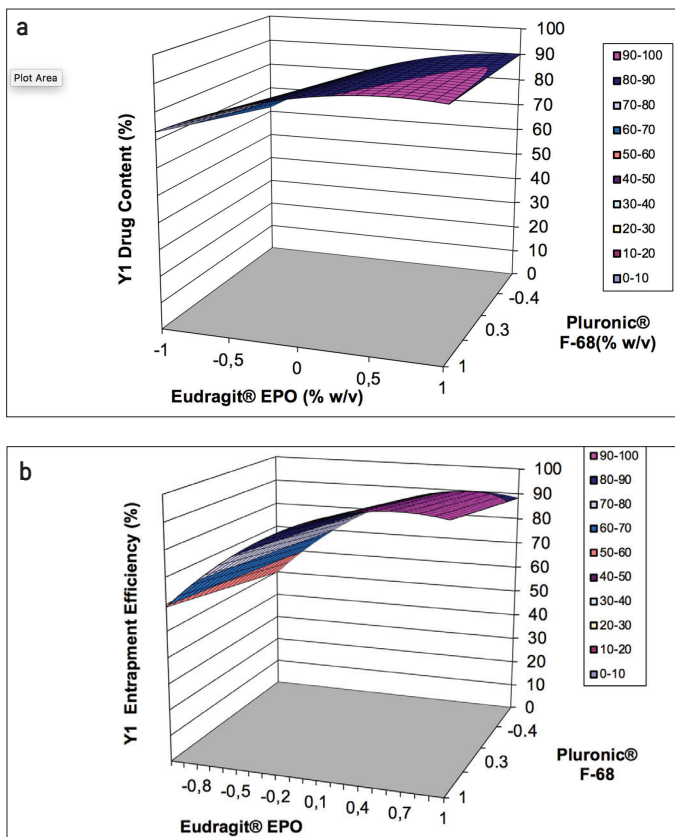


Figure 1. Response surface plot showing the influence of polymer surfactant ratio on drug content (a), Response surface plot showing the influence of polymer surfactant ratio on encapsulation efficiency (b)

As shown in Table 2, particle size of the nanoparticle suspension was in the range of 114 to 136 nm, which was almost smaller than the etoposide (1120 nm). An increase in particle size of the nanoparticle suspension with a decrease in polydispersity index was observed with an increase in polymer content. The smaller particle size obtained at low polymer content may be due to high distribution efficiency of the internal polymer-solvent phase into the external phase.<sup>20-22</sup> An increase in the viscosity of the internal phase with increased amount of polymer also provides resistance for mass transfer and in turn diffusion of polymer solvent phase into the external phase, leading to particle enlargement. The zeta potential values of the nanoparticle suspension are presented in Table 2. All formulations exhibited strongly positive zeta potential values due to polycationic Eudragit® EPO comprising various ammonium groups. The increased zeta potential values in initial batches may be attributed to Eudragit® EPO available at the surface of the particles due to high viscosity of the external aqueous phase. The subsequent decline in values of zeta potential is an inverse function of particle size.<sup>23</sup> As solid state pharmaceuticals have many advantages over liquid formulations, mainly improved physicochemical stability and less susceptibility to microbial contamination, attempts were made to obtain dry powder nanoparticle suspensions by lyophilization. Based on the results of the factorial design batch F6 having drug content of 88.36±0.075%, encapsulation efficiency of 94.28±0.198%, and zeta potential of 26.2±0.208 mV was further processed to obtain dry powder. When it was compared with the blank batch no significant variations in particle size or zeta potential were observed (Table 2). The lyophilized nanoparticles (F6)

Table 1. Coded levels and actual values of the variables along with the measured responses of the 3<sup>2</sup> factorial design

Batches	Coded levels		Concentration of Eudragit® EPO (% w/v)	Concentration of Pluronic® F-68 (% w/v)	Drug content# (%)	Entrapment efficiency# (%)
Etoposide	X1	X2	-	-	-	-
F1	-1	-1	0.3	0.4	61.86±0.130	48.96±0.135
F2	-1	0	0.3	0.5	67.43±0.075	54.40±0.150
F3	-1	+1	0.3	0.6	72.87±0.015	59.97±0.198
F4	0	-1	0.45	0.4	82.21±0.075	81.82±0.274
F5	0	0	0.45	0.5	86.25±0.075	88.23±0.276
F6	0	+1	0.45	0.6	88.36±0.075	94.28±0.198
F7	+1	-1	0.6	0.4	89.90±0.080	89.95±0.202
F8	+1	0	0.6	0.5	87.66±0.130	94.42±0.430
F9	+1	+1	0.6	0.6	89.5±0.130	94.10±0.135

#All the determinations were performed in triplicate and values were expressed as mean ± standard deviation, n=3; X1: Polymer Eudragit® EPO; X2: Stabilizer Pluronic® F-68

Table 1a. Prediction of regression value

Variable	Constant	X <sub>1</sub>	X <sub>2</sub>	X <sub>1</sub> X <sub>2</sub>	X <sub>1</sub> X <sub>1</sub>	F	R <sup>2</sup>
Drug content (R1)	85.6067	11.2727	2.7933	2.7364	6.9473	721.12	0.9986
Entrapment efficiency (R2)	88.1100	19.1767	4.6033	-	14.4633	194.77	0.9915

have an average particle size of  $131.4 \pm 0.057$  nm. The almost twofold increase in size of particles could be due to changes in the internal structure of the particles, originated during the freeze drying process caused by the formation of ice crystals in the water phase, or, more likely, to particle aggregation during freeze drying, resulting in poor redispersion.<sup>24</sup> Figures 2, 3 and 4 show the DSC thermogram of etoposide and lyophilized nanoparticles. Etoposide exhibits a sharp melting endotherm at  $266.9^\circ\text{C}$  ( $78.39$  J/g), whereas the thermogram of the lyophilized nanoparticle suspension displays a sharp endotherm at  $262.7^\circ\text{C}$  ( $60.38$  J/g). It explains the monotectic behavior of the system, where the drug gets completely dissolved below its melting temperature in a molten mass of the excipients. Similar behavior was also reported for the nifedipine with Pluronic® F-68, Gelucire, and paracetamol with PEG.<sup>25,26</sup> The PXRD diffraction patterns, as shown in Figure 4, reveal characteristic peaks at 4.2, 9.46, 10.22, 13.18, 16.15, 17.08, 17.67, 19.26, 19.89, 22.14, 23.03, 23.67, 24.17, and 26.78, which can be inferred to show a high crystalline structure. The complete disappearance of peaks in lyophilized powder may be due to the formation of an amorphous complex while undergoing the nanoprecipitation with an intermolecular interaction occurring within the matrix. Peaks of reduced intensity were observed in the physical mixture. The intermolecular interaction in the nanoparticle suspension was established by FTIR as shown in Figures 5 and 6. Etoposide exhibits the characteristic intensities of a C=O stretching absorption band at  $1764\text{ cm}^{-1}$  and the O-H stretch at  $3452\text{ cm}^{-1}$ . However, FTIR spectra of the lyophilized powder showed a C=O stretching absorption band of etoposide and O-H stretching. These result suggested no interaction between drug and polymer. The surface topography of the nanoparticle suspension was studied using SEM, which displayed uniform sized spherical nanoparticles with size range correlating with particle size studies. A SEM photograph of nanoparticles is

**Table 2. Zeta potential, particle size, and polydispersity of polymeric nanoparticles**

Batches	Zeta potential* (mV)	Mean particle size* (nm)	Polydispersity*
Etoposide	-	$1120 \pm 0.200$	$1.547 \pm 0.005$
F1	$18.30 \pm 0.135$	$114.4 \pm 0.305$	$0.734 \pm 0.002$
F2	$19.46 \pm 0.305$	$125.5 \pm 0.862$	$0.715 \pm 0.001$
F3	$20.2 \pm 0.115$	$134.6 \pm 0.200$	$0.707 \pm 0.002$
F4	$24.6 \pm 0.200$	$128.5 \pm 0.100$	$0.564 \pm 0.005$
F5	$25.6 \pm 0.200$	$129.3 \pm 0.100$	$0.548 \pm 0.001$
F6	$26.2 \pm 0.208$	$131.4 \pm 0.057$	$0.522 \pm 0.001$
F7	$22.3 \pm 0.152$	$134.4 \pm 0.115$	$0.693 \pm 0.001$
F8	$23.6 \pm 0.200$	$135.3 \pm 0.152$	$0.684 \pm 0.002$
F9	$24.60 \pm 0.152$	$136.7 \pm 0.100$	$0.353 \pm 0.005$
Blank (F6)	$26.50 \pm 0.208$	$136.3 \pm 0.208$	$0.526 \pm 0.002$

\*All the determinations were performed in triplicate and values were expressed as mean  $\pm$  standard deviation, n=3

shown in Figure 7. The *in vitro* drug release profiles of etoposide and lyophilized nanoparticles in phosphate pH 7.4 buffer are shown in Figures 8, 9, and 10. The formulated nanoparticles showed the most favorable release within 24 h. Only  $14.09 \pm 0.19\%$  drug release was obtained from the raw material of etoposide. At 24 h, the drug release was  $79.09 \pm 0.58\%$ ,  $81.34 \pm 0.37\%$ ,  $82.81 \pm 0.63\%$ ,  $94.22 \pm 0.56\%$ ,  $96.02 \pm 0.31\%$ ,  $99.22 \pm 0.50\%$ ,  $86.02 \pm 0.18\%$ ,  $89.90 \pm 0.33\%$ , and  $91.93 \pm 0.28\%$  for F1, F2, F3, F4, F5, F6, F7, F8, and F9, respectively. This followed a steady state drug release pattern.

These above data showed that formulation F6 released the drug most at the end of 24 h. The release rate of Etoposide decreased with increasing concentration of Eudragit. However, an increase in the rate of release was found with increasing amount of Pluronic.

As compared with pure drug, lyophilized nanoparticles showed a significant increase in dissolution rate with maximum and complete drug release with F6. However, lyophilization retarded the drug release. The retardation of drug release of lyophilized formulation is probability due to aggregation of the particles in lyophilization, but still particles exhibited size below  $1\text{ }\mu\text{m}$ . The kinetics of *in vitro* drug release was determined by applying the drug release data to various kinetic models such as zero order, first order, Higuchi, and Korsmeyer–Peppas. The results obtained are shown in Table 3.

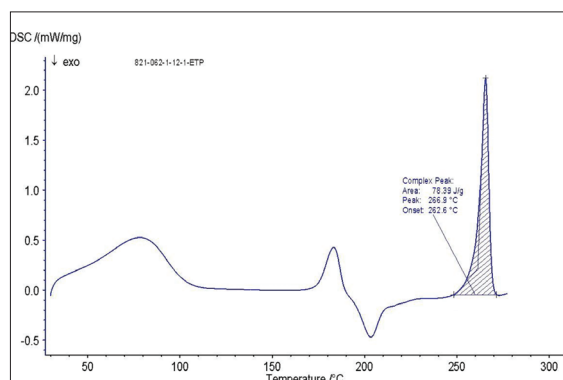


**Figure 2.** DSC thermogram of etoposide

DSC: Differential scanning calorimetric

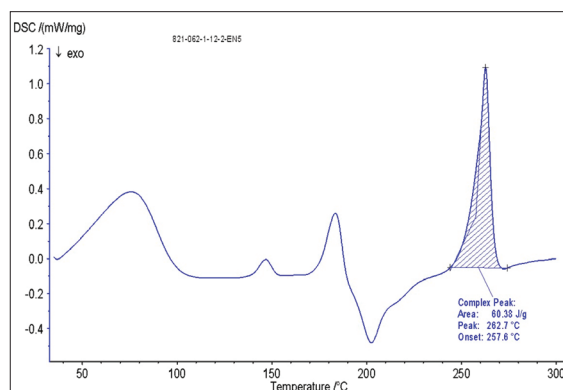


**Figure 3.** DSC thermogram of etoposide nanoparticles

The optimized nanoparticle suspension was subjected to a stability study at 4±1°C. During that stability study, no significant difference in drug content (87.69±0.043%),

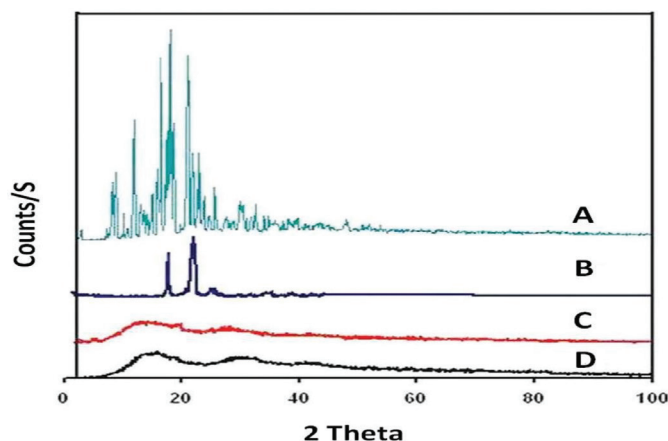


Figure 4. XRD spectra of (A) etoposide, (B) physical mixture of etoposide and polymers, (C) polymeric nanoparticles (before lyophilization), and (D) etoposide loaded polymeric nanoparticles (after lyophilization)

XRD: X-ray diffraction

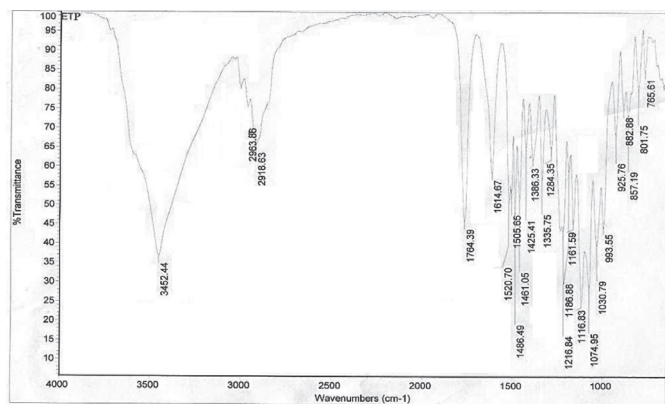


Figure 5. FTIR spectrum of etoposide

FTIR: Fourier transform infrared

encapsulation efficiency (93.32±0.015%), or *in vitro* drug release (97.92±0.037%) was observed over the period of 1 year. The stability results are shown in Table 4. There was no significant difference in physical instability like change in appearance and settling behavior was also observed. The average targeting efficiency of drug loaded nanoparticles was 41.88±0.030% of the injected dose in the liver, 25.66±0.320% in the spleen, 13.82±0.090% in the lungs, 4.52±0.300% in the kidney, and 4.18±0.490% in the brain as compared to the concentration of pure drug of 28.47±0.041% in the liver, 16.40±0.080% in the spleen, 13.79±0.195% in the lungs, 11.83±0.065% in the kidney,

Table 4. Stability testing parameters of optimized nanoparticles (F6)

Evaluation parameters	Fresh formulation	Storage condition at 4±1°C (end of 1 year)
% Drug content	88.36±0.075	87.69±0.043
% Entrapment efficiency	94.28±0.190	93.03±0.020
Percentage drug release	99.22±0.50	97.92±0.037

\*Results are expressed as mean ± standard deviation (n=3)

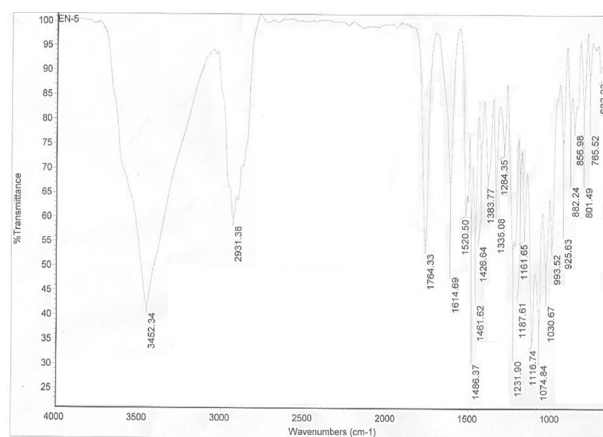
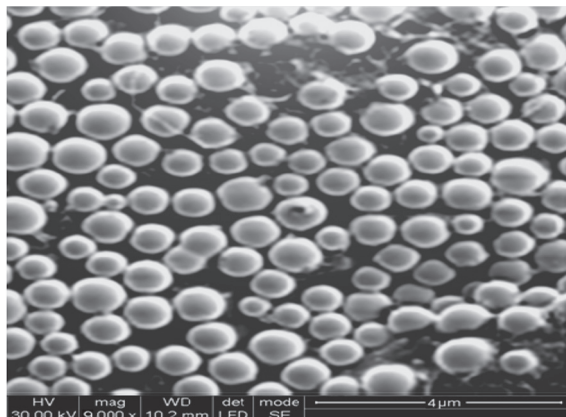


Figure 6. FTIR spectrum of etoposide nanoparticles

Table 3. Kinetics of *in vitro* drug release profile for all etoposide nanoparticles

Formulation code	Zero order R <sup>2</sup> value	First order R <sup>2</sup> value	Higuchi's R <sup>2</sup> value	Korsmeyer Peppas		Best fit models
				R <sup>2</sup> value	n value	
F1	0.9043	0.9940	0.9880	0.9943	0.6513	Peppas
F2	0.8976	0.9946	0.9898	0.9950	0.6303	Peppas
F3	0.8846	0.9946	0.9926	0.9955	0.6061	Peppas
F4	0.9058	0.9630	0.9914	0.9963	0.5978	Peppas
F5	0.9013	0.9493	0.9923	0.9958	0.5848	Peppas
F6	0.8895	0.8677	0.9940	0.9964	0.5617	Peppas
F7	0.8769	0.9935	0.9938	0.9946	0.5873	Peppas
F8	0.8789	0.9875	0.9938	0.9956	0.5982	Peppas
F9	0.8787	0.9803	0.9938	0.9946	0.5959	Peppas

\*Results are expressed as mean ± standard deviation (n=3)



**Figure 7.** SEM photograph of the etoposide nanoparticle suspension  
SEM: Scanning electron microscopy

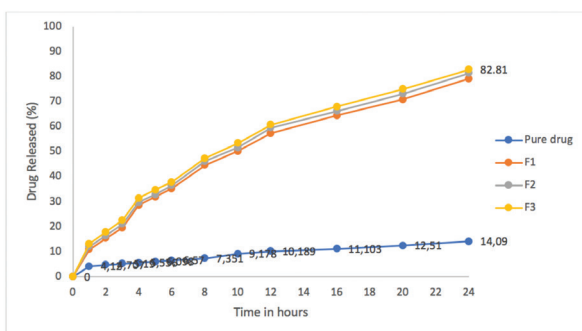


**Figure 8.** Comparative *in vitro* drug release of the etoposide nanoparticles (F1, F2, F3). All the values expressed as mean ± standard deviation, n=3

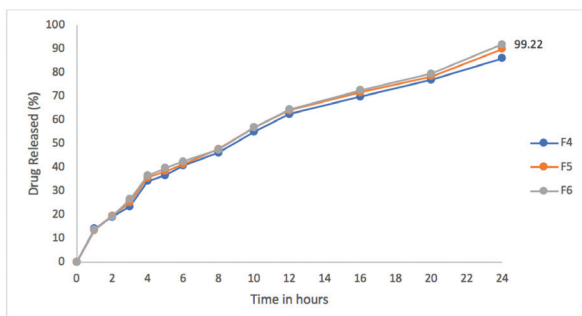


**Figure 9.** Comparative *in vitro* drug release of the etoposide nanoparticles (F4, F5, F6). All the values expressed as mean ± standard deviation, n=3

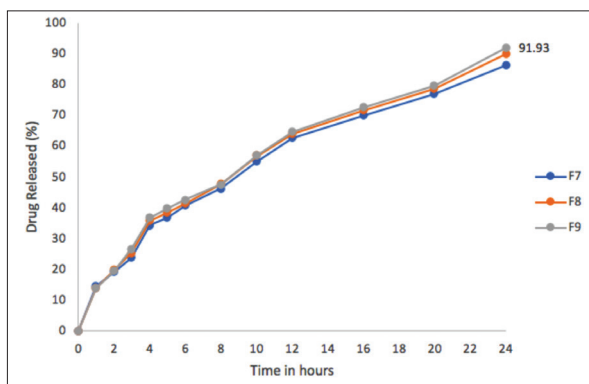


**Figure 10.** Comparative *in vitro* drug release of the etoposide nanoparticles (F7, F8, F9). All the values expressed as mean ± standard deviation, n=3

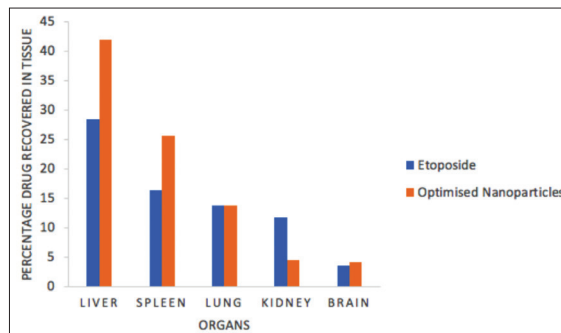


**Figure 11.** Comparative *in vivo* drug targeting. Each data point is the mean ± standard deviation of 3 experiments

and 3.63±0.180% in the brain. The results are shown in Figure 11. The drug loaded nanoparticles showed preferential drug targeting to the liver followed by the spleen, lungs, kidney, and brain.

### CONCLUSIONS

Generally, oral etoposide administration compared to intravenous administration may result in an improvement in the patient's quality of life and reduced costs. Several studies have confirmed the comparable safety and efficacy of oral and intravenous etoposide. However, greater use of oral etoposide is limited by its incomplete and variable bioavailability. The present study utilized particle engineering to improve the primary properties of etoposide. The novel polymeric nanoparticles containing etoposide were prepared by nanoprecipitation. The polycationic polymers Eudragit® EPO and Pluronic® F-68 as stabilizer can be used to obtain stable nanoparticle suspensions. In addition, ionic interactions between cationic polymers with GI mucosa may improve bioavailability. The drug:polymer ratio and concentration of stabilizer were found to influence the drug content and entrapment efficacy of etoposide nanoparticles but the concentration of stabilizer had great influence of both dependent variables. In the *in vitro* drug release study of selected factorial formulations F6 showed 99.22% drug release in 24 h. The drug release was found to follow Peppas release kinetics with a Fickian diffusion mechanism for all batches. Therefore, it was concluded that etoposide nanoparticles could be effective in sustained release.

These results show that the etoposide loaded polymeric nanoparticles showed preferential targeting of the drug to the liver followed by the spleen, lungs, kidney, and brain. It also revealed that, as compared to pure drug, higher concentrations of drug targeted the organs like the liver and lungs after administering the dose in the form of nanoparticles. This may be attributed to the high macrophage load in these organs and large size of the liver as compared to the spleen and lungs.

The relatively high concentration of drug etoposide present in the liver suggests its usefulness in the targeting of liver cancer. The etoposide nanoparticles of smaller particle size coupled with the prolonged blood circulating property could be a beneficial delivery system for tumor targeting. Further investigations are required on the anticancer activity and pharmacokinetics of



selected factorial formulations of F6 etoposide nanoparticles. Those studies are in progress in our laboratory.

## ACKNOWLEDGMENTS

Financial support from the Tamilnadu Dr. M.G.R. Medical University, [Sw (1)/26221/2015] Chennai, India, is gratefully acknowledged. The Director, Indian Institute of Technology, Chennai, India, is acknowledged for providing necessary facilities to carry out the analytical studies. The authors are also thankful to Azidus Laboratories Ltd, Chennai, India, for their help in carrying out the animal studies.

*Conflict of Interest: No conflict of interest was declared by the authors.*

## REFERENCES

- Montecucco A, Biamonti G. Cellular response to etoposide treatment. *Cancer Lett.* 2007;252:9-18.
- Ezoe S. Secondary leukemia associated with the anti-cancer agent, etoposide, a topoisomerase II inhibitor. *Int J Environ Res Public Health.* 2012;9:2444-2453.
- McLeod HL, Evans WE. Clinical pharmacokinetics and pharmacodynamics of epipodophyllotoxins. *Cancer Surv.* 1993;17:253-268.
- Rodman JH, Murry DJ, Madden T, Santana VM. Altered etoposide pharmacokinetics and time to engraftment in pediatric patients undergoing autologous bone marrow transplantation. *J Clin Oncol.* 1994;12:2390-2397.
- Hande KR. Etoposide pharmacology. *Semin Oncol.* 1992;19(6 Suppl 13):3-9.
- Joel SP, Shah R, Slevin ML. Etoposide dosage and pharmacodynamics. *Cancer Chemother Pharmacol.* 1994;34(Suppl):69-75.
- Chellampillai B, Pawar AP. Improved bioavailability of orally administered andrographolide from pH-sensitive nanoparticles. *Eur J Drug Metab Pharmacokinet.* 2011;35:123-129.
- Huang KJ, Zhu CH. The production and characteristics of solid lipid nanoparticles (SLNs). *Biomaterials.* 2003;24:1781-1785.
- Kaliks R, Guerra C, Giglio AD. Efficacy and toxicity of mitoxantrone and oral etoposide in the treatment of hormone refractory prostate cancer: pilot study. *Einstein (Sao Paulo).* 2010;8:336-338.
- Patloll RR, Vobalaboina V. Folate-targeted etoposide-encapsulated lipid nanospheres. *J Drug Target.* 2008;16:269-275.
- Patlolla RR, Vobalaboina V. Pharmacokinetics and tissue distribution of etoposide delivered in parenteral emulsion. *J Pharma Sci.* 2005;94:437-445.
- Abdelbary G, Fahmy RH. Diazepam loaded solid lipid nanoparticles: design and characterization. *AAPS PharmSciTech.* 2009;10:211-219.
- Kreuter J. *Nanoparticles in Colloidal Drug Delivery Systems.* New York; Marcel Dekker Inc; 1994:2019-220.
- Huynh NT, Passirani C, Saulnier P, Benoit JP. Lipid nanocapsules: A new platform for nanomedicine. *Int J Pharm.* 2009;379:201-209.
- Xing J, Zhan, D, Tan T. Studies on the oridonin-loaded poly(D,L-lactic acid) nanoparticles *in vitro* and *in vivo*. *Int J Biol Macromol.* 2007;40:153-158.
- Lee ES, Oh YT, Youn YS, Nam M, Park B, Yun J, Kim JH, Song HT, Oh KT. Binary mixing of micelles using pluronics for a nano-sized drug delivery system. *Colloids Surf B Biointerfaces.* 2011;82:190-195.
- Kocbek P, Baumgartner S, Kristl J. Preparation and evaluation of nanosuspensions for enhancing the dissolution of poorly soluble drugs. *Int J Pharm.* 2006;312:179-186.
- Ubrich N, Schmidt C, Bodmeier R, Hoffman M, Maincent P. Oral evaluation in rabbits of cyclosporin-loaded Eudragit RS or RL nanoparticles. *Int J Pharm.* 2005;288:169-175.
- Wu TH, Yen FL, Lin LT, Tsai TR, Lin CC, Cham TM. Preparation, physicochemical characterization, and antioxidant effects of quercetin nanoparticles. *Int J Pharm.* 2008;346:160-168.
- Haznedar S, Dortunc B. Preparation and *in vitro* evaluation of Eudragit microspheres containing acetazolamide. *Int J Pharm.* 2004;269:131-140.
- Hoffart V, Ubrich N, Simonin C, Babak V, Vigneron C, Hoffman M, Lecompte T, Maincent P. Low molecular weight heparin-loaded polymeric nanoparticles: formulation, characterization, and release characteristics. *Drug Dev Ind Pharm.* 2002;28:1091-1099.
- Rodriguez SG, Allemann E, Doelker E, Fessi H. Versatility of three techniques for preparing ibuprofen-loaded methacrylic acid copolymer nanoparticles of controlled sizes. *Pharm Res.* 2005;15:347-354.
- Dillen K, Vandervoort J, Van den Mooter G, Ludwig A. Evaluation of ciprofloxacin-loaded Eudragit RS100 or RL100/PLGA nanoparticles. *Int J Pharm.* 2006;314:72-82.
- Kocbek P, Baumgartner S, Kristl J. Preparation and evaluation of nanosuspension for enhancing the dissolution of poorly water soluble drugs. *Int J Pharm.* 2006;312:179-186.
- Vippagunta SR, Maul KA, Tallavajhala S, Grant DJ. Solid-state characterization of nifedipine solid dispersions. *Int J Pharm.* 2002;236:111-123.
- Lloyd GR, Craig DQ, Smith A. An investigation into the melting behavior of binary mixes and solid dispersions of paracetamol and PEG 4000. *J Pharm Sci.* 1997;86:991-996.



# Quantitative Structure–Activity Relationship Analysis of Selective Rho Kinase Inhibitors as Neuro-regenerator Agents

## Nöro-rejeneratör Ajan Olarak Seçici Rho Kinaz İnhibitörlerinin Kantitatif Yapı-Etkinlik İlişki Analizi

Seema KESAR\*, Sarvesh K. PALIWAL, Pooja MISHRA, Monika CHAUHAN  
Banasthali University, Faculty of Pharmacy, Department of Pharmacy, Rajasthan, India

### ABSTRACT

**Objectives:** To understand the role of Rho (serine/threonine) kinases in the treatment of neurological segments, attempts have been made to find potent inhibitors of Rho enzyme by a 2D quantitative structure–activity relationship (QSAR) model.

**Materials and Methods:** QSAR studies were executed on urea-based scaffolds from aniline and benzylamine analogues, which were aligned for generation of a chemometric-based model. Multivariate statistical approaches were applied including linear and nonlinear analysis such as multiple linear regression, partial least square and artificial neural network for the generation of model, and also an application of (*in silico*) absorption, distribution, metabolism, excretion studies was performed to ascertain the novelty and drug-like properties of the intended molecules.

**Results:** Ligand based analysis was implemented and showed excellent statistical relevance such as S value=0.38, F value=48.41,  $r=0.95$ ,  $r^2=0.91$ , and  $r_{cv}^2=0.86$ . Five illuminating variables, i.e., vesicle-associated membrane protein (VAMP) polarization YY component (whole molecule), VAMP dipole Y component (whole molecule), VAMP dipole Z component (whole molecule), Kier ChiV6 path index (whole molecule), and moment of inertia 2 size (whole molecule), were found and they have a profound influence on the potency of the compounds.

**Conclusion:** The values of standard statistical parameters reveal the predictive power and robustness of this model and also provide valuable insight into the significance of five descriptors. The acquired physicochemical properties (electronic, topological, and steric) show the important structural features required for activity against Rho kinase. After performing Lipinski's rule of five on urea-based derivatives no molecule was violating the rule. Therefore, these features can be effectively employed for the modeling and screening of active neurological agents as novel Rho kinase inhibitors.

**Key words:** Quantitative structure–activity relationship, chemometric analysis, Lipinski's rule of five

### ÖZ

**Amaç:** Rho (serin/treonin) kinazların nörolojik segmentlerin tedavisinde rolünü anlamak üzere, 2 boyutlu kantitatif yapı-aktivite ilişkisi (QSAR) modeli ile Rho enziminin potansiyel inhibitörlerini bulmak üzere girişimlerde bulunulmuştur.

**Gereç ve Yöntemler:** QSAR çalışmaları, kemometrik tabanlı bir modelin üretilmesi için anilin ve benzilamin analoglarından üre bazlı yapı iskeleleri üzerinde gerçekleştirildi. Modelin üretilmesi ve ayrıca (*in silico*) absorpsiyon, dağılım, metabolizma, eliminasyon çalışmalarının uygulaması, amaçlanan moleküllerin yenilik ve ilaç benzeri özelliklerinin kesin olarak anlaşılması için çoklu doğrusal regresyon, kısmi en küçük kare ve yapay sinir ağı gibi doğrusal ve doğrusal olmayan analizleri içeren çok değişkenli istatistiksel yaklaşımlar uygulandı.

**Bulgular:** Ligand bazlı analiz ile  $S=0.38$ ,  $F=48.41$ ,  $r=0.95$ ,  $r^2=0.91$  ve  $r_{cv}^2=0.86$  ile istatistiksel olarak mükemmel bir ilişki gösterdi. Beş aydınlatıcı değişkenin; vezikülle ilişkili zar proteini (VAMP) polarizasyonu YY bileşeni (bütün molekül), VAMP dipol Y bileşeni (bütün molekül), VAMP dipol Z bileşeni (bütün molekül), Kier ChiV6 yol indeksi (bütün molekül) ve atalet momenti 2 büyüklüğü (bütün molekül); bileşiklerin potensleri üzerinde önemli bir etkiye sahip oldukları bulundu.

**Sonuç:** Standart istatistiksel parametrelerin değerleri, bu modelin gücünü ve sağlamlığını ortaya koymakta ve aynı zamanda beş tanımlayıcıya ait değerli bilgiler sağlamaktadır. Elde edilen fizikokimyasal özellikler (elektronik, topolojik ve sterik), Rho kinaza karşı aktivite için gerekli olan önemli yapısal özellikleri göstermektedir. Üre bazlı türevler üzerinde Lipinski'nin beş kuralı uygulandığında bütün bileşikler bu kurala uymuştur. Bu nedenle, bu özellikler, yeni Rho kinaz inhibitörü aktif nörolojik ajanların modellenmesi ve taranmasında etkili bir şekilde kullanılabilir.

**Anahtar kelimeler:** Kantitatif yapı-etki ilişkisi, kemometrik analiz, Lipinski'nin beşer kuralı

\*Correspondence: E-mail: kesar.seema15@gmail.com, Phone: 08302916491 ORCID-ID: orcid.org/0000-0002-2307-9618

Received: 09.12.2017, Accepted: 25.01.2018

©Turk J Pharm Sci, Published by Galenos Publishing House.

## INTRODUCTION

Inhibition of the Rho-associated protein kinase (ROCK) signaling pathway induces various neuronal functions such as activation of neurite outgrowth, axonal regeneration, and pro-survival Akt. A recent outcome revealed the new site of ROCK as a new strategy to treat neurological disorders. One of the best-defined effectors of the small guanosine triphosphate (GTP) binding proteins of the Rho subfamily (RhoGTPases) is Rho-associated coiled-coil-containing protein kinase/ROCK/Rho kinase (ROK), associated with the protein kinase A/G and C family of serine-threonine kinases. Rho GTPases are members of the Ras superfamily of GTP hydrolase enzymes, used as molecular devices that can handle various signaling pathways by converting biochemically GDP-bound (inactive) to GTP-bound (active) state,<sup>1-3</sup> and the whole process is controlled by two main classes of proteins: GTPase-activating proteins and guanine nucleotide-exchange factors, which increase intrinsic GTPase activity, and gear up the conversion of GDP to GTP, respectively, which activates numerous downstream effectors such as (ROK/ROCK).<sup>4</sup> Activation of downstream Nogo receptor family members or chondroitin sulfate proteoglycan receptors by ROCK signaling stimulates axon growth inhibition; thus ROCK signaling pathway inhibition may be considered a promising strategy for the axon regeneration process.<sup>5</sup> In the treatment of spinal cord injuries, analysis of 30 preclinical studies reported that inhibition of ROCK improves locomotor recovery by 15%.<sup>6</sup> A phase 1 and 2 clinical trial (Japan Primary Registries Network identifier UMIN00000825) was designed to consider the safety and viability of the combination of fasudil and olfactory mucosa autograft in patients, but the results were not divulged, and no results have been found effectual for spinal cord injury. Thus, there is an urgent call for safe and affordable neuro-regenerative agents.

Optimization and development of a new drug involve a lot of effort and cost nearly \$900 million to pharmaceutical or biotechnology companies. To overcome these unavoidable problems, applications of computer assisted drug design or *in silico* techniques have been exclusively used to develop new safe, cheap, and biologically active chemical entities and establish their role of specificity in determining the biological activity of ROK, and also gave the prospect of possible molecular interactions of a specific inhibitor that binds to the active site of the concerned ROK enzyme. Thus, the current study aimed to build a Quantitative structure-activity relationship (QSAR) model by implementing diverse chemometric techniques to achieve improved inhibitory action towards ROK enzyme as a neuro-regenerative agent.

### 2D QSAR or Hansch-Fujita analysis

QSAR analysis ascertains mathematical correlations among structural and/or physicochemical properties called descriptors and correlated to the experimentally measured (biological) activity. The most important recent developments in the field involve a substantial increase in the size of experimental datasets available for analysis and an increased application of QSAR models as virtual screening tools to discover biologically

active molecules in chemical databases and/or virtual chemical libraries. To date no data (QSAR model) have been reported for the treatment of the central nervous system (CNS) spinal cord injuries, and thus we rely on our current model, which provided important information for finding improved new and safe oral bioavailable molecules.

## MATERIALS AND METHODS

### *Experimental data set (generation of 3D structure, charge calculation, and optimization)*

The chemical structures of compounds<sup>7</sup> were sketched using ChemDraw (8.0) and were imported in the Tools for structure-activity relationship (TSAR) 3.3 sheet, i.e. TSAR (TSAR: assimilated analysis package). Once the structures are imported, the negative logarithm of the IC<sub>50</sub> is necessary as actual activities are often skewed and are measures of the free energy of binding and so it was introduced in another column of the TSAR sheet. Prior to the descriptors' calculation, the structures were subjected to CORINA, which is often used to create 3D structures of typically drug-like molecules.<sup>8</sup> The geometry and energy were optimized in order to obtain the minimum potential energy conformer, which is a measure of the stability of the conformer.<sup>9</sup> Molecular energies are evaluated by summing (bond length, bond angle, torsion angle, Van der Waal's, and coulombic) terms for all suitable sets of atoms.

### *Preparation of the data set and data reduction*

The main reason behind descriptor calculation is to decode the information concerning the physicochemical properties of each and every molecular structure liable for specific biological activity of the molecule. Up to 500 descriptors were computed in the TSAR 3D sheet (inbuilt programming of calculating physicochemical properties) for a single molecule. In order to choose only relevant and significant sets of descriptors, data reduction was carried out to eliminate the prevalence of coincidental correlations as well as data redundancy. Firstly, descriptors with "0" values for each compound were deleted. The data were reduced on the basis of a correlation matrix developed between two descriptors. These correlation values indicate the height of co-linearity. Values somewhat close to 1 indicate the extent of better fitting of the regression model. If the intercorrelation values of the two variables were 0.5 or higher then those descriptors were retained, but if they were below 0.5 then they were eliminated from the data sheet. Finally, five descriptors, i.e., inertia moment 2 size (WM), vesicle-associated membrane protein (VAMP) polarization YY (WM), VAMP dipole Y component (WM), VAMP dipole Z component (WM), and Kier chiV6 path (WM), were found to be highly correlated with the actual activity.

### *Training and test set<sup>10</sup>*

Series of 41 analogues were segregated into training (29 compounds) and test (11 compounds) sets on the basis of diversity in the structures and the biological activity of the compounds. The compounds in the training and test sets

were employed to develop and validate the predictability of the concerned model. Some of the compounds may behave as outliers and thus they have to be discarded during the process of model development.

#### Model development and its validation

##### Linear regression analysis

Linear regression analysis helps to establish the correlation between the independent and dependent variables ( $\log 1/IC_{50}$ ) of the series. The construction of the regression model was done using training set compounds and the significance of every model was determined on the basis of statistical values<sup>11</sup> such as  $r^2$  value (correlation between dependent and independent variables), cross validation  $r^2_{cv}$  of the training set (which should be greater than 0.8),  $f$  value (degree of statistical confidence, which should be high) and  $s$ -value (standard error of estimate, which ought to be minimum). The various statistical parameters are shown in Table 1. Compounds of the test set are for the prognostic ability of the purposed model.<sup>12</sup> For a predictive model, the value of the correlation coefficient ( $r^2$ ) of the test set should be greater than 0.6 and less than the  $r^2$  of the training set.

Partial least square analysis was used to check the robustness of the model generated by the multiple least square regression analysis. To validate the results obtained from the multiple linear

regression (MLR) technique, the same data set was subjected to partial least squares (PLS) analysis. The correlation coefficient  $r^2$  and the  $r^2_{cv}$  value of the training and test sets were evaluated to ascertain the quality of the developed PLS models.<sup>13</sup>

##### Nonlinear regression analysis<sup>14</sup>

Artificial neural networks mimic the functioning of simulating the learning process by neural networks. They employ interconnections of artificial neurons with the help of computational studies and are capable of dealing with nonlinear and irregular data. Neural network analysis was carried out on the same descriptors of MLR analysis. The NNA involved three layers: input, hidden, and output layers. The input layer worked by receiving data, whereas the output layer generated the dependent variable. The hidden layer interconnected the two abovementioned layers. The final structural design of the generated NN model was (5-2-1).

##### Validation of the model

**Cross-validation ( $r^2_{cv}$ ):** This validation technique was employed to appraise the reliability of the developed statistical models. Number of compounds was shuffled from the test to the training set and vice versa for generation of the precise model. Leave-one-out methodology (when a molecule is removed from the training set and included in the test set and vice versa to predict the activity of a compound) was performed to get the final model. The cross-validation test ( $r^2_{cv}$ ) value should be greater than 0.60.<sup>15</sup>

**Activity prediction of test set compounds:** In general,  $r^2$  of the test set greater than 0.6 represents good prognostic ability of the model.<sup>16</sup>

##### Outliers

Outliers are the data points that are fitted far apart from the linear model and have some different mode of binding. An outlier of a QSAR model refers to a data point that falls outside the confidence interval of the regression line. The compounds with higher residual values that deviated from the regression line were deleted as outliers and they adversely affected the robustness of the prospective model.

## RESULTS AND DISCUSSION

Data sets of various analogues were employed for the present studies. Their chemical structures and biological activity ( $\log 1/IC_{50}$ ) are presented in Table 2. In order to assess the major molecular factors that greatly affect the ROK inhibition of derivatives belonging to anilines and benzylamines, three chemometric tools (MLR, PLS, and NN) were used to construct classical descriptor-based (QSAR) models. The compounds were divided into training and test sets and the training set comprised 29 compounds (excluding 1 outlier) and the test set 11.

##### Statistical analysis

##### MLR and PLS (linear regression method)

Initially, more than 200 descriptors were calculated for regression analysis. Due to the copious and redundant data,

**Table 1. Description of various statistical parameters**

Statistical parameters	Descriptions
$r$ (Correlation coefficient)	Correlation coefficient is a measure of quality of fit of the model. It constitutes the variance in the data and should be above 0.9.
$r^2$ (Coefficient of determination)	Coefficient of determination, also known as square of correlation coefficient, is a measure of the proportion of variability in the biological activity that can be explained by a linear relationship between independent variables and dependent variable and gives information about the goodness of fit of a model.
Standard deviation	Standard deviation is the typical amount by which an observation deviates from the regression line; it is an absolute measure of quality of fit of the model. The value of standard deviation should be small but cannot have a value lower than the standard deviation of experimental data and the magnitude of standard deviation may be attributed to some experimental error in the data as well as imperfection in the biological model.
F (Sequential Fisher test)	It is a measure of the level of statistical significance of the regression model. A higher value of F implies that a more significant correlation has been attained.
t (Test for statistical significance)	The t-test measures the statistical significance of the regression coefficients. The higher t-test values correspond to the more significant regression coefficients.

Table 2. Data set used for QSAR model development

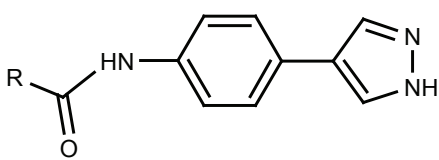
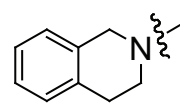
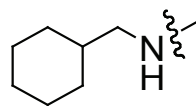
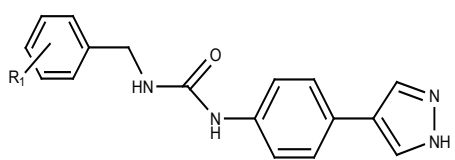
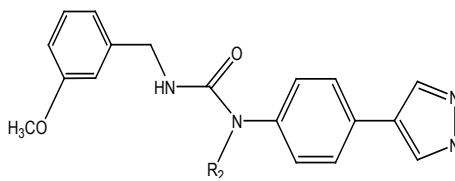
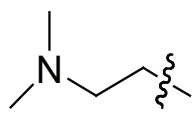
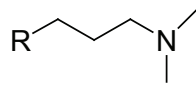
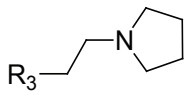
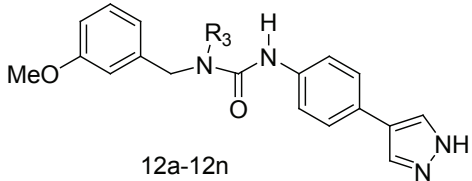
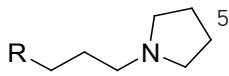
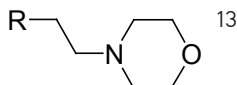
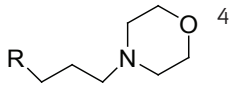
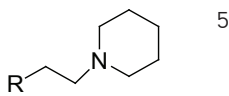
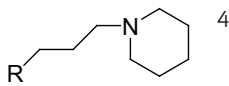
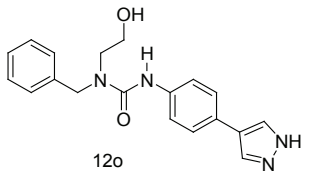
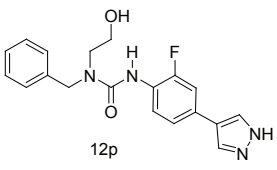
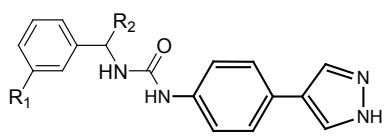
Compound no	Basic scaffold	R	ROCK-II IC <sub>50</sub> (nM)
5a		PhNH	304
5b		PhCH <sub>2</sub> NH	18
5c		PhCH <sub>2</sub> CH <sub>2</sub> NH	88
5d		PhCH <sub>2</sub> CH <sub>2</sub> CH <sub>2</sub> NH	1017
5e		PhCH <sub>2</sub> O	7
5f		PhCH <sub>2</sub> CH <sub>2</sub> O	55
5g		PhCH <sub>2</sub> CH <sub>2</sub>	24
5h			280
5i		751	
5j		3-OCH <sub>3</sub>	2
5k		2,3-di-OCH <sub>3</sub>	253
5l		2,4-di-OCH <sub>3</sub>	331
5m		2,5-di-OCH <sub>3</sub>	570
5n		2,6-di-OCH <sub>3</sub>	924
5o		3,4-di-OCH <sub>3</sub>	425
5p		3,5-di-OCH <sub>3</sub>	281
5q		3-F, 4-OCH <sub>3</sub>	357
8a		CH <sub>3</sub>	87
8b		CH <sub>2</sub> CH <sub>2</sub> OH	611
8c			2984
8e			3324

Table 2. Continued

Compound no	Basic scaffold	R	ROCK-II IC <sub>50</sub> (nM)	
12a		CH <sub>3</sub>	1	
12b		CH <sub>2</sub> CH <sub>3</sub>	1	
12c		Cyclopropyl	1	
12d		Isopropyl	3	
12e		CH <sub>2</sub> CH <sub>2</sub> OH	1	
12f		CH <sub>2</sub> CH <sub>2</sub> OCH <sub>3</sub>	17	
12h		CH <sub>2</sub> CH <sub>2</sub> N(CH <sub>3</sub> ) <sub>2</sub>	1	
12i			3	
12j	 <p>12a-12n</p>		5	
12k			13	
12l			4	
12m			5	
12n			4	
12o	 <p>12o</p>	CH <sub>2</sub> CH <sub>2</sub> OH	12	
12p	 <p>12p</p>	CH <sub>2</sub> CH <sub>2</sub> OH	14	
		R <sub>1</sub>	R <sub>2</sub>	
14a		OCH <sub>3</sub>	CH <sub>2</sub> CH <sub>2</sub> OH	2
14b		F	CH <sub>2</sub> CH <sub>2</sub> OH	2
14c		H	CH <sub>2</sub> CH <sub>2</sub> OH	2
14d		H	CH <sub>2</sub> OH	1
14e		H	CH <sub>2</sub> CH <sub>2</sub> N(CH <sub>3</sub> ) <sub>2</sub>	2

QSAR: 2D quantitative structure–activity relationship, ROCK: Rho-associated protein kinase

there was a very low value for  $r_{cv}^2$  (0.312), implying inadequate internal predictability. There was a strong necessity to build a reliable and informative set of descriptors having good correlation with the biological activity with no intercorrelation. After the deletion of the undesirable set of descriptors, the correlation matrix technique was employed and eventually five distinct physicochemical descriptors were obtained: inertia moment 2 size, VAMP polarization YY, VAMP dipole Y component, VAMP dipole Z component, and Kier chiV6 path. For QSAR analysis, the training set molecules were used to construct (linear and nonlinear) models so that a precise relationship could be established between molecules and biological activity and the molecules of test set served to check the robustness of the model. During the creation of the purposed model, one compound was shown as an outlier and not to fit either the training set or the test set; also the residual value was more than two orders of magnitude. Owing to this, outlier 5b with different prediction was omitted from the training set. The correlation matrixes of the descriptors are shown in Table 3. The selected model was assessed on the basis of different statistical values, such as regression coefficient ( $r$ ), coefficient of determination ( $r^2$ ), prognostic power of the model ( $r_{cv}^2$ ), standard deviation (SD), sequential Fisher's ratio (F), and test for statistical significance (t). The value of  $r^2$  ought to be  $>0.6$  and the value of  $r_{cv}^2 >0.7$ . Statistical outputs of the MLR and PLS models are summarized in Table 4. The statistical worthiness of the developed model was evaluated in terms of square of the correlation coefficient, where  $r^2$  (MLR=0.913 and PLS=0.912) values explain 91% variance in activity, which indicates a measure of good fit by the regression equation. A small difference in (MLR)  $r^2$  (0.913) and  $r_{cv}^2$  (0.862) values implies high prognostic ability of the model. Similarly in the PLS analysis, there is a slight difference in  $r^2$  (0.912) and  $r_{cv}^2$  (0.869) values, which further ascertains the robustness of the model. The  $r_{cv}^2$  values for the MLR and PLS models ( $r_{cvMLR}^2=0.862$  and  $r_{cvPLS}^2=0.869$ ) were evaluated and both models had comparable  $r_{cv}^2$  values. The F-test indicates the significance level of the

model. The F-value of the final MLR model, 48.41, clearly shows the statistical significance of the derived model. The 's' value is the (standard) error of the regression model, and it should be low for better QSAR model generation; this is an approximation of how precisely the model will predict unknown 'Y' values. The value of 's' for the best MLR model is 0.373 and for PLS 0.307. It signifies that regression with an 's' value of 0.3 should predict Y values with a standard error of 0.3 units. The final model has the highest correlation coefficient (0.91), confirming the robustness of the model and also the model was cross validated and the  $r_{cv}^2$  value of 0.86 depicted the strength of the model. For further assurance of the significance of the descriptors, their t-test values, coefficient values, jackknife standard error (SE), and covariance SE values (Table 5) were evaluated. The values of all these parameters for all five descriptors confirmed the significance of an individual descriptor in determining the importance of structural design in exhibiting ROK inhibitory activity by a molecule. The generated model was used to understand the structural dependency of the biological activity demonstrated by the certain set of ROK inhibitors, and generated following equation 1:

*Original data*

$$Y = -0.0012895674 * X_1 + 0.092464715 * X_2 + 0.22125481 * X_3 + 0.34796265 * X_4 + 1.5525457 * X_5 - 3.9303896$$

*Standardized data*

$$Y = -0.2757968 * S_1 + 0.45911208 * S_2 + 0.35567212 * S_3 + 0.4776836 * S_4 - 0.64006561 * S_5 - 1.344354$$

Here  $X_1$ = inertia moment 2 size (whole molecule),  $X_2$ = VAMP polarization YY (whole molecule),  $X_3$ = VAMP dipole Y component (whole molecule),  $X_4$ = VAMP dipole Z component (whole molecule),  $X_5$ = Kier ChiV6 (path) index (whole molecule), and Y represents the biological activity.

The PLS method is an addition to the MLR approach that evaluates the results to obtain assurance of the consequences when

**Table 3. Correlation matrix of the independent variables used in the final model demonstrating the degree of correlation**

Descriptors	Inertia moment 2 size (WM)	VAMP polarization YY (WM)	VAMP dipole Y component (WM)	VAMP dipole Z component (WM)	Kier ChiV6 path (WM)	Log1/IC <sub>50</sub>
Inertia moment 2 size (WM)	1	-0.0706	-0.1137	-0.3832	0.4636	-0.6950
VAMP polarization YY (WM)	-0.0706	1	-0.1074	-0.2828	0.0541	0.2270
VAMP dipole Y component (WM)	-0.1137	-0.1074	1	-0.0480	0.0266	0.2497
VAMP dipole Z component (WM)	-0.3832	-0.2828	-0.0480	1	-0.2635	0.5075
Kier ChiV6 path (WM)	0.4636	0.0541	0.0266	-0.2635	1	-0.7209
Log1/IC <sub>50</sub>	-0.6950	0.2270	0.2497	0.5075	-0.7209	1

they show minimal variation and have comparable results. Statistically, the PLS equation evaluated the robustness of the developed model on the basis of statistical parameters, i.e.,  $r^2$ . The regression equation obtained by the PLS method generated: *Equation 2*;

$$Y = -0.0013*X_1 + 0.0914*X_2 + 0.2306*X_3 + 0.3482*X_4 - 1.5262*X_5 - 3.8318$$

#### Prediction of test set compounds

The predictive ability of the intended model was validated by a set of eleven compounds. The difference between (actual and predicted) activity values of MLR and PLS analysis should be minimal for assessment of the quality of the developed models.

#### Artificial neural networks (artificial nonlinear regression analysis method)

Artificial neural networks (ANN) analyses were carried out with the same descriptors that were used for linear regression analysis in an endeavor to improve the results

obtained for ROK inhibition. In the present study, inputs for the neural network were the descriptors, while the output was the  $\log_1/IC_{50}$  values. In artificial neural network analysis, TSAR software automatically computes the number of hidden neurons, as well as patterns of the training and test sets. The number of neurons in the hidden layer and the number of rows in the training set are balanced to achieve the optimum predictive power for the neural network. The NN with three hidden neurons and 30% of compounds excluded as the test set was the most successfully trained NN model for *in vitro* ROK inhibition data as compared to the other NN models. Each analysis was repeated several times so that test RMS fit and best RMS fit were nearer to each other. Values of actual and predicted activity of the training/test set of compounds and their corresponding graph and also dependence plots of the descriptors with the output value ( $\log_1/IC_{50}$ ) clearly demonstrate that three descriptors, VAMP polarization YY, VAMP dipole Y component, and VAMP dipole Z component, are positively correlated to the output value ( $\log_1/IC_{50}$  value), while two descriptors, inertia moment 2 size and Kier chiV6

**Table 4. Equations, statistical values, and the descriptors used for the development of MLR and PLS models**

Equation Y=Biological Activity X=Descriptors	r	r <sup>2</sup>	r <sup>2</sup> <sub>cv</sub>	s value	F value	Descriptors				
						X <sub>1</sub>	X <sub>2</sub>	X <sub>3</sub>	X <sub>4</sub>	X <sub>5</sub>
MLR Y = -0.00128*X <sub>1</sub> + 0.09246*X <sub>2</sub> + 0.22125*X <sub>3</sub> + 0.34796*X <sub>4</sub> - 1.55254*X <sub>5</sub> - 3.93038	0.955	0.913	0.862	0.387	48.41	Inertia moment 2 size (whole molecule)	VAMP polarization YY (whole molecule)	VAMP dipole Y component (whole molecule)	VAMP dipole Z component (whole molecule)	Kier ChiV6 path (whole molecule)
PLS Y = -0.0013*X <sub>1</sub> + 0.0914*X <sub>2</sub> + 0.2306*X <sub>3</sub> + 0.3482*X <sub>4</sub> - 1.5262*X <sub>5</sub> - 3.8318	0.943	0.912	0.869	0.307	46.0					

In linear regression analysis the dependence has the following linear form:

$$Y = b_1X_1 + b_2X_2 + \dots + b_pX_p + b,$$

where  $b_1, b_2, \dots, b_p$  are regression coefficients;  $b$  is the intercept;  $X_1, X_2, \dots, X_p$  are independent variables; and  $Y$  represents expected values of the dependent variable by the regression model. The regression coefficients  $b_1, b_2, \dots, b_p$  and the intercept are calculated by applying the method of least squares to give the smallest possible sum of squared differences between the true  $Y$  values of the dependent variable and the  $Y'$  values calculated by the regression model.

MLR: Multiple linear regression, PLS: Partial least squares, VAMP: Vesicle-associated membrane protein

**Table 5. The t-test values, jackknife SE, and covariance SE values of the descriptors used for regression analysis**

Statistical parameters	Descriptors	Coefficient <sup>a</sup>	Jackknife SE <sup>b</sup>	Covariance SE <sup>c</sup>	t-value <sup>d</sup>	T-probability <sup>e</sup>
Inertia moment 2 size (WM)		-0.0012896	0.00038428	0.00042338	-3.0459	0.0057359
VAMP polarization YY (WM)		0.092465	0.019823	0.015956	5.795	6.6441e-006
VAMP dipole Y component (WM)		0.22125	0.052874	0.046879	4.7197	9.3614e-005
VAMP dipole Z component (WM)		0.34796	0.065733	0.062124	5.6011	1.0638e-005
Kier ChiV6 path (WM)		-1.5525	0.23786	0.20289	-7.6521	9.1178e-008

<sup>a</sup>Represents the regressions coefficient for each variable in the QSAR equations, <sup>b</sup>Represents the standard error estimation on each regression coefficient derived from a jackknife method on the final regression model, <sup>c</sup>Represents an estimate of the standard error on each regression coefficient derived from the covariance matrix, <sup>d</sup>Measurement of the significance of each variable incorporated in the model, <sup>e</sup>Represents statistical significance for t-values, VAMP: Vesicle-associated membrane protein, QSAR: 2D quantitative structure-activity relationship, SE: Standard error



path index, are negatively correlated to  $\log 1/IC_{50}$ , which is in agreement with the results of MLR analysis.

#### Comparison between linear and nonlinear methods

Different statistical approaches were employed to quantify the predictive ability of the generated models in terms of statistical fit ( $r^2$ ). Both MLR and PLS (two linear methods) were studied and had comparable results. The  $r^2$  values for the training set for QSAR analysis were  $r^2_{MLR}=0.91$ ,  $r^2_{PLS}=0.91$ , and  $r^2_{ANN}=0.93$  and for the test set the values were  $r^2_{MLR}=0.75$ ,  $r^2_{PLS}=0.75$ , and  $r^2_{ANN}=0.73$ . On the basis of the predictive power of the model it is very clear that conventional MLR and PLS as well as ANN analysis generated a highly robust and predictive model. The actual and predicted activity for the compounds of the training and test sets were obtained after MLR, PLS, and NNA and are shown in Table 6 and their corresponding graph are shown in Figures 1-3. A summary of the performance of the different prediction models is given in Table 7.

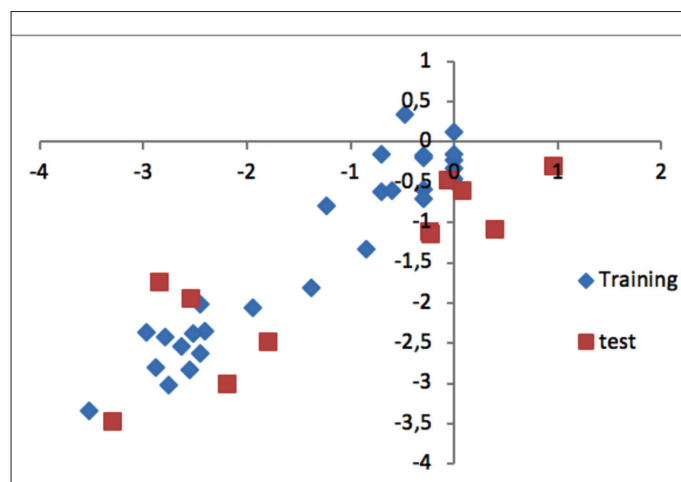


**Figure 1.** Graph plotted between actual and predicted activity of training and test set through MLR analysis

MLR: Multiple linear regression

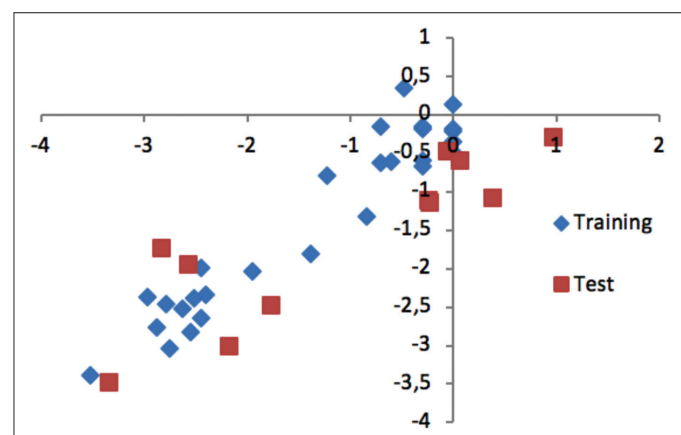


**Figure 2.** Graph plotted between actual and predicted activity of training and test set through PLS analysis

PLS: Partial least squares

#### Mechanistic interpretation of the descriptors

The results of MLR, PLS, and NN reveal the importance of inertia moment 2 size (WM), VAMP polarization YY (WM), VAMP dipole Y component (WM), VAMP dipole Z component (WM), and Kier chiV6 path (WM) and in fact a strong correlation was observed between ROK inhibitory activity and the five descriptors (Table 8). The dependence plots of the descriptors with the output value ( $\log 1/IC_{50}$ ) are shown in Figure 4 and the structure-activity relationship derived from QSAR analysis is shown in Figure 5.

#### Kier ChiV6 path index

Out of the five parameters, Kier ChiV6 path index (WM) was shown to be an essential descriptor in defining the biological activity of urea-based derivatives as evident from the correlation matrix and the t-value. Kier ChiV6 path index was initially defined by Randic and subsequently by Kier and Hall. It illustrates a number of series represented by "order" and "subgraph" type. By definition, a chi index is a calculation of a known type of subgraph such as path (P), cluster (C), path/cluster (PC), and ring (CH), weighted by a function of the delta values. The descriptor highlights different aspects of atom connectivity within a molecule. It also helps us to examine the substitution pattern in benzene rings and the amount of branching rings.<sup>17</sup> In our study it was observed that the KierchiV6 (path index) descriptor is negatively correlated with permeability; according to the study the sixth order valence connectivity index (KierchiV6) encodes structural complexity, such as the size and heteroatom content of the rings. This complexity is observed in the least and most active compound. As the size of the compound decreases, biological activity increases.

#### VAMP polarization YY

VAMP polarization YY is a spatial descriptor that calculates the electronic properties of a compound and projects polarization towards YY planes. There is a direct relation between polarizability and the number of valence electrons on every atom.<sup>18</sup> A positive correlation of VAMP polarization YY with the

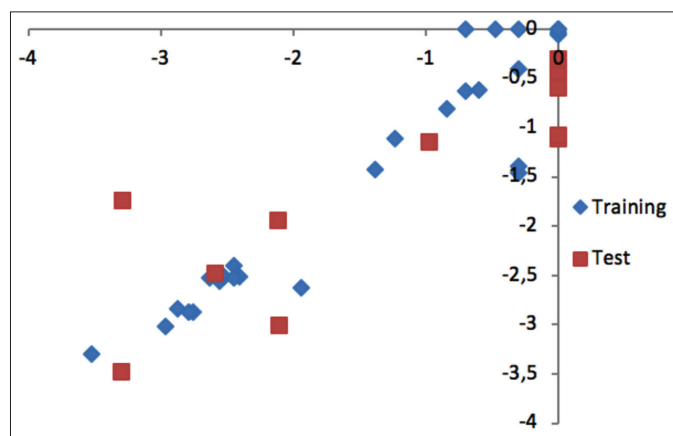


**Figure 3.** Graph plotted between actual and predicted activity of training and test set through FFNN analysis

FFNN: Feed forward neural network

**Table 6. Actual activity versus predicted activity and corresponding residual for the training set of compound**

Compound no.	Actual activity (Log1/IC <sub>50</sub> values)	Predicted activity (Log1/IC <sub>50</sub> values)		
		MLR	PLS	FFNN
<b>Training set compounds</b>				
5c	-1.94	-2.05	-2.08	-2.62
5e	-0.84	-1.33	-1.37	-0.80
5g	-1.38	-1.80	-1.85	-1.42
5h	-2.44	-2.02	-2.10	-2.39
5i	-2.87	-2.79	-2.87	-2.84
5k	-2.40	-2.34	-2.34	-2.51
5l	-2.51	-2.38	-2.37	-2.51
5m	-2.75	-3.02	-3.02	-2.87
5n	-2.96	-2.37	-2.37	-3.02
5o	-2.62	-2.53	-2.49	-2.52
5p	-2.44	-2.63	-2.62	-2.60
5q	-2.55	-2.83	-2.82	-2.65
8b	-2.78	-2.43	-2.39	-2.74
8e	-3.52	-3.34	-3.30	-3.09
12a	0	-0.23	-0.29	-0.06
12b	0	-0.45	-0.45	-0.23
12c	0	-0.32	-0.32	-0.16
12d	-0.47	0.34	0.37	-0.04
12e	0	-0.15	0.13	-0.07
12f	-1.23	-0.79	-0.79	-0.09
12h	0	-0.50	-0.50	-0.09
12j	-0.69	-0.61	-0.64	-0.68
12l	-0.60	-0.61	-0.59	-0.79
12m	-0.69	-0.15	-0.14	-0.13
14a	-0.30	-0.58	-0.55	-0.07
14b	-0.30	-0.20	-0.22	-0.20
14d	-0.30	-0.17	-0.15	-0.06
14c	0	0.11	0.13	-0.05
14e	-0.30	-0.70	-0.80	-0.35
<b>Test set compounds</b>				
5a	-2.48	-2.28	-2.38	-0.60
5d	-3.00	-2.46	-2.15	-2.48
5f	-1.74	-2.54	-2.75	-2.68
8a	-1.93	-2.03	-1.85	-2.76
8c	-3.47	-3.09	-3.21	-3.09
12i	-0.47	-0.88	-0.93	-0.07

**Table 6. Continued**

Compound no.	Actual activity (Log1/IC <sub>50</sub> values)	Predicted activity (Log1/IC <sub>50</sub> values)		
		MLR	PLS	FFNN
12k	-1.11	-0.45	-0.81	-0.16
12n	-0.60	-0.93	-0.84	-0.10
12o	-1.07	-1.49	-1.04	-0.03
12p	-1.14	-0.84	-1.06	-0.20
5j	-0.30	-0.32	-0.29	-0.03

MLR: Multiple linear regression, PLS: Partial least squares, FFNN: Feed forward neural network

**Table 7. Correlation coefficients (r<sup>2</sup>) between predicted and experimental values of the MLR, PLS, and NN models**

r <sup>2</sup> <sub>training</sub>			r <sup>2</sup> <sub>test</sub>		
MLR	PLS	NN	MLR	PLS	NN
0.91	0.91	0.90	0.75	0.75	0.72

MLR: Multiple linear regression, PLS: Partial least squares, NN: Neural network

biological activity reveals a direct link between the chemical reactivity index and biological activity. The compounds 12a, 12b, 12c, 12e, and 14c, having high values of VAMP polarization YY, are the most active, whereas compound 8e, with low VAMP polarization YY, is the least active.

#### VAMP dipole Y component

VAMP dipole Y component is an electronic parameter and is due to the degree of charge separation in a molecule. It describes the substituent point of attachment with the bond sited along the Y-axis.<sup>19</sup> A positive correlation between VAMP dipole Y and biological activity reveals a direct link between the chemical reactivity index and biological activity.

#### Moment of inertia 2 (size)

Inertia moment 2 size (WM) with reference to an axis is defined as the product of the mass times the distance from the axis squared. The higher positive correlation coefficient of inertia moment with permeability data and the high t-values (t-values define the statistical significance of a descriptor) suggest that the orientation behavior with respect to the size of whole molecule is of utmost importance in the binding interaction with the receptor site as well as in imparting greater permeability. In the present study the biological activity increases with a decrease in moment of inertia 2 (size) of the whole molecule. This phenomenon can be explained by taking the example of most active compound that has low value of moment of inertia 2 (size) of the whole molecule in comparison to the least active compound that has high value of moment of inertia 2 (size) of the whole molecule. Hence it can be concluded that by decreasing the moment of inertia 2 (size) ROK inhibitory activity can be increased.

#### VAMP dipole X component

Vamp is a semiempirical molecular orbital package used to determine electrostatic properties and perform optimizing

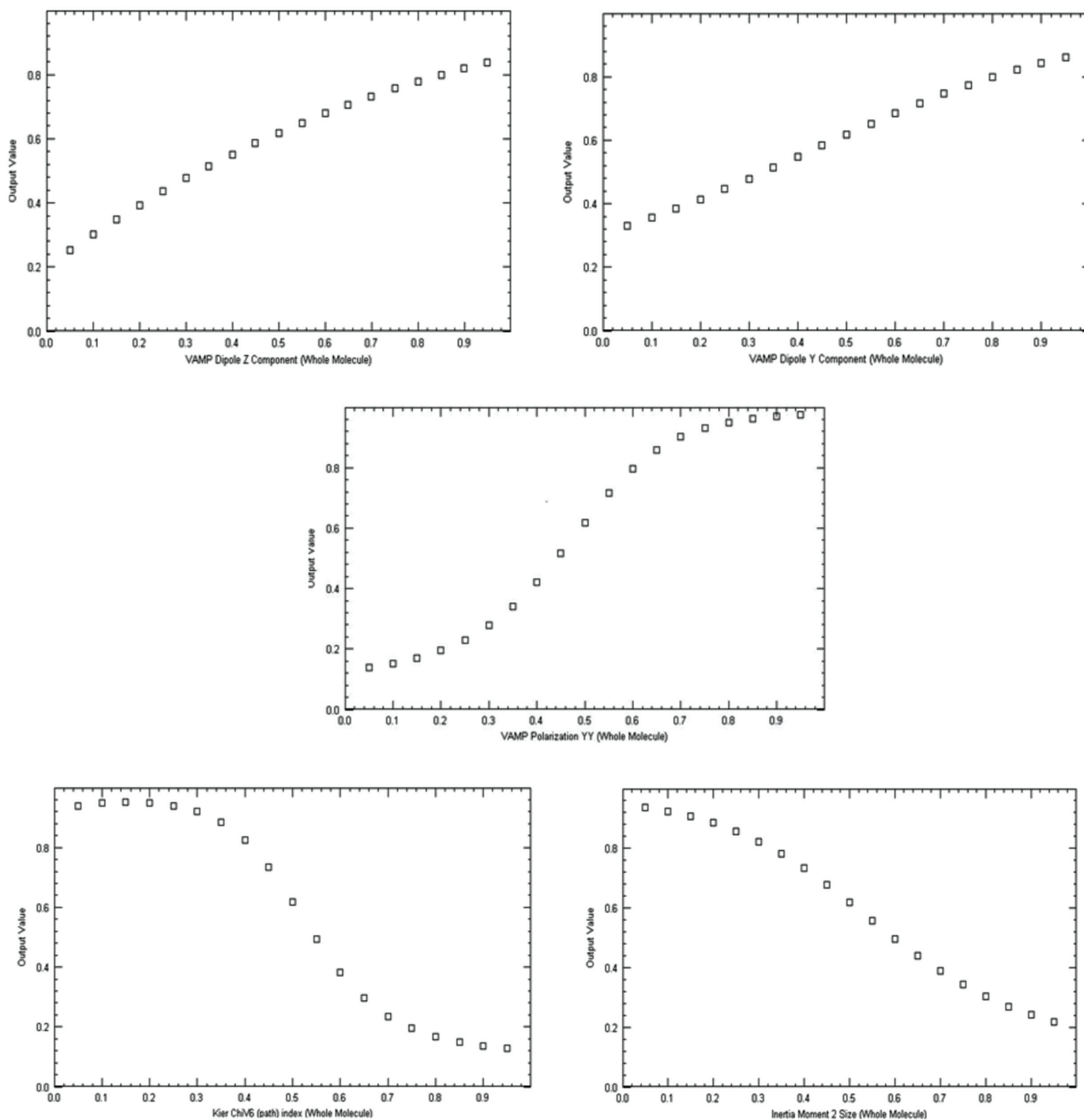


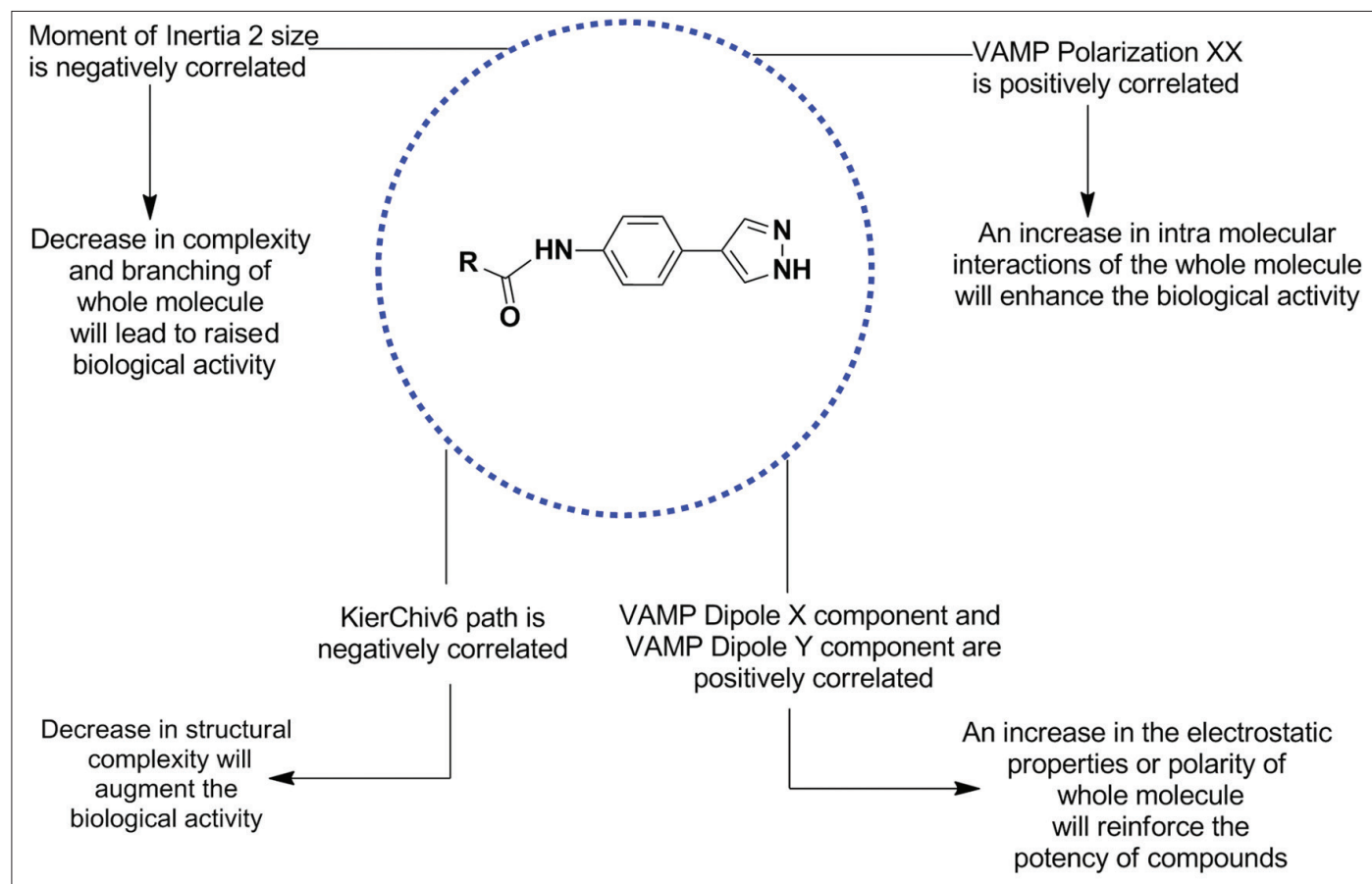
**Figure 4.** Dependency graph illustrating correlation between all five descriptors and actual activity data

of structure such as total energy, electronic energy, nuclear repulsion energy, accessible surface area, atomic charge, mean polarizability, heat of formation, highest occupied molecular orbital and lowest unoccupied molecular orbital eigenvalues, ionization potential, total dipole, polarizability, and dipole components. The positive coefficient of this expression in the proposed model elucidates that the higher the value, the better is the activity, and indicates that biological activity with respect to ROK inhibition is directly dependent upon the chemical

permanence of the compounds in biochemical systems. Some exciting facts were revealed during the analysis of the derived descriptors and their correlation with the structural design of the molecules. In the comparison of the least active molecule with the most active compound of the selected series, we found that when the least active compound (8e) was substituted with dimethylamine the shape and volume of the molecule were altered, which eventually changed the optimal binding affinity of the molecule. However, in the most

active compounds (12a, 12b, 12c, 14c, and 12e) dimethylamine was replaced with either simple alkyl or oxygen-containing alkyl substitutions, which gradually reduced the size and volume of the molecule, thus resulting in enhancement of the

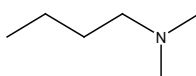
ROK inhibitory activity. Interestingly, both alkyl and oxygen-containing alkyl chains have analogous molecular mass and, thus, no further bulk was loaded onto the molecule. Attribution of alkyl or oxygen-containing alkyl substitutions



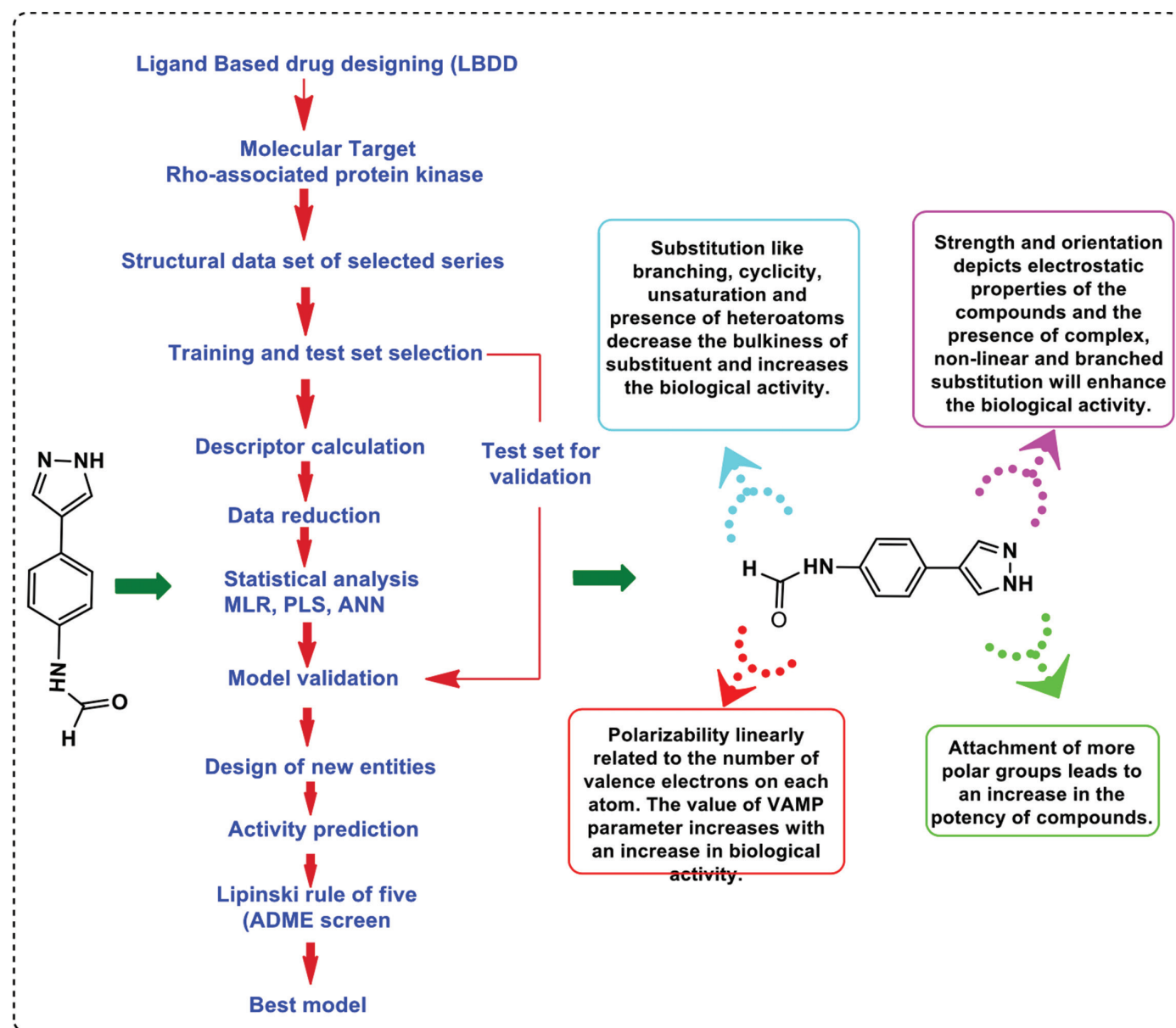
**Figure 5.** Systematic interpretation of the physicochemical descriptors used in the model, which briefly explained the structure–activity relationship

VAMP: Vesicle-associated membrane protein

**Table 8.** Correlation of biological activity of active and inactive molecules with all five descriptors

Name of compound	Substitution at R <sub>3</sub> (12a - 12h)	Biological activity LogIC <sub>50</sub> (nM)	Inertia moment 2 size (WM)	VAMP polarization YY (WM)	VAMP dipole Y (WM)	VAMP dipole Z (WM)	KierChiV6 (path) (WM)
12a	CH <sub>3</sub>	1	1090.7	55.661	0.032	3.045	0
12b	CH <sub>2</sub> CH <sub>3</sub>	1	1080.4	62.251	-3.086	-0.588	0
12c	Cyclopropyl	1	1099	63.302	-3.274	-0.314	0
12e	CH <sub>2</sub> CH <sub>2</sub> OH	1	1115.4	60.45	-2.487	0.492	0
12h	CH <sub>2</sub> CH <sub>2</sub> N(CH <sub>3</sub> ) <sub>2</sub>	1	1216.1	54.60	-0.622	0.224	0
Substitution at R <sub>1</sub> , R <sub>4</sub>							
14c	H CH <sub>2</sub> CH <sub>2</sub> OH	1	1171.8	55.684	1.552	0.199	0
Inactive compound	8e 	3324	1537.5	43.504	-3.134	-4.05	0

VAMP: Vesicle-associated membrane protein



## Graphical Abstract

MLR: Multiple linear regression, PLS: Partial least squares, ANN: Artificial neural network, ADME: Association of destination management executives

positively affects the electrostatic nature of the substituent and thus additional atoms contributing to the energy, resulting in enhanced biological activity, and also showing clearly that hydroxyl or oxygen substitutions are highly electronegative, which augments the overall polarizability of the molecule. However, the negative correlation of Kier Chiv6 (path) index at  $R_1$  clearly reveals that reductions in the bulkiness and volume at certain positions in the whole molecule lead to an increased biological profile. Additionally, compounds 12a, 12b, 12c, 14c, and 12e have lower molecular mass (378.52, 350.46, 362.47, 336.43, and 366.46) than compound 8e (407.57), also confirming the authentication of the descriptor, which leads to compression in the shape of the molecule, allowing it to conveniently enter the binding site and align in such a way that it fits snugly with the walls of the active site.

*Absorption, distribution, metabolism, and excretion studies*

The 'rule of five', given by Lipinski, is known as the therapeutic relevance or property of drug-likeness. It is an empirical approach traditionally utilized for calculating drug-like properties in a molecule that clearly postulates that molecules with a molecular weight less than 500,  $\log p < 5$ , hydrogen bond donors less than 5, and hydrogen bond acceptors less than 10 exhibit an excellent pharmacokinetics profile in terms of absorption or permeation through the biological membrane.<sup>20</sup> This rule explains the absorption, distribution, metabolism, and excretion of bioactive compounds in a superior organism. Lipinski's rule of five was calculated for the particular series of compounds and no molecule was found to have violated the above stated set of rules (Table 9). This overtly indicates that all compounds showed adequate pharmacokinetic profiles.

**Table 9. Illustrating the values of various parameters constituting Lipinski's rule of five**

Compound	ADME weight (WM)	ADME H-bond acceptors (WM)	ADME H-bond donors (WM)	ADME log P (WM)	ADME violations (WM)
4	306.4	2	3	2.910	0
5	293.35	3	2	3.309	0
6	291.38	2	2	3.149	0
7	318.41	2	2	2.887	0
8	298.43	2	3	2.781	0
9	352.43	4	3	2.153	0
15	352.43	4	3	2.153	0
16	352.43	4	3	2.153	0
17	352.43	4	3	2.153	0
18	352.43	4	3	2.153	0
19	352.43	4	3	2.153	0
20	340.39	3	3	2.546	0
21	366.46	4	3	2.209	0
22	407.57	4	2	2.684	0
23	378.52	3	2	3.486	0
27	350.46	3	2	2.995	0
28	362.47	3	2	3.049	0
29	364.49	3	2	3.408	0
30	366.46	4	3	2.209	0
31	380.49	4	2	2.488	0
32	393.54	4	2	2.632	0
33	433.61	4	2	3.009	0
34	449.61	5	2	2.341	0
43	433.61	4	2	3.354	0
44	306.4	3	3	2.406	0
45	293.35	4	4	2.086	0
46	291.38	3	4	2.478	0

ADME: Association of destination management executives

### Study limitations

The findings of the present QSAR analysis will be advantageous only for the modeling of potent ROK inhibitors as active neurological agents. For the future aspects we will try to screen multitargeted novel ROK inhibitors.

## CONCLUSIONS

A 2D QSAR study was performed to establish a structural and physicochemical relationship required for the inhibition of a molecular target against a neurological disease, i.e., ROK. The

statistically significant model highlighted the significance of electronic, topological, and steric descriptors. The authenticity of the projected model was checked by validation and cross-validation ( $r^2_{cv}$ ) based on leave-one-out methodology. Overfitting of the models was checked by considering the difference between  $r^2$  and  $r^2_{cv}$ . In a planned study, an attempt was made to understand the dependence of biological activity on the structural design accountable for their specific ROK inhibition. The main problem regarding the CNS-related drug is its ability to cross the blood-brain barrier, and for crossing this barrier there should be optimal log P, volume, shape, molecular mass, and polarizability. The proposed model overtly points towards the introduction of optimal bulk or charge distribution along with the shape and size of the molecules to determine the binding efficacy of the molecule to the receptor domain, which eventually increases the inhibitory profiles of the selected molecules. VAMP polarization YY component (WM), VAMP dipole Y component (WM), and VAMP dipole Z component (WM) descriptors were positively correlated with activity while the other two, Kier ChiV6 path index (WM) and moment of inertia 2 (size) (WM), were negatively correlated descriptors, and projected molecular structure information with reference to a specific rotation axis or the rotational analogue to mass, and groups that decrease Kier ChiV6 and inertia of moment at substitutions will increase the predictability of the model. The above final model reveals the significance of selected descriptors and their correlation with biological activity and provided substantial insights to plan new chemical scaffolds with improved selectivity outlines. Design of ROK inhibitors incorporating the appropriate essential features or descriptors will increase the chances of getting new better molecules with enhanced inhibitory profiles.

## ACKNOWLEDGEMENT

The authors are thankful to the Vice-chancellor of Banasthali University for providing the necessary research facilities.

*Conflict of Interest:* No conflict of interest was declared by the authors.

## REFERENCES

1. Van Aelst L, D'Souza-Schorey C. Rho GTPases and signaling networks. *Genes Dev.* 1997;11:2295-2322.
2. Burridge K, Wennerberg K. Rho and Rac take center stage. *Cell.* 2004;116:167-179.
3. Bishop AL, Hall A. Rho GTPases and their effector proteins. *Biochem J.* 2000;348:241-255.
4. Rossman KL, Der CJ, Sondek J. GEF means go: turning on RHO GTPases with guanine nucleotide-exchange factors. *Nat Rev Mol Cell Biol.* 2005;6:167-180.
5. Fujita Y, Yamashita T. Axon growth inhibition by RhoA/ROCK in the central nervous system. *Front Neurosci.* 2014;8:338.
6. Watzlawick R, Sena ES, Dirnagl U, Brommer B, Kopp MA, Macleod MR, Howells DW, Schwab JM. Effect and reporting bias of RhoA/ROCK-

- blockade intervention on locomotor recovery after spinal cord injury: a systematic review and meta-analysis. *JAMA Neurol.* 2014;71:91-99.
- Lum C, Kahl J, Kessler L, Kucharski J, Lundström J, Miller S, Nakanishi H, Pei Y, Pryor K, Roberts E, Sebo L, Sullivan R, Urban J, Wang Z. 2,5-Diaminopyrimidines and 3,5-disubstituted azapurines as inhibitors of glycogen synthase kinase-3 (GSK-3). *Bioorg Med Chem Lett.* 2008;18:3578-3581.
  - Dwivedi N, Mishra BN, Katoch VM. 2D-QSAR model development and analysis on variant groups of anti-tuberculosis drugs. *Bioinformation.* 2011;7:82-90.
  - Abraham MH, Whiting GS. Hydrogen bonding: XXI. Solvation parameters for alkylaromatic hydrocarbons from gas-liquid chromatographic data. *J Chrom.* 1992;594:229-241.
  - Wu W, Walczak B, Massart DL, Heuerding S, Erni F, Last IR, Prebble KA. Artificial neural networks in classification of NIR spectral data: design of the training set. *Chemometrics Intell Lab Syst.* 1996;33:35-46.
  - Rose K, Hall LH. E-State Modeling of Fish Toxicity Independent of 3D Structure Information. *SAR QSAR Environ Res.* 2003;14:113-129.
  - Rose K, Hall LH, Kier LB. Modeling Blood-Brain Barrier Partitioning Using the Electrotopological State. *J Chem Inf Comput Sci.* 2002;42:651-666.
  - Voelkel A. Structural descriptors in organic chemistry - new topological parameter based on electrotopological state of graph vertices. *Computers & Chemistry.* 1994;18:1-4.
  - Bottcher CJF. *Theory of Electric Polarization.* (2nd ed). Amsterdam; Elsevier Press; 1973.
  - Hopfinger AJ. *Conformational Properties of Macromolecules.* New York; Academic Press; 1973.
  - TSAR reference guide.
  - Rinaldi D, Rivail JL. Molecular polarisability and dielectric effect of medium in the liquid phase: Theoretical study of the water molecule and its dimers. *Theor Chim Acta.* 1973;32:57-70.
  - Hall LH, Kier LB. The molecular connectivity chi indices and kappa shape indices in structure-property modeling. In: Lipkowitz KB, Boyd DB, eds. *Reviews of Computational Chemistry.* New York; VCH publishers; 1991;2:367-412.
  - Vadlamudi SM, Kulkarni MV. 3D-QSAR of Protein Tyrosine Phosphatase 1B Inhibitors by Genetic Function Approximation. *Internet Electron J Mol Des.* 2004;3:586-609.
  - Lipinski CA, Lombardo F, Dominy BW, Feeney PJ. Experimental and Computational approaches to estimate solubility and permeability in drug discovery and development settings. *Adv Drug Deliv Rev.* 1997;23:3-26.



# Investigation of the Polyphenol Composition, Biological Activities, and Detoxification Properties of Some Medicinal Mushrooms from Turkey

## Türkiye'deki Bazı Tıbbi Mantarların Polifenol Bileşiminin, Biyolojik Aktivitelerinin ve Detoksifikasyon Özelliklerinin Araştırılması

© Naznoosh SHOMALI<sup>1\*</sup>, © Okan ONAR<sup>1</sup>, © Tuğçe ALKAN<sup>1</sup>, © Nergiz DEMİRTAŞ<sup>2</sup>, © Ilgaz AKATA<sup>1</sup>, © Özlem YILDIRIM<sup>1</sup>

<sup>1</sup>Ankara University, Faculty of Science, Department of Biology, Ankara, Turkey

<sup>2</sup>The Ministry of Food, Agriculture and Livestock, Food Control Laboratory, Food Chemical Analysis Laboratory, Ankara, Turkey

### ABSTRACT

**Objectives:** Ethanolic extracts of the mushroom species *Ganoderma adspersum*, *Inonotus hispidus*, *Russula chloroides*, and *Sarcodon imbricatus* were investigated for their polyphenolic contents and biological activities.

**Materials and Methods:** The radical scavenging activity of the extracts was evaluated by 2,2-diphenyl-1-(2,4,6-trinitrophenyl) (DPPH) method and their polyphenolic compounds were determined by high performance liquid chromatography (HPLC) analysis. Furthermore, the activity effects of mushroom extracts on the enzyme glutathione-S-transferase (GST) were also examined. Additionally, the antimicrobial activity of mushroom extracts was evaluated by disc diffusion method.

**Results:** Ethanolic extract of *I. hispidus* demonstrated the highest total phenolic content and total flavonoid contents, with 227.23±4.96 mg gallic acid equivalent/g and 42.14±0.20 quercetin equivalent/g, respectively. The highest DPPH radical scavenging activity was observed for ethanolic extracts of *I. hispidus*, with 10.687±1.643 µg/mL IC<sub>50</sub>. HPLC analysis demonstrated that *R. chloroides* was composed of ferulic acid, gallic acid, and myricetin compounds. The highest GST enzyme activity effect was detected with the ethanol extracts of *I. hispidus* and *S. imbricatus*. None of the mushroom extracts demonstrated significant inhibition of the bacterial strains used.

**Conclusion:** These results indicate that *I. hispidus* may be proposed as a new potential source of natural medicine and its potential may be related to its polyphenolic content, which needs further investigation.

**Key words:** Wild mushrooms, polyphenolic compounds, antioxidant, glutathione-S-transferase, detoxification properties

### ÖZ

**Amaç:** *Ganoderma adspersum*, *Inonotus hispidus*, *Russula chloroides* ve *Sarcodon imbricatus* mantar türlerinin etanolü ekstraktları, polifenolik içerikleri ve biyolojik aktiviteleri açısından araştırılmıştır.

**Gereç ve Yöntemler:** Ekstrelerin radikal süpürücü etkileri 2,2-difenil-1-(2,4,6-trinitrofenil) (DPPH) yöntemi kullanılarak ve polifenolik içerikleri yüksek performanslı sıvı kromatografisi (HPLC) analizleri ile belirlendi. Ayrıca, mantar ekstraktlarının glutatyon-S-transferaz (GST) enzim aktivatör etkisi incelendi. Bunlara ek olarak, mantar ekstraktlarının antimikrobiyal aktivitesi, disk difüzyon yöntemi ile değerlendirildi.

**Bulgular:** *I. hispidus*'un etanol ekstresi sırasıyla 227.23±4.96 mg GAE/g ve 42.14±0.20 QE/g değerleri ile en yüksek toplam fenol ve toplam flavonoid içeriği göstermiştir. DPPH radikalini en yüksek süpürme aktivitesi de *I. hispidus*'un etanol ekstresinde, 10.687±1.643 µg/mL IC<sub>50</sub> değeri ile gözlenmiştir. HPLC analizi, *R. chloroides*'in ferulik asit, gallik asit ve mirisetin bileşiklerini içerdiğini göstermiştir. En yüksek GST enzim aktivatör etkisi *I. hispidus* ve *S. imbricatus*'un etanol ekstraktlarında belirlenmiştir. Mantar ekstraktlarının hiçbirini kullanılan bakteri suşları üzerinde belirgin bir inhibisyon göstermemiştir.

**Sonuç:** Bu sonuçlar, ileri araştırmalar gerektirip *I. hispidus*'un yeni bir potansiyel doğal ilaç kaynağı olabileceğini ve bu etkinin polifenolik içerik ile ilişkili olabileceğini göstermektedir.

**Anahtar kelimeler:** Yabani mantarlar, polifenolik bileşikler, antioksidan, glutatyon-S-transferaz, detoksifikasyon özellikleri

\*Correspondence: E-mail: naznoosh\_shomali@yahoo.com, Phone: +90 554 281 63 36 ORCID-ID: orcid.org/0000-0002-7366-1569

Received: 08.10.2017, Accepted: 25.01.2018

©Turk J Pharm Sci, Published by Galenos Publishing House.



## INTRODUCTION

Recently, exploration of natural sources for novel bioactive compounds has gained considerable attention and it has helped to provide therapeutic drugs and principal compounds. Mushrooms, traditionally known as a valuable source of natural bioactive compounds, have been studied widely for their therapeutic capabilities. Medicinal mushrooms have been proved to contain many biologically active compounds, and many effective drugs and agrochemical fungicides are derived due to secondary metabolites extracted and isolated from mushrooms.<sup>1,2</sup> Some of the most recent isolated and identified compounds from mushrooms have shown promising antiviral, antibacterial, antioxidant, antidiabetic, immunomodulatory, antitumor, and hepatoprotective properties. Moreover, they contain a number of valuable nutrients, including protein, enzymes, B vitamins (especially niacin), and vitamin D.<sup>3,4</sup>

*Ganoderma adspersum* is a species of Basidiomycetes. Several species of *Ganoderma* are rich in bioactive compounds such as triterpenoids and polysaccharides. Traditionally, *Ganoderma* species have been widely used in the treatment of hepatopathy, chronic hepatitis, nephritis, hypertension, arthritis, neurasthenia, insomnia, bronchitis, asthma, and gastric ulcers.<sup>5</sup> They were also investigated for a variety of potential therapeutic benefits such as reducing blood pressure, as well as their blood cholesterol, antioxidant, anticancer, antidiabetic, antiviral, and antibacterial properties.<sup>6-9</sup> Wong et al.<sup>10</sup> demonstrated that extract of *Ganoderma lucidum* prepared in hot water had a protective effect on the cardiovascular system. Their study suggested that it reduces superoxide-induced damage to the heart. Additionally, Çayan-Tel et al.<sup>11</sup> isolated applanoxidic acid G, applanoxidic acid E, applanoxidic acid A, and 22-stigmastenol compounds from *G. adspersum* and investigated the antioxidant and anticholinesterase activities of mushroom extracts and isolated pure compounds. They reported that applanoxidic acid E and 22-stigmastenol showed significant antioxidant activities in the inhibition of lipid peroxidation. The same authors also demonstrated that applanoxidic acid G and 22-stigmastenol compounds exhibited moderate inhibiting activity against the enzyme butyrylcholinesterase.

*Sarcodon imbricatus* (Bankeraceae) is an edible mushroom. It is commonly known as the shingled hedgehog or scaly hedgehog. In folk medicine, it is used for lowering cholesterol levels, relaxing muscles, and regulating blood circulation.<sup>12</sup> Many studies have demonstrated that *S. imbricatus* is a good source of sterol compounds. In previous studies, the compounds ergosterol, ergostane, and cholestane have been isolated from *S. imbricatus*.<sup>13,14</sup> In particular, the presence of ergosterol peroxide in the methanol extract of *S. imbricatus* is important because it shows various biological activities, such as antileukemic, anticancer, apoptotic-inducing, and anti-inflammatory.<sup>15-17</sup>

*Inonotus hispidus* (Hymenochaetaceae) is commonly known as shaggy bracket. It is known as a pathogen on plants. However, it has numerous medicinal properties. In previous studies, the antiviral activity of two phenolic compounds, hispolon and hispidin, which were isolated from the fruit bodies

of *I. hispidus*, was investigated. The results obtained showed that hispidin and hispolon exhibit considerable antiviral activity against influenza viruses type A and B.<sup>18</sup>

*Russula chloroides* is a member of the genus *Russula*, which belongs to the family Russulaceae. Even though there is a high number of species, the biological properties of *Russula* have not been investigated in detail.

Glutathione-S-transferases (GSTs) comprise a phase II metabolic isozyme family existing in both eukaryotes and prokaryotes. These isozymes are best known for their ability to catalyze the conjugation of the reduced form of glutathione (GSH) to xenobiotic substrates for the purpose of detoxification. This eukaryotic species has multiple GST isozymes that are found in the cytosol and membrane. They catalyze the process of glutathione conjugation in electrophilic regions using a sulfhydryl group, which increases the solubility of xenobiotic and endogenous compounds. During this process, endogenous compounds like peroxidase lipids are detoxified together with the disintegration of compounds and xenobiotics.<sup>19,20</sup>

The main aims of this work were to investigate the polyphenolic contents and biological activities of ethanol extracts of several wild mushrooms from the local environment (*G. adspersum*, *I. hispidus*, *R. chloroides*, and *S. imbricatus*). Furthermore, the GST enzyme activity of these mushroom extracts was evaluated for the first time.

## MATERIALS AND METHODS

### Chemical materials

All chemicals used in the study were supplied by Sigma Aldrich (USA), except 1-chloro-2,4-dinitrobenzene (CDNB), which was purchased from Gerbu (Germany), and nutrient broth, malt extract, and malt extract agar, which were obtained from Merck (USA).

### Mushroom materials

Mushroom samples of *G. adspersum*, *I. hispidus*, *R. chloroides*, and *S. imbricatus* were collected from Belgrad Forest, İstanbul, and Yomra, Trabzon. They were identified by Dr. Ilgaz Akata and they are kept at the *Fungarium* of Ankara University with the code numbers Akata 6355, Akata 6052, Akata 5895 and Akata & Yuzun 757.

### Extraction of mushrooms

For ethanol extraction, 10 g of dried samples were weighed and ground into a fine powder with liquid nitrogen, and then mixed with 100 mL of ethyl alcohol (96%) at room temperature for 24 h. The extract obtained was filtered using Whatman No. 1 paper. In the next step, the existing ethanol was removed using a rotary evaporator at 40°C and the remaining solution was lyophilized. Finally, the samples were then kept in dark and cold (4°C) conditions to prevent oxidative damage.<sup>21</sup>

### Determination of total phenolic content

The Folin-Ciocalteu method was used to evaluate the content of total phenolic compounds of mushroom extracts.<sup>22</sup> Each 0.1 mL of extract solution was mixed with 2 mL of a 2% (w/v)

sodium carbonate solution using strong vortexing. After 5 min, 0.1 mL of 50% Folin–Ciocalteu reagent (w/v) was added and the resulting mixture was vortexed and then incubated for 1 h at room temperature. Afterwards, the absorbance of each mixture was measured at 750 nm with a UV-VIS spectrophotometer. The results were evaluated using 0.05, 0.1, 0.15, and 0.2 mg/mL gallic acid (GA) as standard curve and recorded as milligrams of GA equivalent per gram of dried sample.

#### Determination of total flavonoid content

The aluminum chloride colorimetric method was utilized to determine the total content of flavonoids in samples.<sup>23</sup> This test was conducted by mixing 0.1 mL of each extract solution with 0.15 mL of 95% ethanol, 0.01 mL of 10% aluminum chloride, 0.01 mL of 1 M sodium acetate, and 0.25 mL of dimethyl sulfoxide. The mixture was then incubated at room temperature for 30 min and the absorbance of the reaction was measured at 415 nm with a UV-VIS spectrophotometer. Finally, the standard curve was produced using different concentrations of quercetin solutions (0.025, 0.05, 0.1, 0.15, and 0.2 mg/mL). The total flavonoid content of the extract was expressed as milligrams of quercetin equivalent per gram of dried sample.

#### High performance liquid chromatography analysis

The high performance liquid chromatography (HPLC) assay was performed to investigate the phenolic compound profiles of ethanol mushroom extract. For this purpose, a lyophilized sample was dissolved in 2 mL of 80% methanol and then filtered using 0.45 µm cellulose membrane filters before injection. Aliquots of 20 µL were injected into the ultra-performance liquid chromatography system (Shimadzu Nexera X2, Shimadzu Corporation, Kyoto, Japan) equipped with a diode array detector set at 280, 320, and 360 nm. A 250×4.6 mm i.d., 5 µm, C18 ODS-3 column (Intersil) was used. The mobile phase was composed of 5% formic acid (A) and methanol (B) at flow rate of 0.9 mL/min. The elution gradient was 5–80% (B) from 0 to 60 min. Calibration curves for each phenolic standard (the best wavelength) were prepared for quantification. For this purpose, myricetin, quercetin hydrate, ferulic, gallic, vanillic, caffeic, chlorogenic, and p-coumaric acids were used as positive controls. The HPLC analysis was carried out by the Central Laboratory of the General Directorate of the Food and Control Institute.

#### Free radical scavenging activity by DPPH assay

The radical scavenging activities of mushroom extracts were measured according to the methods described by Sharma and Bhat<sup>24</sup> with some modifications. The antioxidant activities of the extracts were determined on the basis of the radical scavenging effect of the DPPH-free radical. According to the procedure, 0.2 mL of mushroom extract at different concentrations was mixed with 0.5 mL of DPPH ethanol solution (0.12 mM) and 0.5 mL of ethanol (96%). Then samples were incubated for 30 min at room temperature and in darkness. Next absorbance was read at 517 nm by UV-VIS spectrophotometer with GA employed as reference. The DPPH radical scavenging activity of each sample was expressed as the half maximal inhibitory concentration

(IC<sub>50</sub>) value and calculated from the dose-response inhibition curve.

#### Isolation of cytosol from bovine liver

The bovine liver used in this study was provided by a slaughterhouse in Kazan, Ankara, Turkey. The liver samples were homogenized in 10 mM potassium phosphate buffer (pH 7.0), containing 0.15 M KCl, 1 mM EDTA, and 1 mM DTT, using a glass Teflon homogenizer and then centrifuged at 10,000×g for 20 min. The supernatant was filtered through cheesecloth and the filtrate was centrifuged at 30,000×g for 60 min. The collected supernatants were filtered again and the resultant filtrate was referred to as cytosol.<sup>25</sup> The prepared homogenates were kept at -80°C for future analysis. Total protein content was determined by the Lowry method.<sup>26</sup>

#### Testing activity of GST

GST activity was determined against the substrate CDNB by monitoring thioether formation at 340 nm.<sup>27</sup> In line with the protocol, an assay mixture composed of mushroom extract solutions (concentration in the range of 10–0.625 mg/mL), 200 mM potassium phosphate buffer (pH 6.5) with 20 mM CDNB and 50 mM GSH, and bovine liver cytosolic fractions was prepared and used as the enzyme source to measure GST activity. GSH-CDNB conjugate formation was followed in 1 mL total volume assay by UV-VIS spectrophotometer at 340 nm for 2 min. Initial rates of enzymatic reactions were determined as nanomoles of the conjugation product of GSH and reported as nmol/min/mL.

#### Antimicrobial assay

The antibacterial activities of mushroom extracts were determined against the gram (+) bacterial strain *Staphylococcus aureus* ATCC 25923 and the gram (-) bacterial strains *Escherichia coli* ATCC 25922 and *Pseudomonas aeruginosa* ATCC 27853 using the disc diffusion method.<sup>28</sup> The bacterial strains were incubated at 37°C in Nutrient Broth culture for 24 h. Inoculants were prepared by transferring colonies of each organism into 0.9% sterile saline solution until the visible turbidity was equal to 0.5 McFarland standard containing approximately 10<sup>8</sup> cfu/mL bacteria. Nutrient Agar was used as culture for antibacterial activities. Afterwards, 0.02 mL of each extract was applied to 6-mm-diameter sterile paper discs and to eliminate any residual solvent the discs were left to dry overnight at room temperature. The surface of the plates was inoculated by using prepared inoculant containing saline suspension of microorganisms. The discs were placed in the center of the agar surface of each petri plate. Zones of inhibition were measured in mm after incubating the petri plates at 30°C for 24 h. For this study, streptomycin (10 mg) and tetracycline (30 mg) were used as positive controls for all samples.

## RESULTS

The ethanol extracts of *G. adpersum*, *I. hispidus*, *R. chloroides*, and *S. imbricatus* were used to investigate their polyphenolic contents and antioxidant and antimicrobial activities. Moreover, for the first time, their effects on GST activity were evaluated. With this research, each extract was prepared by dissolving

10 g of dry samples in 100 mL of ethanol (96%) solvent. The extraction yields of *G. adspersum*, *I. hispidus*, *R. chloroides*, and *S. imbricatus* were in the range of 3.71% to 13%. In addition, total phenolic contents, total flavonoid contents, and radical scavenging activity of the extract were determined using spectrophotometric assays. The percentage of the yields, total phenolic contents, total flavonoid contents, and results of DPPH scavenging activity are shown in Table 1. The total phenolic contents of extracts were 227.23±4.96 to 3.125±0.12 mg GAE/g of the dry samples. The total flavonoid contents varied from 42.14±0.20 to 1.99±0.27 mg QE/g of the dry samples. Phenolic and flavonoid contents of the ethanol extract of *I. hispidus* were 227.23±4.96 mg GAE/g and 42.14±0.20 QE/g, respectively, and these are higher values compared to the other mushroom species. Free radical scavenging activity results are presented as percentage of DPPH radical scavenging activity of different extracts (mg/mL) according to concentration inhibition curves and IC<sub>50</sub> values. The results showed that the highest amount of free radical scavenging activity was in the extracts of *G. adspersum* and *I. hispidus*, with 48.002±0.861 and 10.687±1.643 µg/mL IC<sub>50</sub>, respectively (Figure 1, Table 1). The IC<sub>50</sub> value for GA solution, which was used as a reference, was 4.000±0.002 µg/mL.

**Table 1.** The percent (%) yield, total phenolics content, total flavonoid content, and DPPH results of mushroom extracts

Mushroom	Yield (%)	TPC (mg GAE/g)	TF (mg QE/g)	DPPH IC <sub>50</sub> µg/mL
<i>Inonotus hispidus</i>	3.71	227.23±4.96	42.14±0.20	10.687±1.643
<i>Ganoderma adspersum</i>	6.44	109.20±8.83	13.6±0.22	48.002±0.861
<i>Sarcodon imbricatus</i>	11.88	13.20±0.1	5.45±0.11	950.878±11.418
<i>Russula chloroides</i>	13.00	3.125±0.12	1.99±0.27	2637.709±55.857
Gallic acid	-	-	-	4.000±0.002

DPPH: 2,2-diphenyl-1-(2,4,6-trinitrophenyl), TPC: Total phenolic contain, TF: Total flavonoid

**Table 2.** HPLC analysis of the phenolic profiles of mushrooms extracts

Mushroom	<i>Inonotus hispidus</i>	<i>Ganoderma adspersum</i>	<i>Sarcodon imbricatus</i>	<i>Russula chloroides</i>
	Content of selected polyphenol compound mg/g			
Caffeic acid	-	-	-	-
Chlorogenic acid	-	-	-	-
<i>p</i> -coumaric acid	-	-	-	-
Ferulic acid	-	-	-	4.6020±0.23
Gallic acid	-	-	0.7510±0.04	0.3027±0.02
Myricetin	0.6010±0.03	0.6370±0.03	2.8910±0.15	1.7460±0.09
Quercetin hydrate	-	1.3040±0.07	-	-
Vanillic acid	-	-	-	-

HPLC: High performance liquid chromatography

The phenolic profiles of the ethanol extracts from *G. adspersum*, *I. hispidus*, *R. chloroides*, and *S. imbricatus* were studied by HPLC assay. In this assay, myricetin, quercetin hydrate, ferulic, gallic, vanillic, caffeic, chlorogenic, and *p*-coumaric acids were used as references. According to these results, *R. chloroides* included ferulic acid, GA, and myricetin compounds, with 4.6020±0.23, 0.3027±0.02, and 1.7460±0.09 mg/g values, respectively. Moreover, myricetin was found in all of the ethanol extract solutions. However, none of the extract solutions contained vanillic, caffeic, chlorogenic, or *p*-coumaric acids. The results are given in Table 2.

With this study, it was shown that the *G. adspersum*, *I. hispidus*, *R. chloroides*, and *S. imbricatus* extracts had effects on GST enzyme activity. The extracts were used within the range of 0.625-10 mg/mL concentration while measuring the activity on GST. The best activity profile for GST was observed with the crude ethanol extracts of *I. hispidus* and *S. imbricatus* (Figure 2). The activities of the ethanol extracts of mushrooms are presented in Figure 2.

Moreover, we also demonstrated the antimicrobial activity of *G. adspersum*, *I. hispidus*, *R. chloroides*, and *S. imbricatus* extracts against the *S. aureus*, *E. coli*, and *P. aeruginosa* strains by disc diffusion assay. However, in comparison with the positive

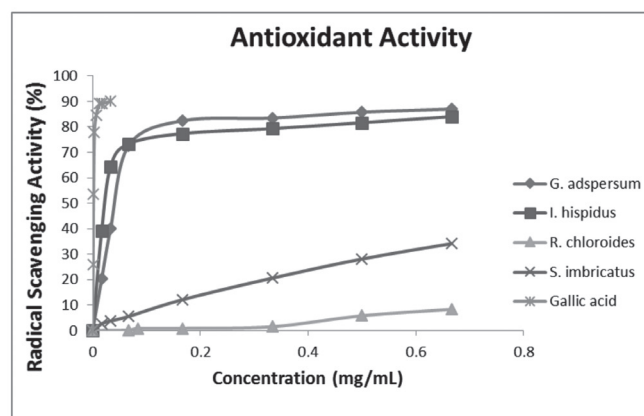


**Figure 1.** Percent free radical scavenging activity of mushroom extracts. The data represent the mean ± standard deviation (n=3)

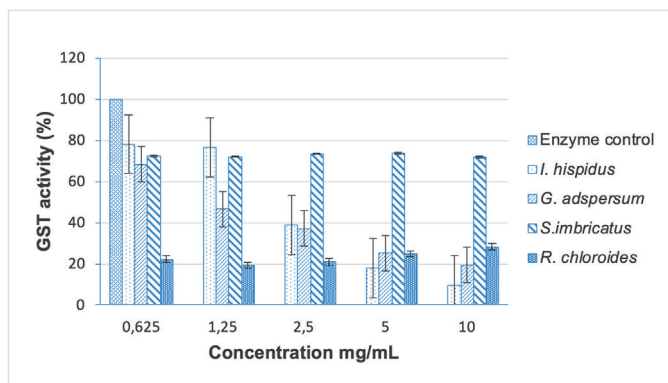


**Figure 2.** Effects of mushroom extracts on glutathione-S-transferase enzyme activity (%). The data represent the mean  $\pm$  standard deviation (n=3)

controls, none of the mushroom extracts showed significant inhibitory effects on the bacterial strains. The results of the disc diffusion assay of mushroom extracts are presented in Table 3.

**Table 3. Results of disc diffusion of mushroom extracts**

Mushroom	<i>Escherichia coli</i> ATCC 25922	<i>Staphylococcus aureus</i> ATCC 25923	<i>Pseudomonas aeruginosa</i> ATCC 27853
	Inhibition zone (mm)		
<i>Inonotus hispidus</i>	10	10	10
<i>Ganoderma adspersum</i>	10	10	8
<i>Sarcodon imbricatus</i>	9	9	9
<i>Russula chloroides</i>	8	8	8
Streptomycin	20	23	15
Tetracycline	13	35	20

## DISCUSSION

In the present study, we found that the ethanol extract of *G. adspersum* contained significant amounts of phenolic and flavonoid compounds. It was also shown that *G. adspersum* extract exhibited significant free radical scavenging effect. Moreover, the ethanol extract from *G. adspersum* included remarkable amounts of myricetin and quercetin hydrate compounds, which have benefits to health. These compounds possess antioxidant and anticancer properties.<sup>29-31</sup> It should also be noted that *G. adspersum* extract revealed weak antimicrobial activity against *S. aureus*, *E. coli*, and *P. aeruginosa* strains. Kuruni et al.<sup>32</sup> evaluated the antioxidant activity of methanol extracts of *G. applanatum* using *in vitro* models. They reported that high amounts of phenolic and flavonoid compounds in the extract were determined and, therefore, the extract exhibited a significant antioxidant capacity in the DPPH radical scavenging assay.

Furthermore, we demonstrated that the ethanol extract from *S. imbricatus* included small amounts of phenolic and flavonoid

compounds; therefore, it showed lower antioxidant and antimicrobial activity profiles. Using the HPLC assay we found that the ethanol extract of *S. imbricatus* also included GA and myricetin compounds. It was highly effective on GST activity at all doses. Marcotullio et al.<sup>33</sup> reported that the methanol extract of *S. imbricatus* contained high amounts of polyphenol contents, which can explain the radical scavenging activity.

In the present study, it was found that the ethanol extract of *I. hispidus* contained high amounts of phenolic and flavonoid contents, which suggests that the high potential effects of free radical scavenging activity may be raised due to the large amounts of polyphenolic profiles. The low dosage of *I. hispidus* extracts showed an elevated effect on GST activity. The ethanol extract of *I. hispidus* also demonstrated a slight antimicrobial effect on the bacterial strains. In another study, the inhibitory effect of phenolic compounds and alkaloids of *I. hispidus* was investigated on the lipase of *Candida rugosa*.<sup>34</sup> It was observed that the phenolic and alkaloid extracts were efficient inhibitors of the lipase of *C. rugosa*. Therefore, it was suggested that these compounds could be used in the treatment of candidiasis. The obtained results also indicated that the phenolic extracts showed stronger radical scavenging activity than the alkaloids extracts.<sup>34</sup>

In our study, *R. chloroides* included very low amounts of polyphenolic contents and showed antioxidant and antimicrobial activities. On the other hand, HPLC analysis showed that the ethanol extract of *R. chloroides* contained remarkable amounts of ferulic acid, myricetin, and GA compounds. However, the effect of this extract on GST enzyme activity was negligible.

## CONCLUSIONS

In the present research, the biological activity and detoxification potential of the polyphenol contents isolated from *G. adspersum*, *I. hispidus*, *R. chloroides*, and *S. imbricatus* species were investigated for their free radical scavenging and GST enzyme activities. It was found that the ethanol extract of *I. hispidus* had large amounts of phenolic and flavonoid contents. It was also observed that this ethanol extract had a high level of free radical scavenging potential. This activity may be attributed to the high concentration of polyphenol compounds in the ethanol extract of *I. hispidus*. Moreover, the ethanol extract of *I. hispidus* had a significant potential to increase GST enzyme activity, which plays a critical role in detoxification pathways. Therefore, *I. hispidus* was suggested to be a new potential source of natural medicine.

## ACKNOWLEDGEMENTS

This work was financially supported by the Coordination of Scientific Research Projects of Ankara University (Research Project No: 16H0430011 and 15H0430001) in Turkey.

*Conflict of Interest:* No conflict of interest was declared by the authors.

## REFERENCES

- De Silva DD, Rapior S, Sudarman E, Stadler M, Xu J, Alias SA, Hyde KD. Bioactive metabolites from macrofungi: ethnopharmacology, biological activities and chemistry. *Fung Diver*. 2013;62:1-40.
- Loria-Kohen V, Lourenco-Nogueira T, Espinosa-Salinas I, Marin FR, Soler-Rivas C, Ramirez de Molina A. Nutritional and functional properties of edible mushrooms: A food with promising health claims. *J Pharm Nutr Sci*. 2014;4:187-198.
- Hansen MB, Jensen ML, Carstensen B. Causes of death among diabetic patients in Denmark. *Diabetologia*. 2012;55:294-302.
- Kozarski M, Klaus A, Jakovljevic D, Todorovic N, Vunduk J, Petrović P, Niksic M, Vrvic MM, Van Griensven L. Antioxidants of Edible Mushrooms. *Molecules*. 2015;20:19489-19525.
- Liu GT. Recent advances in research of pharmacology and clinical applications of *Ganoderma* (P. Korst.) species (Aphyllphoromycetideae) in china. *IJ of Med Mushrooms*. 1999:63-67.
- Smina TP, Mathew J, Janardhanana KK, Devasagayam TP. Antioxidant activity and toxicity profile of total triterpenes isolated from *Ganoderma lucidum* (Fr.) P. Karst occurring in South India. *Environ Toxicol Pharmacol*. 2011;32:438-446.
- Vazirian M, Dianat S, Manayi A, Ziari R, Mousazadeh A, Habibi E, Saeidnia S, Amanzadeh Y. Anti-inflammatory effect, total polysaccharide, total phenolics content and antioxidant activity of the aqueous extract of three basidiomycetes. *Res J of Pharma*. 2014;1:15-21.
- Rajoriya A, Tripathy SS, Gupta N. *In vitro* antioxidant activity of selected *Ganoderma* species found in Odisha, India. *Trop Plant Res*. 2015;2:72-77.
- Ivone HA, Jorge MT, Guadalupe GRM, Berenice YJ. Total Polyphenols and Antioxidant Activity of *Ganoderma curtisii* extracts. *J of Med Plants Studies*. 2016;4:136-141.
- Wong KL, Chao HH, Chan P, Chang LP, Liu CF. Antioxidant Activity of *Ganoderma lucidum* in Acute Ethanol-induced Heart Toxicity. *Phytother Res*. 2004;18:1024-1026.
- Çayan-Tel G, Öztürk M, Duru ME, Rehman MU, Adhikari A, Türkoğlu A, Choudhary MI. Phytochemical investigation, antioxidant and anticholinesterase activities of *Ganoderma adspersum*. *Indust Crops and Prod*. 2015;76:749-754.
- Kim SK. Method for making seasoned pork ribs by using *Sarcodon aspratus* and *Acanthopanax senticosus* broth for aging pork ribs. Patent KR. 2006:128485.
- Ueno T, Yaoita Y, Kakuda R, Machida K, Kikuchi M. Studies on the constituents of mushrooms. VII. On the sterol constituents from the fruit bodies of *Sarcodon aspratus*. *J of Tohoku Pharma Uni*. 1999;46:71-76.
- Yue H, Zejun D, Jikai L. Chemical constituents from the basidiocarp of *Sarcodon aspratum*. *Acta Botanica Yunnanica*. 2002;24:125-128.
- Takei T, Yoshida M, Ohnishi-Kameyama M, Kobori M. Ergosterol peroxide, an apoptosis-inducing component isolated from *Sarcodon aspratus* (Berk.) S. Ito. *Biosci Biotechnol Biochem*. 2005;69:212-215.
- Kobori M, Yoshida M, Ohnishi-Kameyama M, Takei T, Shinmoto H. 55alpha,8alpha-Epidoxy-22E-ergosta-6,9(11),22-trien-3beta-ol from an edible mushroom suppresses growth of HL60 leukemia and HT29 colon adenocarcinoma cells. *Biol Phar Bull*. 2006;29:755-759.
- Kobori M, Yoshida M, Ohnishi-Kameyama M, Shinmoto H. Ergosterol peroxide from an edible mushroom suppresses inflammatory responses in RAW264.7 macrophages and growth of HT29 colon adenocarcinoma cells. *Br J Pharmacol*. 2007;150:209-219.
- Awadh Ali NA, Mothanaa RA, Lesnau A, Pilgrim H, Lindequist U. Antiviral activity of *Inonotus hispidus*. *Fitoterapia*. 2003;76:483-485.
- Sheehan D, Meade G, Foley VM, Dowd CA. Structure, function and evolution of glutathione transferases: implications for classification of non-mammalian members of an ancient enzyme superfamily. *Biochem J*. 2001;360:1-16.
- Nebert DW, Vasiliou V. Analysis of the glutathione-S-transferase (GST) gene family. *Human Genomics*. 2004;1:460-464.
- Onar O, Akata I, Celep GS, Yildirim O. Antioxidant Activity of Extracts from the Red-Belt Conk Medicinal Mushroom, *Fomitopsis pinicola* (Agaricomycetes), and Its Modulatory Effects on Antioxidant Enzymes. *Int J Med Mushrooms*. 2016;18:501-508.
- Slinkard K, Singleton VL. Total phenol analyses: Automation and comparison with manual methods. *Am J Enol Vitic*. 1977;28:49-55.
- Chang CC, Yang MH, Wen HM, Chern JC. Estimation of total flavonoid content in propolis by two complementary colorimetric methods. *J Food Drug Anal*. 2002;10:178-182.
- Sharma OP, Bhat TK. DPPH antioxidant assay revisited. *Food Chem*. 2009;113:1202-1205.
- Moghaddam NS, Isgor BS, Isgor YG, Geven F, Yildirim O. The Evaluation of Inhibitory Effects of Selected Plant Extracts on Antioxidant Enzymes. *Fresenius Environ Bull*. 2015;4:63-70.
- Lowry OH, Rosebrough NJ, Farr AL, Randall RJ. Protein measurement with the Folin phenol reagent. *J Biol Chem*. 1951;193:265-275.
- Habig WH, Pabst MJ, Jakoby WB. Glutathione-S-transferases the first enzymatic step in mercapturic acid formation. *J Biol Chem*. 1974;249:7130-7139.
- Silici S, Koc AN. Comparative study of *in vitro* methods to analyse the antifungal activity of propolis against yeasts isolated from patients with superficial mycoses. *Lett Appl Microbiol*. 2006;43:318-324.
- Kandaswami C, Lee LT, Lee PP, Hwang JJ, Ke FC, Huang YT, Lee MT. The antitumor activities of flavonoids. *In Vivo*. 2005;19:895-909.
- Chirumbolo S. The role of quercetin, flavonols and flavones in modulating inflammatory cell function. *Inflamm Aller Drug Targets*. 2010;9:263-285.
- Yao Y, Lin G, Xie Y, Ma P, Li G, Meng Q, Wu T. Preformulation studies of myricetin: a natural antioxidant flavonoid. *Pharmazie*. 2014;69:19-26.
- Kuruni N, Mallikarjun N, Naika R, Venugopal TM. Antioxidative Activities of Wild Macro Fungi *Ganoderma applanatum* (PERS.) PAT. *Asian J Pharm Clin Res*. 2014;7:166-171.
- Marcotullio MC, Oball-Mond Mwankie GN, Cossignani L, Tirillini B, Pagiotti R. Phytochemical analysis and antiradical properties of *Sarcodon imbricatus* (L.:Fr) Karsten. *Natu Prod Commun*. 2008;3:1907-1910.
- Benarous K, Bombarda I, Iriepea I, Moraleta I, Gaetan H, Linari A, Tahri D, Sebaa M, Yousfi M. Harmaline and hispidin from *Peganum harmala* and *Inonotus hispidus* with binding affinity to *Candida rugosa* lipase: *In silico* and *in vitro* studies. *Bio Chem*. 2015;62:1-7.



# Study of the Tableting Properties of MCR, a Newly Coprocessed Cellulose-based Direct Compression Excipient

## Yeni Koproses Selüloz Bazlı Doğrudan Basım Yardımcı Maddesi Olan MCR'nin Tabletleme Özelliklerinin İncelenmesi

Salah ALY\*

Al Jouf University, Pharmacy College, Department of Pharmaceutics, Sekake, Saudi Arabia  
Present Address: Chemical Industries Development, Cid, Assiut Branch, Assiut, Egypt

### ABSTRACT

**Objectives:** In this work, the aim was to coprocess and evaluate a new cellulose-based direct compression tableting excipient (MCR) of improved functionalities by granulation and slugging from locally extracted microcrystalline cellulose and regenerated cellulose (CRC).

**Materials and Methods:** Model tablet formulations of metronidazole (MZ) as a model of nonfreely flowing and directly incompressible active pharmaceutical ingredient were designed to study the tableting properties of MCR.

**Results:** The results showed that the optimum concentration of CRC needed to produce excipient of accepted flow properties and high compression characteristics was 20% w/w. MCR performed better than the parent components either singly or in a simple binary mixture. MZ tablets of enhanced mechanical properties and fast disintegrating and dissolving rates were compressed from MCR. The crushing strength (H) and the disintegration rate constant ( $k_d$ ) increased from 3.76 to 11.08 kg and from 0.92 to  $13.1 \times 10^{-3} \text{ s}^{-1}$  for the tablets made with 50% w/w MCR, respectively.

**Conclusion:** Both the H and  $k_d$  values of a given MZ tablet batch were found to be functions of the total number of bonding sites ( $\alpha$ ) available in the excipient in the given batch. MCR was unfortunately sensitive to magnesium stearate. The obtained result revealed that MCR is a successful complementary direct compression excipient.

**Key words:** Microcrystalline cellulose, regenerated cellulose, MCR co-processing, MCR tableting properties

### ÖZ

**Amaç:** Bu çalışmada, lokal olarak ekstrakte edilmiş mikrokristal selülozdan ve rejenere selülozdan (CRC) granülasyon ve slugging ile gelişmiş işlevsellikli yeni selüloz bazlı doğrudan basım tabletleme yardımcı maddesini (MCR) koprosesini ve değerlendirmeyi amaçladık.

**Gereç ve Yöntemler:** Serbest akmayan ve dolaylı olarak sıkıştırılabilir bir aktif farmasötik bileşen modeli olarak metronidazolün (MZ) model tablet formülasyonları, MCR'nin tabletleme özelliklerini incelemek için tasarlanmıştır.

**Bulgular:** Kabul edilen akış özellikleri ve yüksek sıkıştırma özelliklerindeki yardımcı maddeyi üretmek için gereken optimum CRC konsantrasyonunun, %20 (a/a) olduğunu göstermiştir. MCR, bileşenlerin tek başına veya basit bir ikili karışım içerisinde olmasından daha iyi performans göstermiştir. MCR ile geliştirilmiş mekanik özelliklere ve hızlı dağılma ve çözünme hızlarına sahip olan MZ tabletleri basılmıştır.

**Sonuç:** Kırma dayanımı (H) ve dağılma hız sabiti ( $k_d$ ), %50 a/a MCR ile yapılan tabletler için sırasıyla 3.76'dan 11.08 kg'a ve 0.92'den  $13.1 \times 10^{-3} \text{ s}^{-1}$ 'e yükselmiştir. Belirli bir MZ tablet partisinin hem H hem de  $k_d$ 'sinin, verilen partideki yardımcı maddenin içinde mevcut olan toplam bağlanma bölgesi sayısının ( $\alpha$ ) fonksiyonu olduğu bulunmuştur. MCR ne yazık ki magnezyum stearata karşı duyarlıydı. Elde edilen sonuç, MCR'nin başarılı bir tamamlayıcı doğrudan basım yardımcı maddesi olduğunu ortaya koymuştur.

**Anahtar kelimeler:** Mikrokristal selüloz, rejenere selüloz, MCR koproses, MCR tabletleme özelliği

\*Correspondence: E-mail: sasalytout@hotmail.com, Phone: 002 010 264 70816 ORCID-ID: orcid.org/0000-0003-3108-6209

Received: 14.09.2017, Accepted: 08.02.2018

©Turk J Pharm Sci, Published by Galenos Publishing House.

## INTRODUCTION

The coprocessing technique has been utilized to develop excipients of improved and/or desired functionalities. The technique is defined as the concept of two or more excipients interacting physically at the subparticle level to provide a synergy of functionality and improvements as well as masking the undesirable properties of individual excipients.<sup>1</sup> It provides a broad platform for the manipulation of excipient functionality or particle engineering of two or more existing excipients.<sup>2,3</sup> Silicified microcrystalline cellulose (MCC) (Prosolve), Cellactose, and Avicel CE-15 are commercially available coprocessed excipients that have improved flow and consolidation properties.<sup>4-10</sup> Controlling particle size and particle-size distribution as coprocessing means were used to produce excipients of improved flow with no need to add glidants.<sup>5-7</sup> However, cases of some coprocessed powders with enhanced mechanical properties but having similar particle-size distribution of the parent powders were reported.<sup>4-10</sup>

One of the major limitations challenging the coprocessing technique is the fixed ratio of the excipients in a coprocessed mixture, which may not be an optimum choice for the active ingredient(s) and the dose for a formulation under development.<sup>11</sup> MCC tableting properties are close to optimal. The excipient has high degrees of compressibility and compactibility, and high dilution potential. However, the bad flow properties and the sensitivity to magnesium stearate (MS) are the main drawbacks of this excipient.<sup>12</sup> Cellulose regenerated (RC) from microfibril showed high physicochemical and tableting properties.<sup>13</sup> Ahmad<sup>14</sup> reported that RC has glidant activity. Rojas et al.<sup>15</sup> found that RC has strong disintegration activity. Due to its large specific surface area, RC was successfully employed with olive oil to produce Dis-Lub-Tout, a newly coprocessed tablet excipient of bifunctional activity.<sup>16,17</sup>

Metronidazole (MZ) is an antimicrobial agent effective against anaerobic bacteria and protozoa. It is primarily used to treat bacterial vaginosis, pelvic inflammatory disease, wounds, intraabdominal infections, trichomoniasis, and infections caused by susceptible anaerobic organisms. Tablets are the commonly used dosage form of this drug.<sup>18</sup> Trials were conducted to coprocess excipients to manufacture direct compression MZ tablets.<sup>19,20</sup>

Our objective in this work was to coprocess and evaluate the tableting properties of cellulose-based direct compression tableting excipient (MCR), a new cellulose-based tableted excipient produced from the granules of colloidal microcrystalline cellulose (CMCC)/regenerated cellulose (CRC) slugs. CMCC was locally extracted from the dried leaves and hollow stems of the common reed plant [*Phragmites australis* (Gramineae)] and was used to prepare CRC. Metronidazole, a model of nonfreely flowing incompressible active pharmaceutical ingredient (API) powder, was employed to evaluate the tableting properties of MCR.

## MATERIALS AND METHODS

### *Materials*

Dried leaves and hollow stems of the common reed plant were collected from different areas near water resources and sewages in the town of Assiut (upper Egypt) at harvest time (March-June). Analytical-grade chemicals, namely absolute ethanol and sodium hydroxide pellets given by Krishna Chemicals, Mumbai-40078, Maharashtra, and 98% sulfuric acid obtained from Scharalab, S.L., Gato Prez, Spain, were used in this investigation. Metronidazole (Provizer Pharma, India), a model of nonfreely flowing incompressible API, and MS, the commonly used tablet lubricant (Scharalab, S.L., Gato Prez, Spain), were employed in this investigation.

### *Methods*

#### *CMCC and CRC processing*

The collected plant material was thoroughly examined and the decayed parts were discarded. The selected parts were thoroughly washed, dried, and ground using a suitable grinder. A 500-g sample of the powdered plant material was boiled in 2% sulfuric acid for 2 h to destroy the lignin content in order to separate the cellulose fibers. The acid and the acid soluble materials were filtered out and the collected solid material was washed to remove the acid, neutralized, and boiled in 12% sodium hydroxide solution for 4 h to completely get rid of the lignin. The solid material was thoroughly washed to remove the alkali, neutralized, and subjected to acid hydrolysis by boiling in 3 L of 10% sulfuric acid solution for 3 h to produce CMCC. The yield was thoroughly washed to remove the acid, neutralized, and bleached by boiling in 3 L of 6% sodium hypochlorite for 2 h. The CMCC was thoroughly washed with distilled water, neutralized, dried, pulverized, and stored in a screw-capped brown powder bottle until use. A 100-g sample of CMCC was suspended in 300 mL of 20% sodium hydroxide solution. The suspension was frozen at  $-28^{\circ}\text{C}$  for 12 h to dissolve the cellulose. The frozen cellulose solution was kept at room temperature ( $25\pm 2^{\circ}\text{C}$ ) for 18 h. CRC precipitated with 1 N sulfuric acid solution was thoroughly washed with distilled water, neutralized, dried, pulverized, and stored at room temperature ( $25\pm 2^{\circ}\text{C}$ ) in screw-capped brown powder bottles until use.

#### *Infrared characterization of cellulose powders*

The infrared (IR) spectra of authentic MCC sample and samples of CMCC and CRC powders were run using the technique described by Rojas et al.<sup>21</sup> In this technique, 1 mg of a given sample was mixed with 100 mg of KBr in an agate mortar. Pellets of this mixture were prepared on a portable press (CrushIR Digital Hydraulic Press 161-1900, PIKE, Madison, WI, USA) at a dwell time of 5 min and at a force of 4540 kg. The infrared spectra were run between 650 and 4000  $\text{cm}^{-1}$  using a PerkinElmer IR spectrometer (Spectrum BX, PerkinElmer, San Jose, CA, USA) equipped with the software Ommic (Nicolet Corp., Madison, WI, USA). The resolution and interval length were 16 and 2  $\text{cm}^{-1}$ , respectively, and the number of scans employed was 16  $\text{cm}^{-1}$ .

### *Physical properties of cellulose and MZ powders*

#### *Particle shape and effective mean particle diameter*

The shapes of CMCC and CRC particles were characterized by scanning electron microscopy (SEM) (BM-180, Bo-eco, GmbH, Frankfurt, Germany) attached to a digital camera (S8000fd, Fujifilm Corp., Japan). A suitable volume of the given powder sample was mounted in the specimen stub of the SEM for microphotographing (no sputtering was noticed). The effective mean diameters of CMCC and MZ particles were determined by the sieving technique using a set of stainless steel sieves (Fritsch, GmbH, FRG) arranged in descending order as described earlier.<sup>16</sup> The effective mean diameter of CRC particles was determined using a size analyzer (Brookhaven Instruments Corp., Holtsville, NY, USA) equipped with default particle sizing software (ver. 3.74). A sample of dilute CRC/water suspension was used for the test. The refractive index of the sample was 1.33, while the beam angle and the wavelength were 90° and 678 nm, respectively.

#### *Flow properties, density, and moisture content determinations of powders*

The funnel technique was employed to determine the volumetric flow rates and repose angles of the powders under investigation. The apparent density,  $\rho_a$ , of a given powder was determined using the liquid displacement technique. The bulk,  $\rho_B$ , and tap,  $\rho_T$ , densities and packing fraction,  $q_f$ , were determined using earlier reported techniques.<sup>16</sup> The mean of five determinations of each experiment was calculated and taken as the determined value. The moisture content (dry weight basis) was determined by drying technique as described earlier.<sup>16</sup>

#### *Moisture sorption isotherm study*

The moisture sorption isotherm exhibited by MCR was studied and compared with that of the parent components. For the test, accurately weighed 1-g samples of MCR CRC, and CMCC were stored on a shelf in ambient conditions [25±2°C - relative humidity (RH) 45±2%] and at 40°C - RH 75%. The RH% conditions were achieved using a saturated solution of sodium chloride. A Gallenkamp humidity oven (Gallenkamp, London, United Kingdom) was employed for the test. At a predetermined time interval, a sample of a stored powder was evaluated for the amount of adsorbed moisture (dry weight basis).

#### *Swelling index and hydration capacity determinations*

The swelling index (SI) of a given cellulose powder was determined as follows:<sup>16</sup> an accurately weighed 1-g sample of the given cellulose powder was suspended in 25 mL of distilled water and vigorously shaken at 10-min time intervals for 1 h. The suspension was equilibrated for 24 h and the volume occupied by the powder under the test was precisely determined. SI was calculated from:  $SI = \frac{v - v^0}{v^0} \times 100$ , where  $v$  and  $v^0$  stand for the volumes of the test powder sample before and after the test, respectively. The mean of such 5 determinations was taken as the SI of the given powder. The hydration capacity (HC) of a given cellulose powder was measured as follows: a 2-g sample of a given powder was suspended in 10 mL of distilled water in a centrifuge tube and shaken intermittently for 2 h. The tube was

left to stand for 30 min and centrifuged at 3000 rpm for 10 min. HC was calculated from the weight ( $w$ ) of the powder before the test as  $HC = \frac{w - 2}{2} \times 100$  as reported earlier.<sup>16</sup> The mean of 5 such determinations was taken as the HC of the given powder

#### *MCR coprocessing*

Binary mixtures of CMCC/CRC containing varying portions of CRC were prepared using a laboratory assembled 0.75-kg capacity drum mixer. The preliminary tests carried out showed that the optimum concentration of CRC needed to produce a mixture of improved flow properties (flow rate and repose angle) was 20% w/w (1 part CRC to 4 parts CMCC). A batch of 500 g of this physical mixture was prepared and employed to coprocess MCR as follows. The mixture was placed into a porcelain mortar of suitable capacity and kneaded with a sufficient volume (400 mL) of absolute ethanol. The damp mass was forced through a 350- $\mu$ m-mesh sieve and the resulting granules were dried at 50°C for 6 h using a Binder oven (FRG). The granules were placed on a tray and put into the oven. The obtained dried granules were equilibrated at room conditions for 24 h. Although the fourier-transform infrared spectroscopy technique to test for the residual alcohol in pharmaceutical solids is limited by the high detection limit (above 100 ppm), it was decided to employ it using the above-mentioned method and equipment to test for residual alcohol in the prepared granules since the allowed limit for residual ethanol in pharmaceutical solids is high (5000 ppm).<sup>22</sup> The IR spectrum run showed that the produced granules were alcohol-free. The produced granules were compressed into large slugs using a single punch tableting machine (F3, Manesty Machines Ltd., Liverpool, UK). The machine settings were adjusted to produce slugs of 5-g mean weight and of the highest tensile strength that could be achieved. The machine was manually run and the surfaces of the punches were frequently cleaned of sticky powder. The produced slugs were crushed using a laboratory oscillating granulator and sifted through a 90- $\mu$ m-mesh sieve. The obtained MCR powder was stored at room temperature (25±2°C) in a screw-capped wide mouth brown powder bottle until use.

#### *Characterization of MCR*

The flow rate, repose angle, packing fraction,  $q_f$ , and density (apparent, bulk and tap) of MCR were determined using the above-mentioned techniques. The moisture content, swelling index, and hydration capacity determinations were also carried out employing the above-mentioned methods.<sup>16</sup> The mean of 5 determinations of each experiment was calculated and taken as the determined value.

#### *Formulation, compression, and evaluation of MZ tablets*

A simple mixing technique was adopted to prepare MZ tablets. Tablets batches formulated with 20%, 30%, 50%, and 75% w/w of a given excipient were prepared. Lubrication was carried out just before compression. Tablets were compressed using a Manesty single punch tableting machine fitted to flat faced punches adopting the modified compression technique.<sup>17</sup> The machine was adjusted to compress tablets of 250±0.05 mg



mean weight,  $9.0 \pm 0.02$  mm mean diameter, and of the highest crushing strength, H, and lowest friability, F, levels that could be achieved from the batch formulated with 75% w/w (the highest concentration) of a given excipient. The machine settings were kept constant throughout compressing the rest of the batches formulated with the lower concentration of the given excipient. Altogether 1000 tablets were compressed from each batch. The machine settings were readjusted whenever formulations of a new excipient were compressed. The produced tablets were evaluated for uniformity of weight and thickness, mechanical properties, (H, F, and porosity,  $\epsilon$ ), and disintegration times (Dt).

#### Determination of H, $\epsilon$ , and F of MZ tablets

A digital recording hardness tester, Erweka TBH-28 (Erweka, Darmstadt, Germany), was used to determine the mean crushing strength of a given MZ tablet batch. For the test, a sample of 10 tablets was randomly collected from a given batch. The tablets were individually tested for crushing strength and the mean was calculated and taken as the crushing strength of the given batch.  $\epsilon$  of a given tablet batch was calculated from the relation  $\epsilon = (v_t - v_o)/v_o$ , where  $v_t$  and  $v_o$  equal the tablet volume and the true volume(s) of the powder (s) in the given tablet batch. The mean of five calculations was considered the porosity of the given tablet batch. F of a MZ tablet batch was determined using a Roche friabilator (Erweka, Darmstadt, Germany). A sample of 20 tablets randomly collected from the given batch was brushed free of adhering dust and precisely weighed and placed into the friabilator drum. The apparatus was adjusted to revolve at 25 rpm for 4 min. At the end of the test, the tablets were rebrushed and precisely reweighed. The percent loss in weight was calculated as F of the tablets. The mean of such five determinations was used as F of the tested MZ tablet batch.

#### Determination of Dt and $k_d$ of tablets

Neutral buffer solution of pH 7.2 was employed to carry out the disintegration and dissolution rate determination tests. This was to exclude the effect of pH of the medium on the disintegration and dissolution rates.

#### Determination of Dt of tablets

A USP disintegration test apparatus (ZT 220, Erweka, Darmstadt, Germany) was employed to determine the disintegration times of the compressed tablets. A sample of 6 tablets randomly selected from a given MZ batch was used in this investigation. Each tablet was accurately weighed and placed into a disintegration tube of the apparatus. The time when the fragments of the tested tablet completely passed through the screen mesh at the base of the disintegration tube was recorded as the Dt. The mean of such 10 determinations was calculated as the Dt of a given MZ batch.

#### Study of dissolution behavior of MZ tablets

A rotating basket USP dissolution rate test apparatus (model DT-D, Erweka, Germany) was employed to determine the dissolution rate of MZ tablets in 900 mL of 7.2 buffer solution. All the USP requirements for dissolution rate test were kept constant. The

test was carried out at  $37 \pm 0.5^\circ\text{C}$ . A sample of 6 tablets randomly collected from a given batch was employed to carry out the test. For the test, one tablet was precisely weighed and placed into the basket of the apparatus. The revolution of the basket was adjusted to 100 rpm. At a predetermined time interval accommodated with the disintegration time of the batch under the test, a 5-mL aliquot sample was withdrawn from the dissolution chamber and was immediately substituted by an equal volume of freshly prepared dissolution medium maintained at  $37 \pm 0.5^\circ\text{C}$ . The amount of MZ in the withdrawn sample was determined spectrophotometrically at 340 nm with reference to a calibration curve constructed using a pure MZ sample as used in the formulation. The mean of such 6 determinations was taken as a point on the dissolution curve.

#### Study of MCR sensitivity against MS

The effects of lubrication with 1.0%, 1.5%, and 3% w/w of MS on the H, F, and Dt values of the MZ tablet batch formulated with 75% w/w of MCR were studied.

## RESULTS

#### IR characterization of CMCC and CRC

The IR spectra of MCC and CRC powders given in Figure 1 show the following characteristic vibration peaks of cellulose: 3445/cm corresponding to intramolecular OH stretching, including hydrogen bonds; 2898/cm due to CH and  $\text{CH}_2$  stretching; 1650/cm corresponding to OH from absorbed water; 1430/cm due to  $\text{CH}_2$  symmetric bending; 1375/cm due to CH bending; 1330/cm due to OH in-plane bending; 1161/cm due to C-O-C asymmetric stretching ( $\beta$ -glucosidic linkage); 1061/cm due to C-O/C-C stretching; and 898/cm corresponding to the asymmetric (rocking) C-1 ( $\beta$ -glycosidic linkage) out-of-plane stretching vibrations. No new peaks were seen in the spectra, suggesting that CMCC and CRC are chemically similar to microcrystalline cellulose.

#### Physical properties of cellulose and MZ powders

Figure 2 shows that CMCC and CRC particles were morphologically similar. They were elongated and amorphous particles. Table 1

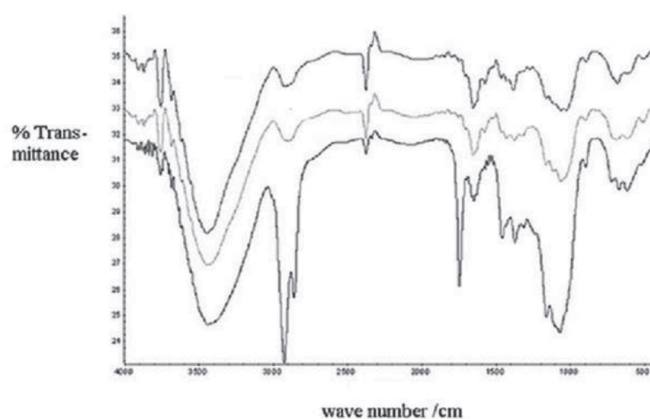


**Figure 1.** IR spectra for MCC (upper curve), CRC (middle curve), and CMCC (lower curve)

MCC: Microcrystalline cellulose, CRC: Regenerated cellulose, CMCC: Colloidal microcrystalline cellulose, IR: Infrared

shows that their effective mean particle diameters were 90 and 3  $\mu\text{m}$ , respectively. Such elongated particles have a tendency to intermesh and create internal resistance against the flow of the powder.<sup>12</sup>

Table 1 also shows that the moisture contents and SI and HC values of the studied powders were high. Figure 3 shows that the investigated excipients exhibited more or less equal moisture sorption isotherm patterns.

#### Physical properties of MZ tablets

##### Uniformity of MZ tablets

The data in Table 2 show that more uniform MZ tablets were compressed with CRC followed by MCR and CMCC, in that order. The uniformity generally increased (estimated by the decrease in % CV) as the concentration of the excipient in an examined tablet batch increased. Powder metallurgy (PM) produced nonuniform tablets due to the segregation observed during compression.

##### Mechanical properties of MZ tablets

##### Compressibility and compactibility of excipients

The yield value obtained from the Heckel<sup>23</sup> plot and the energy consumption during compression determined from the force-displacement plot<sup>24</sup> are usually parameters used to measure powders' compressibility. In this investigation since a given tablet

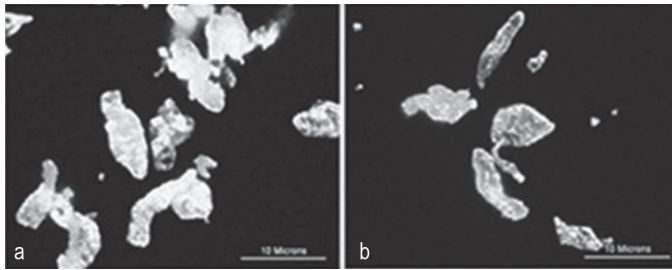


Figure 2. Microphotographs for a) CMCC, and b) CRC

CMCC: Colloidal microcrystalline cellulose, CRC: Regenerated cellulose

formulation was compressed under confined machine settings, it follows that the number of sites available for bonding in a given concentration of an excipient in a formulation is the sole working parameter. In other words, the mechanical properties of the excipient in the given formulation are excipient concentration dependent factors. An excipient concentration-displacement plot was constructed (see Figure 4a) and the area under the curve (AUC) was taken as a parameter indicative of the compressibility of a studied excipient. The compressibility index,  $k_c$ , of an excipient in a given formulation was calculated from the relation;

$$\varepsilon = \varepsilon^0 \exp. - k_c C$$

where  $\varepsilon$  and  $\varepsilon^0$  stand for the porosity fractions for compacts made from a given excipient and the lubricated drug only (control tablets batch) (see Figure 4b), respectively. On the other hand, Figure 4c was constructed to calculate the compactibility index,  $k_p$ , of the given excipient. It was calculated from the relation;

$$H = H^0 \exp. k_p C$$

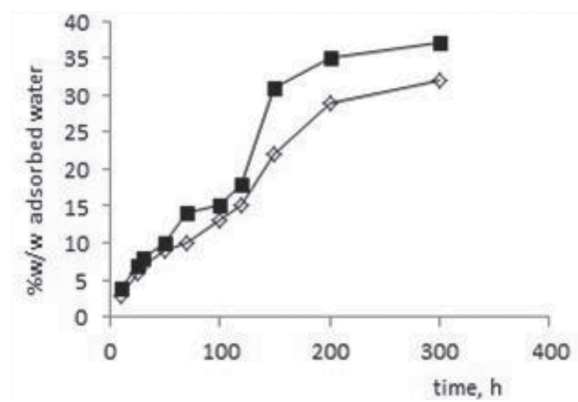


Figure 3. Moisture sorption isotherm exhibited by MCR stored at  $\square$ , ambient condition and at  $\blacksquare$ , 40°C-75% RH

MCR: Cellulose-based direct compression tableting excipient, RH: Relative humidity

Table 1. Physical properties of metronidazole and the investigated cellulose powders

Drug and excipient used	Mean part diam $\mu\text{m}$	Flow rate $\text{g s}^{-1} \pm \text{SD}$	Repose angle degree $\pm \text{SD}$	Density ( $\text{g/cm}^{-3}$ )			Moist contact $\%w/w \pm \text{SD}$	Packing fraction of $\% \text{ calculated}$	Compressibility index $\%$	Hausner ratio (h)	Surface area $\text{m}^2\text{g}^{-1} \times 10^{-2}$ calculated	Hydration capacity $\text{g/g} \pm \text{SD}$	Swell index $\text{g/g} \pm \text{SD}$
				App $\pm \text{SD}$	Bulk $\pm \text{SD}$	Tap $\pm \text{SD}$							
MZ	90	0.11 (0.03)	40 (2.11)	1.5 (0.34)	0.90 (0.11)	1.30 (0.31)	3.50 (0.34)	59	31	1.44	6.5	-	-
CMCC	90	0.21 (0.10)	42 (4.30)	1.50 (0.76)	0.91 (0.18)	1.32 (0.52)	4.76 (0.19)	61	31	1.45	8.2	2.31 (0.41)	1.50 (0.33)
CRC	3	1.20 (0.05)	38 (6.70)	1.52 (0.32)	0.28 (0.27)	0.41 (0.13)	6.4 (0.08)	18	32	1.46	132.0	2.87 (0.65)	1.75 (0.53)
MCR	-	0.94 (0.09)	38 (3.92)	1.62 (0.18)	0.78 (0.20)	1.25 (0.16)	5.38 (0.54)	48	38	1.60	-	2.67 (0.34)	1.73 (0.22)
PM	-	0.52 (0.06)	40 (2.43)	1.65 (0.25)	0.71 (0.31)	1.28 (0.11)	5.11 (1.10)	43	45	1.64	-	2.61 (0.24)	1.66 (0.19)

SD: Standard deviation, MZ: Metronidazole, CMCC: Colloidal microcrystalline cellulose, CRC: Regenerated cellulose, MCR: Cellulose-based direct compression tableting excipient, PM: Powder metallurgy

**Table 2. Physical properties of metronidazole tablets compressed directly with increasing concentrations of the named cellulose excipients**

Excipient used	Concentration % w/w	Weight (g)		Thickness (cm)		Friability, (Loss % w/w)	
		Mean	CV %	Mean	CV %	Mean	CV %
CMCC	20	0.2502	9.1	0.360	2.4	0.23	11.5
	30	0.2533	12.2	0.351	5.5	0.37	14.2
	50	0.2603	16.4	0.343	3.2	0.41	3.1
	75	0.2696	8.2	0.336	2.1	0.49	1.1
MCR	20	0.2521	2.2	0.356	1.6	0.18	8.1
	30	0.2576	6.1	0.341	12.4	0.25	3.8
	50	0.2651	4.9	0.332	12.4	0.31	1.1
	75	0.2708	1.5	0.326	12.4	0.38	6.1
CRC	20	0.2517	4.7	0.362	6.4	0.18	6.3
	30	0.2571	3.2	0.357	9.2	0.31	3.4
	50	0.2599	1.3	0.352	12.6	0.39	7.2
	75	0.2601	0.8	0.330	14.8	0.48	1.9
PM	20	0.2500	49.2	0.359	11.6	0.43	9.8
	30	0.2276	36.1	0.211	12.4	0.95	3.8
	50	0.2151	14.9	0.212	12.4	1.91	1.1
	75	0.2208	35.5	0.216	12.4	4.38	6.1

CMCC: Colloidal microcrystalline cellulose, MCR: Cellulose-based direct compression tableting excipient, CRC: Regenerated cellulose, PM: Powder metallurgy

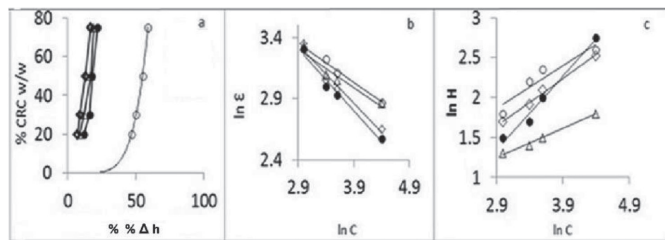


**Figure 4.** a) The reduction in tablet height as a function of % MCR concentration, C; b)  $\ln \epsilon$  vs C; and c),  $\ln H$  vs C. Key:  $\diamond$ , MCC;  $\Delta$ , CMCC;  $\bullet$ , CRC, and  $\square$ , MCR

MCR: Cellulose-based direct compression tableting excipient, MCC: Microcrystalline cellulose, CMCC: Colloidal microcrystalline cellulose, CRC: Regenerated cellulose

where H and H<sup>0</sup> represent the crushing strengths of the batches made with the given excipient and the control tablets batch, respectively. The data given in Table 3 show that more compressed formulation was produced by MCR, followed by CRC, CMCC, and PM, in that order.

*Disintegration and dissolution behaviors of MZ tablets*

Figure 5 shows that the disintegration rate constant,  $k_d$ , generally decreased as the excipient concentration, C, increased in a given tablet batch and the relation;

$$k_d = k_d^0 \exp. x C$$

where x is the disintegration activity of the excipient in a given formulation, worked. The constants  $k_d$  and  $k_d^0$  stand for the disintegration rate constants of the batches made with a given excipient and the control tablets batch, respectively. The data

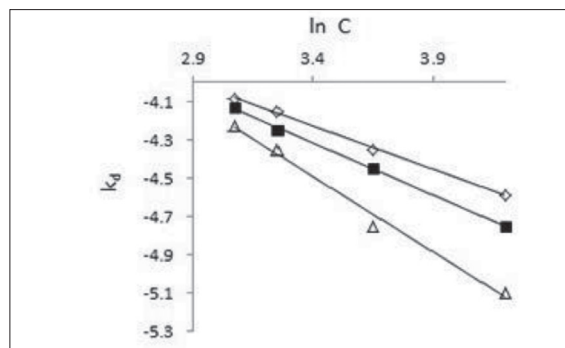


**Figure 5.**  $\ln k_d$  vs  $\ln C$  for the tested MZ tablets

MZ: Metronidazole

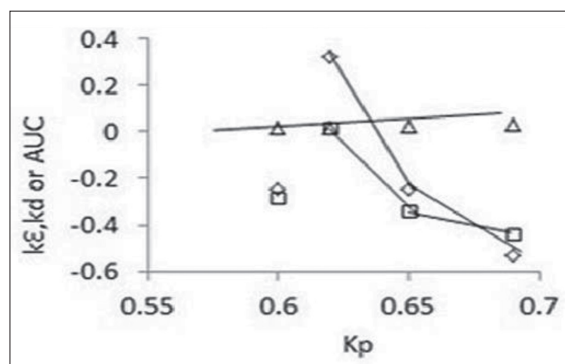


**Figure 6.**  $k_\epsilon$ ,  $k_d$ , or AUC as functions of  $k_p$  for the tested MZ tablets

MZ: Metronidazole, AUC: Area under the curve

**Table 3. Some parameters determined for the tested cellulose excipients using the mathematical expressions in the text**

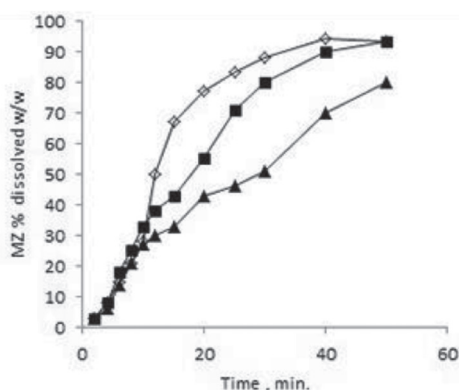
Excipients used	AUC $\text{cm}^2 \times 10^{-2}$	$k_p$	$k_e$	$x$
CMCCMCC	1.1	0.61	-0.24	-0.43
MCR	2.3	0.69	-0.20	-0.35
CRC	1.9	0.59	-0.49	-0.38
PM	1.0	0.38	-0.46	-0.48

CMCC: Colloidal microcrystalline cellulose, MCR: Cellulose-based direct compression tableting excipient, CRC: Regenerated cellulose, PM: Powder metallurgy, AUC: Area under the curve

**Table 4. % Change in some physicochemical properties of tablets compressed with the named excipients and lubricated with different concentrations of MS**

Excipient used	% Change in								
	H	F	Dt	H	F	Dt	H	F	Dt
	For tablets lubricated with % MS w/w								
	1		2		3				
CMCC	-11	14	23	-18	20	43	-30	27	53
MCR	-9	16	27	-14	19	33	-33	29	47
CRC	-22	18	43	-33	22	51	-42	34	62

CMCC: Colloidal microcrystalline cellulose, MCR: Cellulose-based direct compression tableting excipient, CRC: Regenerated cellulose, MS: Magnesium stearate

**Figure 7.** Dissolution profiles of MZ tablets compressed from ♦, CRC; □, MCR; and Δ, CMCC

MZ: Metronidazole, CRC: Regenerated cellulose, MCR: Cellulose-based direct compression tableting excipient, CMCC: Colloidal microcrystalline cellulose

in Figure 6 disclose that  $k_e$  and  $x$  of a given excipient were functions of  $k_p$  of the given excipient. In other words, the compressibility and the disintegration activity of an excipient are excipient compactibility dependent parameters. Figure 7 shows that tablets made from CR and MCR dissolved in more or less equal rates faster than those of the tablets made from CMCC.

#### MCR sensitivity against MS

Lubrication with MS generally produced less hard and more friable and slower disintegrating tablets. These adverse effects

increased as the concentration of MS in a tested tablet batch increased. The changes in H, F, and Dt of tablets lubricated with 3% w/w MS are given in Table 4.

## DISCUSSION AND CONCLUSIONS

The IR spectra in Figure 1 indicate that the tested powders are chemically similar. No new peaks suggesting the development of new materials were seen. The differences in the shape and intensity of the peaks were due to the different crystal lattices of the tested powders.

CMCC and CRC particles were elongated and amorphous. Such particles have a tendency to intermesh and create resistance (due to interparticle friction) to the flow of the bulk powder.<sup>12-15</sup> This explains why CMCC is not a freely flowing powder (0.21 g s<sup>-1</sup>). Although the Hausner ratio ( $h$ ) and the % compressibility determined for MCR were 1.6 and 38, MCR showed an improved flow rate. This is supported by the concept that the Hausner ratio and Carr's index, which are empirically derived parameters, failed in many cases to give a reliable base to judge powder flowability. The improved flow properties of MCR may be due to the glidant effect of CRC. It seems that CRC reduced the interparticle friction of the powder and improved its flow.

Since CRC had a large specific surface area wherein a large  $\alpha$  is available, it is expected that MCR has improved compression and compaction properties and generates larger AUC,  $k_e$ , and  $k_p$  values.  $\alpha$  of a given excipient may be calculated as;

$$\alpha = L \cdot k_p \cdot \text{wt.} \cdot \sum (r_i / MW_i)$$

where  $L$ ,  $\text{wt.}$ ,  $r_i$ , and  $MW_i$  stand for Avogadro's number ( $6.022 \times 10^{23}$ ), the weight of the excipient in a batch, the fraction of a parent excipient used in coprocessing, and its molecular weight, respectively. CRC and MCR showed almost the same level of disintegration activity and they generated smaller  $x$  values as shown in Table 3. CRC followed by MCR produced fast dissolving tablets. This is due to the powerful disintegrant effect of CRC.<sup>15</sup> Incorporating a powerful disintegrant in formulating tablets would contribute to the bioresponse of the tablets. MCR was unfortunately sensitive to MS.

In response to the increasing demand for inexpensive and multifunctional excipients with minimum risk to the products, MCR was engineered from MCC and regenerated cellulose. MCR has high functionality in terms of flow and compression, good binding properties, and strong disintegrating activity. However, it is sensitive to MS and exhibits high moisture uptake and therefore it is recommend as a complementary direct compression excipient.

## ACKNOWLEDGEMENT

The author is grateful to Prof. Dr. J. Rojas for the technical assistance.

*Conflict of Interest: No conflict of interest was declared by the authors.*

## REFERENCES

1. Reimerdes D. The near future of tablet excipients. *Manufacturing Chemist*. 1993;64:14-15.
2. Saha S, Shahiwala AF. Multifunctional co-processed excipients for improved tableting performance. *Expert Opin Drug Deliv*. 2009;6:197-208.
3. Mirani AG, Patankar SP, Borole VS, Pawar AS, Kadam VJ. Direct compression high functionality excipient using co-processing technique: A brief review. *Curr Drug Deliv*. 2011;8:426-435.
4. Builders PF, Bonaventure AM, Tiwalade A, Okpako LC, Attama AA. Novel multifunctional pharmaceutical excipients derived from microcrystalline cellulose-starch microparticulate composites prepared by compatibilized reactive polymer blending. *Int J Pharm*. 2010;388:159-167.
5. Gonnissen Y, Remon JP, Vervaet C. Development of directly compressible powders via co-spray drying. *Eur J Pharm Biopharm*. 2007;67:220-226.
6. Gohel MC, Jogani PD. Exploration of melt granulation technique for the development of co-processed directly compressible adjuvant containing lactose and microcrystalline cellulose. *Pharm Dev Technol*. 2003;8:175-185.
7. Sherwood BE, Becker JW. A New class of high functionality excipients: silicified microcrystalline cellulose. *Pharm Technol*. 1998;22:78-88.
8. Nachaegari SK, Bansal AK. Co-processed excipient for solid dosage forms. *Pharm Technol*. 2004;28:52-64.
9. York P. Crystal engineering and particle design for the powder compaction process. *Drug Dev Ind Pharm*. 1992;18:677-721.
10. Gohel MC, Jogani PD. A review of co-processed directly compressible excipients. *J Pharm Pharm Sci*. 2005;8:76-93.
11. Reier GE, Shangraw RF. Microcrystalline cellulose in tableting. *J Pharm Sci*. 1966;55:10-15.
12. Zuurman K, Maarschalk VV, Bolhuis GK. Effect of magnesium stearate on bonding and porosity expansion of tablets produced from materials with different consolidation properties. *Int J Pharm*. 1999;179:107-115.
13. Kumar V. Powdered micro-fibrillated cellulose, US Patent 6,821,531 B2, 2004.
14. Ahmad FAS. Evaluation of regenerated cellulose as a glidant for Common Reed cellulose. *IJPJ's J Pharm Cosmet*. 2013;3:18-22.
15. Rojas J, López A, Gamboa Y, González C, Montoya F. Assessment of processing and polymorphic form effect on the powder and tableting properties of microcrystalline celluloses I and II. *Chem Pharm Bull (Tokyo)*. 2011;59:603-607.
16. Aly SAS. Evaluation of Dis-Lub-Tout, a new co-processed tableting excipient I. Physico-chemical properties. *J Drug Del Sci Tech*. 2014;24:503-506.
17. Aly SAS. Evaluation of Dis-Lub-Tout, a new co-processed tableting excipient II. Lubricant property. *J Drug Del Sci Tech*. 2014;24:678-683.
18. Phillips MA, Samuel SL. Chemotherapy of protozoa infections. In: Brunton LL, Lazo JS, Parker KL, eds. *The Pharmacological Basis of Therapeutics*. 10th ed. New York; McGraw-Hill Medical Publishing Division; 2006:1049-1069.
19. Chime SA, Onyishi VI, Onyechi JO. Co-processed metronidazole granules for tableting: Formulation and *in vitro* evaluation. *Int J Pharm Sci Rev*. 2013;22:13-17.
20. Adebowale BO, Oluwatomi O, Bakre L. Compressional properties of metronidazole tablet formulations containing aloe vera as binding agent. *Int J Pharm Pharm Sci*. 2014;10:261-264.
21. Rojas J, Lopez A, Guisao S, Ortiz C. Evaluation of several microcrystalline celluloses obtained from agricultural by-products. *J Adv Pharm Technol Res*. 2011;2:144-150.
22. Hu C, Liu Y. Quality Control in Pharmaceuticals: Residual Solvents Testing and Analysis. In: Akyar I, eds. *Wide Spectra of Quality Control*. INTECH; 2011 p.183-210. URL: <http://www.intechopen.com/books/wide-spectra-of-quality-control>.
23. Heckel RW. Density/pressure relationship in powder compaction. *Trans Metall Soc AIME*. 1961;22:1671-1675.
24. Antikainen O, Yliruusi J. Determining the compression behaviour of pharmaceutical powders from the force-distance compression profile. *Inter J Pharm*. 2003;61:253-261.



# Decreased Protein Kinase C Expression in the Cochlear Fibroblasts of Diabetic Rat Models Induced by Curcumin

## Kurkumin Tarafından İndüklenen Diyabetik Sıçan Modellerinin Koklear Fibroblastlarındaki Azalmış Protein Kinaz C Ekspresyonları

© Tengku Siti Hajar HARYUNA\*, © Farhat FARHAT, © Siska INDRIANY

Universitas Sumatera Utara, Faculty of Medicine, Department of Otorhinolaryngology-Head and Neck Surgery, Medan, Indonesia

### ABSTRACT

**Objectives:** Microcirculation and hemodynamic disturbances, including in the cochlea, are commonly found in diabetic patients. A study on diabetic rats discovered histopathological changes in outer hair cells and the spiral ganglion and mitochondrial damage in the ear. Hyperglycemia can increase the activation of protein kinase C (PKC). Curcumin as an antioxidant also affects the regulation of PKC and  $Ca^{2+}$ . The aim of this study was to determine the role of curcumin in decreasing PKC expression in the cochlear fibroblasts of diabetic rats.

**Materials and Methods:** An experimental study was performed on 24 Wistar rats divided into the following 6 groups: group 1: control group; group 2: diabetic group without curcumin administration; groups 3 and 4: diabetic groups with curcumin administration (200 mg/kg and 400 mg/kg for 3 days, respectively); groups 5 and 6: diabetic groups with curcumin administration (200 mg/kg and 400 mg/kg for 8 days, respectively). Cochlear tissues were taken from all groups and immunohistochemistry-stained, and the PKC expression scores were analyzed with one-way ANOVA (a significance level of 0.05).

**Results:** Significant differences in PKC expression ( $p < 0.05$ ) were found between group 1 and group 2, and group 2 and groups 3, 4, 5, and 6. There was no significant difference in PKC expression regarding the different doses and the duration of curcumin administration.

**Conclusion:** Curcumin can reduce PKC expression in the cochlear fibroblasts of diabetic rats.

**Key words:** Diabetes mellitus, curcumin, fibroblast, cochlea, protein kinase C

### ÖZ

**Amaç:** Kokleada dahil olmak üzere mikrodolaşım ve hemodinamik bozukluklar, diyabetli hastalarda yaygın olarak görülür. Diyabetik sıçanlar üzerine yapılan bir çalışma, dıştaki saç hücrelerindeki histopatolojik değişiklikleri, sarmal gangliyon ve kulaktaki mitokondriyal hasarı ortaya koymuştur. Hiperglisemi, protein kinaz C (PKC) aktivasyonunu artırabilir. Bir antioksidan olan kurkumin, PKC ve  $Ca^{2+}$  düzenini de etkiler. Bu çalışmanın amacı, diyabetik sıçanlarda koklear fibroblastlarda PKC ekspresyonlarının azaltılmasında kurkuminin rolünü öğrenmektir.

**Gereç ve Yöntemler:** Yirmi dört adet Wistar sıçan 6 gruba ayrılmıştır. Grup 1: kontrol grubu; grup 2: kurkumin uygulanmayan diyabetik grup; grup 3 ve 4: kurkumin uygulanan diyabetik gruplar (sırasıyla 3 gün süreyle 200 mg/kg ve 400 mg/kg); grup 5 ve 6: kurkumin uygulaması olan diyabetik gruplar (sırasıyla 8 gün boyunca 200 mg/kg ve 400 mg/kg). Koklear dokular tüm gruplardan alındı ve immünohistokimyasal olarak boyandı ve PKC ekspresyon skorları, tek-yönlü ANOVA (0.05'lik önem derecesi) ile analiz edildi.

**Bulgular:** Grup 1 ile grup 2, grup 2 ve grup 3, 4, 5, 6 arasında PKC ekspresyonlarında önemli farklılıklar bulundu ( $p < 0.05$ ). Farklı dozlar ve kurkuminin uygulama süresi ile ilgili olarak PKC ekspresyonunda önemli bir fark yoktu.

**Sonuç:** Kurkumin, diyabetik sıçanların koklear fibroblastlarındaki PKC ekspresyonlarını azaltabilir.

**Anahtar kelimeler:** Şeker hastalığı, kurkumin, fibroblast, koklea, protein kinaz C

\*Correspondence: E-mail: tengkusitihajarharyuna@gmail.com, Phone: +628126061694 ORCID-ID: orcid.org/0000-0003-2779-3285

Received: 03.10.2017, Accepted: 08.02.2018

©Turk J Pharm Sci, Published by Galenos Publishing House.

## INTRODUCTION

Diabetes mellitus (DM) is a chronic disease caused by inadequate production of insulin or ineffective usage of the provided insulin, marked by an increase in blood glucose (hyperglycemia), and found as an inherited disease. It is estimated that there will be 300 million diabetic patients worldwide in 2025.<sup>1</sup>

Diabetes has the potential to cause various complications due to angiopathy and neuropathy. There have been several studies over the years about the relationship between DM and hearing loss. Disturbances in microcirculation and hemodynamic changes (including in the cochlea) are often found in diabetic patients. Further research on experimental animals such as diabetic rats has reported pathological changes in outer hair cells and the spiral ganglion and mitochondrial damage.<sup>2</sup>

A similar result can also be found in a study conducted by Lee et al.,<sup>3</sup> which found histologic abnormalities, such as degeneration of the organ of Corti and spiral ganglion cells, related to hyperglycemia and obesity.

Several biochemical pathways have also been studied to discover the effect of hyperglycemia, such as the diacylglycerol (DAG) activation pathway, protein kinase C (PKC) activation, increased polyol, increased oxidative stress, and overproduction of advanced glycation end products. These biochemical pathways are strongly related to reactive oxygen species (ROS), leading to vascular damage.<sup>4,5</sup>

Some existing hypotheses explain the harmful side effects of hyperglycemia; one of them is the constant activation of PKC. PKC has been linked to vascular changes, such as increased permeability, contractility, extracellular matrix synthesis, cell growth and apoptosis, angiogenesis, cytokines activity, and inhibition.<sup>6</sup>

Curcumin is an active, yellow component of turmeric, isolated from the plant *Curcuma longa*. This molecule has a therapeutic effect on various diseases, especially anti-inflammatory, antimicrobial, and antioxidant. It has been reported that curcumin is a bifunctional antioxidant possessing direct and indirect antioxidant activity by scavenging ROS and neutralizing them and inducing upregulation of various cytoprotective proteins and antioxidants such superoxide dismutase, catalase, and glutathione peroxidase. The presence of phenolic OH and CH<sub>2</sub> groups in the β-diketone part of this natural compound significantly contributes to its potent antioxidant property.<sup>7-9</sup>

Curcumin affects PKC and Ca<sup>2+</sup> regulation. The effect of inhibited ROS caused by curcumin depends on the curcumin dose through its effect on PKC activity and Ca<sup>2+</sup> regulation.<sup>10</sup>

The role of curcumin in the treatment and prevention of hearing loss through its inhibitory mechanism towards PKC in the cochlear fibroblasts of diabetic rats (*Rattus norvegicus*) has never been studied, and so the objective of the present study was to demonstrate the role of curcumin in reducing PKC expression in the cochlear fibroblasts of diabetic rats.

## MATERIALS AND METHODS

### *Animal subjects*

This study was an experimental study with a randomized posttest-only control group design using Wistar rats (*R. norvegicus*) that were male, healthy, and average weight 200 g. The 24 rats were divided into 6 groups, with 4 rats in each group. The rats were obtained from the Laboratory of Biochemistry, Faculty of Medicine, Universitas Airlangga, Surabaya, Indonesia. To ensure that all the procedures were ethically acceptable, a proposal was submitted to the Research Ethics Committee. This study earned approval from the Health Research Ethics Committee of Universitas Sumatera Utara, Indonesia, no. 433/KOMET/FKUSU/2015.

### *Treatments*

In the study, after the white rats had adapted to the cage environment in the laboratory for 2 weeks, they were treated according to the plan.

Group 1 (control group) was injected with a single dose of sodium citrate, obtained from 1.47 g of sodium citrate solution in 50 mL of dH<sub>2</sub>O intraperitoneally on the 1<sup>st</sup> day, and then terminated on the 5<sup>th</sup> day.

Group 2 was injected with a single dose of streptozotocin (STZ) (Bioworld, USA) 60 mg/kgbw, and then terminated on the 5<sup>th</sup> day.

Group 3 was injected with a single dose of STZ 60 mg/kgbw followed by curcumin 200 mg/kgbw/day orally for 3 days and terminated on the 5<sup>th</sup> day.

Group 4 was injected with a single dose of STZ 60 mg/kgbw followed by curcumin 400 mg/kgbw/day orally for 3 days and terminated on the 5<sup>th</sup> day.

Group 5 was injected with a single dose of STZ 60 mg/kgbw followed by curcumin 200 mg/kgbw/day orally for 8 days and terminated on the 10<sup>th</sup> day.

Group 6 was injected with a single dose of STZ 60 mg/kgbw followed by curcumin 400 mg/kgbw/day orally for 8 days and terminated on the 10<sup>th</sup> day.

### *Procedures*

#### *STZ-induced diabetes*

The rats were fasted for 4 h to empty the stomach and decrease the risk of aspiration. Induction was performed on the rats by injecting STZ solution 60 mg/kgbw<sup>11</sup> intraperitoneally with the required doses mentioned above (diabetic groups: groups 2-6). In order to avoid sudden postinjection hypoglycemia, the rats were given sucrose 10% or dextrose 10% solution throughout the 1<sup>st</sup> night. Every morning, the fasting blood sugar levels of the rats were examined with an Advance Glucometer (Boehringer Mannheim, Germany) by taking blood from the peripheral blood vessel in the tail. Hyperglycemia is diagnosed when the blood sugar level is >200 mg/dL after 48 h of STZ induction.<sup>12</sup> If the blood sugar is <200 mg/dL then the rats are eliminated from the sample.

After being diagnosed as hyperglycemic, the rats were given curcumin according to the required dose per group and they were terminated after the procedure.

#### Procedure of curcumin administration

Powdered curcumin was used at the level of  $16.62 \pm 0.14\%$  b/b using thin layer chromatography – densitometry. The given preparation included powdered curcumin at a dose of 200 mg/kgbw/day and 400 mg/kgbw/day per rat suspended in carboxymethyl cellulose 0.5% and administered orally into the stomach of the rat via a nasogastric tube.

#### Procedure of rat cochlear tissue collection

Termination was conducted on rats in all groups by temporal bone necropsy. The tissue sample taken was fixated with buffered formalin solution 10% and decalcified with EDTA for 4 weeks. Each tissue sample was prepared in paraffin blocks and sliced into 4- $\mu$ m-thick sections and placed inside the glass object and then stained with hematoxylin-eosin and immunohistochemical staining of PKC was performed with polyclonal anti-PKC antibody (catalogue#: ENT3752, Elabscience).

#### Cell-counting method

All slides were examined using an Olympus XC 10 microscope (under 40 $\times$  magnification) by two anatomical pathologists separately with the double-blind method. PKC expression scores were evaluated by multiplying the area score (0=0%, 1=<10%, 2=10%-50%, 3=>50%) by the intensity score (0, 1, 2, or 3).<sup>13</sup>

#### Statistical analysis

To analyze the mean differences between more than two groups, one-way ANOVA was used (a significance level of 0.05). Before one-way ANOVA, we used the Shapiro–Wilk test to prove that the data were normally distributed and post-hoc tests to see the differences of groups.

## RESULTS

Mean differences in PKC expression were seen in all groups. The lowest PKC expression was found in the control group and the highest PKC expression was found in the diabetic group without curcumin administration (Chart 1).

It is also shown in Chart 1 that the diabetic groups administered curcumin (groups 3-6) had lower mean values of PKC expression compared to the diabetic group not administered curcumin (group 2).

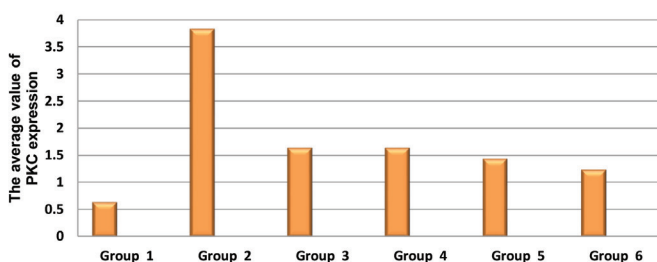


**Chart 1.** The average value of PKC expression in the cochlear lateral fibroblast wall of all groups

PKC: Protein kinase C

In order to get a proper and detailed view of the cochlear tissue histopathologically, hematoxylin-eosin staining was performed and used as a comparison for further immunohistochemical staining (Figure 1).

Clinical test results of curcumin in decreasing PKC expression in the cochlear fibroblasts of diabetic rats can be seen in Figure 2.

The fibroblasts in the diabetic group (group 2) showed higher density compared to the other groups, whereas the fibroblasts within the diabetic group administered curcumin (groups 3-6) showed lower density.

The results obtained from the histopathological examination above were then processed and analyzed statistically to find

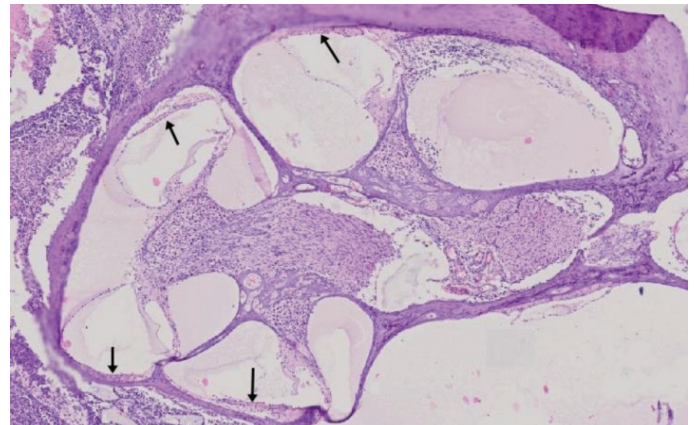


**Figure 1.** The cochlear lateral wall section of *Rattus norvegicus* (black arrow) with hematoxylin-eosin staining (under 40 $\times$  magnification)

**Table 1.** The ANOVA test results in various groups

Groups	PKC expression		
	Mean $\pm$ SD	p value	
Group 1	Group 2	-3.2 $\pm$ 0.374	0.000*
	Group 3	-1.0 $\pm$ 0.374	0.200
	Group 4	-1.0 $\pm$ 0.374	0.200
	Group 5	-0.8 $\pm$ 0.374	0.643
	Group 6	-0.6 $\pm$ 0.374	1.000
	Group 2	Group 3	2.2 $\pm$ 0.374
Group 4		2.2 $\pm$ 0.374	0.000*
Group 5		2.4 $\pm$ 0.374	0.000*
Group 6		2.6 $\pm$ 0.374	0.000*
Group 3	Group 4	0 $\pm$ 0.374	1.000
	Group 5	0.2 $\pm$ 0.374	1.000
	Group 6	0.4 $\pm$ 0.374	1.000
Group 4	Group 5	0.2 $\pm$ 0.374	1.000
	Group 6	0.4 $\pm$ 0.374	1.000
Group 5	Group 6	0.2 $\pm$ 0.374	1.000

\*statistically significant, PKC: Protein kinase C, SD: Standard deviation



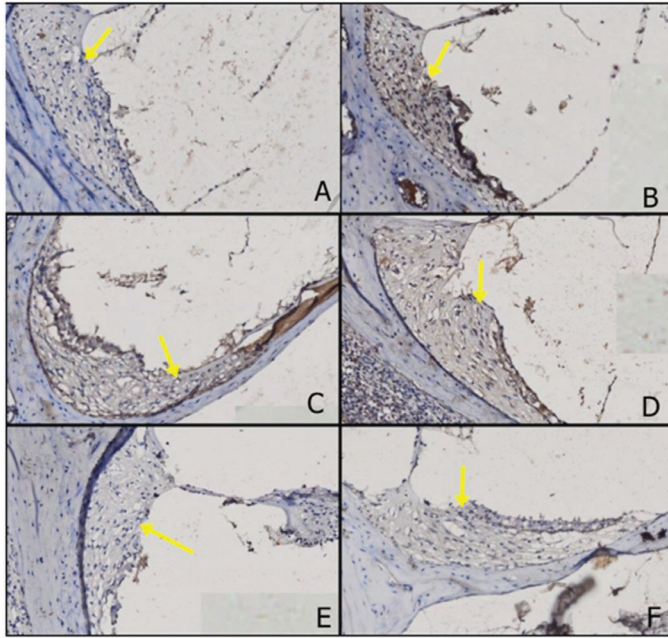


**Figure 2.** The expressions of PKC in each group (under 100× magnification): a) Group 1; b) Group 2; c) Group 3; d) Group 4; e) Group 5; f) Group 6. The yellow arrow indicates the expressions of PKC in cochlear fibroblasts marked by brown stains

PKC: Protein kinase C

the differences between each group and the interpreted results are shown in Table 1.

According to Table 1, there was a statistically significant difference ( $p < 0.05$ ) in the mean value of PKC expression between group 1 and the diabetic group not administered curcumin (group 2).

As shown in Table 1, the administration of curcumin in the diabetic groups (groups 3-6) decreased PKC expression significantly ( $p < 0.05$ ) compared to the diabetic group not administered curcumin (group 2).

According to Table 1, the different doses (200 and 400 mg/kgbw/day) and the duration of curcumin administration (3 and 8 days) showed no statistically significant differences ( $p > 0.05$ ) in PKC expression.

## DISCUSSION

Sensorineural hearing loss in diabetic patients is caused by cochlear angiopathy characterized by dilatation of the blood vessels of the stria vascularis, atrophy, and loss of outer hair cells. Research on diabetic rats found that microangiopathy occurs inside the inner ear and thickening of basement membranes of capillaries in the stria vascularis.<sup>14,15</sup>

To help identify the gene that plays a role in the human auditory system, rats were used as the experimental animal since they are genetically similar to humans (>70%).<sup>16</sup> The objective of this study was to determine the role of curcumin in decreasing PKC expression in the cochlear fibroblasts of diabetic rats (*R. norvegicus*).

Earlier studies have not proved any effect of curcumin on PKC expression in the lateral wall of cochlear fibroblasts in diabetic model rats. This study is the first to prove that curcumin is able to decrease the expression of PKC in the lateral wall of cochlear fibroblasts in these rats.

The dose of curcumin used in this study was 200 mg/kgbw according to the previous study, in which that dose of curcumin acted as an antioxidant<sup>17</sup> due to its inhibitory effect on ROS by affecting the PKC pathway and calcium regulation.<sup>10</sup> In order to find the optimal dose and duration of curcumin administration to decrease PKC expression, we compared the doses of 200 mg/kgbw/day and 400 mg/kgbw/day with the durations of administration of 3 and 8 days. In regard to the present study, curcumin is a compound that functions dependently on the dose and duration of administration. Thus, the dose and duration of administration can affect gene expression.<sup>18</sup>

A significant difference in the mean value of PKC expression between the control group and the diabetic group not administered curcumin was found in this study. Curcumin as an antioxidant can inhibit ROS via the PKC pathway and calcium regulation.<sup>10</sup> This discovery strengthens the presumption that hyperglycemia will cause cellular dysfunction that activates PKC persistently and stimulates the continuous synthesis of endogenous ROS, leading to cell damage, including cochlear fibroblasts.

In the present study, there were differences in the mean values of PKC expression in all groups. The lowest PKC expression was found in group 1 and the highest PKC expression was found in group 2.

Chronic hyperglycemia can cause various cellular reactions that play a role in the pathomechanism of various complications, caused by cell dysfunction and damage. The cellular reactions caused by chronic hyperglycemia are nonenzymatic glycation, activation of the signal transduction pathway increasing DAG synthesis, increased ROS synthesis as the waste product of energy catabolism leading to cell and tissue oxidative stress, and activation of aldolase reductase.<sup>19</sup> In DM, increased ROS production also occurs via several mechanisms, such as polyol pathway, increased AGEs production, excessive radical superoxide production, and PKC activation. The increased PKC activity may also result in increased ROS production.<sup>20</sup>

The increased DAG synthesis in hyperglycemia via the signal transduction pathway, especially that coming from the transformation of glucose into glycerol 3-phosphate, may lead to increased DAG synthesis *de novo*. DAG is partially synthesized from phosphatidylcholine and phosphatidylinositol of the "insulin-sensitive" cell membrane continuously. The perpetual DAG synthesis and the potentiation effect from the free fatty acid in the blood may initiate the PKC activation pathway persistently, leading to cellular response via the modification of various proteins controlling signal transduction and cytokine expression.<sup>19,21,22</sup>

The modification of transcription factor and cell cycle may cause cell dysfunction and damage due to the disturbance in cell proliferation and differentiation as well as the abnormality in

apoptosis. Additionally, the modification of transcription factor and postprotein translation can also stimulate the synthesis of endogenous ROS, resulting in cell damage.<sup>19</sup>

Thereby, in the STZ-induced diabetes group, PKC expression was increased due to the continuous activation of the PKC pathway.

In the present study, groups 3, 4, 5, and 6 (diabetic groups administered curcumin) showed lower mean values of PKC expression compared to group 2 (diabetic group not administered curcumin). The decreased mean values of PKC expression in the STZ-induced diabetes groups receiving curcumin was due to the activity of curcumin, which can eliminate the formation of ROS, thereby inhibiting PKC activation at the cellular level.

A similar study conducted by Kao et al.<sup>23</sup> found significant inhibition in PKC expression in patients with hepatocellular carcinoma (Hep 3B cell) treated by curcumin. The decreased expression mechanism of PKC is not fully understood, but many previous *in vivo* and *in vitro* studies have shown a strong indication of decreased expression of PKC caused by curcumin acting as a noncompetitive and selective inhibitor of phosphorylase kinase.

Phosphorylase kinase is the key enzyme in glycogen metabolism; if this enzyme is inhibited then autocrine effect as cell growth factor is also inhibited, which affects the cell proliferation disturbance. Curcumin is also a potent antioxidant to neutralize ROS and inhibit lipid peroxidation.<sup>24</sup>

Similarly, the study carried out by Jancinova et al.<sup>25</sup> observed that curcumin can inhibit PKC in the neutrophils of Lewis rats suffering from arthritis *in vitro* or experimentally.

Another study demonstrated that curcumin can serve as an antioxidant by eliminating phorbol-12, myristate-13 acetate to inhibit ROS. This inhibitory pattern shows that curcumin mechanically inhibits PKC and calcium regulation.<sup>10</sup>

The antioxidant activity of curcumin is based on the phenolic group in it through donation of a hydrogen atom. Moreover, the phenolic group plays a key role for the activity of free radicals scavenging.<sup>26</sup>

In the present study, the different doses of curcumin, 200 mg/kgbw/day and 400 mg/kgbw/day, with duration of 3 and 8 days showed no statistically significant differences ( $p > 0.05$ ) in PKC expression. Nevertheless, the administration of a higher dose of curcumin with a longer duration (group 6) demonstrated more decreased PKC expression compared to a lower dose of curcumin with a shorter duration (group 3).

## CONCLUSIONS

According to this study, we conclude that curcumin is an antioxidant that mechanically inhibits PKC expression in the cochlear fibroblasts of diabetic rats administered curcumin of either 200 mg/kgbw/day or 400 mg/kgbw/day for 3 days or 8 days. Curcumin is considered a therapeutic agent that is effective in repairing fibroblast damage in the cochlear lateral wall caused by DM, which was determined through the expression of PKC. This study can act as basic scientific

research in traditional therapy to manage hearing loss caused by DM in the future.

## ACKNOWLEDGEMENTS

This study was supported by DIPA Direktorat Penelitian dan Pengabdian kepada Masyarakat, Universitas Sumatera Utara 2015.

*Conflict of Interest: No conflict of interest was declared by the authors.*

## REFERENCES

- Malucelli DA, Malucelli FJ, Fonseca VR, Zeigeboim B, Ribas A, Trotta FD, Silva TP. Hearing loss prevalence in patients with diabetes mellitus type 1. *Braz J Otorhinolaryngol.* 2012;78:105-115.
- Xipeng L, Ruiyu L, Meng L, Yanzhuo Z, Kaosan G, Liping W. Effect of Diabetes on Hearing and Cochlear Structures. *J Otolaryngol.* 2013;8:82-87.
- Lee HS, Kim KR, Chung WH, Cho YS, Hong SH. Early Sensorineural Hearing Loss in Ob/Ob Mouse, an Animal Model of Type 2 Diabetes. *Clin Exp Otorhinolaryngol.* 2008;1:211-216.
- Noh H, King GL. The role of protein kinase C activation in diabetic nephropathy. *Kidney Int Suppl.* 2007;72:49-53.
- Aronson D. Hyperglycemia and the pathobiology of diabetic complications. 2nd ed. Fisman EZ, Tenenbaum A. *Cardiovascular Diabetology: Clinical, Metabolic and Inflammatory Facets.* Adv Cardiol. 2008;1:16.
- Geraldes P, King GL. Activation of Protein Kinase C Isoform and Its Impact on Diabetic Complications. *Circ Res.* 2010;106:1319-1331.
- Correa F, Buelna-Chontal M, Hernández-Reséndiz S, García-Niño WR, Roldán FJ, Soto V, Silva-Palacios A, Amador A, Pedraza-Chaverrí J, Tapia E, Zazueta C. Curcumin maintains cardiac and mitochondrial function in chronic kidney disease. *Free Radic Biol Med.* 2013;61:119-129.
- Trujillo J, Chirino YI, Molina-Jijón E, Andérica-Romero AC, Tapia E, Pedraza-Chaverrí J. Renoprotective effect of the antioxidant curcumin: Recent Findings. *Redox Biol.* 2013;1:448-456.
- Yadav SK, Sah AK, Jha RK, Sah P, Shah DK. Turmeric (curcumin) remedies gastroprotective action. *Pharmacogn Rev.* 2013;7:42-46.
- Balasubramanyam M, Koteswari AA, Kumar RS, Monickaraj SF, Maheswari JU, Mohan V. Curcumin-induced inhibition of cellular reactive oxygen species generation: Novel therapeutic implications. *J Biosci.* 2003;28:715-721.
- Ragbetli C, Ebubekir C. Effect of Streptozotocin on Biochemical Parameters in Rats. *Asian J Chem.* 2010;22:2376-2378.
- Wongekain N, Sridulyakul P, Jariyapongskul A, Suksamrarn A, Patumraj S. Effects of curcumin and tetrahydrocurcumin on diabetes induced endothelial dysfunction. *Afr J Biochem Res.* 2009;3:259-265.
- Tan KB, Putti TC. Cyclooxygenase 2 expression in nasopharyngeal carcinoma: immunohistochemical findings and potential implication. *J Clin Pathol.* 2005;5:535-538.
- Austin DF, Konrad-Martin D, Griest S, McMillan GP, McDermott D, Fausti S. Diabetes-Related Change in Hearing. *Laryngoscope.* 2009;119:1788-1796.
- Maia CA, Campos CA. Diabetes Mellitus as etiological factor of hearing loss. *Braz J Otorhinolaryngol.* 2005;71:208-214.

16. Gravel JS, Ruben RJ. Auditory Deprivation and Its Consequences: From Animal Models to Human. In: Van De Water TR, Popper AN, Fay RR, eds. *Clinical Aspect of Hearing*. New York; Springer; 1996:86-92.
17. González-Salazar A, Molina-Jijón E, Correa F, Zarco-Márquez G, Calderón-Oliver M, Tapia E, Zazueta C, Pedraza-Chaverri J. Curcumin Protects from Cardiac Reperfusion Damage by Attenuation of Oxidant Stress and Mitochondrial Dysfunction. *Cardiovasc Toxicol*. 2011;11:357-364.
18. Van Erk MJ, Teuling E, Staal YC, Huybers S, Van Bladeren PJ, Aarts JM, Van Ommen B. Time- and dose-dependent effects of curcumin on gene expression in human colon cancer cells. *J Carcinog*. 2004;3:8.
19. Koya D, King GL. Protein Kinase C Activation and the Development of Diabetic Complications. *Diabetes*. 1998;47:859-866.
20. Oshiro Y, Lee Y, King G. Mechanism of diabetic nephropathy: role of protein kinase-c activation. *Advanced Studies in Medicine*. 2005;5:10-19.
21. Nishizuka Y. Intracellular Signaling by Hydrolysis of Phospholipids and Activation of Protein Kinase C. *Science*. 1992;258:607-614.
22. Gutterman D. Vascular Dysfunction in Hyperglycemia: Is Protein Kinase C the Culprit? *Circ Res*. 2002;90:5-7.
23. Kao HH, Wu CJ, Won SJ, Shin JW, Liu HS, Su CL. Kinase Gene Expression and Subcellular Protein Expression Pattern of Protein Kinase C Isoform in Curcumin-treated Human Hepatocellular Carcinoma Hep 3B Cells. *Plant Foods Hum Nutr*. 2011;66:136-142.
24. Reddy S, Aggarwal BB. Curcumin is a non-competitive and selective inhibitor of phosphorylase kinase. *FEBS Lett*. 1994;94:19-22.
25. Jancinova V, Perecko T, Nosal R, Kostalova D, Bauerova K, Drabikova K. Decreased activity of neutrophils in the presence of diferuloylmethane (curcumin) involves protein kinase C inhibition. *Eur J Pharmacol*. 2009;612:161-166.
26. Menon VP, Sudheer AR. Antioxidant and inflammatory properties of curcumin. *Adv Exp Med Biol*. 2007;595:105-125.



# Investigation of the Antioxidant, $\alpha$ -Glucosidase Inhibitory, Anti-inflammatory, and DNA Protective Properties of *Vaccinium arctostaphylos* L.

## *Vaccinium arctostaphylos* L.'nin Antioksidan, $\alpha$ -Glukozidazı İnhibe Edici, Anti-inflamatuvar ve DNA Koruyucu Özelliklerinin İncelenmesi

© Burak BARUT<sup>1\*</sup>, © Elif Nur BARUT<sup>2</sup>, © Seçkin ENGİN<sup>2</sup>, © Arzu ÖZEL<sup>1</sup>, © Feride Sena SEZEN<sup>2</sup>

<sup>1</sup>Karadeniz Technical University, Faculty of Pharmacy, Department of Biochemistry, Trabzon, Turkey

<sup>2</sup>Karadeniz Technical University, Faculty of Pharmacy, Department of Pharmacology Trabzon, Turkey

### ABSTRACT

**Objectives:** The scope of this study was to investigate the total phenolic, anthocyanin, and flavonoid contents and the biological properties of ethanol extract (EE), methanol extract (ME), and aqueous extract (AE) from *Vaccinium arctostaphylos* L.

**Materials and Methods:** EE, ME, and AE of *V. arctostaphylos* were prepared. Various biological activities such as total phenolic, anthocyanin, and flavonoid contents, and antioxidant (2,2'-diphenyl-1-picrylhydrazyl ferrous ion-chelating, and ferric reducing antioxidant power assays),  $\alpha$ -glucosidase inhibitory, anti-inflammatory, and DNA protective properties of these extracts were studied.

**Results:** EE exhibited the highest total phenolic, anthocyanin, and flavonoid contents with 44.42±1.22 mg gallic acid equivalents/g dry weight, 8.46±0.49 mg/Cyaniding-3-glucoside equivalents/g dry weight, and 9.22±0.92 mg quercetin equivalents/g dry weight, respectively. The antioxidant activities of the extracts followed the order: EE>ME>AE. EE and ME inhibited  $\alpha$ -glucosidase enzyme and their IC<sub>50</sub> values were 0.301±0.002 mg/mL and 0.477±0.003 mg/mL, respectively. In addition, EE and ME were determined as noncompetitive inhibitors with inhibitory constant (K<sub>i</sub>) values of 0.48±0.02 mg/mL and 0.46±0.01 mg/mL, respectively. EE in 100 and 300 mg/kg doses caused a significant reduction in formalin-induced edema in mice, demonstrating the anti-inflammatory effect of EE. In DNA protective studies, all of the extracts protected supercoiled plasmid pBR322 DNA against damage caused by Fenton's reagents due to their radical scavenging activities.

**Conclusion:** Our results demonstrated that EE of *V. arctostaphylos* L. had strong antioxidant, anti-inflammatory,  $\alpha$ -glucosidase inhibitory, and DNA protective effects, suggesting that it might be an effective medical plant to prevent or treat diseases associated with oxidative damage and inflammation.

**Key words:** Antioxidant, anti-inflammatory, DNA,  $\alpha$ -glucosidase, *Vaccinium arctostaphylos*

### ÖZ

**Amaç:** Bu çalışmanın amacı *Vaccinium arctostaphylos* L.'den hazırlanan etanol (EE), metanol (ME) ve su (AE) ekstraktlarının toplam fenolik, antosiyanin, flavonoid içerikleri ve biyolojik özelliklerinin incelenmesidir.

**Gereç ve Yöntemler:** *V. arctostaphylos*'un EE, ME ve AE ekstraktları hazırlanmıştır. Bu ekstraktların total fenolik, antosiyanin ve flavonoid içerikleri, antioksidan (2,2'-difeniil-1-pikrilhidrazil, metal iyon şelatlama ve ferrik indirgeyici antioksidan gücü metotları),  $\alpha$ -glukozidaz, anti-inflamatuvar ve DNA koruma özellikleri araştırılmıştır.

**Bulgular:** EE, 44.42±1.22 mg galik asit eşdeğeri/g kuru ağırlık, 8.46±0.49 mg/siyanidin-3-glukozid eş değerleri/g kuru ağırlık ve 9.22±0.92 mg quercetin eş değerleri/g kuru ağırlık değerleriyle en yüksek toplam fenolik, antosiyanin ve flavonoid içeriğine sahip olduğu görülmüştür. Bununla birlikte ekstraktların antioksidan aktiviteleri sırasıyla EE>ME>AE olduğu belirlendi. EE ve ME  $\alpha$ -glukozidaz enzimini sırasıyla 0.301±0.002 mg/mL ve 0.477±0.003 mg/mL IC<sub>50</sub> değerleriyle inhibe etmiştir. Ayrıca, EE ve ME'nin inhibisyon sabiti (K<sub>i</sub>) değerleri 0.48±0.02 mg/mL ve 0.46±0.01 mg/mL bulunarak, yarışmasız inhibisyon gerçekleştirdikleri belirlenmiştir. EE'nin 100 ve 300 mg/kg dozları farelerde formalin ile indüklenen ödemi önemli derecede azalttığı belirlenmiştir. DNA koruma çalışmalarında, ekstraktlar radikal süpürme aktivitesinden dolayı Fenton reaktifıyla oluşturulan hasara karşı süpersarmal plasmid pBR322 DNA'yı korumuştur.

**Sonuç:** Sonuçlarımız, *V. arctostaphylos* L.'nin EE'sinin güçlü antioksidan, anti-inflamatuvar,  $\alpha$ -glukozidaz inhibisyon ve DNA koruyucu etkilere sahip olduğunu göstermiştir; bu, oksidatif hasar ve iltihaplanma ile ilişkili hastalıkları önlemek veya tedavi etmek için etkili bir tıbbi bitki olabileceğini düşündürmektedir.

**Anahtar kelimeler:** Antioksidan, anti-inflamatuvar, DNA,  $\alpha$ -glukozidaz, *Vaccinium arctostaphylos*

\*Correspondence: E-mail: burakbarut@ktu.edu.tr, Phone: +90 537 592 44 89 ORCID-ID: orcid.org/0000-0002-7441-8771

Received: 14.02.2018, Accepted: 15.03.2018

©Turk J Pharm Sci, Published by Galenos Publishing House.

## INTRODUCTION

Medicinal plants containing secondary metabolites such as phenolic, anthocyanin, and flavonoid compounds have been used as alternative therapeutic tools to treat many diseases throughout medical history.<sup>1</sup> Many plants are considered able to scavenge and hinder free radicals, including reactive oxygen species (ROS) such as hydroxyl radical (OH<sup>•</sup>), hydrogen peroxide (H<sub>2</sub>O<sub>2</sub>), and superoxide anion radical (O<sub>2</sub><sup>•-</sup>), which induce oxidative damage in biomolecules due to these secondary metabolites possessing antioxidant activity.<sup>2</sup> In addition, plant-based natural antioxidants are preferred to synthetic ones due to their good safety profiles.<sup>3</sup> Therefore, there is growing interest in finding natural compounds that could prevent oxidative damage underlying the pathogenesis of many diseases.

The genus *Vaccinium* belongs to the family *Ericaceae*; it includes approximately 450 species distributed in the Northern Hemisphere and tropical mountains of America and Asia.<sup>4,5</sup> Numerous studies have reported that *Vaccinium* possesses several biological and pharmacological activities, making it an attractive medical plant.<sup>6</sup> Previous studies reported that *Vaccinium* species have been used for memory improvement, eyesight protection, cardiovascular protection, and for their antioxidant, antidiabetic, and anticancer activities.<sup>7-10</sup>

*Vaccinium arctostaphylos* L., commonly named the Caucasian whortleberry, is the only member of the genus *Vaccinium* and is widely used as an antidiabetic and antihypertensive agent.<sup>11,12</sup> To date, this plant has been reported to contain phenolic compounds such as anthocyanin, flavanol, and procyanidins that are responsible for numerous biological activities such as reducing serum glucose concentration and improving lipid profile, antioxidant and urinary antiseptic activities, etc.<sup>12,13</sup> Ayaz reported that delphinidin, petunidin, and malvidin were the most predominant anthocyanins of *V. arctostaphylos* L. fruits, while caffeic acid and *p*-coumaric acid were the major phenolic compounds.<sup>14,15</sup>

Diabetes mellitus (DM) is one of the most prevalent metabolic disorders, characterized by hyperglycemia triggered by inherited and acquired formation of insulin or by insulin resistance.<sup>16,17</sup> According to the International Diabetes Federation, 425 million people are living with DM; this number is expected to increase to 629 million by 2045 approximately. In addition, 352 million adults are at risk of developing DM.<sup>18</sup>

$\alpha$ -Glucosidase (EC 3.2.1.20) catalyzes the break of the glycosidic bond in oligosaccharides into  $\alpha$ -glucose, resulting in postprandial hyperglycemia.<sup>19</sup> Thus, an  $\alpha$ -glucosidase inhibitor could be useful to treat obesity and DM. Commercial  $\alpha$ -glucosidase inhibitors such as acarbose, voglibose, and miglitol are currently used against DM, but many adverse effects have been observed such as abdominal pain, renal tumors, hepatic injury, diarrhea, and flatulence.<sup>20</sup> Therefore, scientists seek novel natural  $\alpha$ -glucosidase inhibitors against DM.

To the best of our knowledge, there is no report on kinetic studies of the  $\alpha$ -glucosidase inhibition, anti-inflammatory, and DNA protective properties of *V. arctostaphylos*. The goal of the present study was to evaluate the antioxidant, anti-

inflammatory,  $\alpha$ -glucosidase inhibitory, and DNA protective properties of ethanol extract (EE), methanol extract (ME), and aqueous extract (AE) of *V. arctostaphylos* L. from Turkey.

## EXPERIMENTAL

### *Plant material and sample preparation*

*V. arctostaphylos* fruits were collected from Uzungöl, Trabzon, Turkey, in August 2013 and identified by Prof. Kamil Coşkunçelebi. The fruits were dried at room temperature for 2 weeks and the dried samples were pulverized using an automatic herbal grinder. Then the pulverized fruits were extracted with solvent (ethanol, methanol, and water) in a shaker for 6 h $\times$ 3. After shaking, the mixtures were filtered with Whatman filter paper No: 1. The solvent was evaporated under reduced pressure by a Heidolph Hei-VAP rotary evaporator. The extracts were kept +4°C until further use.<sup>21</sup>

### *Total phenolic content*

The total phenolic content of extracts was evaluated using the Folin–Ciocalteu reagent method described by Keser. The calibration curve was obtained with gallic acid (GA) and the results expressed as mg gallic acid equivalents (GAE) per g dry weight of the sample.<sup>22</sup>

### *Total anthocyanin content*

The total anthocyanin content of extracts was determined with the pH differential absorbance method, as described by Cheng and Breen, and expressed as  $\mu$ g cyaniding-3-glucoside equivalents (CGE) per g dry weight of the fruit.<sup>23</sup>

### *Total flavonoid content*

The total flavonoid content of extracts was investigated using an Al(NO<sub>3</sub>)<sub>3</sub> assay and expressed as mg quercetin equivalents (QEE) per g dry weight of the sample.<sup>24</sup>

### *Antioxidant activities*

#### *2,2-diphenyl-1-picrylhydrazyl radical scavenging assay*

The 2,2-diphenyl-1-picrylhydrazyl (DPPH) radical scavenging activities of extracts were investigated using the method described by Blois and the inhibition percentage was calculated using Formula 1.<sup>25</sup>

$A_{\text{control}}$  is the antioxidant activity without extracts and  $A_{\text{extract}}$  is the antioxidant activity with extracts at various concentrations.  $SC_{50}$  values represented the concentration of the extracts that caused 50% inhibition of radical formation. GA was used as a positive control.

#### *Ferrous ion-chelating assay*

The ferrous ion-chelating activity of the extract was investigated using Chua et al.'s<sup>26</sup> method and the ferrous ion chelating capacities were calculated using Formula 1.

#### *Ferric reducing antioxidant power assay*

The ferric reducing antioxidant power (FRAP) effects of extracts were evaluated using the method described by Oyaizu and expressed as butylated hydroxyanisole equivalents (BHA-E) per g dry weight of the sample.<sup>27</sup>

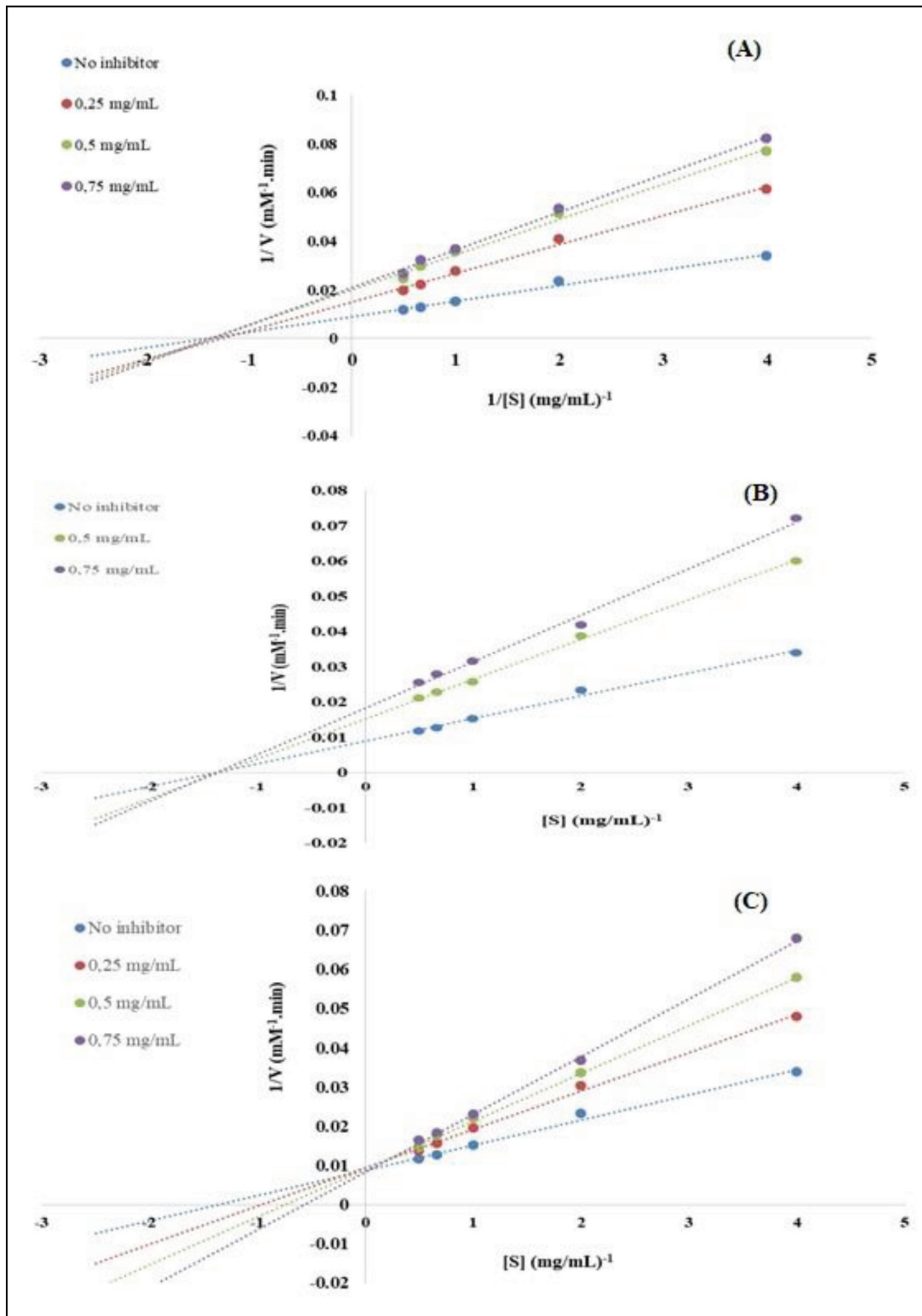


**Figure 1.** Lineweaver–Burk plots for kinetic analysis of  $\alpha$ -glucosidase inhibition by a) EE, b) ME, and c) AE

EE: Ethanol extract, ME: Methanol extract, AE: Aqueous extract

### Enzyme inhibition

#### $\alpha$ -Glucosidase inhibition assay

The  $\alpha$ -glucosidase inhibitory properties were examined according to a previous study with a slight modification.<sup>28</sup> In the

present study, the extracts and 0.5 U/mL  $\alpha$ -glucosidase enzyme were mixed in a 96-well microplate and left to react for 10 min. After that, 5 mM 4-pNPG was added and the reaction mixture was incubated for 10 min. The absorbance was measured at

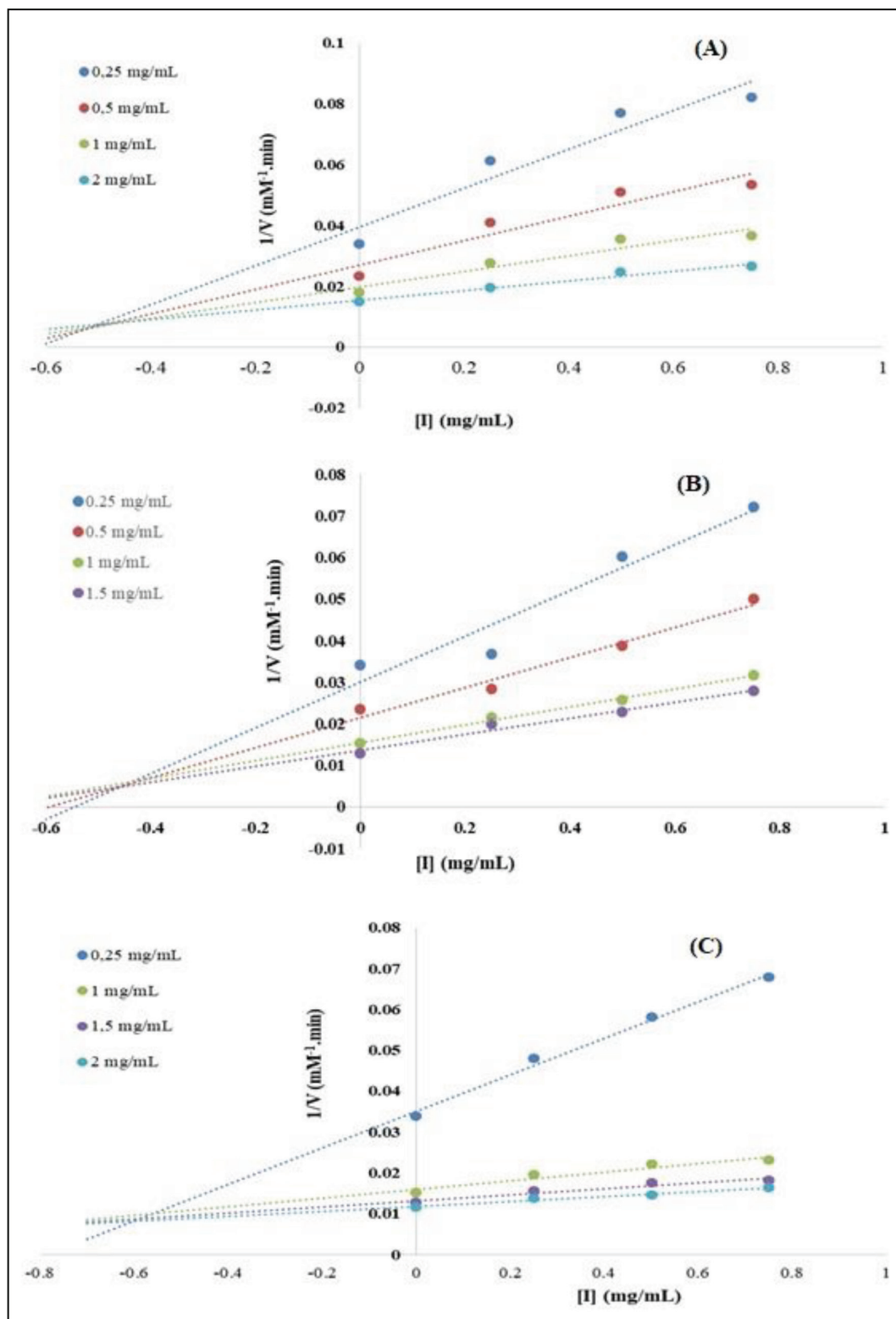


**Figure 2.** Dixon plot kinetic analysis of  $\alpha$ -glucosidase inhibition by a) EE, b) ME and c) AE  
 EE: Ethanol extract, ME: Methanol extract, AE: Aqueous extract

405 nm using a 96-well microplate reader. Acarbose was used as a standard reference. The percentage of  $\alpha$ -glucosidase inhibition was calculated as follows:

$$\alpha\text{-glucosidase inhibition (\%)} = \left[ \frac{(A_{\text{control}} - A_{\text{extract}})}{A_{\text{control}}} \right] \times 100$$

Here  $A_{\text{control}}$  is the activity of enzyme without extract and  $A_{\text{extract}}$  is the activity of enzyme with extract at various concentrations.

#### Kinetic analysis of $\alpha$ -glucosidase inhibition

In order to investigate the inhibition type and inhibition constant ( $K_i$ ) values of extracts, Lineweaver–Burk and Dixon plots were used against  $\alpha$ -glucosidase enzyme.<sup>29</sup> The kinetic analysis was conducted with various 4-pNPG concentrations in the absence and presence of extracts.<sup>30</sup>

#### DNA protective properties

The DNA protective properties of extracts of *V. arctostaphylos* fruits against oxidative damage caused by OH $\cdot$  were monitored by conversion of supercoiled plasmid pBR322 DNA to open circular form as described by Yeung et al.<sup>31</sup> In the present study, the total volume of the mixture was 10  $\mu$ L, containing Tris-HCl buffer (pH 7.0), supercoiled plasmid pBR322 DNA, 1 mM FeSO $_4$ , 2% H $_2$ O $_2$ , and various concentration of extracts (0.125, 0.25, and 0.5 mg/mL). The mixtures were incubated at 37°C for 1 h. After incubation, loading buffer (bromophenol, glycerol, SDS, and xylene cyanol) was added to the mixture. The mixtures were loaded on agarose gel and electrophoresis was performed at 100 V for 90 min using the wide Mini-Sub cell GT system from Bio-Rad. The results were visualized with the Bio-Rad Gel Doc XR system.<sup>32</sup>

#### In vivo anti-inflammatory activity

##### Animals

The male Balb/c mice (25–35 g; n=24) used in this study were kept in temperature controlled (24 $\pm$ 1°C) rooms with food and water given *ad libitum*. They were allowed to acclimatize to the laboratory conditions for 1 week. The experiments were carried out between 9 am and 4 pm. The experimental protocol was approved by the Institutional Animal Ethical Committee of Karadeniz Technical University (2017/45).

##### Formalin-induced hind paw edema

The anti-inflammatory activity of EE was evaluated by formalin-induced edema. The mice were divided into the following 4 groups with 6 mice in each group: 1) control (saline, 10 mL/kg p.o.), 2) diclofenac (10 mg/kg, i.p.), 3) EE 100 mg/kg p.o., 4) EE 300 mg/kg p.o. Extract was administered orally to the mice for three consecutive days. Then 60 min after the last dose of extracts and 30 min after administration of diclofenac and saline, 20  $\mu$ L of 1% formalin (in 0.9% saline) solution was injected into the dorsal surface of the right hind paws of the animals to form edema. Edema was expressed as the increment in paw thickness and was measured 30 min before and 30, 60, and 120 min after the formalin injection by micrometer caliper.<sup>33</sup>

#### Statistical analysis

The data were analyzed using GraphPad Prism 5.0 and Microsoft Excel Windows 10. *In vitro* tests were performed in triplicate and the data were expressed as the mean  $\pm$  standard deviation. Statistical analysis was performed with two-way analysis of variance followed by Bonferroni tests. P<0.05 was considered statistically significant.<sup>34</sup>

## RESULTS

#### Determination of total phenolic, anthocyanin, and flavonoid contents

The total phenolic, total anthocyanin, and total flavonoid contents of extracts are shown in Table 1. EE had the highest total phenolic, anthocyanin, and flavonoid contents, with 44.42 $\pm$ 1.22 mg GAE/g dry weight, 8.46 $\pm$ 0.49 mg CGE/g dry weight, and 9.22 $\pm$ 0.92 mg QEE/g dry weight, respectively. In addition, ME had higher total phenolic, anthocyanin, and flavonoid contents than AE, about 1.63-, 1.40-, and 5.57-fold, respectively.

#### Evaluation of antioxidant activity

The SC $_{50}$  values of DPPH and metal chelating radical scavenging activities of extracts are presented in Table 2. All extracts demonstrated scavenging activities against DPPH radical in a concentration-dependent manner. The DPPH radical scavenging assay showed that EE had significant antioxidant activities, with an SC $_{50}$  value of 0.141 $\pm$ 0.009 mg/mL. The extracts

**Table 1. Total phenolic, anthocyanin, and flavonoid contents of *Vaccinium arctostaphylos* L. fruit extracts**

Extracts	Total phenolic content (mg GAE/g dry weight)	Total anthocyanin content (mg CGE/g dry weight)	Total flavonoid content (mg QEE/g dry weight)
EE	44.42 $\pm$ 1.22	8.46 $\pm$ 0.49	9.22 $\pm$ 0.92
ME	26.78 $\pm$ 0.67	6.02 $\pm$ 1.20	7.80 $\pm$ 0.44
AE	16.42 $\pm$ 0.15	4.29 $\pm$ 0.33	1.40 $\pm$ 0.02

EE: Ethanol extract, ME: Methanol extract, AE: Aqueous extract, GAE: Gallic acid equivalents, CGE: Cyaniding-3-glucoside equivalents, QEE: Quercetin equivalents

**Table 2. DPPH radical scavenging, metal chelating, and FRAP activities of *Vaccinium arctostaphylos* L. fruit extracts**

Extracts	DPPH (IC $_{50}$ values mg/mL)	Metal chelating effect (IC $_{50}$ values mg/mL)	FRAP (mg BHAE/g dry weight)
EE	0.141 $\pm$ 0.009	0.453 $\pm$ 0.007	62.06 $\pm$ 2.13
ME	0.211 $\pm$ 0.011	0.757 $\pm$ 0.004	47.70 $\pm$ 2.77
AE	0.263 $\pm$ 0.003	0.909 $\pm$ 0.006	15.39 $\pm$ 0.98
GA	0.068 $\pm$ 0.001	1.243 $\pm$ 0.010	-
EDTA	-	0.020 $\pm$ 0.001	-

EE: Ethanol extract, ME: Methanol extract, AE: Aqueous extract, GA: Gallic acid, EDTA: Ethylenediaminetetraacetic acid, FRAP: Ferric reducing antioxidant power, DPPH: 2,2-diphenyl-1-picrylhydrazyl, BHAE: Butylated hydroxyanisole equivalents



demonstrated moderate metal chelating activities compared to ethylenediaminetetraacetic acid. EE had the highest chelating activities, with an  $SC_{50}$  value of  $0.453 \pm 0.007$  mg/mL, whereas AE had the lowest activities, with an  $SC_{50}$  value of  $0.909 \pm 0.006$  mg/mL.

The FRAP activities of the extracts are presented in Table 2 and expressed as mg BHA/g dry weight. EE had the highest reducing activities, with  $62.06 \pm 2.13$  mg BHA/g dry weight, while ME and AE were  $47.70 \pm 2.77$  and  $15.39 \pm 0.98$  mg BHA/g dry weight, respectively.

#### Enzyme inhibition and kinetic analysis of $\alpha$ -glucosidase inhibition

The  $\alpha$ -glucosidase inhibitory effects of extracts were evaluated using the da Silva Pinto method when compared to acarbose as a standard reference. The results obtained in the present study were expressed as  $IC_{50}$  values and are presented in Table 3. The extracts demonstrated an inhibitory effect against  $\alpha$ -glucosidase ranging from  $0.301 \pm 0.003$  mg/mL to  $0.591 \pm 0.007$  mg/mL as  $IC_{50}$  values. EE exhibited the most potent inhibitory activity against  $\alpha$ -glucosidase, with an  $IC_{50}$  value of  $0.301 \pm 0.003$  mg/mL.

The kinetic analysis of extracts was carried out using Lineweaver–Burk and Dixon plots and is presented in Table 3 and Figures 1 and 2. These data obtained were plotted as  $1/\text{activity}$  ( $1/V$ ) against  $1/\text{substrate concentration}$  ( $1/[S]$ ) for Lineweaver–Burk plots. These results revealed that the inhibition type EE and ME were noncompetitive, while AE was competitive.  $K_i$  values using Dixon plots were plotted as  $1/\text{enzyme velocity}$  versus inhibitor concentration with varying concentrations of the substrate. The  $K_i$  values of EE, ME, and AE were  $0.48 \pm 0.02$  mg/mL,  $0.46 \pm 0.01$  mg/mL, and  $0.58 \pm 0.04$  mg/mL, respectively.

**Table 3.**  $IC_{50}$  values (mg/mL), inhibition type, and  $K_i$  values (mg/mL) of *Vaccinium arctostaphylos* L. fruit extracts against  $\alpha$ -glucosidase enzyme

Extracts	$IC_{50}$ values	Inhibition type	$K_i$ values
EE	$0.301 \pm 0.003$	Noncompetitive	$0.48 \pm 0.02$
ME	$0.477 \pm 0.003$	Noncompetitive	$0.46 \pm 0.01$
AE	$0.591 \pm 0.007$	Competitive	$0.58 \pm 0.04$
Acarbose	$0.031 \pm 0.001$	-	-

EE: Ethanol extract, ME: Methanol extract, AE: Aqueous extract

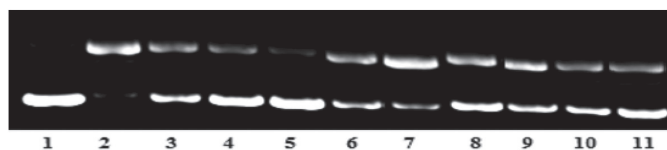


**Figure 3.** DNA protective properties of *Vaccinium arctostaphylos* L. fruit extracts. Lane 1: DNA control; Lane 2: DNA + 1 mM  $FeSO_4$  + 2%  $H_2O_2$ ; Lane 3: DNA + 1 mM  $FeSO_4$  + 2%  $H_2O_2$  + 0.125 mg/mL EE; Lane 4: DNA + 1 mM  $FeSO_4$  + 2%  $H_2O_2$  + 0.25 mg/mL EE; Lane 5: DNA + 1 mM  $FeSO_4$  + 2%  $H_2O_2$  + 0.5 mg/mL EE; Lane 6: DNA + 1 mM  $FeSO_4$  + 2%  $H_2O_2$  + 0.125 mg/mL ME; Lane 7: DNA + 1 mM  $FeSO_4$  + 2%  $H_2O_2$  + 0.25 mg/mL ME; Lane 8: DNA + 1 mM  $FeSO_4$  + 2%  $H_2O_2$  + 0.5 mg/mL ME; Lane 9: DNA + 1 mM  $FeSO_4$  + 2%  $H_2O_2$  + 0.125 mg/mL AE; Lane 10: DNA + 1 mM  $FeSO_4$  + 2%  $H_2O_2$  + 0.25 mg/mL AE; Lane 11: DNA + 1 mM  $FeSO_4$  + 2%  $H_2O_2$  + 0.5 mg/mL AE

AE: Aqueous extract, EE: Ethanol extract, ME: Methanol extract

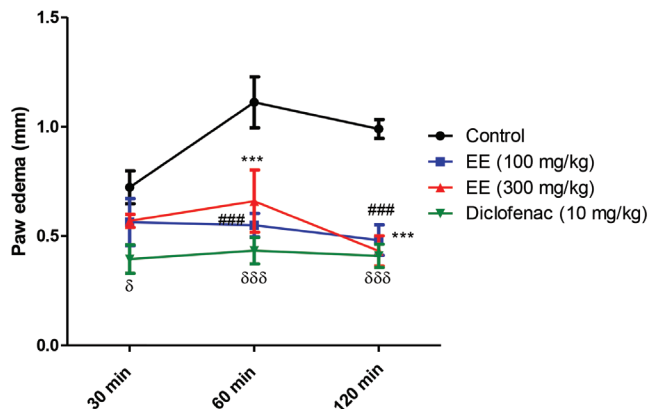


**Figure 4.** Effect of EE of *Vaccinium arctostaphylos* L. fruits in formalin-induced paw edema in mice ( $n=6$ )

### $p < 0.001$  EE (100 mg/kg) vs control group, \*\*\* $p < 0.001$  EE (300 mg/kg) vs control group,  $\delta p < 0.05$ ;  $\delta\delta\delta p < 0.001$  diclofenac (10 mg/kg) vs control group (two-way ANOVA, post-hoc Bonferroni), EE: Ethanol extract

#### In vivo anti-inflammatory activity

The *in vivo* anti-inflammatory activity of EE was also evaluated due to its higher antioxidant activity than the other extracts. As presented in Figure 3, the intraplantar injection of formalin solution induced edema in the control group significantly with a peak at 60 min. Pretreatment with 100 and 300 mg/kg doses of EE significantly reduced the edematogenic response at 60 and 120 min compared to the control group ( $p < 0.001$ ). As expected, diclofenac treatment markedly reduced edema thickness at 30, 60, and 120 min compared to the control group ( $p < 0.05$ ;  $p < 0.001$ ). However, there was no statistically significant difference between extract doses or extract doses and the diclofenac group in anti-edematogenic response.

#### DNA protective properties

The DNA protective properties of extracts were investigated using supercoiled pBR322 plasmid DNA against damage caused by hydroxyl ( $\cdot OH$ ) radicals and the results are shown in Figure 4. When supercoiled pBR322 plasmid DNA (form I) was exposed to Fenton's reagent ( $FeSO_4$  and  $H_2O_2$ ), form I converted to nicked pBR322 plasmid DNA (form II) by single-strand breaks as shown in lane 2 in Figure 4. Upon increasing concentration of the extracts treated with pBR322 DNA, form II decreased and form I increased in a concentration dependent manner. At 500  $\mu g/mL$ , EE almost converted form II to form I; thereby it had the highest protective effect among the extracts.

## DISCUSSION

The phenolic compounds, acting as hydrogen donors, ROS scavengers, and reducing agents, are responsible for many biological activities such as hepatoprotective, anti-allergic, anticancer, anti-inflammatory, antimutagenic, antioxidant, and antidiabetic effects.<sup>35</sup> In the present work, EE had the highest total phenolic content, with  $44.42 \pm 1.22$  mg GAE/g dry weight. According to the literature, Ayaz et al.<sup>14</sup> reported that 13 phenolic compounds were identified in *V. arctostaphylos* fruits from Turkey, including gallic, protocatechuic, *p*-hydroxybenzoic, *m*-hydroxybenzoic, gentisic, sinapic, chlorogenic, *p*-coumaric,

ferulic, syringic, caffeic, salicylic, and trans-cinnamic acids. Saral et al.<sup>36</sup> reported that total phenolic contents of ME in *V. arctostaphylos* fruits from different regions were  $20.74 \pm 0.24$  mg GAE/g weight of samples. Hasanloo et al.<sup>37</sup> reported that acidic ME of the plants was found to contain 9.48 mg GAE/g dry weight. The higher amount of total phenolic content was determined as 42.73 mg GAE/g dry weight in Iran and the highest phenolic content was determined in May. Anthocyanins, which are responsible for colors ranging from red to blue in most vegetables, flowers, and fruits, are water-soluble pigments that are extensively spread throughout the plant kingdom. These compounds have been reported to have anti-inflammatory and protective effects against chronic disorders such as hypertension, DM, and metabolic syndromes.<sup>38</sup> Latti et al.<sup>15</sup> identified that delphinidin, petunidin, malvidin were the most predominant anthocyanidins in *V. arctostaphylos* fruits from Turkey using high performance liquid chromatography (HPLC)-diode array detection and HPLC-electrospray ionization-mass spectrometer. In the present study, EE had the highest total anthocyanin content, with  $8.46 \pm 0.49$  mg CGE/g dry weight among the extracts tested. Similar to our findings, Saral et al.<sup>36</sup> reported that ME of *V. arctostaphylos* was  $6.14 \pm 0.01$  mg CGE/g dry weight. The results obtained in the present study demonstrated that *V. arctostaphylos* is a rich source of secondary metabolites.

The flavonoid compounds, which are secondary metabolites, are crucial constituents due to their active hydroxyl groups.<sup>39</sup> In the present study, the results for total flavonoid were found to range from  $9.22 \pm 0.92$  mg QEE/g dry weight to  $1.40 \pm 0.02$  mg QE/g dry weight. According to the results of Mohaddese et al.'s<sup>11</sup> study, total flavonoid contents of AE, EE, and ME of *V. arctostaphylos* fruits were 5.4, 7.2, and 5.5 mg QEE/g dry weight, respectively, while Saral et al.<sup>36</sup> reported that ME of it ranged from  $1.93 \pm 0.10$  to  $2.16 \pm 0.46$  mg QEE/g dry weight. In the present work, we determined the antioxidant activities of EE, ME, and AE of *V. arctostaphylos* fruits on the basis of DPPH and metal chelating, radical scavenging, and reducing power. DPPH, a stable nitrogen free radical, is generally used to determine the scavenging activities of compounds that eliminate this radical with electron donation or hydrogen atom transfer.<sup>40</sup> EE showed higher DPPH scavenging activity and was positively correlated with total phenolic content. The correlation of total phenolic, total anthocyanin, and total flavonoid contents with DPPH was determined using GraphPad Prism 5.0. The Pearson's correlation coefficient ( $r$ ) and coefficient of determination ( $R^2$ ) results for total phenolic, total anthocyanin, and total flavonoid contents with DPPH were  $r=0.996$  and  $R^2=0.992$ ,  $r=0.830$  and  $R^2=0.689$ , and  $r=0.990$  and  $R^2=0.980$ , respectively. In addition, there is a correlation between total anthocyanin and metal chelating effects with  $r=0.972$  and  $R^2=0.945$ . Mohaddese et al.<sup>11</sup> reported that  $SC_{50}$  values of DPPH radical scavenging of AE, EE, and ME were 75, 45, and 35  $\mu\text{g/mL}$ , respectively. In addition, Jooyandeh et al.<sup>13</sup> prepared ultrasound-assisted extract and reported that *V. arctostaphylos* fruits were scavenged at a rate of 32.21% at 1 mg/mL. The FRAP assay is an antioxidant method to determine the reducing capacity of samples *in vitro*.

In the present study, the FRAP of extracts was demonstrated in the following order: EE>ME>AE. Güder et al.<sup>12</sup> reported that *V. arctostaphylos* fruits have remarkable reducing activities at different temperatures. The correlation between the FRAP with total anthocyanin and total phenolic was determined as  $r=0.950$  and  $R^2=0.903$  and  $r=0.933$  and  $R^2=0.870$ .

There are many reports that suggest that phenolic, anthocyanin, and flavonoid compounds included in medicinal herbs are responsible for  $\alpha$ -glucosidase inhibition.<sup>41,42</sup> According to these results, the  $\alpha$ -glucosidase inhibitory effect with total phenolic and total anthocyanin contents is more compatible than that between the  $\alpha$ -glucosidase inhibitory effect with total flavonoid content. Feshani et al.<sup>43</sup> reported that EE of *V. arctostaphylos* fruits showed antihyperglycemic activity against diabetic rats. The correlation between the  $\alpha$ -glucosidase inhibitory effect with total phenolic, total anthocyanin, and total flavonoid contents was determined as  $r=0.993$  and  $R^2=0.986$ ,  $r=0.986$  and  $R^2=0.972$ , and  $r=0.815$  and  $R^2=0.665$ .

The results from the Lineweaver-Burk plots are presented in Table 3 and Figure 1. EE and ME inhibited  $\alpha$ -glucosidase in a noncompetitive manner with  $K_i$  values of  $0.48 \pm 0.02$  mg/mL and  $0.46 \pm 0.01$  mg/mL, respectively. The noncompetitive inhibitors increase  $V_{max}$  values and do not change  $K_m$  values against enzymes. The noncompetitive inhibitors bind to different sites on the enzyme or enzyme-substrate complex, but do not bind to active sites. Otherwise, AE did not change the  $V_{max}$  value and decreased the  $K_m$  value and so it was a competitive inhibitor with  $K_i$  values of  $0.58 \pm 0.04$  mg/mL.

The formalin-induced paw edema test is widely used to screen new potential anti-inflammatory agents.<sup>44</sup> In the present work, we used this model to evaluate the anti-inflammatory effect of EE and we found a significant reduction in formalin-induced edema for both doses of EE at 60 and 120 min when compared with the control group. This result suggested that EE of *V. arctostaphylos* could have a significant effect on the prevention of inflammatory response. In addition, it is well known that especially free radicals play a major role in several inflammatory diseases. In the present study, we have shown that *V. arctostaphylos* extracts exhibited potent antioxidant activity due to the diversity of their chemical compounds such as anthocyanins, phenolics, and flavonoids.<sup>45,46</sup> The antioxidant activity of EE might be related to its anti-inflammatory activity.

It is well known that Fenton's reagent triggers oxidative damage to the bases of DNA via formation of hydroxyl radicals. Medicinal plants including antioxidants prevent hydroxyl radical-induced DNA damage due to their scavenging activities.<sup>47</sup> According to the literature, several phenolic and flavonoid compounds protect DNA against the toxic and mutagenic effects of  $\text{H}_2\text{O}_2$ .<sup>48</sup> In the present work, increasing concentrations of the extracts prevented the cleavage of supercoiled plasmid DNA when exposed to Fenton's reagent. All of the extracts in our study demonstrated remarkable reduction in the formation of form II and increase in the formation form I. EE was remarkably effective in protecting DNA by inhibiting form II and these results may be associated with its antioxidant activities.

## CONCLUSIONS

This study presented the antioxidant,  $\alpha$ -glucosidase inhibitory, anti-inflammatory, and DNA protective properties of *V. arctostaphylos* fruit extracts from Turkey. The study data demonstrated that EE had the highest total phenolic, anthocyanin, and flavonoid contents and exhibited significant scavenging and reducing activities compared to the other extracts. In addition, there was a correlation between antioxidant results and total phenolic, anthocyanin, and flavonoid contents. The  $\alpha$ -glucosidase inhibitory studies revealed that EE and ME inhibited enzyme with  $IC_{50}$  values of  $0.301 \pm 0.002$  mg/mL and  $0.477 \pm 0.003$  mg/mL and were determined as noncompetitive inhibitors, while AE was a competitive inhibitor. The  $\alpha$ -glucosidase inhibitory properties of extracts were in the following order: EE>ME>AE. In the anti-inflammatory experiment, EE indicated a significant reduction in formalin-induced edema in mice. In addition, when DNA was exposed to Fenton's reagent, all of extracts protected the DNA from damage, especially EE due to its antioxidant capacity. These results suggest that EE of *V. arctostaphylos* L. might be promising for the treatment or prevention of many diseases associated with oxidative damage and inflammation. Further studies are required to confirm these biological activities and mechanisms of action.

## ACKNOWLEDGEMENTS

This work was supported by grants from Karadeniz Technical University. We are grateful to Professor Kamil Coşkunçelebi for his help with the authentication of the species.

*Conflict of interest: There are no conflicts of interest among the authors.*

## REFERENCES

1. Seebaluck-Sandoram R, Lall N, Fibrich B, Bloom van Staden A, Mahomoodally F. Antibiotic-potential, antioxidant, cytotoxic, anti-inflammatory and anti-acetylcholinesterase potential of *Antidesma madagascariense* Lam. (Euphorbiaceae). *S Afr J Bot.* 2017;111:194-201.
2. Supasuteekul C, Nonthitipong W, Tadtong S, Likhitwitayawuid K, Tengamnuay P, Sritularak B. Antioxidant, DNA damage protective, neuroprotective, and  $\alpha$ -glucosidase inhibitory activities of a flavonoid glycoside from leaves of *Garcinia gracilis*. *Rev Bras Farmacol.* 2016;26:312-320.
3. Hyun TK, Kim HC, Ko YJ, Kim JS. Antioxidant,  $\alpha$ -glucosidase inhibitory and anti-inflammatory effects of aerial parts extract from Korean crowsberry (*Empetrum nigrum* var *japonicum*). *Saudi J Biol Sci.* 2016;23:181-188.
4. Feng CY, Wang WW, Ye JF, Li SS, Wu Q, Yin DD, Li B, Xu YJ, Wang LS. Polyphenol profile and antioxidant activity of the fruit and leaf of *Vaccinium glaucoalbum* from the Tibetan Himalayas. *Food Chem.* 2017;219:490-495.
5. Ahmadi A, Khalili M, Mashaei F, Nahri-Niknafs B. The effects of solvent polarity on hypoglycemic and hypolipidemic activities of *Vaccinium arctostaphylos* L. Unripe fruits. *Pharm Chem J.* 2017;50:746-752.
6. Kraujalyte V, Venskutonis PR, Pukalskas A, Cesoniene L, Daubaras R. Antioxidant properties, phenolic composition and potentiometric sensor array evaluation of commercial and new blueberry (*Vaccinium corymbosum*) and bog blueberry (*Vaccinium uliginosum*) genotypes. *Food Chem.* 2015;188:583-590.
7. Cambers BK, Camire ME. Can cranberry supplementation benefit adults with type 2 diabetes. *Diabetes Care.* 2003;26:2695-2696.
8. Kraft TFB, Schmidt BM, Yousef GG, Knight CTG, Cuendet M, Kang YH, Pezzuto JM, Sieglar DS, Lila MA. Chemopreventive potential of wild lowbush blueberry fruits in multiple stages of carcinogenesis. *J Food Sci.* 2005;70:159-166.
9. Krikorian R, Shidler MD, Nash TA, Kalt W, Vinqvist-Tymchuk MR, Shukitt Hale B, Joseph JA. Blueberry supplementation improves memory in older adults. *J Agric Food Chem.* 2010;58:3996-4000.
10. Liu Y, Song X, Han Y, Zhou F, Zhang D, Ji B, Hu J, Lv Y, Cai S, Wei Y, Gao F, Jia X. Identification of anthocyanin components of wild Chinese blueberries and amelioration of light induced retinal damage in pigmented rabbit using whole berries. *J Agric Food Chem.* 2011;59:356-363.
11. Mohaddese M, Kazempour N, Taghizadeh M. *In vitro* antimicrobial and antioxidant activity of *Vaccinium arctostaphylos* L. extracts. *Journal of Biologically Active Products from Nature.* 2013;3:241-247.
12. Güder A, Engin MS, Yolcu M, Gür M. Effect of processing temperature on the chemical composition and antioxidant activity of *Vaccinium arctostaphylos* fruit and their jam. *J Food Process Preserv.* 2014;38:1696-1704.
13. Jooyandeh H, Noshad M, Khamirian RA. Modeling of ultrasound-assisted extraction, characterization and *in vitro* pharmacological potential of polysaccharides from *Vaccinium arctostaphylos* L. *Int J Biol Macromol.* 2018;107:938-948.
14. Ayaz FA, Hayırlıoğlu Ayaz S, Gruz J, Novak O, Strnad M. Separation, characterization, and quantitation of phenolic acids in a little-known blueberry (*Vaccinium arctostaphylos* L.) fruit by HPLC-MS. *J Agric Food Chem.* 2005;53:8116-8122.
15. Latti AK, Kainulainen PS, Hayırlıoğlu-Ayaz S, Ayaz FA, Riihinen KR. Characterization of anthocyanins in caucasian blueberries (*Vaccinium arctostaphylos* L.) native to Turkey. *J Agric Food Chem.* 2009;57:5244-5249.
16. Deliorman Orhan D, Orhan N. Assessment of *In Vitro* Antidiabetic and Antioxidant Effects of *Helianthus tuberosus*, *Cydonia oblonga* and *Allium porrum*. *Turk J Pharm Sci.* 2016;13:181-188.
17. Şöhretoğlu D, Sari S, Soral M, Barut B, Özel A, Liptaj T. Potential of *Potentilla inclinata* and its polyphenolic compounds in  $\alpha$ -glucosidase inhibition: Kinetics and interaction mechanism merged with docking simulations. *Int J Biol Macromol.* 2018;108:81-87.
18. International Diabetes Federation, *Diabetes Atlas.* www.idf.org/diabetesatlas (Accessed 9 March 2018) 2017.
19. Sulistiyani, Safithri M, Sari YP. Inhibition of  $\alpha$ -glucosidase activity by ethanolic extract of *Melia azedarach* L. leaves. *IOP Conf Ser Earth Environ Sci.* 2016;31:1-5.
20. Zhang J, Zhao S, Yin P, Yan L, Han J, Shi L, Zhou X, Liu Y, Ma C.  $\alpha$ -Glucosidase Inhibitory Activity of Polyphenols from the Burs of *Castanea mollissima* Blume. *Molecules.* 2014;19:8373-8386.
21. Barut EN, Barut B, Engin S, Yıldırım S, Yaşar A, Türkiş S, Özel A, Sezen FS. Antioxidant capacity, anti-acetylcholinesterase activity and inhibitory effect on lipid peroxidation in mice brain homogenate of *Achillea millefolium*. *Turk J Biochem.* 2017;42:493-502.
22. Keser S, Çelik S, Türkoğlu S, Yılmaz O, Türkoğlu I. Antioxidant activity, total phenolic and flavonoid content of water and ethanol extracts from *Achillea millefolium* L. *Turk J Pharm Sci.* 2013;10:385-392.

23. Cheng GW, Breen PJ. Activity of phenylalanine ammonia-lyase (PAL) and concentrations of anthocyanins and phenolics in developing strawberry fruit. *J Am Soc Hortic Sci.* 1991;116:865-869.
24. Chang CC, Yang MH, Wen HM, Chern JC. Estimation of total flavonoid content in propolis by two complementary colorimetric methods. *J Food Drug Anal.* 2002;10:178-182.
25. Bakar F, Bahadır Acıkara Ö, Ergene B, Nebioğlu S, Saltan Çitoğlu G. Antioxidant activity and phytochemical screening of some Asteraceae Plants. *Turk J Pharm Sci.* 2015;12:123-132.
26. Chua MT, Tung YT, Chang ST. Antioxidant activities of ethanolic extracts from the twigs of *Cinnamomum osmophleum*. *Bioresour Technol.* 2008;99:1918-1925.
27. Oyaizu M. Studies on products of browning reactions-antioxidative activities of products of browning reaction prepared from glucosamine. *Jpn J Nutr.* 1986;44:307-315.
28. da Silva Pinto M, Kwon YI, Apostolidis E, Lajolo FM, Genovese MI, Shetty K. Functionality of bioactive compounds in Brazilian strawberry (*Fragaria × Ananassa* Duch.) cultivars: evaluation of hyperglycemia and hypertension potential using *in vitro* models. *J Agric Food Chem.* 2008;56:4386-4392.
29. Lineweaver H, Burk D. The determination of enzyme dissociation constant. *J Am Chem Soc.* 1934;56:658-666.
30. Şöhretoglu D, Sari S, Özel A, Barut B.  $\alpha$ -Glucosidase inhibitory effect of *Potentilla astracanica* and some isoflavones: inhibition kinetics and mechanistic insights through *in vitro* and *in silico* studies. *Int J Biol Macromol.* 2017;105:1062-1070.
31. Yeung SY, Lan WH, Huang CS, Lin CP, Chan CP, Chang MC, Jeng JH. Scavenging property of three cresol isomers against H<sub>2</sub>O<sub>2</sub>, hypochlorite, superoxide and hydroxyl radicals. *Food Chem Toxicol.* 2002;40:1403-1413.
32. Barut B, Demirbaş Ü, Özel A, Kantekin H. Novel water soluble morpholine substituted Zn(II) phthalocyanine: Synthesis, characterization, DNA/BSA binding, DNA photocleavage and topoisomerase I inhibition. *Int J Biol Macromol.* 2017;105:499-508.
33. Kumar T, Jain V. Antinociceptive and anti-inflammatory activities of *Bridelia retusa* methanolic fruit extract in experimental animals. *Scientific World Journal.* 2014;2014:890151.
34. Kumar S, Sandhir R, Ojha S. Evaluation of antioxidant activity and total phenol in different varieties of *Lantana camara* leaves. *BMC Res Notes.* 2014;7:560.
35. Alam MA, Zaidul IS, Ghafoor K, Sahena F, Hakim MA, Rafii MY, Abir HM, Bostanudin MF, Perumal V, Khatib A. *In vitro* antioxidant and  $\alpha$ -glucosidase inhibitory activities and comprehensive metabolite profiling of methanol extract and its fractions from *Clinacanthus nutans*. *BMC Complement Altern Med.* 2017;17:181.
36. Saral Ö, Ölmez Z, Şahin H. Comparison of Antioxidant Properties of Wild Blueberries (*Vaccinium arctostaphylos* L. and *Vaccinium myrtillus* L.) with Cultivated Blueberry Varieties (*Vaccinium corymbosum* L.) in Artvin Region of Turkey. *Turk J Ag Food Sci Techn.* 2015;3:40-44.
37. Hasanloo T, Sepehrifar R, Hajimehdipoor H. Levels of phenolic compounds and their effects on antioxidant capacity of wild *Vaccinium arctostaphylos* L. (Qare-Qat) collected from different regions of Iran. *Turk J Biol.* 2011;35:371-377.
38. Yıldırım S, Kadioğlu A, Sağlam A, Yaşar A, Sellitepe HE. Fast determination of anthocyanins and free pelargonidin in fruits, fruit juices, and fruit wines by high-performance liquid chromatography using a core-shell column. *J Sep Sci.* 2016;39:3927-3935.
39. Raffa D, Maggio B, Raimondi MV, Plescia F, Daidone G. Recent discoveries of anticancer flavonoids. *Eur J Med Chem.* 2017;142:213-228.
40. Kazeem MI, Ashafa AOT. *In vitro* antioxidant and antidiabetic potentials of *Dianthus basuticus* Burt & Davy whole plant extracts. *J Herb Med.* 2015;5:158-164.
41. Jimenez-Suarez V, Nieto-Camacho A, Jimenez-Estrada M, Alvarado Sanchez B. Anti-inflammatory, free radical scavenging and  $\alpha$ -glucosidase inhibitory activities of *Hamelia patens* and its chemical constituents. *Pharm Biol.* 2016;54:1822-1830.
42. Zlotek U, Szychowski KA, Swieca M. Potential *in vitro* antioxidant, anti-inflammatory, antidiabetic, and anticancer effect of arachidonic acid-elicited basil leaves. *J Funct Foods.* 2017;36:290-299.
43. Feshani AM, Kouhsari SM, Mohammadi S. *Vaccinium arctostaphylos*, a common herbal medicine in Iran: Molecular and biochemical study of its antidiabetic effects on alloxan-diabetic Wistar rats. *J Ethnopharmacol.* 2011;133:67-74.
44. Mohammad FE, Hasan WA, Mohamed EG. Natural antioxidant flavonoids in formalin-induced mice paw inflammation; inhibition of mitochondrial sorbitol dehydrogenase activity. *J Biochem Mol Toxicol.* 2017;31:21896.
45. Bowen-Forbes CS, Zhang Y, Nair MG. Anthocyanin content, antioxidant, anti-inflammatory and anticancer properties of blackberry and raspberry fruits. *J Food Compos Anal.* 2010;23:554-560.
46. Alhakmani F, Kumar S, Khan SA. Estimation of total phenolic content, *in vitro* antioxidant and anti-inflammatory activity of flowers of *Moringa oleifera*. *Asian Pac J Trop Biomed.* 2013;3:623-627.
47. Jiang Y, Han W, Shen T, Wang MH. Antioxidant activity and protection from DNA damage by water extract from pine (*Pinus densiflora*) bark. *Prev Nutr Food Sci.* 2012;17:116-121.
48. Kada S, Bouriche H, Senator A, Demirtaş I, Özen T, Çeken Toptancı B, Kızıl G, Kızıl M. Protective activity of *Hertia cheirifolia* extracts against DNA damage, lipid peroxidation and protein oxidation. *Pharm Biol.* 2017;55:330-337.



# Electroanalytical Determination of the Anti-inflammatory Drug Tenoxicam in Pharmaceutical Dosage Forms

## Anti-enflamatuvar İlaç Tenoksikamın Farmasötik Dozaj Formlarından Elektroanalitik Miktar Tayini

© Fatma AĞIN\*, © Sena ATAL

Karadeniz Technical University, Faculty of Pharmacy, Department of Analytical Chemistry, Trabzon, Turkey

### ABSTRACT

**Objectives:** The electro-oxidation behavior of the non-steroidal anti-inflammatory drug tenoxicam (TX) was studied on multiwalled carbon nanotube (MWCNT)-modified glassy carbon electrode (GCE) by cyclic voltammetry, differential pulse voltammetry (DPV), and square wave voltammetry (SWV).

**Materials and Methods:** The GCE was modified with MWCNT for sensitive determination of TX by voltammetric methods.

**Results:** The current peaks for TX occurred at around 0.520 V for DPV and 0.570 V for SWV when the potential was scanned in the positive direction. The oxidation process of TX showed irreversible and diffusion-controlled behavior. The linear responses were obtained in the range from  $2 \times 10^{-7}$  to  $1 \times 10^{-5}$  M with the limit of detection (LOD)  $1.43 \times 10^{-9}$  for DPV and from  $8 \times 10^{-9}$  to  $8 \times 10^{-6}$  with the LOD  $9.97 \times 10^{-10}$  for SWV in 1 M acetate buffer solution at pH 5.5.

**Conclusion:** Fully validated DPV and SWV were successfully applied for the determination of TX from pharmaceutical dosage form and yielded satisfying results.

**Key words:** Glassy carbon electrode, multiwalled carbon nanotubes, tenoxicam, voltammetry

### ÖZ

**Amaç:** Non-steroidal antienflamatuvar ilaç etken maddesi tenoksikamın (TX) elektro-oksidasyon davranışı çok duvarlı karbon nanotüple (MWCNT) modifiye edilmiş camı karbon elektrot (GCE) ile dönüşümlü voltametri, diferansiyel puls voltametri (DPV) ve kare dalga voltametri (SWV) ile çalışılmıştır.

**Gereç ve Yöntemler:** GCE, TX'in voltammetrik metodlarla hassas tayini için MWCNT ile modifiye edilmiştir.

**Bulgular:** Potansiyel pozitif yönde tarandığında TX'in pik akımı 0.520 V civarında DPV ile, 0.570 V civarında SWV ile oluşmuştur. TX'in oksidasyon prosesi tersinmez ve diffüzyon kontrollü davranış göstermiştir. DPV ve SWV için doğrusal cevaplar sırasıyla  $2 \times 10^{-7}$ - $1 \times 10^{-5}$  M,  $1.43 \times 10^{-9}$  M yakalama alt sınırı (LOD) ile,  $8 \times 10^{-9}$ - $8 \times 10^{-6}$  M,  $9.97 \times 10^{-10}$  M LOD ile 1 M asetat tamponu pH 5.5 içinde elde edilmiştir.

**Sonuç:** Tamamen valide edilmiş DPV ve SWV başarılı bir şekilde TX'in farmasötik dozaj formundan miktar tayini için uygulanmış ve memnun edici sonuçlar elde edilmiştir.

**Anahtar kelimeler:** Camı karbon elektrot, çok duvarlı karbon nanotüp, tenoksikam, voltametri

\*Correspondence: E-mail: fagin@ktu.edu.tr, Phone: +90 536 948 99 22 ORCID-ID: orcid.org/0000-0002-6973-4323

Received: 24.01.2018, Accepted: 15.03.2018

©Turk J Pharm Sci, Published by Galenos Publishing House.

## INTRODUCTION

Tenoxicam (TX) (Figure 1) is a non-steroidal anti-inflammatory drug and shows analgesic, anti-inflammatory, and antirheumatic properties. TX, a member of the oxicams class, is widely used to relieve swelling, inflammation, stiffness, and pain associated with osteoarthritis, rheumatoid arthritis, arthrosis, ankylosing spondylitis, arthritic diseases such as tendinitis, bursitis, shoulder or hip peri-arthritis (shoulder-hand syndrome), sprains and injuries, and acute gout. TX inhibits prostaglandin biosynthesis both *in vitro* and *in vivo*. It shows a strong inhibitory effect *in vitro* on human metalloproteinase (stromelysin and collagenase) enzymes that stimulate cartilage destruction.<sup>1</sup>

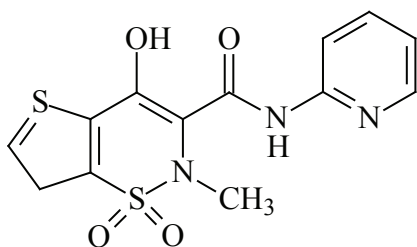


**Figure 1.** Chemical structure of TX

TX: Tenoxicam

In the literature, high performance liquid chromatography,<sup>2-7</sup> thin layer chromatography,<sup>8</sup> flow injection spectrophotometric analysis,<sup>9-11</sup> and spectrophotometric and spectrofluorimetric methods<sup>12-15</sup> are reported as methods for the determination of TX in pharmaceuticals and biological samples. These methods require mostly time-consuming sample preparation procedures such as extraction and the costly instrumentation makes their usage inconvenient. Electrochemical methods are user friendly, no pretreatment is required for them, and they use low-cost instrumentation and minimum amount of organic solvent compared to the reported analytical methods. Additionally, electrochemical methods supply high sensitivity, precision, accuracy, and wider linear dynamic range.<sup>16,17</sup>

TX was determined using a differential pulse polarographic method in pharmaceuticals and blood, with a static mercury drop electrode.<sup>18</sup> El-Maali et al.<sup>19</sup> investigated the electro-reduction behavior of TX and piroxicam at the static mercury drop electrode. The electro-reduction of TX was also investigated using a hanging mercury drop electrode.<sup>20</sup>

In recent years, working electrodes were modified with carbon nanotubes (CNTs) for electrochemical and bio-electrochemical studies.<sup>21,22</sup> CNTs can be used as electrode materials with useful properties; they show excellent high chemical stability, high mechanical strength, and a wide range of electrical conductivity. CNTs supply a modifier to promote electron transfer reactions between many biologically important species and the surface of the electrode. CNT-modified electrodes have been reported to have excellent electroanalytical properties such as low background current, wide potential window, high sensitivities, and low detection limits.<sup>23</sup> The excellent properties of CNTs

make them extremely popular for obtaining chemical sensors and they are used for electrochemical detection.<sup>24</sup>

The aim of the present study was to develop a multiwalled (MW)CNT-modified glassy carbon electrode (GCE) for electroanalytical determination of TX and to investigate the electro-oxidative behavior of TX with voltammetric methods. The obtained MWCNT-modified GCE and fully validated voltammetric methods indicated a low detection limit, high selectivity and sensitivity, and good recovery results in the electroanalytical determination of TX.

## EXPERIMENTAL

### Instrumentation

All experiments were carried out using a three-electrode electrochemical cell with a GCE (Bioanalytical Systems,  $\phi$ : 3 mm diameter) as the working electrode, a platinum wire as the counter electrode (Bioanalytical Systems), and a Ag/AgCl electrode (Bioanalytical Systems, 3.0 M KCl) as the reference electrode. All voltammetric measurements were performed using an Autolab Pgstat128n potentiostat/galvanostat with Nova 10.0 software (Metrohm-Autolab, The Netherlands). The pH measurements were carried out using a Hanna HI2211 pH meter (Romania) with an accuracy of  $\pm 0.05$  pH at room temperature. All of the electrochemical measurements were performed at room temperature ( $25 \pm 1^\circ\text{C}$ ).

### Reagents

TX was supplied by Deva (Turkey) and its pharmaceutical dosage form (Tilcotil® tablets, 20 mg of TX per tablet) was purchased from a pharmacy and was used without further purification. TX stock solutions ( $1 \times 10^{-3}$  M) were prepared in methanol and stored at  $+4^\circ\text{C}$  away from light. TX working solutions for the voltammetric investigation were prepared by direct dilution of the stock solution with the selected supporting electrolyte containing a constant amount of methanol (20% V/V). MWCNT were purchased from Nano-Lab (USA) with  $\sim 95\%$  purity, 1-5  $\mu\text{m}$  lengths and  $30 \pm 10$  nm diameter. *N,N*-Dimethylformamide (DMF) was from Fluka (Switzerland).

Britton-Robinson buffer solutions (0.04 M) were prepared at pH 3.0-8.0 from 0.04 M  $\text{CH}_3\text{COOH}$  (Merck, Germany), 0.04 M  $\text{H}_3\text{BO}_3$  (Aldrich, USA), and 0.04 M  $\text{H}_3\text{PO}_4$  (Merck, Germany). Acetate buffer solutions (1 M) at pH 3.5, 4.5, and 5.5 were prepared from 1 M  $\text{CH}_3\text{COOH}$  (Merck, Germany). Phosphate buffer solutions (0.1 M) were prepared from  $\text{H}_3\text{PO}_4$  (Merck, Germany) for pH 2.0-4.0 and  $\text{Na}_2\text{HPO}_4$  (Aldrich, USA) and  $\text{NaH}_2\text{PO}_4$  (Merck, Germany) for pH 5.0-8.0. The pH values were adjusted with 5 M NaOH (Aldrich, USA) solution.

Sartorius Arium proUV nanopure water (resistivity  $\geq 18$  M $\Omega$  cm) and analytical reagents were used for the preparation of solutions.

### Preparation of the MWCNT-modified GCE

First 0.2% and 0.5% (mg mL<sup>-1</sup>) MWCNT dispersions in DMF were sonicated for 4 h to obtain a homogeneous mixture. The GCE was polished with aqueous slurry of alumina powder ( $\phi$ : 0.01

$\mu\text{M}$ ) on a polishing pad (Bioanalytical Systems polishing pad) and then rinsed with nanopure water before coating it. Four different suspensions of MWCNT in DMF 2.5 and 5  $\mu\text{L}/0.2\%$  and 1 and 5  $\mu\text{L}/0.5\%$  were dropped on the surface of the GCE to select suspension of MWCNT according to the optimum peak current obtained for TX. The selected dispersion of MWCNT in DMF for voltammetric determination of TX was dropped on the surface of the GCE. The resulting modified electrode was named an MWCNT-modified GCE. The MWCNT-modified GCE electrode dried overnight at room temperature. After each measurement, the electrode surface was cleaned using cyclic voltammetry (CV) in the potential range between  $-0.4\text{ V}$  and  $+1.0\text{ V}$  (3 cyclic) in buffer solution.

#### Pharmaceutical assay

Ten Tilcotil® tablets (each tablet includes 20 mg of TX) were first weighed and then powdered in a mortar. The needed amount of powder equivalent to  $1 \times 10^{-3}\text{ M}$  of TX was diluted to 25 mL with methanol and sonicated for 10 min. The analyzed solutions were prepared by taking aliquots of the clear supernatant liquor and diluting with the selected supporting electrolyte. TX working solutions for voltammetric inquiries were prepared by direct dilution of the stock solution with 1 M acetate buffer solution at pH 5.5 containing a constant amount of methanol (20% V/V).

## RESULTS AND DISCUSSION

The fabrication of the MWCNT-modified GCE was optimized to obtain the best MWCNT suspension for TX oxidation. The effect of the volume of MWCNT in DMF suspension on the peak current was investigated at four different loadings of MWCNT (2.5 and 5  $\mu\text{L}/0.2\%$ , 1 and 5  $\mu\text{L}/0.5\%$ ) on the surface of the GCE. The coated electrodes with 2.5  $\mu\text{L}$  and 5  $\mu\text{L}$  for 0.2% and 1  $\mu\text{L}$  and 5  $\mu\text{L}$  for 0.5% of MWCNT suspension were used to determine  $4 \times 10^{-5}\text{ M}$  TX by CV, differential pulse voltammetry (DPV), and square wave voltammetry (SWV). As shown in Figure 2, in DP voltammograms obtained from TX the peak current reaches its maximum value ( $2.47\text{ }\mu\text{A}$ ) when the amount of MWCNT suspension (0.2%) is 2.5  $\mu\text{L}$ . Thus, 2.5  $\mu\text{L}$  for 0.2% MWCNT suspension was chosen to modify the GCE and this electrode was used for all electrochemical studies. Moreover, Figure 2 shows the response of TX obtained on a bare GCE ( $0.040\text{ }\mu\text{A}$ ). The peak current of TX on the MWCNT-modified GCE (a) increased about 60-fold compared to the peak current of TX on the bare GCE (e).

#### Voltammetric behavior of TX at the MWCNT-modified GCE

Voltammetric responses of TX were checked out in detail by CV, DPV, and SWV using the MWCNT-modified GCE over the pH range of 2.0–8.0 in different buffer solutions. The cyclic voltammograms of  $1 \times 10^{-5}\text{ M}$  TX solution exhibited an irreversible electrochemical oxidation process on the MWCNT-modified GCE in all working solutions (Figure 3). The CV scan was carried out from  $-0.40\text{ V}$  to  $1.0\text{ V}$  in the positive direction and an anodic response of TX was observed at about  $+0.55\text{ V}$  at a scan rate of  $100\text{ mV s}^{-1}$ .

The influence of pH on the peak current and potential was examined from pH 2.0 to 8.0 using CV, DPV, and SWV. The results acquired from CV, DPV and SWV showed similarity. Therefore, only DPV results for the main oxidation step are shown as  $E_p$ -pH and  $I_p$ -pH plots in Figure 4. The peak potentials of the responses were shifted to more negative potentials by increased pH. This is based on the oxidation of conjugate base at less positive potentials compared to the corresponding acid form. The TX oxidation peak that corresponds to the electroactive group in acid-base equilibrium with a  $\text{pK}_a$  of about 5.5<sup>25</sup> indicates pH dependence. Above pH 5.5, the peak potential is pH independent (Figure 4a). The linear relationship between

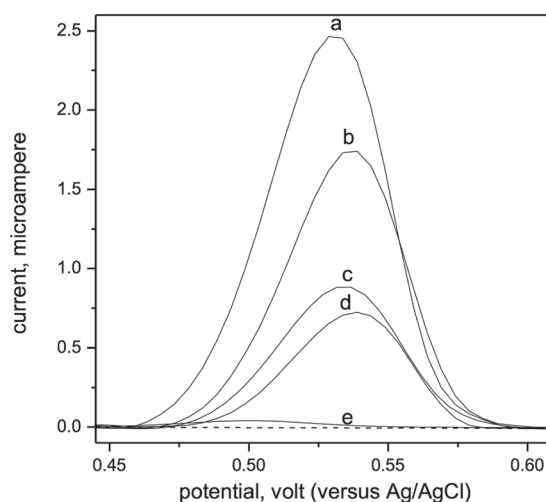


**Figure 2.** Differential pulse voltammograms  $4 \times 10^{-5}\text{ M}$  of TX in 0.04 M Britton–Robinson buffer at pH 5.0 a) 0.2% 2.5  $\mu\text{L}$ , b) 0.2% 5  $\mu\text{L}$ , c) 0.5% 1  $\mu\text{L}$ , d) 0.5% 2.5  $\mu\text{L}$  of MWCNT-modified GCE, e) bare GCE. Dash line; 0.04 M Britton–Robinson buffer solution on 0.2% 2.5  $\mu\text{L}$  of MWCNT-modified GCE  
TX: Tenoxicam, MWCNT: Multiwalled carbon nanotube, GCE: Glassy carbon electrode

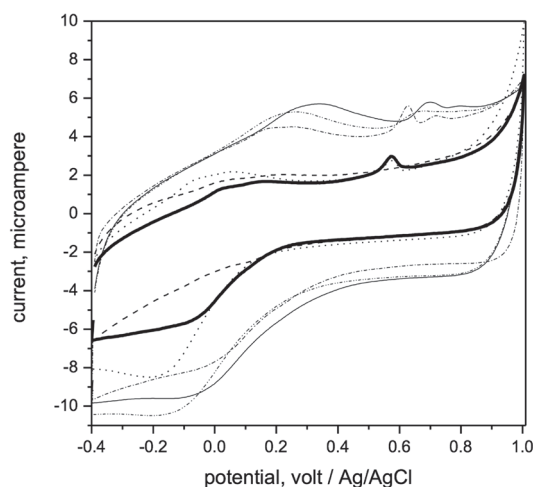


**Figure 3.** Cyclic voltammograms of  $1.0 \times 10^{-5}\text{ M}$  TX in 1 M acetate buffer at pH 3.5 (---), pH 5.5 (—), 0.04 M Britton–Robinson buffer pH 3.0 (— · —), pH 4.0 (— · · —), 0.1 M phosphate buffer at pH 7.0 (·····) with MWCNT-modified GCE. 1 M acetate buffer at pH 5.5 (---); scan rate  $100\text{ mV s}^{-1}$

TX: Tenoxicam, MWCNT: Multiwalled carbon nanotube, GCE: Glassy carbon electrode

$E_p$  and pH can be clarified according to the following equation between 2.0 and 5.5 in all supporting electrolytes:  $E_p(\text{mV}) = -24.7\text{pH} + 654.2$  ( $r=0.9987$ ). The slope value (-24.7) was about half of -59.0 mV/pH, and so it was inferred that the number of protons is half of the number of electrons transferred in the TX reaction. This can be attributed to the oxidation of the amide group in the structure of TX.

The impact of pH on the TX peak current on the MWCNT-modified GCE indicated that the peak current of TX was maximum in 1 M acetate buffer at pH 5.5 (Figure 4b). Thus, 1 M acetate buffer was selected as the supporting electrolyte for the quantitative determination of TX from pharmaceutical dosage forms.

Scan rate studies were performed to understand the electrochemical process for TX at the surface of the MWCNT-

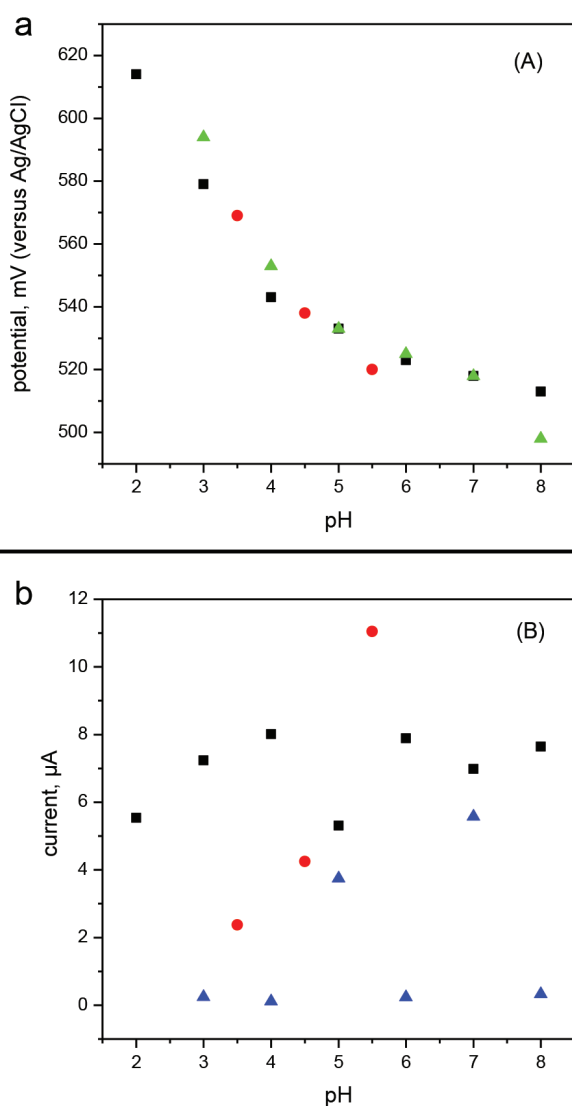


**Figure 4.** Plots of peak potential ( $E_p$ ), versus pH a) and peak current ( $I_p$ ), versus pH b) from differential pulse voltammograms of  $1.0 \times 10^{-5}$  M TX with MWCNT-modified GCE. Squares indicate 0.1 M phosphate buffer solution, triangles 0.04 M Britton-Robinson buffer solution, and circles 1 M acetate buffer solution

TX: Tenoxicam, MWCNT: Multiwalled carbon nanotube, GCE: Glassy carbon electrode

modified GCE. The electrochemical behavior of  $8 \times 10^{-5}$  M TX in 1 M acetate buffer at pH 5.5 was investigated at different scan rates ranging from 5 to 200  $\text{mV s}^{-1}$  by CV. The peak potential of TX solution was shifted in the anodic direction when the scan rate was increased (Figure 5). A plot of peak current versus the scan rate showed a straight line with a slope of 0.0118 (equation 1). This indicated that the electrochemical reaction is checked by the diffusion of the electroactive species to the MWCNT-modified GCE surface.<sup>26,27</sup> Related equations are noted below:

$$I_p = 0.0118 v + 0.15; r=0.997 (n=8) \text{ (Equation 1)}$$

It was also observed that the anodic peak current of TX shifted to a higher positive value when the scan rate was increased. This shows the irreversibility of the oxidation reaction of TX on the MWCNT-modified GCE.<sup>28</sup>

#### Calibration curve and method validation

Quantitative analysis of TX for validation studies was performed using DPV and SWV. The calibration curves for DPV and SWV were drawn by plotting the peak current versus the TX concentration. TX responses were linear between the ranges of  $2 \times 10^{-7}$  and  $1 \times 10^{-5}$  M for DPV and  $8 \times 10^{-9}$  and  $8 \times 10^{-6}$  M for SWV. Equations obtained from the calibration data were as follows:

$$I_p(\mu\text{A}) = 52349 \mu\text{M} - 0.0209; r=0.997 (n=10) \text{ for DPV (Equation 2)}$$

$$I_p(\mu\text{A}) = 25472 \mu\text{M} + 0.0039; r=0.997 (n=14) \text{ for SWV (Equation 3)}$$

DP and SW voltammograms for various concentrations of TX are shown in Figures 6a and 6b, respectively.

Limit of detection (LOD) and limit of quantification values were calculated according to  $3s/m$  and  $10s/m$ , respectively ( $s$  is the standard deviation of the peak currents obtained from three sequential measurements and  $m$  is the slope of the related calibration graph).<sup>29-32</sup> The characteristics of the calibration curve results for DPV and SWV are shown in Table 1.

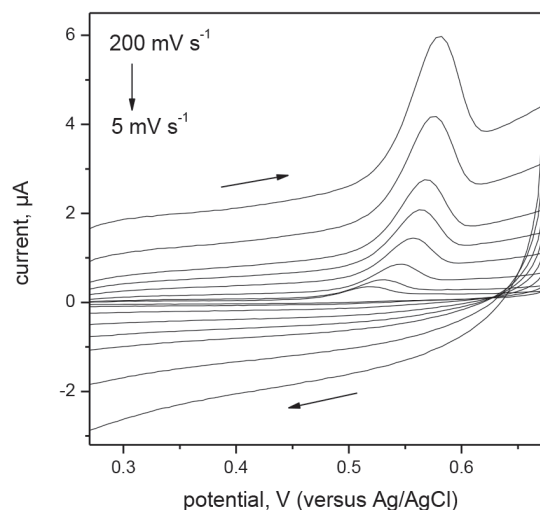


**Figure 5.** Cyclic voltammograms of  $8.0 \times 10^{-5}$  M of TX in 1 M acetate buffer solution at pH 5.5 at scan rates of 5, 10, 25, 50, 75, 100, 150, and 200  $\text{mV s}^{-1}$  with MWCNT-modified GCE

TX: Tenoxicam, MWCNT: Multiwalled carbon nanotube, GCE: Glassy carbon electrode



We determined the precision of the improved methods by repeatability and reproducibility studies. For the experiments  $6 \times 10^{-6}$  M TX solution in 1 M acetate buffer at pH 5.5 was used. To calculate relative standard deviation (RSD %) values for DPV and SWV, five measurements were taken from different

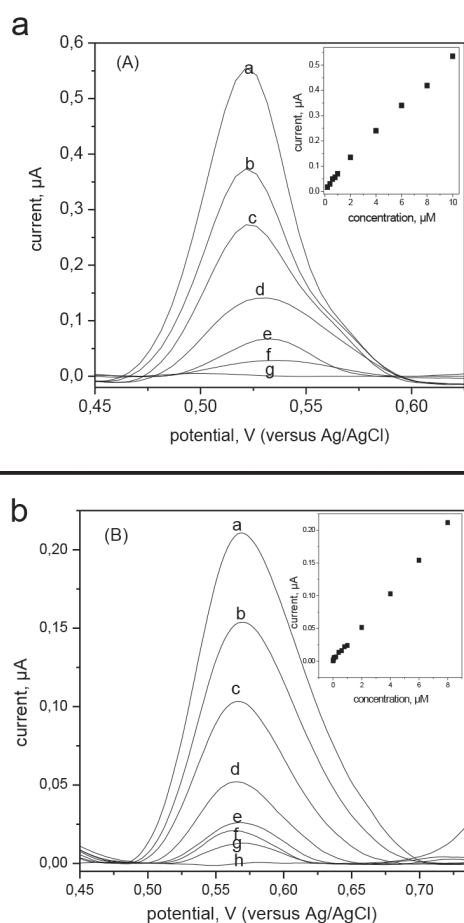


**Figure 6.** (a) Differential pulse voltammograms a)  $1 \times 10^{-5}$  M, b)  $6 \times 10^{-6}$  M, c)  $4 \times 10^{-6}$  M, d)  $2 \times 10^{-6}$  M, e)  $1 \times 10^{-6}$  M, f)  $4 \times 10^{-7}$  M TX in 1 M acetate buffer solution at pH 5.5, g) 1 M acetate buffer solution at pH 5.5 with MWCNT-modified GCE; (b) Square wave voltammograms a)  $8 \times 10^{-6}$  M, b)  $6 \times 10^{-6}$  M, c)  $4 \times 10^{-6}$  M, d)  $2 \times 10^{-6}$  M, e)  $1 \times 10^{-6}$  M, f)  $6 \times 10^{-7}$  M, g)  $4 \times 10^{-7}$  M TX in 1 M acetate buffer solution at pH 5.5, h) 1 M acetate buffer solution at pH 5.5 with MWCNT-modified GCE

TX: Tenoxicam, MWCNT: Multiwalled carbon nanotube, GCE: Glassy carbon electrode

solutions with the same TX concentrations in a day for repeatability and on different days of a week for reproducibility. These results (Table 1) demonstrated that the developed methods with the MWCNT-modified GCE were good in terms of precision, accuracy, repeatability, and reproducibility.

Stability studies of the MWCNT-modified GCE were performed as a function of time. For the purpose of the peak current  $4 \times 10^{-5}$  M TX was examined with DPV for 1 M acetate buffer solution at pH 5.5 on the same MWCNT-modified GCE stored at room temperature 2 months. After 4 and 8 weeks, the modified electrode kept 99.65% and 98.41% of the peak current of TX, respectively. After 2 weeks the peak current value kept only

**Table 1.** Validation data of calibration lines for the quantitative determination of TX by DPV and SWV on MWCNT-modified GCE in 1 M acetate buffer at pH 5.5

	MWCNT-modified GCE	
	DPV	SWV
Peak potential (V)	0.520	0.570
Linearity range (M)	$2.0 \times 10^{-7}$ - $1.0 \times 10^{-5}$	$8.0 \times 10^{-9}$ - $8.0 \times 10^{-6}$
Slope ( $\mu\text{A } \mu\text{M}^{-1}$ )	52349	25472
Intercept ( $\mu\text{A}$ )	-0.0209	+0.0039
Correlation coefficient	0.997	0.997
Limit of detection (M)	$1.43 \times 10^{-9}$	$9.97 \times 10^{-10}$
Limit of quantification (M)	$4.33 \times 10^{-9}$	$3.02 \times 10^{-9}$
Repeatability of peak current (Relative standard deviation %)*	0.675	0.411
Repeatability of peak potential (Relative standard deviation %)*	0.044	0.319
Reproducibility of peak current (Relative standard deviation %)*	0.704	0.896
Reproducibility of peak potential (Relative standard deviation %)*	0.961	0.538

TX: Tenoxicam, DPV: Differential pulse voltammetry, SWV: Square wave voltammetry, MWCNT: Multiwalled carbon nanotube, GCE: Glassy carbon electrode, \*Obtained from five experiments

**Table 2.** Compared parameters obtained using different electrodes for the determination of TX

Electrode	Method	Linear range (M)	Limit of detection (M)	References
Static mercury drop electrode	Differential pulse polarography	$7.41 \times 10^{-8}$ - $5.90 \times 10^{-5}$	$7.41 \times 10^{-8}$	18
Static mercury drop electrode	Square wave adsorptive stripping voltammetry	$8.0 \times 10^{-10}$ - $1.0 \times 10^{-5}$	$1 \times 10^{-10}$	19
Hanging mercury drop electrode	Differential pulse polarography	$1.24 \times 10^{-6}$ - $9.79 \times 10^{-6}$	-	20
MWCNT-modified GCE	Differential pulse voltammetry	$2.0 \times 10^{-7}$ - $1.0 \times 10^{-5}$	$1.43 \times 10^{-9}$	This work
GCE	Square wave voltammetry	$8.0 \times 10^{-9}$ - $8.0 \times 10^{-6}$	$9.97 \times 10^{-10}$	

TX: Tenoxicam, MWCNT: Multiwalled carbon nanotube, GCE: Glassy carbon electrode

95.12%. Consequently, the MWCNT-modified GCE demonstrated long-term stability.

In the literature, electroanalytical determination of TX has been achieved with various electrodes. In Table 2, the results obtained in the present study and from other voltammetric studies in the literature were compared in terms of electrode, linearity range, and LOD. El-Maali et al.'s<sup>19</sup> study demonstrated a wider linearity range and a lower LOD value. However, the use of a mercury electrode is a disadvantage because of the highly toxic nature of the mercury. In the present study, the MWCNT-modified GCE provided a good linear range and detection limit with SWV and the MWCNT-modified GCE. Additionally, it has some advantages such as easy preparation, user friendliness, and long-term stability. As a result, the MWCNT-modified GCE can be used more safely and sensitively in the electroanalytical determination of TX.

#### Tablet analysis

DPV and SWV methods developed using the MWCNT-modified GCE were applied for the determination of TX in pharmaceutical dosage forms (Tilcotil® tablets). Each tablet in pharmaceutical dosage form contains 20 mg of TX. The DPV and SWV methods were applied in direct determination of TX in pharmaceutical dosage form without pretreatment such as extraction or evaporation steps. Furthermore, recovery studies with the proposed methods and modified electrode were also carried out via adding known amounts of pure TX to pharmaceutical form. Five repetitive experiments were done using the related calibration curve, which is a straight line, and the obtained results are demonstrated in Table 3. As shown in Table 3, the results were satisfactory and indicated the validity of the methods and modified electrode for the determination of TX in pharmaceutical form.

**Table 3. The results for the determination of TX from tablet dosage forms and recovery experiments in 1 M acetate buffer at pH 5.5 by DPV and SWV on MWCNT-modified GCE**

	Tablet (mg)	
	Differential pulse voltammetry	Square wave voltammetry
Labeled claim (mg)	20	20
Amount found (mg)*	19.871	20.260
Relative standard deviation %	0.714	0.638
Bias %	0.645	-1.3
Added (mg)	20.00	20.00
Found (mg)*	20.035	20.018
Average recovered (%)	100.865	100.307
Relative standard deviation % of recovery	0.799	0.704
Bias %	-0.865	-0.307

TX: Tenoxicam, DPV: Differential pulse voltammetry, SWV: Square wave voltammetry, MWCNT: Multiwalled carbon nanotube, GCE: Glassy carbon electrode

## CONCLUSIONS

In the present study, a MWCNT-modified GCE was prepared for sensitive determination of TX. The fully validated DPV and SWV results demonstrated high sensitivity and reproducibility and repetitively via the developed sensor. The developed sensor was used for the determination of TX in pharmaceutical form by DPV and SWV without any pretreatment. The results were recovered in high percentages. In addition, the prepared electrode in this study is very useful in voltammetric studies of TX due to its high accuracy, sensitivity, stability, and repeatability, as well as its practical preparation. The sensor and method for determining accurate TX concentrations can be used in biological samples for pharmacokinetic studies and quality control laboratories.

*Conflicts of Interest: No conflict of interest was declared by the authors.*

## REFERENCES

- Guzmán-Hernández DS, Ramírez-Silva MT, Palomar-Pardavé M, Corona-Avendano S, Galano A, Rojas-Hernández A, Romero-Romo M. Electrochemical characterization of tenoxicam using a bare carbon paste electrode under stagnant and forced convection conditions. *Electrochimica Acta*. 2012;59:150-155.
- Múnera-Jaramillo MI, Botero-Garcés S. Determination of tenoxicam in plasma by high-performance liquid chromatography. *J Chromatogr Biomed Sci Appl*. 1993;616:349-352.
- Semreen MH, Aboul-Enein HY. LC-UV method development and validation for the nonsteroidal anti-inflammatory agent tenoxicam. *J Liq Chromatogr RT*. 2010;33:720-729.
- Sora I, Galaon T, Udrescu S, Negru J, David V, Medvedovici A. Fast RPLC-UV method on short sub-two micron particles packed column for the assay of tenoxicam in plasma samples. *J Pharm Biomed Anal*. 2007;43:1437-1443.
- Mason JL, Hobbs GJ. Simple method for the analysis of tenoxicam in human plasma using high-performance liquid chromatography. *J Chromatogr B Biomed Appl*. 1995;665:410-415.
- Sultan M, Stecher G, Stöggel WM, Bakry R, Zaborski P, Huck CW, El Kousy NM, Bonn GK. Sample pretreatment and determination of non-steroidal anti-inflammatory drugs (NSAIDs) in pharmaceutical formulations and biological samples (blood, plasma, erythrocytes) by HPLC-UV-MS and micro-HPLC. *Curr Med Chem*. 2005;12:573-588.
- Ji HY, Lee HW, Kim YH, Jeong DW, Lee HS. Simultaneous determination of piroxicam, meloxicam and tenoxicam in human plasma by liquid chromatography with tandem mass spectrometry. *J Chromatogr B Analyt Technol Biomed Life Sci*. 2005;826:214-219.
- Taha EA, Salama NN, Fattah LeI-S. Stability-indicating chromatographic methods for the determination of some oxicams. *J AOAC Int*. 2004;87:366-373.
- Al-Momani IF. Indirect flow-injection spectrophotometric determination of meloxicam, tenoxicam and piroxicam in pharmaceutical formulations. *Anal Sci*. 2006;22:1611-1614.
- García MS, Sánchez-Pedreo C, Alberio MI, Gimenez MJ. Flow-injection spectrophotometric methods for the determination of tenoxicam. *J Pharm Biomed Anal*. 1999;21:731-738.

- Al-Tamrah SA. Flow injection spectrophotometric determination of tenoxicam. *Anal Chim Acta*. 1998;375:277-283.
- El-Ries MA, Mohamed G, Khalil S, El-Shall M. Spectrophotometric and potentiometric determination of piroxicam and tenoxicam in pharmaceutical preparations. *Chem Pharm Bull*. 2003;51:6-10.
- Amin AS. Spectrophotometric determination of piroxicam and tenoxicam in pharmaceutical formulations using alizarin. *J Pharm Biomed Anal*. 2002;29:729-736.
- Barary MH, Abdel-Hay MH, Sabry SM, Belal TS. Spectrofluorimetric determination of 2-aminopyridine as a potential impurity in piroxicam and tenoxicam within the pharmacopoeial limit. *J Pharm Biomed Anal*. 2004;34:221-226.
- El Walily AFM, Blaih SM, Barary MH, El Sayed MA, Abdine HH, El Kersh AM. Simultaneous determination of tenoxicam and 2-aminopyridine using derivative spectrophotometry and high-performance liquid chromatography. *J Pharm Biomed Anal*. 1997;15:1923-1928.
- Arcos MJ, Alonso M, Ortiz MC. Genetic-algorithm-based potential selection in multivariate voltammetric determination of indomethacin and acetaminophen by partial least squares. *Electrochimica Acta*. 1988;43:479-485.
- Nikolic K, Bogovac M, Arsenijevik L. Coulometric determination of some anti-inflammatory compounds. *Farmaco*. 1993;48:1131-1136.
- Özaltın N. Differential pulse polarographic determination of tenoxicam in pharmaceuticals and added to blood. *Anal Chim Acta*. 2000;406:183-189.
- El-Maali NA, Vire JC, Patriarche GJ, Ghandour MA, Christian G. Square wave and square wave adsorptive stripping comparison of the anti-inflammatory drugs piroxicam and tenoxicam. *Analytical Sciences*. 1990;6:245-250.
- Reguera C, Ortiz MC, Arcos MJ. Differential pulse voltammetric simultaneous determination of four anti-inflammatory drugs by using soft modelling. *Electroanalysis*. 2002;14:1699-1706.
- Ağın F, Serdaroğlu V. Voltammetric determination of nimesulide using multiwalled carbon nanotubes modified carbon paste electrode. *Turk J Pharm Sci*. 2016;13:335-341.
- Bozal-Palabiyik B, Uslu B. Comparative study for voltammetric investigation and trace determination of pramipexole at bare and carbon nanotube-modified glassy carbon electrodes. *Ionics*. 2016;22:2519-2528.
- Patil RH, Hegde RN, Nandibewoor ST. Electro-oxidation and determination of antihistamine drug, cetirizine dihydrochloride at glassy carbon electrode modified with multi-walled carbon nanotubes. *Colloids Surf B Biointerfaces*. 2011;83:133-138.
- Wang J. Carbon-nanotube based electrochemical biosensors: a review. *Electroanalysis*. 2005;17:7-14.
- Rodríguez-Barrientos D, Rojas-Hernández A, Gutiérrez A, Moya-Hernández R, Gómez-Balderas R, Ramírez-Silva MT. Determination of pKa values of tenoxicam from <sup>1</sup>H NMR chemical shifts and of oxycams from electrophoretic mobilities (CZE) with the aid of programs SQUAD and HYPNMR. *Talanta*. 2009;80:754-762.
- Laviron E, Roullier L, Degrand C. A multilayer model for the study of space distributed redox modified electrodes: Part II. Theory and application of linear potential sweep voltammetry for a simple reaction. *Journal of Electroanalytical Chemistry*. 1980;112:11-23.
- Doğan-Topal B, Uslu B, Ozkan SA. Investigation of Electrochemical Behavior of Lipid Lowering Agent Atorvastatin Calcium in Aqueous Media and its Determination from Pharmaceutical Dosage Forms and Biological Fluids Using Boron-Doped Diamond and Glassy Carbon Electrodes. *Comb Chem High Throughput Screen*. 2007;10:571-582.
- Amare M, Aklog S. Electrochemical determination of caffeine content in ethiopian coffee samples using lignin modified glassy carbon electrode. *J Anal Methods Chem*. 2017;2017:3979068.
- Riley CM, Rosanske TM. *Development and Validation of Analytical Methods* (1st ed). New York; Elsevier; 1996:1-349.
- Swartz ME, Krull SI. *Analytical Method Development and Validation*, New York; Marcel Dekker; 1997:17-34.
- Ermer J, Miller HMcB. *Method Validation in Pharmaceutical Analysis*. Weinheim; Wiley-VCH; 2005:21-120.
- Gumustas M, Ozkan SA. The role of and the place of method validation in drug analysis using electroanalytical techniques. *The Open Analytical Chemistry Journal*. 2011;5:1-21.



# Flavonoid Glycosides from *Heracleum pastinaca* Fenzl

## *Heracleum pastinaca* Fenzl'in Flavonoit Glikozitleri

Perihan GÜRBÜZ\*

Erciyes University, Faculty of Pharmacy, Department of Pharmacognosy, Kayseri, Turkey

### ABSTRACT

**Objectives:** The objective was to isolate and characterize the secondary metabolites of *Heracleum pastinaca*, which has not been previously investigated.

**Materials and Methods:** Conventional chromatographic procedures were carried out for isolation of the compounds. The structures of the compounds were elucidated by extensive 1D and 2D nuclear magnetic resonance spectroscopic analysis in combination with mass spectrometry experiments and comparison with the relevant literature data.

**Results:** This first phytochemical investigation on all parts of *H. pastinaca* Fenzl led to the isolation and identification of seven known flavonoid glycosides: isoquercetin (1), rutin (2), afzelin (3), astragalin (4), isorhamnetin 3-O-glucoside (5), nicotiflorin (6), and narcissoside (7).

**Conclusion:** This is the first report on the isolation of these flavonoid glycosides from *H. pastinaca* and compounds 3, 5, 6, and 7 from the genus *Heracleum*.

**Key words:** *Heracleum*, Apiaceae, isorhamnetin, flavonoid glycosides, chemotaxonomy

### ÖZ

**Amaç:** Bu çalışmanın amacı, üzerinde daha önce herhangi bir fitokimyasal çalışma bulunmayan *Heracleum pastinaca*'nın sekonder bileşiklerinin izolasyonu ve karakterizasyonudur.

**Gereç ve Yöntemler:** Maddelerin izolasyonları, klasik kromatografik prosedürlere göre yapılmıştır. Saf bileşiklerin yapıları, kütle spektrometresi deneyleri ile 1D ve 2D nükleer manyetik rezonans spektroskopik analizleri kullanılarak aydınlatılmış; literatür verileriyle de doğrulanmıştır.

**Bulgular:** *H. pastinaca* Fenzl'in tüm kısımlarının ilk defa fitokimyasal açıdan incelenmesinde, yedi adet bilinen; izokersetin (1), rutin (2), afzelin (3), astragalin (4), izoramnetin 3-O-glukozit (5), nikotiflorin (6) ve narkisozit (7) isimli flavonoit glikozitleri izole edilerek tanımlanmıştır.

**Sonuç:** Bu çalışma ile izole edilen flavonoitlerin tamamı, *H. pastinaca*'dan, 3, 5, 6, 7 nolu bileşikler ise *Heracleum* cinsinden ilk defa tanımlanmıştır.

**Anahtar kelimeler:** *Heracleum*, Apiaceae, izoramnetin, flavonoit glikozitleri, kemotaksonomi

\*Correspondence: E-mail: pgorbuz@erciyes.edu.tr, Phone: +90 553 355 38 70 ORCID-ID: orcid.org/0000-0002-3056-411X

Received: 16.01.2018, Accepted: 15.03.2018

©Turk J Pharm Sci, Published by Galenos Publishing House.

## INTRODUCTION

The genus *Heracleum*, which is known as hogweed, is one of the largest genera of Apiaceae, containing more than 120 species widely distributed in Central Europe and Asia as well as 17 species with 41% endemism in the flora of Turkey.<sup>1,2</sup>

*Heracleum* species have been traditionally used as spices and food additives as well as in the treatment of inflammation, flatulence, stomachache, epilepsy, and psoriasis. They also act as carminative, antiseptic, antimicrobial, analgesic, and anticonvulsant agents.<sup>3</sup> Some *Heracleum* species are used traditionally for different purposes in Turkey, i.e., *Heracleum crenatifolium* as a vegetable and condiment,<sup>4</sup> *Heracleum trachyloma* against asthma and bronchitis,<sup>5</sup> *Heracleum spondylium* L. subsp. *ternatum* as a galactagogue,<sup>6</sup> and *Heracleum persicum* and *Heracleum platytaenium* for gastritis and epilepsy and as a sedative.<sup>7</sup>

There are many phytochemical studies on *Heracleum* species that mainly focused on furanocoumarins<sup>8,9</sup> and furanocoumarin glycosides,<sup>10,11</sup> together with alkaloids,<sup>12</sup> polyacetlenes,<sup>13</sup> and flavonoids.<sup>14-16</sup> Essential oil compounds of the genus were also studied.<sup>17-19</sup> While the phytochemical studies and bioactivity studies were mostly conducted with the coumarin compounds of the genus, we wanted to examine the flavonoid content of *Heracleum pastinaca* Fenzl (Figure 1), which is a tiny rare endemic plant mainly distributed in the inner and southwest region of Anatolia.<sup>20</sup>

Conventional chromatographic purification procedures were carried out to isolate the compounds of *H. pastinaca*. The structures of the compounds were elucidated by extensive 1D and 2D nuclear magnetic resonance (NMR) and electrospray ionization (ESI)-mass spectrometry (MS) experiments confirmed by the relevant literature data. The chemotaxonomic significance of the compounds was discussed.

## EXPERIMENTAL

### General

NMR spectra (400 MHz for <sup>1</sup>H NMR, 100 MHz for <sup>13</sup>C NMR, both use TMS as internal standard) were measured on a Bruker AM



Figure 1. *Heracleum pastinaca* Fenzl

400 spectrometer and MS spectra on a LC/MS Shimadzu 8040 instrument. Kieselgel 60 (Merck, 0.063-0.200 mm) was used for open column chromatography (CC). Sephadex (SP) LH-20 (SP LH-20) (General Electrics Healthcare) was used for gel permeation chromatography. LiChroprep C<sub>18</sub> (Merck, 40-63 µm) was used for medium pressure liquid chromatography (MPLC) (Buchi Pump Module: C-601, ultraviolet (UV)-Photometer: C-640, control unit: C-620, Fr. Collector: C-660). Thin layer chromatography (TLC) analyses were carried out on pre-coated Kieselgel 60 F<sub>254</sub> aluminum plates (Merck). Compounds were detected by UV fluorescence and spraying 1% vanillin/H<sub>2</sub>SO<sub>4</sub>, followed by heating at 100°C for 1-2 min.

### Plant material

Whole parts (aerial parts and roots) of *H. pastinaca* were collected from the Maden-Kızıltepe region (Niğde-Ulukışla), at about 2600 m altitude from calcareous rock clefts on August 2017. A voucher specimen was deposited at the Herbarium of Hacettepe University Faculty of Pharmacy (code HUEF-17015).

### Extraction and isolation

The dried and powdered whole parts of *H. pastinaca* (90 g) were extracted with MeOH (500 mL×4) at 37°C. After the evaporation of the solvent (yield 18%), the crude MeOH extract (17 g) was first dissolved in water and then partitioned between *n*-hexane and *n*-BuOH. *n*-BuOH (4.5 g) extract was first submitted to CC on Sephadex LH-20 (2.5×60 cm) and eluted with MeOH. Four main fractions (Fr) [Fr. 1 (1.7 g); Fr. 2 (2.2 g), Fr. 3 (332.6 mg), Fr. 4 (130 mg)] were obtained. Fr. 3 (332.6 mg) was submitted to a reverse phase column (1.5 cm×15 cm) and eluted with a gradient H<sub>2</sub>O:MeOH solvent system (10%→50%; 10 mL/min; 4-5 mbar) with the MPLC system coupled with a fraction collector to give four subfractions (Fr. 3a-d).

Fr. 3d gave compound **3** (4 mg). Further purification of Fr. 3a (116 mg) with a reverse phase column (1.5 cm×15 cm) and elution with a gradient H<sub>2</sub>O:MeOH solvent system (20%→30%; 10 mL/min; 4-5 mbar) yielded two subfractions. These two fractions were submitted to a TLC plate (20×20 cm) separately and eluted with 70:30:3 (CHCl<sub>3</sub>:MeOH:H<sub>2</sub>O) to yield compounds **1** (22 mg) and **2** (32 mg), respectively. Fr. 3c (63 mg) was submitted to two different TLC plates (20×20 cm) and eluted with 70:30:3 (CHCl<sub>3</sub>:MeOH:H<sub>2</sub>O). After elution, the bands belonging to the compounds were detected under UV<sub>254</sub> light and scraped to obtain compounds **4** and **5** (24 mg) and compounds **6** and **7** (16 mg), respectively, as mixtures.

### Structure elucidation

The structures of the compounds (Figure 2) were elucidated by 1D and 2D NMR experiments. The positions of the sugar units were confirmed by 2D HMBC experiments. Together with ESI-MS data and comparison with the relevant literature the compounds were elucidated as follows: isoquercetin (**1**),<sup>21</sup> rutin (**2**),<sup>21,22</sup> afzelin (**3**),<sup>23</sup> astragalín (**4**),<sup>21,24</sup> isorhamnetin 3-*O*-β-glucopyranoside (**5**),<sup>25</sup> kaempferol 3-*O*-rutinoside (**6**),<sup>21,22</sup> and isorhamnetin 3-*O*-rutinoside (**7**).<sup>22</sup>

**Quercetin 3-O- $\beta$ -glucopyranoside (Isoquercetin) (1)**

Yellow powder; Negative ESI/MS m/z: 463 [M-H]<sup>-</sup>; <sup>1</sup>H NMR (400 MHz, MeOH-*d*<sub>4</sub>)  $\delta$  7.72 (d, *J*=2.1 Hz, 1H, H-2'), 7.58 (dd, *J*=8.5, 2.1 Hz, 1H, H-6'), 6.86 (d, *J*=8.5 Hz, 1H, H-5'), 6.24 (d, *J*=2.0 Hz, 1H, H-8), 6.08 (d, *J*=2.0 Hz, 1H, H-6), 5.11 (d, *J*=7.6 Hz, 1H, H-1''), 3.71 (dd, *J*=11.8, 2.3 Hz, 1H, H-6a''), 3.59 (dd, *J*=12.5, 4.6 Hz, 1H, H-6b''), 3.56–3.17 (m, 4H, remaining sugar signals).

**Quercetin 3-O- $\alpha$ -rhamnopyranosyl (1 $\rightarrow$ 6)- $\beta$ -glucopyranoside (Rutin) (2)**

Yellow powder; Negative ESI/MS m/z: 609 [M-H]<sup>-</sup>; <sup>1</sup>H NMR (400 MHz, MeOH-*d*<sub>4</sub>)  $\delta$  7.68 (brs, 1H, H-2'), 7.64 (brd, *J*=8.0 Hz, 1H, H-6'), 6.87 (d, *J*=8.2 Hz, 1H, H-5'), 6.30 (brs, 1H, H-8), 6.13 (brs, 1H, H-6), 5.03 (d, *J*=7.6 Hz, 1H, H-1''), 4.53 (brs, 1H, H-1'''), 3.81 (brd, *J*=10.5 Hz, 1H, H-6a''), 3.70–3.20 (m, 9H, remaining sugar signals), 1.15 (d, *J*=6.2 Hz, 3H).

**Kaempferol 3-O- $\alpha$ -rhamnopyranoside (Afzelin) (3)**

Yellow powder; Negative ESI/MS m/z: 431 [M-H]<sup>-</sup>; <sup>1</sup>H NMR (400 MHz, MeOH-*d*<sub>4</sub>)  $\delta$  7.78 (d, *J*=8.9 Hz, 2H, H-2', 6'), 6.95 (d, *J*=8.8 Hz, 2H, H-3', 5'), 6.39 (d, *J*=2.1 Hz, 1H, H-8), 6.21 (d, *J*=2.1 Hz, 1H, H-6), 5.38 (d, *J*=1.6 Hz, 1H, H-1''), 4.23 (dd, *J*=3.3, 1.6 Hz, 1H, H-2''), 3.76–3.68 (m, 1H, H-3''), 3.53–3.40 (m, 2H, H-4'', 5''), 0.93 (d, *J*=5.7 Hz, 3H, H-6'').

**Kaempferol 3-O- $\beta$ -glucopyranoside (Astragalin) (4)**

Yellow powder; Negative ESI/MS m/z: 447 [M-H]<sup>-</sup>; <sup>1</sup>H NMR (400 MHz, MeOH-*d*<sub>4</sub>)  $\delta$  8.04 (d, *J*=8.8 Hz, 2H, H-2', 6'), 6.89 (d, *J*=8.2

Hz, 2H, H-3', 5'), 6.24 (d, *J*=1.9 Hz, 1H, H-8), 6.09 (d, *J*=1.9 Hz, 1H, H-6), 5.27 (d, *J*=7.3 Hz, 1H, H-1''), 3.76–3.57 (m, 2H, H-6''), 3.56–3.16 (m, 4H, remaining sugar signals).

**Isorhamnetin 3-O- $\beta$ -glucopyranoside (5)**

Yellow powder; Negative ESI/MS m/z: 477 [M-H]<sup>-</sup>; <sup>1</sup>H NMR (400 MHz, MeOH-*d*<sub>4</sub>)  $\delta$  7.91 (d, *J*=1.9 Hz, 1H, H-2'), 7.59 (dd, *J*=8.5, 1.9 Hz, 1H, H-6'), 6.89 (d, *J*=8.5 Hz, 1H, H-5'), 6.24 (d, *J*=1.9 Hz, 1H, H-8), 6.09 (d, *J*=1.9 Hz, 1H, H-6), 5.10 (d, *J*=7.4 Hz, 1H, H-1''), 3.94 (s, 3H, OCH<sub>3</sub>), 3.76–3.57 (m, 2H, H-6''), 3.56–3.16 (m, 4H, remaining sugar signals).

**Kaempferol 3-O-rutinoside (Nicotiflorin) (6)**

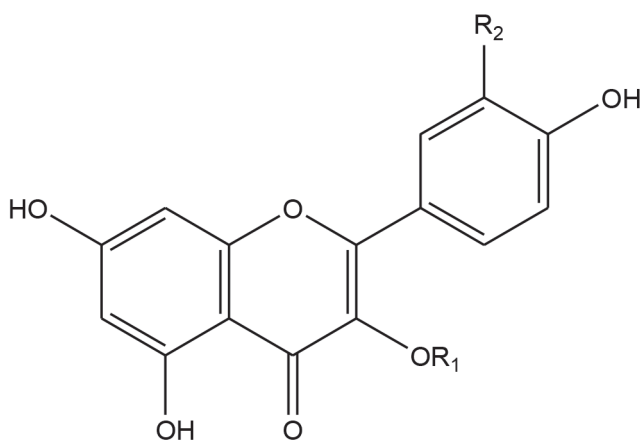
Yellow powder; Negative ESI/MS m/z: 593 [M-H]<sup>-</sup>; <sup>1</sup>H NMR (400 MHz, MeOH-*d*<sub>4</sub>)  $\delta$  8.06 (d, *J*=8.8 Hz, 2H, H-2', 6'), 6.89 (d, *J*=8.0 Hz, 2H, H-3', 5'), 6.28 (brs, 1H, H-8), 6.12 (d, *J*=1.8 Hz, 1H, H-6), 5.14 (d, *J*=7.3 Hz, 1H, H-1''), 4.51 (brs, 1H, H-1'''), 3.86–3.62 (m, 2H, H-6''), 3.61–3.22 (m, 8H, remaining sugar signals), 1.15 (d, 6.2 Hz, 3H, H-6'').

**Isorhamnetin 3-O-rutinoside (Narcissoside) (7)**

Yellow powder; Negative ESI/MS m/z: 623 [M-H]<sup>-</sup>; <sup>1</sup>H NMR (400 MHz, MeOH-*d*<sub>4</sub>)  $\delta$  7.95 (d, *J*=1.8 Hz, 1H, H-2'), 7.62 (dd, *J*=8.5, 1.8 Hz, 1H, H-6'), 6.89 (d, *J*=8.0 Hz, 1H, H-5'), 6.28 (brs, 1H, H-8), 6.12 (d, *J*=1.8 Hz, 1H, H-6), 5.02 (d, *J*=7.3 Hz, 1H, H-1''), 4.52 (brs, 1H, H-1'''), 3.95 (s, 3H, OCH<sub>3</sub>), 3.86–3.62 (m, 2H, H-6''), 3.61–3.22 (m, 8H, remaining sugar signals), 1.12 (d, 6.2 Hz, 3H, H-6'').

**RESULTS AND DISCUSSION**

The present work reports for the first time the characterization of seven flavonoid glycosides, 1–7, from all parts of *H. pastinaca*. To the best of our knowledge, this is the first report of compounds 3, 5, 6, and 7 from the genus *Heracleum*, while others were reported from different *Heracleum* species before, i.e., isoquercetin (1) from *H. napalense*<sup>26</sup> and *H. mollendorffii*,<sup>15</sup> astragalin from *H. mollendorffii*,<sup>15</sup> and rutin from *H. sphondylium*.<sup>27,28</sup> The presence of flavonoids in higher plants has been associated with various environmental conditions, such as high-light/UV stress, cold stress, nutritional deficiencies, and pathogen protection.<sup>29–31</sup> The habitats of the samples were at about 2600 m altitude, where the plants were exposed to high UV radiation. This fact should affect the production of different types and quantities of flavonoids in the plant. Phytochemical investigations of *Heracleum* species have mostly focused on the linear and angular type furanocoumarins, and different biological activities of the genus such as insecticidal, antibacterial, antiviral, and antifungal may be attributed to these coumarin-type compounds.<sup>3</sup> There are limited phytochemical studies about the isolation of flavonoids from *Heracleum* species. A number of flavonoids, i.e., kaempferol, quercetin, isorhamnetin,<sup>16</sup> rutin,<sup>28</sup> astragalin,<sup>15</sup> flavantaside, and epirutin<sup>32</sup> were reported from different *Heracleum* species. In the present study, the isolated and elucidated flavonols were mainly kaempferol, quercetin, and isorhamnetin glycosides. Flavonoids possess many important biological activities such as antimicrobial,<sup>33</sup> antioxidant,<sup>34</sup> and antiviral.<sup>35</sup> The presence of those valuable flavonoids in *Heracleum* species definitely



	R <sub>1</sub>	R <sub>2</sub>
1	Glucose	OH
2	Rutinoside	OH
3	Rhamnose	H
4	Glucose	H
5	Glucose	OCH <sub>3</sub>
6	Rutinoside	H
7	Rutinoside	OCH <sub>3</sub>

Figure 2. Structures of compounds (1–7)

enriches their chemical diversity and provides evidence for chemotaxonomic studies of *Heracleum* species and the family Apiaceae as well.

## CONCLUSIONS

This first phytochemical study of *H. pastinaca* led to the isolation and structure identification of seven flavonoid glycosides. The structures of the isolated compounds were elucidated by 1D and 2D NMR analyses, together with ESI-MS data and comparison with relevant literature data: isoquercetin (1),<sup>21</sup> rutin (2),<sup>21,22</sup> afzelin (3),<sup>23</sup> astragalinalin (4),<sup>21,24</sup> isorhamnetin 3-O- $\beta$ -glucopyranoside (5),<sup>25</sup> nicotiflorin (6),<sup>21,22</sup> and narcissoside (7).<sup>22</sup> Notably this is the first report of these flavonol glycosides from *H. pastinaca* and compounds 3, 5, 6, and 7 from the genus *Heracleum*. In conclusion, when considering the relationship between the bioactivities and the chemistry of *Heracleum* species, it is a possible that flavonoids can also play an important role in contributing to the bioactivity and traditional uses of *Heracleum* species.

## ACKNOWLEDGEMENTS

The author is indebted to Dr. Şengül Dilem Doğan (Erciyes University) for her help with the structure elucidation and Dr. Ahmet Savran for identifying the plant material and providing the high-resolution photo of the plant.

*Conflict of Interest: No conflict of interest was declared by the authors.*

## REFERENCES

- The Plant List (2013). Version 1.1. Published on the Internet; <http://www.theplantlist.org/>. (accessed 1st January).
- <http://www.bizimbitkiler.org/Heracleum>. (accessed 1st January).
- Bahadori MB, Dinparast L, Zengin G. The genus *Heracleum*: a comprehensive review on its phytochemistry, pharmacology, and ethnobotanical values as a useful herb. *Compr Rev Food Sci Food Saf*. 2016;15:1018-1039.
- Özgökçe F, Özçelik H. Ethnobotanical aspects of some taxa in East Anatolia, Turkey. *Econ Bot*. 2004;58:697.
- Polat R, Cakilcioglu U, Satil F. Traditional uses of medicinal plants in Solhan (Bingöl-Turkey). *J Ethnopharmacol*. 2013;148:951-963.
- Kültür Ş. Medicinal plants used in Kırklareli province (Turkey). *J Ethnopharmacol*. 2007;111:341-364.
- Yıldırım B, Terzioğlu Ö, Özgökçe F, Türközü D. Ethnobotanical and pharmacological uses of some plants in the districts of Karpuzalan and Adıgüzel (Van-Turkey). *J Anim Vet Adv*. 2008;7:873-878.
- Razdan TK, Kachroo V, Harkar S, Koul GL. Furanocoumarins from *Heracleum canescens*. *Phytochemistry*. 1982;21:923-927.
- Steck W. Leaf furanocoumarins of *Heracleum lanatum*. *Phytochemistry*. 1970;9:1145-1146.
- Fischer FC, Jasperse PH, Karlsen J, Svendsen AB. Ein neues furanocoumaringlykosid aus *Heracleum mantegazzianum*. *Phytochemistry*. 1974;13:2334-2335.
- Mi J, Peng Y, Zhang H, Wang X, Huo Y, Wang Z, Gao Y, Zhang H. A new benzofuran derivative glycoside and a new coumarin glycoside from roots of *Heracleum dissectum* Ledeb. *Med Chem Res*. 2017;1-6.
- upta BD, Banerjee SK, Handa KL. Alkaloids and coumarins of *Heracleum wallichii*. *Phytochemistry*. 1976;15:576.
- Nakano Y, Matsunaga H, Saita T, MORI M, KATANO M, OKABE H. Antiproliferative Constituents in Umbelliferae Plants II.: Screening for Polyacetylenes in Some Umbelliferae Plants, and Isolation of Panaxyndiol and Falcarindiol from the Root of *Heracleum moellendorffii*. *Biol Pharm Bull*. 1998;21:257-261.
- Ghods B. Flavonoids of three *Heracleum* species: *H. persicum* L., *H. sphondylium* L. and *H. montanum* Schl. *Bull Trav Soc Pharm Lyon*. 1976;20:3-8.
- Park H-J, Nugroho A, Jung B-R, Won Y-H, Jung Y-J, Kim W-B, Choi J-S. Isolation and Quantitative Analysis of Flavonoids with Peroxynitritescavenging Effect from the Young Leaves of *Heracleum moellendorffii*. *Korean J Plant Resour*. 2010;23:393-398.
- Siwon J, Karlsen J. The isolation and identification of flavonoid aglycones from *Heracleum mantegazzianum* Somm. et Lev. *Medd Nor Farm Selsk*. 1976;38:11-12.
- Skalicka-Woźniak K, Grzegorzczak A, Świątek Ł, Walasek M, Widelski J, Rajtar B, Polz-Dacewicz M, Malm A, Elansary HO. Biological activity and safety profile of the essential oil from fruits of *Heracleum mantegazzianum* Sommier & Levier (Apiaceae). *Food Chem Toxicol*. 2017;109:820-826.
- Firuzi O, Asadollahi M, Gholami M, Javidnia K. Composition and biological activities of essential oils from four *Heracleum* species. *Food Chem*. 2010;122:117-122.
- Isçan G, Ozek T, Ozek G, Duran A, Baser K. Essential oils of three species of *Heracleum*. Anticandidal activity. *Chem Nat Comp*. 2004;40:544-547.
- Babaç MT. Possibility of an information system on plants of South-West Asia with particular reference to the Turkish plants data service (TUBIVES). *Turk J Botany*. 2004;28:119-127.
- Han JT, Bang MH, Chun OK, Kim DO, Lee CY, Baek NI. Flavonol glycosides from the aerial parts of *Aceriphyllum rossii* and their antioxidant activities. *Arch Pharm Res*. 2004;27:390-395.
- Chaurasia N, Wichtl M. Flavonolglykoside aus *Urtica dioica* 1, 2. *Planta Med*. 1987;53:432-434.
- Lee SY, So YJ, Shin MS, Cho JY, Lee J. Antibacterial effects of afzelin isolated from *Cornus macrophylla* on *Pseudomonas aeruginosa*, a leading cause of illness in immunocompromised individuals. *Molecules*. 2014;19:3173-3180.
- Wei Y, Xie Q, Fisher D, Sutherland IA. Separation of patuletin-3-O-glucoside, astragalinalin, quercetin, kaempferol and isorhamnetin from *Flaveria bidentis* (L.) Kuntze by elution-pump-out high-performance counter-current chromatography. *J Chromatog A*. 2011;1218:6206-6211.
- Lee YS, Lee HS, Shin KH, Kim B-K, Lee S. Constituents of the halophyte *Salicornia herbacea*. *Arch Pharm Res*. 2004;27:1034-1036.
- Dash S, Nath LK, Bhise S. Antioxidant and antimicrobial activities of *Heracleum nepalense* D Don root. *Trop J Pharm Res*. 2005;4:341-347.
- Benedec D, Hanganu D, Filip L, Oniga I, Tipericiu B, Olah N-K, Gheldiu A-M, Raita O, Vlase L. Chemical, antioxidant and antibacterial studies of Romanian *Heracleum sphondylium*. *Farmacia*. 2017;65:252-256.
- Harborne J, Williams CA. Flavonoid patterns in the fruits of the Umbelliferae. *Phytochemistry*. 1972;11:1741-1750.

29. Dixon RA, Paiva NL. Stress-induced phenylpropanoid metabolism. *Plant Cell*. 1995;7:1085.
30. Kusano M, Tohge T, Fukushima A, Kobayashi M, Hayashi N, Otsuki H, Kondou Y, Goto H, Kawashima M, Matsuda F. Metabolomics reveals comprehensive reprogramming involving two independent metabolic responses of *Arabidopsis* to UV-B light. *Plant J*. 2011;67:354-369.
31. Roberts MR, Paul ND. Seduced by the dark side: integrating molecular and ecological perspectives on the influence of light on plant defence against pests and pathogens. *New Phytologist*. 2006;170:677-699.
32. Komissarenko N, Satsyperova I. Flavonoids and coumarins of leaves of *Heracleum antasiaticum* Manden. *Rastit Resur*. 1974.
33. Cushnie TT, Lamb AJ. Antimicrobial activity of flavonoids. *Int J Antimicrob Agents*. 2005;26:343-356.
34. Burda S, Oleszek W. Antioxidant and antiradical activities of flavonoids. *J Agr Food Chem*. 2001;49:2774-2779.
35. Kaul TN, Middleton E, Ogra PL. Antiviral effect of flavonoids on human viruses. *J Med Vir*. 1985;15:71-79.





# Optimization of Thiazolidone Scaffolds Using Pocket Modeling for Development of Potential Secretory System Inhibitors of *Mycobacterium tuberculosis*

## *Mycobacterium tuberculosis*'in Potansiyel Sekreter Sistem İnhibitörleri Olarak Thiazolidone İskelelerinin Optimizasyonu

Shivratna V. KHARE<sup>1</sup>, Sujata P. CHOUDHARI<sup>2</sup>, Siddharth P. PHALLE<sup>1</sup>, Santosh S. KUMBHAR<sup>1</sup>, Prafulla B. CHOUDHARI<sup>1\*</sup>, Sambhaji R. MASAL<sup>1</sup>, Aakash K. PATIL<sup>1</sup>, Rakesh P. DHAVAL<sup>3</sup>, Durgacharan A. BHAGWAT<sup>3</sup>, Atul M. KADAM<sup>4</sup>

<sup>1</sup>Bharati Vidyapeeth College of Pharmacy, Department of Pharmaceutical Chemistry, Computational Chemistry Research Lab, Kolhapur, India

<sup>2</sup>Sarojini College of Pharmacy, Department of Pharmaceutical Analysis, Kolhapur, India

<sup>3</sup>Bharati Vidyapeeth College of Pharmacy, Department of Pharmaceutics, Kolhapur, India

<sup>4</sup>Shree Santkrupa College of Pharmacy, Department of Pharmaceutics, Ghogaon, India

### ABSTRACT

**Objectives:** *Mycobacterium tuberculosis* is the causative organism of tuberculosis, which is the most lethal disease after cancer in the current decade. The development of multidrug and broadly drug-resistant strains is making the problem of tuberculosis more and more critical. In the last 40 years, only one molecule has been added to the treatment regimen. Generally, drug design and development programs target proteins whose function is known to be essential to the bacterial cell. *M. tuberculosis* possesses specialized protein export systems like the SecA2 export pathway and ESX pathways.

**Materials and Methods:** In the present communication, rational development of an antimycobacterial agent's targeting protein export system was carried out by integrating pocket modeling and virtual analysis.

**Results:** The 23 identified potential lead compounds were synthesized, characterized by physicochemical and spectroscopic methods like infrared and nuclear magnetic resonance spectroscopy, and further screened for antimycobacterial activity using isoniazid as standard. All the designed compounds showed profound antimycobacterial activity.

**Conclusion:** We found that Q30, M9, M26, U8, and R26 molecules had significant desirable biological activity and specific interactions with Sec of mycobacteria. Further optimization of these leads is necessary for the development of potential antimycobacterial drug candidates with fewer side effects.

**Key words:** *Mycobacterium tuberculosis*, Sec, ESX, docking, antimycobacterial, multidrug resistant, pocket modeling

### ÖZ

**Amaç:** *Mycobacterium tuberculosis*, son on yılda kanserden sonra en ölümcül hastalık olan tüberkülozun etkenidir. Çoklu ilaç ve ilaca dirençli suşların gelişimi, tüberküloz problemini daha da kritik kılmaktadır. Son 40 yılda, tedavi rejimine sadece bir molekül eklenmiştir. Genel olarak ilaç tasarımı ve geliştirme programları, bakteri hücresi fonksiyonunda önemi olduğu bilinen proteinleri hedeflemektedir. *M. tuberculosis*, SecA2 ve ESX gibi özel protein ihracat sistemlerine sahiptir.

**Gereç ve Yöntemler:** Bu çalışmada, protein atım sistemini hedefleyen antimikobakteriyel bir bileşiğin rasyonel geliştirilmesi entegre cep modelleme ve sanal analiz kullanılarak gerçekleştirilmiştir.

\*Correspondence: E-mail: praffula12@gmail.com - praffulla.choudhari@bharativedyapeeth.edu ORCID-ID: orcid.org/0000-0002-9137-3982

Received: 10.02.2018, Accepted: 22.03.2018

©Turk J Pharm Sci, Published by Galenos Publishing House.

**Bulgular:** Yirmi üç bileşik tasarlanmış, sentezlenmiş, fizikokimyasal özellikleri ve infrared ve nükleer manyetik rezonans spektroskopisi ile yapıları karakterize edilmiştir. Ayrıca isoniazid standart olarak kullanılarak antimikobakteriyel etkileri saptanmıştır. Tasarlanan bileşiklerin hepsi iyi antimikobakteriyel aktivite göstermiştir.

**Sonuç:** Q30, M9, M26, U8 ve R26 moleküllerinin önemli biyolojik aktiviteye ve mikobakterilerin Sec ile spesifik etkileşime sahip olduğu bulunmuştur. Bu hedef bileşiklerin daha da iyileştirilmesi, daha az yan etkiye sahip potansiyel antimikobakteriyel ilaç adaylarının gelişimi için gereklidir.

**Anahtar kelimeler:** *Mycobacterium tuberculosis*, Sec, ESX, docking, antimikobakteriyel, çoklu ilaç direnci, cep modellemesi

## INTRODUCTION

Tuberculosis is an air-borne disease caused by infection with *Mycobacterium tuberculosis*. In the current decade, tuberculosis has emerged as a global emergency due to its mortality rate.<sup>1-3</sup> Tuberculosis acts as the salient killer in patients suffering from immunocompromising diseases like acquired immune deficiency syndrome (AIDS) and diabetics. In more than 80% cases of AIDS death occurs in the patients due to tuberculosis.<sup>4-7</sup> The problem of multidrug resistant tuberculosis (MDR), extensively drug-resistant tuberculosis, and total drug-resistant tuberculosis has reached its peak.<sup>8-11</sup> Bedaquiline is the only newly developed and approved drug for active MDR tuberculosis in the last two decades. Negligence of pharmaceutical scientists and medicinal chemists towards tuberculosis generated this global problem of tuberculosis. A number of hurdles are normally associated with antitubercular drug discovery; one of them is *M. tuberculosis*. *M. tuberculosis* is lipid-rich gram-negative organism having specialized systems that make it different from other microorganisms.<sup>12-15</sup> Secretary systems are one of the specialized systems present in *M. tuberculosis*, and are key regulators of virulence of *M. tuberculosis*. In *M. tuberculosis* three different secretory systems, secondary translocase pathway (SEC), twin arginine translocation (TAT), and ESX, are present.<sup>16-18</sup> The SEC pathway is a major protein export system present in the mycobacterium, accounting for more than 50% of virulence protein exports in the mycobacterium. The SEC is a conserved protein pathway in the mycobacterium that does not have any homologues in the mammalian systems, and possesses ideal properties to act as a potential antimycobacterial drug target. The SEC pathway is a key enzyme involved in transport of the virulence protein across the cell membrane, which spreads tuberculosis all over the host body. Inhibition of SEC will be able to block the transport of the virulence protein, which will inhibit the spread of the tuberculosis. In recent years, a number of researchers have been trying to develop novel antitubercular agents targeting conserved protein targets. Currently a number of molecules like equisetin derivatives<sup>19</sup> and thiazolo[4,5-d]pyrimidine derivatives<sup>20</sup> are reported as SEC inhibitors. In this research article, an attempt was made to optimize thiazolidine scaffolds as potential SEC inhibitors via integration of pocket and pharmacophore modeling.

## EXPERIMENTAL

### *Selection of target*

*M. tuberculosis* has three specialized protein export systems: SEC, TAT, and ESX. The SEC is major protein export system of *M. tuberculosis*, exporting the bulk of virulent protein, which accounts for the spread of disease. SEC systems do not have

any homologues in mammalian systems and so inhibition of this SEC will not lead to any toxicity to humans. Thus due to its critical role in the growth and virulence of the *M. tuberculosis*, the SEC has been selected as the preferred biomolecular target rather than TAT or ESX.

### *Pocket modeling of the selected protein export systems*

Pocket modeling of the selected SEC of *M. tuberculosis* was carried out using the crystal structure of SEC downloaded from the free protein database [www.rcsb.org](http://www.rcsb.org). The downloaded crystal structure of SEC was first refined by the BioPredicta module, via removal of water molecules and retaining native hydrogen atoms in the protein structure. Pocket modeling of SEC A was carried out using the ProViz module of Vlife MDS 4.4. ProViz is an integrated property visualization module with which electrostatic and hydrophobic mapping of biomolecules can be carried out.

### *Design of molecules*

Pocket modeling of the SEC revealed the binding pocket of SEC is U-shaped and highly hydrophobic, keeping in mind complementary structures on the thiazole template were designed with structural modification on the aromatic moiety carried out. A number of the aromatic benzaldehydes are utilized to generate a number of thiazole derivatives. Total 75×75 benzaldehyde combinations are utilized to generate total 5625 different structures (indicated as R) as shown in Table 1. These 5625 different thiazole derivatives were designed and drawn in 2D geometry using the builder module of Vlife MDS 4.4. 2D structures were converted into 3D geometry and their coordinates were optimized via energy minimization by application of Merck molecular force field.

### *Docking analysis of synthesized ligands*

Molecular docking was performed to identify potent derivatives with the maximum binding affinity for SEC of *M. tuberculosis* amongst the designed set of molecules. Docking analysis was performed in the BioPredicta module of Vlife MDS 4.4 using grip-based docking analysis in which the protein structure was kept rigid and molecules were kept in flexible conformation so that a number of conformations can be achieved. The best 100 confirmations of all designed molecules were generated. Potent molecules were scrutinized based on binding energy and interaction profile. The proposed synthetic scheme of the designed derivatives is shown in Figure 1.

### *Screening based on the drug-like properties and percentage absorption*

The designed set of molecules was analyzed for Lipinski parameters like molecular weight, H-bond acceptor, H-bond

Table 1. Designed set of molecules (total 75×75 benzaldehyde combinations are utilized to generate total 5625 different structures indicated as R)

Sr. no.	R	Sr. no.	R	Sr. no.	R	Sr. no.	R
1.	C <sub>6</sub> H <sub>5</sub>	2.	4-(CH <sub>3</sub> ) <sub>2</sub> N-C <sub>6</sub> H <sub>5</sub>	3.	4CH <sub>3</sub> CONH-C <sub>6</sub> H <sub>5</sub>	4.	2-OCHC <sub>6</sub> H <sub>5</sub>
5.	3-OCHC <sub>6</sub> H <sub>5</sub>	6.	4-OCHC <sub>6</sub> H <sub>5</sub>	7.	3-OCH,4-OCH <sub>3</sub> -C <sub>6</sub> H <sub>4</sub>	8.	5-Br-2-OH-C <sub>6</sub> H <sub>4</sub>
9.	2-Br-C <sub>6</sub> H <sub>5</sub>	10.	3-Br-C <sub>6</sub> H <sub>5</sub>	11.	4-Br-C <sub>6</sub> H <sub>5</sub>	12.	2-Cl-6-F-C <sub>6</sub> H <sub>4</sub>
13.	4-Cl-3-NO <sub>2</sub>	14.	2-Cl-C <sub>6</sub> H <sub>5</sub>	15.	3-Cl-C <sub>6</sub> H <sub>5</sub>	16.	4-Cl-C <sub>6</sub> H <sub>5</sub>
17.	2-(4-Cl-SC <sub>6</sub> H <sub>5</sub> )	18.	3-CN-C <sub>6</sub> H <sub>5</sub>	19.	4-CN-C <sub>6</sub> H <sub>5</sub>	20.	2,3-Cl-C <sub>6</sub> H <sub>4</sub>
21.	2,4-Cl-C <sub>6</sub> H <sub>4</sub>	22.	2,6-Cl-C <sub>6</sub> H <sub>4</sub>	23.	3,5-Cl-C <sub>6</sub> H <sub>4</sub>	24.	4-(C <sub>2</sub> H <sub>5</sub> ) <sub>2</sub> N-C <sub>6</sub> H <sub>5</sub>
25.	2,6-F-C <sub>6</sub> H <sub>4</sub>	26.	3,4-F-C <sub>6</sub> H <sub>4</sub>	27.	2,3-OH-C <sub>6</sub> H <sub>4</sub>	28.	2,4-OH-C <sub>6</sub> H <sub>4</sub>
29.	2,5-OH-C <sub>6</sub> H <sub>4</sub>	30.	3,4-OH-C <sub>6</sub> H <sub>4</sub>	31.	2,3-OCH <sub>3</sub> -C <sub>6</sub> H <sub>4</sub>	32.	2,4-OCH <sub>3</sub> -C <sub>6</sub> H <sub>4</sub>
33.	2,5-OCH <sub>3</sub>	34.	3,4-OCH <sub>3</sub> -C <sub>6</sub> H <sub>4</sub>	35.	3,5-OCH <sub>3</sub> -C <sub>6</sub> H <sub>4</sub>	36.	3,5-OCH <sub>3</sub> ,4-OH- C <sub>6</sub> H <sub>4</sub>
37.	2,4-CH <sub>3</sub> -C <sub>6</sub> H <sub>4</sub>	38.	3,5-CH <sub>3</sub> -C <sub>6</sub> H <sub>4</sub>	39.	3-OC <sub>2</sub> H <sub>5</sub> -4-OH-C <sub>6</sub> H <sub>4</sub>	40.	2-F-C <sub>6</sub> H <sub>5</sub>
41.	3-F-C <sub>6</sub> H <sub>5</sub>	42.	4-F-C <sub>6</sub> H <sub>5</sub>	43.	2-OH-C <sub>6</sub> H <sub>5</sub>	44.	3-OH-C <sub>6</sub> H <sub>5</sub>
45.	4-OH-C <sub>6</sub> H <sub>5</sub>	46.	2-OH,3-OCH <sub>3</sub> -C <sub>6</sub> H <sub>4</sub>	47.	2-OH,4-OCH <sub>3</sub> -C <sub>6</sub> H <sub>4</sub>	48.	2-OH,5-OCH <sub>3</sub> -C <sub>6</sub> H <sub>4</sub>
49.	3-OH,4-OCH <sub>3</sub> -C <sub>6</sub> H <sub>4</sub>	50.	4-OH,3-OCH <sub>3</sub> -5NO <sub>2</sub>	51.	2-OH-5NO <sub>2</sub>	52.	4-CH(CH <sub>3</sub> ) <sub>2</sub> -C <sub>6</sub> H <sub>5</sub>
53.	2-OCH <sub>3</sub> -C <sub>6</sub> H <sub>5</sub>	54.	3-OCH <sub>3</sub> -C <sub>6</sub> H <sub>5</sub>	55.	4-OCH <sub>3</sub> -C <sub>6</sub> H <sub>5</sub>	56.	4-CH <sub>3</sub> -C <sub>6</sub> H <sub>5</sub>
57.	2-CH <sub>3</sub> -C <sub>6</sub> H <sub>5</sub>	58.	3-CH <sub>3</sub> -C <sub>6</sub> H <sub>5</sub>	59.	4-SCH <sub>3</sub> -C <sub>6</sub> H <sub>5</sub>	60.	2-NO <sub>2</sub> -C <sub>6</sub> H <sub>5</sub>
61.	3-NO <sub>2</sub> -C <sub>6</sub> H <sub>5</sub>	62.	4-NO <sub>2</sub> -C <sub>6</sub> H <sub>5</sub>	63.	3-OC <sub>6</sub> H <sub>5</sub>	64.	4-CH(CH <sub>3</sub> ) <sub>3</sub> -C <sub>6</sub> H <sub>5</sub>
65.	2,3,5-Cl C <sub>6</sub> H <sub>3</sub>	66.	3,4,5-F-C <sub>6</sub> H <sub>3</sub>	67.	4-CF <sub>3</sub> OCH <sub>3</sub> -C <sub>6</sub> H <sub>4</sub>	68.	4-CF <sub>3</sub> -C <sub>6</sub> H <sub>5</sub>
69.	2,3,4-OCH <sub>3</sub> -C <sub>6</sub> H <sub>3</sub>	70.	3,4,5-OCH <sub>3</sub> -C <sub>6</sub> H <sub>3</sub>	71.	2,4,6-OCH <sub>3</sub> -C <sub>6</sub> H <sub>3</sub>	72.	3-NO <sub>2</sub> -C <sub>6</sub> H <sub>5</sub>
73.	C <sub>5</sub> H <sub>4</sub> O <sub>2</sub>	74.	C <sub>9</sub> H <sub>10</sub> O <sub>3</sub>	75.	C <sub>5</sub> H <sub>4</sub> OS		

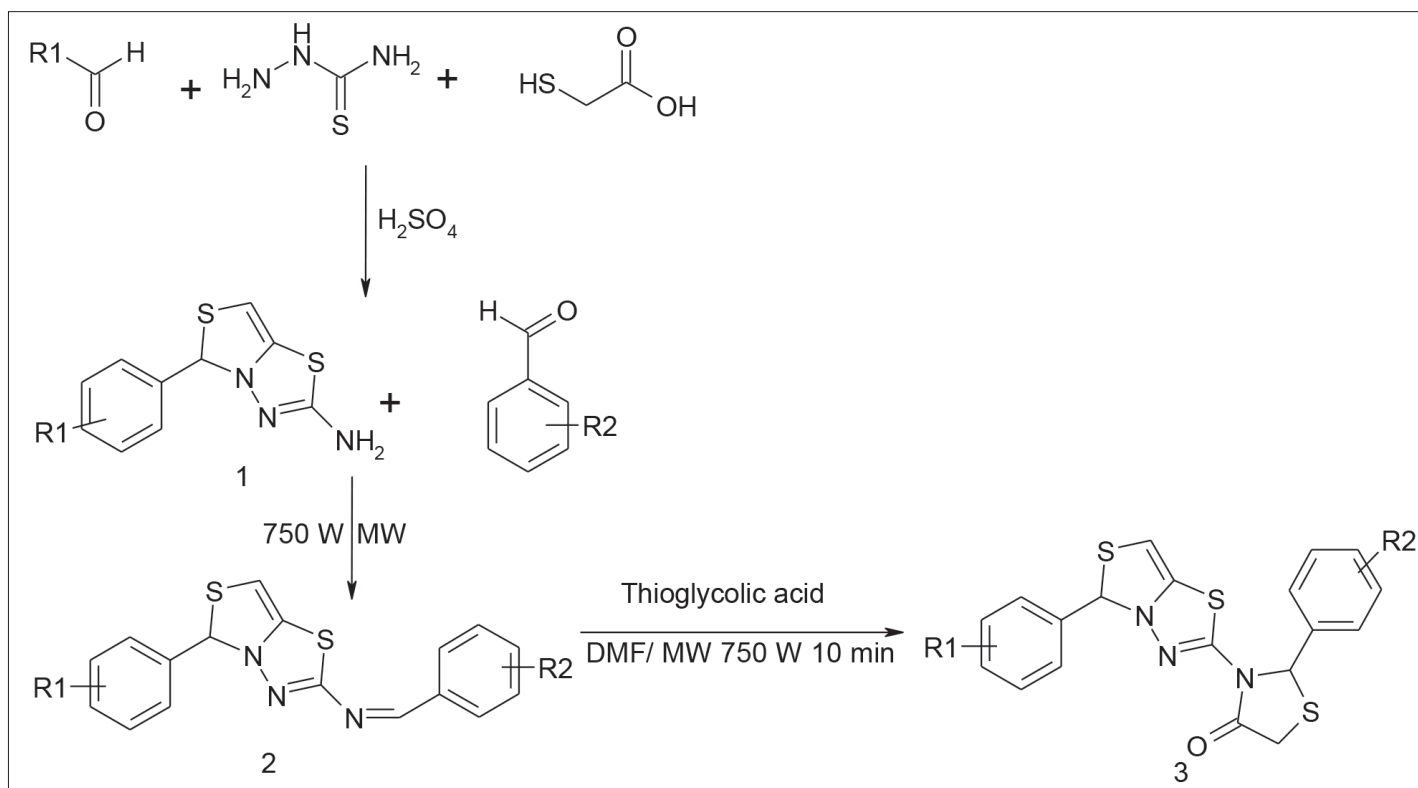


Figure 1. Synthetic scheme of designed derivatives

donor, rotatable bond, and XlogP. The physicochemical descriptors were calculated with the help of the QSAR module of Vlife MDS 4.4. Total polar surface area (TPSA) was calculated from the web server [www.molinspiration.com/cgi-bin/properties](http://www.molinspiration.com/cgi-bin/properties) by drawing the molecules in the drawing area and then calculating the TPSA. Percentage absorption was calculated using the formula;

$$\% \text{ Absorption} = 109 - (0.345 \times \text{TPSA}).^{21}$$

#### Synthesis of selected ligands<sup>22</sup>

#### Synthesis of optimized thiazole derivatives

##### Step 1

#### Synthesis of 2-amino-5-aryl-5H thiazolo[4,3-b]-1,3,4-thiadiazole (1)

To 25 mL of RBF were added aldehyde (0.02 M), thioglycolic acid (0.02 M), thiosemicarbazide (0.022 M), and 10 mL of concentrated H<sub>2</sub>SO<sub>4</sub>. The reaction mixture was mixed and left overnight and the resulting suspension was neutralized with 40% NaOH solution until the product was precipitated out and this resulting compound 1 was recrystallized from aqueous dioxane solution.

#### Synthesis of 1-phenyl-N-{5-phenyl-5H-[1,3]thiazolo[4,3-b][1,3,4]thiadiazol-2-yl}methanimine derivatives (2):

A solution of compound 1 (0.01 M) in ethanol (50 mL) was put in RBF and stirred vigorously for 15 min and to this resulting solution concentrated H<sub>2</sub>SO<sub>4</sub> (2 mL) and aldehyde (0.01 M) were added. The reaction mixture was irradiated in a synthetic microwave (Cata 4R) for 10 min. The separated solid was filtered and recrystallized from ethanol.

#### Synthesis of 2-phenyl-3-{5-phenyl-5H-[1,3]thiazolo[4,3-b][1,3,4]thiadiazol-2-yl}-1,3-thiazolidin-4-one derivatives (3):

In 25 mL of RBF were added compound 2 (0.01 M) and thioglycolic acid (0.01 M) and then 30 mL of DMF was added followed by stirring. The resulting reaction mixture was irradiated in the microwave for 10 min at 750 W. The reaction mixture was cooled to room temperature and the resulting solid was separated and recrystallized from benzene to get compounds 1 to 23. Table 2 shows the list of substituents in the synthesized set of molecules.

#### B3: 3-[5-(4-bromophenyl)-5H-[1,3]thiazolo[4,3-b][1,3,4]thiadiazol-2-yl]-2-phenyl-1,3-thiazolidin-4-one

Color: Brown, Yield: 82%, m. p.: 192-194°C, MASS: [M+1] + 474.94, IR: 1752 cm<sup>-1</sup> (C=O Str.), 1452 cm<sup>-1</sup> (C=C), 2742.84 cm<sup>-1</sup> (Ar. CH), 1580 cm<sup>-1</sup> (-N=CH) NMR: <sup>1</sup>H NMR (DMSO-*d*<sub>6</sub>, 300 MHz,): δ=6.95-7.35 (m, 9H, aromatic H), 4.95-5.90 (s, 2H, methine), 3.35 (s, 2H, methylene), 4.85 (s, 1H, ethylene).

#### C13: 2-(4-chlorophenyl)-3-{5-phenyl-5H-[1,3]thiazolo[4,3-b][1,3,4]thiadiazol-2-yl}-1,3-thiazolidin-4-one

Color: Yellow, Yield: 80%, m. p.: 178-180°C, MASS: [M+1] + 430.99, IR: 1690 cm<sup>-1</sup> (C=O Str.), 1435 cm<sup>-1</sup> (C=C), 2842 cm<sup>-1</sup> (Ar. CH), 1470 cm<sup>-1</sup> (-N=CH), NMR: <sup>1</sup>H NMR (DMSO-*d*<sub>6</sub>, 300 MHz,): δ=6.90-7.25 (m, 9H, aromatic), 4.95-5.90 (s, 2H, methine), 3.38 (s, 2H, methylene), 4.95 (s, 1H, ethylene).

#### C1: 2-(2-chlorophenyl)-3-{5-phenyl-5H-[1,3]thiazolo[4,3-b][1,3,4]thiadiazol-2-yl}-1,3-thiazolidin-4-one

Color: Brown, Yield: 75%, m. p.: 186-188°C, MASS: [M+1] + 430.99, IR: 1625 cm<sup>-1</sup> (C=O Str.), 1400 cm<sup>-1</sup> (C=C), 2830 cm<sup>-1</sup> (Ar. CH), 1476 cm<sup>-1</sup> (-N=CH) NMR: <sup>1</sup>H NMR (DMSO-*d*<sub>6</sub>, 300 MHz,): δ=6.95-7.20 (m, 9H, aromatic), 4.90-5.92 (s, 2H, methine), 3.30 (s, 2H, methylene), 4.90 (s, 1H, ethylene).

#### F1: 2-(2-chlorophenyl)-3-[5-(3,4-dimethoxyphenyl)-5H-[1,3]thiazolo[4,3-b][1,3,4]thiadiazol-2-yl]-1,3-thiazolidin-4-one

Color: Lemon, Yield: 89%, m. p.: 162-164°C, MASS: [M+1] + 492.02, IR: 1640 cm<sup>-1</sup> (C=O Str.), 1490 cm<sup>-1</sup> (C=C), 2790 cm<sup>-1</sup> (Ar. CH), 1520 cm<sup>-1</sup> (-N=CH) NMR: <sup>1</sup>H NMR (DMSO-*d*<sub>6</sub>, 300 MHz,): δ=6.52-7.15 (m, 7H, aromatic), 4.95-5.90 (s, 2H, methine), 3.33 (s, 2H, methylene), 4.85 (s, 1H, ethylene), 3.75 (d, 6H, methyl).

#### O17: 2-(3-chlorophenyl)-3-[5-(2-hydroxyphenyl)-5H-[1,3]thiazolo[4,3-b][1,3,4]thiadiazol-2-yl]-1,3-thiazolidin-4-one

Color: Yellow, Yield: 80%, m. p.: 228-230°C, MASS: [M+1] + 447.97, IR: 1680 cm<sup>-1</sup> (C=O Str.), 1500 cm<sup>-1</sup> (C=C), 2810 cm<sup>-1</sup> (Ar. CH), 1580 cm<sup>-1</sup> (-N=CH) NMR: <sup>1</sup>H NMR (DMSO-*d*<sub>6</sub>, 300 MHz,):

**Table 2. List of substituents in synthesized set of molecules**

Sr. no.	R1	R2	Code
1.	4-Br-C <sub>6</sub> H <sub>4</sub>	-C <sub>6</sub> H <sub>4</sub>	B3
2.	-C <sub>6</sub> H <sub>4</sub>	4-Cl-C <sub>6</sub> H <sub>4</sub>	C13
3.	-C <sub>6</sub> H <sub>4</sub>	2-Cl-C <sub>6</sub> H <sub>4</sub>	C1
4.	3,4-(OCH <sub>3</sub> )-C <sub>6</sub> H <sub>4</sub>	2-Cl-C <sub>6</sub> H <sub>4</sub>	F1
5.	2-(OH)-C <sub>6</sub> H <sub>4</sub>	3-Cl-C <sub>6</sub> H <sub>4</sub>	O17
6.	-C <sub>4</sub> H <sub>3</sub> O	3-OCH <sub>3</sub> -4-OH-C <sub>6</sub> H <sub>3</sub>	Q21
7.	4-N(CH <sub>3</sub> ) <sub>2</sub> -C <sub>6</sub> H <sub>4</sub>	4-Cl-C <sub>6</sub> H <sub>4</sub>	L13
8.	2-(OH)-C <sub>6</sub> H <sub>4</sub>	4-Cl-C <sub>6</sub> H <sub>4</sub>	O13
9.	-C <sub>4</sub> H <sub>3</sub> O	2-(OH)-C <sub>6</sub> H <sub>4</sub>	Q24
10.	4-Cl-C <sub>6</sub> H <sub>4</sub>	4-(OH)-C <sub>6</sub> H <sub>4</sub>	M9
11.	4-F-C <sub>6</sub> H <sub>4</sub>	-C <sub>4</sub> H <sub>3</sub> O	H25
12.	3-Cl-C <sub>6</sub> H <sub>4</sub>	S-C <sub>4</sub> H <sub>3</sub>	R26
13.	3-(OCH <sub>3</sub> )-4-(OH)-C <sub>6</sub> H <sub>3</sub>	-C <sub>6</sub> H <sub>4</sub>	V3
14.	3,5-(OCH <sub>3</sub> ) <sub>2</sub> -4-(OH)-C <sub>6</sub> H <sub>2</sub>	-C <sub>6</sub> H <sub>4</sub>	U8
15.	3-Cl-C <sub>6</sub> H <sub>4</sub>	3-NO <sub>2</sub> -C <sub>6</sub> H <sub>4</sub>	A11
16.	2-Cl-C <sub>6</sub> H <sub>4</sub>	4-NO <sub>2</sub> -C <sub>6</sub> H <sub>4</sub>	A10
17.	-C <sub>4</sub> H <sub>3</sub> O	3-OCH <sub>3</sub> -C <sub>6</sub> H <sub>4</sub>	Q22
18.	-C <sub>4</sub> H <sub>3</sub> O	-C <sub>7</sub> H <sub>5</sub> O <sub>2</sub>	Q30
19.	3-Cl-C <sub>6</sub> H <sub>4</sub>	S-C <sub>4</sub> H <sub>3</sub>	R25
20.	4-Cl-C <sub>6</sub> H <sub>4</sub>	S-C <sub>4</sub> H <sub>3</sub>	M26
21.	3-Cl-C <sub>6</sub> H <sub>4</sub>	3,4-(OCH <sub>3</sub> )-C <sub>6</sub> H <sub>4</sub>	R6
22.	3-(OCH <sub>3</sub> )-C <sub>6</sub> H <sub>4</sub>	4-Cl-C <sub>6</sub> H <sub>4</sub>	W13
23.	3-(OCH <sub>3</sub> )-C <sub>6</sub> H <sub>4</sub>	4-F-C <sub>6</sub> H <sub>4</sub>	W8

$\delta$ =6.62-7.20 (m, 8H, aromatic), 4.95 (s, 1H, methine), 5.92 (s, 1H, methine), 3.38 (s, 1H, methylene), 4.75 (s, 1H, ethylene), 6.05 (s, 1H, aromatic C-OH).

**Q21:** *2-(3-ethoxy-4-hydroxyphenyl)-3-[5-(furan-2-yl)-5H-[1,3]thiazolo[4,3-b][1,3,4]thiadiazol-2-yl]-1,3-thiazolidin-4-one*

Color: Black, Yield: 78%, m. p.: 192-194°C, MASS: [M+1] + 447.54, IR: 1750 cm<sup>-1</sup> (C=O Str.), 1540 cm<sup>-1</sup> (C=C), 2840 cm<sup>-1</sup> (Ar. CH), 1600 cm<sup>-1</sup> (-N=CH) NMR: <sup>1</sup>H NMR (DMSO-*d*<sub>6</sub>, 300 MHz.):  $\delta$ =6.05-7.30 (m, 6H, aromatic benzene and furan), 4.75 (s, 1H, ethylene), 5.15-5.92 (s, 2H, methine), 3.30 (s, 2H, methylene), 3.95 (s, 2H, methylene), 1.58 (s, 3H, methyl), 5.02 (s, 1H aromatic C-OH).

**L13:** *2-(4-chlorophenyl)-3-[5-[4-(dimethylamino)phenyl]-5H-[1,3]thiazolo[4,3-b][1,3,4]thiadiazol-2-yl]-1,3-thiazolidin-4-one*

Color: Brown, Yield: 67%, m. p.: 156-158°C, MASS: [M+1] + 475.04, IR: 1652 cm<sup>-1</sup> (C=O Str.), 1538 cm<sup>-1</sup> (C=C), 2800 cm<sup>-1</sup> (Ar. CH), 1530 cm<sup>-1</sup> (-N=CH) NMR: <sup>1</sup>H NMR (DMSO-*d*<sub>6</sub>, 300 MHz.):  $\delta$ =6.45-7.20 (m, 8H, aromatic benzene), 4.80 (s, 1H, ethylene), 4.95-5.80 (s, 2H, methine), 3.30 (s, 2H, methylene), 2.95 (s, 6H, methyl N-CH<sub>3</sub>).

**O13:** *2-(4-chlorophenyl)-3-[5-(2-hydroxyphenyl)-5H-[1,3]thiazolo[4,3-b][1,3,4]thiadiazol-2-yl]-1,3-thiazolidin-4-one*

Color: Brown, Yield: 67%, m. p.: 236-238°C, MASS: [M+1] + 447.97, IR: 1760 cm<sup>-1</sup> (C=O Str.), 1540 cm<sup>-1</sup> (C=C), 2830 cm<sup>-1</sup> (Ar. CH), 1680 cm<sup>-1</sup> (-N=CH) NMR: <sup>1</sup>H NMR (DMSO-*d*<sub>6</sub>, 300 MHz.):  $\delta$ =6.65-7.25 (m, 8H, aromatic benzene), 4.85 (s, 1H, ethylene), 4.05-4.70 (s, 2H, methine), 3.28 (s, 2H, methylene), 5.25 (s, 1H, aromatic C-OH).

**Q24:** *3-[5-(furan-2-yl)-5H-[1,3]thiazolo[4,3-b][1,3,4]thiadiazol-2-yl]-2-(2-hydroxyphenyl)-1,3-thiazolidin-4-one*

Color: Black, Yield: 75%, m. p.: 216-218°C, MASS: [M+1] + 403.49, IR: 1740 cm<sup>-1</sup> (C=O Str.), 1623 cm<sup>-1</sup> (C=C), 2810 cm<sup>-1</sup> (Ar. CH), 1680 cm<sup>-1</sup> (-N=CH), NMR: <sup>1</sup>H NMR (DMSO-*d*<sub>6</sub>, 300 MHz.):  $\delta$ =6.60-7.30 (m, 7H, aromatic benzene and furan), 4.80 (s, 1H, ethylene), 5.20-5.80 (s, 2H, methine), 3.30 (s, 2H, methylene), 5.25 (s, 1H, aromatic C-OH).

**M9:** *3-[5-(4-chlorophenyl)-5H-[1,3]thiazolo[4,3-b][1,3,4]thiadiazol-2-yl]-2-(4-hydroxyphenyl)-1,3-thiazolidin-4-one*

Color: Brown, Yield: 88%, m. p.: 138-140°C, MASS: [M+1] + 447.97, IR: 1700 cm<sup>-1</sup> (C=O Str.), 1640 cm<sup>-1</sup> (C=C), 2790 cm<sup>-1</sup> (Ar. CH), 1650 cm<sup>-1</sup> (-N=CH), NMR: <sup>1</sup>H NMR (DMSO-*d*<sub>6</sub>, 300 MHz.):  $\delta$ =6.55-7.25 (m, 8H, aromatic benzene), 4.85 (s, 1H, ethylene), 5.10-5.85 (s, 2H, methine), 3.38 (s, 2H, methylene), 6.05 (s, 1H, aromatic C-OH).

**H25:** *3-[5-(4-fluorophenyl)-5H-[1,3]thiazolo[4,3-b][1,3,4]thiadiazol-2-yl]-2-(furan-2-yl)-1,3-thiazolidin-4-one*

Color: Yellow, Yield: 70%, m. p.: 122-124°C, MASS: [M+1] + 405.48, IR: 1688 cm<sup>-1</sup> (C=O Str.), 1589 cm<sup>-1</sup> (C=C), 2690 cm<sup>-1</sup> (Ar. CH), 1580 cm<sup>-1</sup> (-N=CH) NMR: <sup>1</sup>H NMR (DMSO-*d*<sub>6</sub>, 300 MHz.):  $\delta$ =6.30-7.05 (m, 7H, aromatic benzene and furan), 4.82 (s, 1H,

ethylene), 5.10-5.85 (s, 2H, methine), 3.35 (s, 2H, methylene).

**R26:** *3-[5-(3-chlorophenyl)-5H-[1,3]thiazolo[4,3-b][1,3,4]thiadiazol-2-yl]-2-(thiophen-2-yl)-1,3-thiazolidin-4-one*

Color: Yellow, Yield: 72%, m. p.: 206-208°C, MASS: [M+1] + 437.99, IR: 1750 cm<sup>-1</sup> (C=O Str.), 1670 cm<sup>-1</sup> (C=C), 2560 cm<sup>-1</sup> (Ar. CH), 1540 cm<sup>-1</sup> (-N=CH) NMR: <sup>1</sup>H NMR (DMSO-*d*<sub>6</sub>, 300 MHz.):  $\delta$ =6.60-7.10 (m, 7H, aromatic benzene and thiophene), 4.85 (s, 1H, ethylene), 4.95-5.90 (s, 2H, methine), 3.30 (s, 2H, methylene).

**V3:** *3-[5-(3-ethoxy-4-hydroxyphenyl)-5H-[1,3]thiazolo[4,3-b][1,3,4]thiadiazol-2-yl]-2-phenyl-1,3-thiazolidin-4-one*

Color: Brown, Yield: 83%, m. p.: 180-182°C, MASS: [M+1] + 457.58, IR: 1620 cm<sup>-1</sup> (C=O Str.), 1560 cm<sup>-1</sup> (C=C), 2860 cm<sup>-1</sup> (Ar. CH), 1490 cm<sup>-1</sup> (-N=CH) NMR: <sup>1</sup>H NMR (DMSO-*d*<sub>6</sub>, 300 MHz.):  $\delta$ =6.45-7.14 (m, 8H, aromatic benzene), 4.80 (s, 1H, ethylene), 4.90-5.85 (s, 2H, methine), 3.35 (s, 2H, methylene), 5.95 (s, 1H, aromatic C-OH), 3.98 (s, 2H, methylene), 1.75 (s, 3H, methyl).

**U8:** *3-[5-(4-hydroxy-3,5-dimethoxyphenyl)-5H-[1,3]thiazolo[4,3-b][1,3,4]thiadiazol-2-yl]-2-phenyl-1,3-thiazolidin-4-one*

Color: Yellow, Yield: 80%, m. p.: 230-232°C, MASS: [M+1] + 473.58, IR: 1688 cm<sup>-1</sup> (C=O Str.), 1562 cm<sup>-1</sup> (C=C), 2883 cm<sup>-1</sup> (Ar. CH), 1489 cm<sup>-1</sup> (-N=CH) NMR: <sup>1</sup>H NMR (DMSO-*d*<sub>6</sub>, 300 MHz.):  $\delta$ =5.95-7.10 (m, 7H, aromatic benzene), 4.85 (s, 1H, ethylene), 4.92-5.95 (s, 2H, methine), 3.28 (s, 2H, methylene), 5.98 (s, 1H, aromatic C-OH), 3.85 (s, 6H, methoxy).

**A11:** *3-[5-(3-chlorophenyl)-5H-[1,3]thiazolo[4,3-b][1,3,4]thiadiazol-2-yl]-2-(3-nitrophenyl)-1,3-thiazolidin-4-one*

Color: Brown, Yield: 69%, m. p.: 146-148°C, MASS: [M+1] + 476.97, IR: 1679 cm<sup>-1</sup> (C=O Str.), 1575 cm<sup>-1</sup> (C=C), 2896 cm<sup>-1</sup> (Ar. CH), 1523 cm<sup>-1</sup> (-N=CH). NMR: <sup>1</sup>H NMR (DMSO-*d*<sub>6</sub>, 300 MHz.):  $\delta$ =6.90-7.95 (m, 8H, aromatic benzene), 4.75 (s, 1H, ethylene), 4.90-5.92 (s, 2H, methine), 3.33 (s, 2H, methylene).

**A10:** *3-[5-(2-chlorophenyl)-5H-[1,3]thiazolo[4,3-b][1,3,4]thiadiazol-2-yl]-2-(4-nitrophenyl)-1,3-thiazolidin-4-one*

Color: Brown, Yield: 70%, m. p.: 174-176°C, MASS: [M+1] + 476.97, IR: 1590 cm<sup>-1</sup> (C=O Str.), 1456 cm<sup>-1</sup> (C=C), 2675 cm<sup>-1</sup> (Ar. CH), 1563 cm<sup>-1</sup> (-N=CH). NMR: <sup>1</sup>H NMR (DMSO-*d*<sub>6</sub>, 300 MHz.):  $\delta$ =7.04-8.05 (m, 8H, aromatic benzene), 4.85 (s, 1H, ethylene), 4.95-5.90 (s, 2H, methine), 3.28 (s, 2H, methylene).

**Q22:** *3-[5-(furan-2-yl)-5H-[1,3]thiazolo[4,3-b][1,3,4]thiadiazol-2-yl]-2-(3-methoxyphenyl)-1,3-thiazolidin-4-one*

Color: Black, Yield: 78%, m. p.: 176-178°C, MASS: [M+1] + 417.52, IR: 1639 cm<sup>-1</sup> (C=O Str.), 1420 cm<sup>-1</sup> (C=C), 2640 cm<sup>-1</sup> (Ar. CH), 1570 cm<sup>-1</sup> (-N=CH). NMR: <sup>1</sup>H NMR (DMSO-*d*<sub>6</sub>, 300 MHz.):  $\delta$ =6.50-7.30 (m, 7H, aromatic benzene and furan), 4.80 (s, 1H, ethylene), 5.10-5.95 (s, 2H, methine), 3.30 (s, 2H, methylene), 3.75 (s, 3H, methoxy).

**Q30:** *2-(2H-1,3-benzodioxol-5-yl)-3-[5-(furan-2-yl)-5H-[1,3]thiazolo[4,3-b][1,3,4]thiadiazol-2-yl]-1,3-thiazolidin-4-one*

Color: Black, Yield: 70%, m. p.: 240-242°C, MASS: [M+1] + 431.50, IR: 1782 cm<sup>-1</sup> (C=O Str.), 1560 cm<sup>-1</sup> (C=C), 2785 cm<sup>-1</sup> (Ar. CH), 1630 cm<sup>-1</sup> (-N=CH). NMR: <sup>1</sup>H NMR (DMSO-*d*<sub>6</sub>, 300 MHz): δ=6.45-7.25 (m, 6H, aromatic benzene and furan), 4.82 (s, 1H, ethylene), 5.15-5.85 (s, 2H, methine), 3.28 (s, 2H, methylene), 5.95 (s, 2H, 1,3-dioxole).

**R25:** 3-[5-(3-chlorophenyl)-5H-[1,3]thiazolo[4,3-b][1,3,4]thiadiazol-2-yl]-2-(thiophen-2-yl)-1,3-thiazolidin-4-one

Color: Yellow, Yield: 82%, m. p.: 234-236°C, MASS: [M+1] + 437.99 IR: 1700 cm<sup>-1</sup> (C=O Str.), 1590 cm<sup>-1</sup> (C=C), 2693 cm<sup>-1</sup> (Ar. CH), 1578 cm<sup>-1</sup> (-N=CH). NMR: <sup>1</sup>H NMR (DMSO-*d*<sub>6</sub>, 300 MHz): δ=6.65-7.05 (m, 7H, aromatic benzene and thiophene), 4.85 (s, 1H, ethylene), 4.95-5.95 (s, 2H, methine), 3.32 (s, 2H, methylene).

**M26:** 3-[5-(4-chlorophenyl)-5H-[1,3]thiazolo[4,3-b][1,3,4]thiadiazol-2-yl]-2-(thiophen-2-yl)-1,3-thiazolidin-4-one

Color: Brown, Yield: 70%, m. p.: 210-212°C, MASS: [M+1] + 437.99, IR: 1665 cm<sup>-1</sup> (C=O Str.), 1545 cm<sup>-1</sup> (C=C), 2530 cm<sup>-1</sup> (Ar. CH), 1540 cm<sup>-1</sup> (-N=CH). NMR: <sup>1</sup>H NMR (DMSO-*d*<sub>6</sub>, 300 MHz): δ=6.60-7.25 (m, 7H, aromatic benzene and thiophene), 4.82 (s, 1H, ethylene), 4.90-5.92 (s, 2H, methine), 3.35 (s, 2H, methylene).

**R6:** 3-[5-(3-chlorophenyl)-5H-[1,3]thiazolo[4,3-b][1,3,4]thiadiazol-2-yl]-2-(3,4-dimethoxyphenyl)-1,3-thiazolidin-4-one

Color: Brown, Yield: 85%, m. p.: 226-228°C, MASS: [M+1] + 492.02, IR: 1675 cm<sup>-1</sup> (C=O Str.), 1553 cm<sup>-1</sup> (C=C), 2542 cm<sup>-1</sup> (Ar. CH), 1580 cm<sup>-1</sup> (-N=CH). NMR: <sup>1</sup>H NMR (DMSO-*d*<sub>6</sub>, 300 MHz): δ=6.50-7.15 (m, 7H, aromatic benzene), 4.82 (s, 1H, ethylene), 4.92-5.85 (s, 2H, methine), 3.33 (s, 2H, methylene), 3.75 (s, 6H, methoxy).

**W13:** 2-(4-chlorophenyl)-3-[5-(3-methoxyphenyl)-5H-[1,3]thiazolo[4,3-b][1,3,4]thiadiazol-2-yl]-1,3-thiazolidin-4-one

Color: White, Yield: 78%, m. p.: 170-172°C, MASS: [M+1] + 462.00, IR: 1600 cm<sup>-1</sup> (C=O Str.), 1532 cm<sup>-1</sup> (C=C), 2520 cm<sup>-1</sup> (Ar. CH), 1560 cm<sup>-1</sup> (-N=CH). NMR: <sup>1</sup>H NMR (DMSO-*d*<sub>6</sub>, 300 MHz): δ=6.55-7.20 (m, 8H, aromatic benzene), 4.85 (s, 1H, ethylene), 4.92-5.88 (s, 2H, methine), 3.30 (s, 2H, methylene), 3.78 (s, 3H, methoxy).

**W8:** 2-(4-fluorophenyl)-3-[5-(3-methoxyphenyl)-5H-[1,3]thiazolo[4,3-b][1,3,4]thiadiazol-2-yl]-1,3-thiazolidin-4-one

Color: Brown, Yield: 80%, m. p.: 160-162°C, MASS: [M+1] + 445.55 IR: 1750 cm<sup>-1</sup> (C=O Str.), 1682 cm<sup>-1</sup> (C=C), 2540 cm<sup>-1</sup> (Ar. CH), 1670 cm<sup>-1</sup> (-N=CH). NMR: <sup>1</sup>H NMR (DMSO-*d*<sub>6</sub>, 300 MHz): δ=6.65-7.05 (m, 8H, aromatic benzene), 4.80 (s, 1H, ethylene), 4.85-5.90 (s, 2H, methine), 3.34 (s, 2H, methylene), 3.65 (s, 3H, methoxy).

#### Antitubercular activity

The synthesized molecules were evaluated for antimycobacterial activity by culturing *Mycobacterium smegmatis* (NCIM 5138) on Middlebrook 7H9 broth (Difco) containing 0.5% albumin, 0.085% NaCl, 0.2% glucose, 0.05% Tween 80, and 0.5% glycerol at 37°C for 48 h to mid-log phase [optical density at 600 nm (OD<sub>600</sub>)= 0.5]. Minimum inhibitory concentrations (MICs) of antibiotics against *M. smegmatis* were determined in Middlebrook 7H9 broth by the standard microdilution method. All synthesized derivatives were dissolved in dimethyl sulfoxide and utilized for the antimycobacterial assay in the concentration range of 3.25-1000 µg/mL.

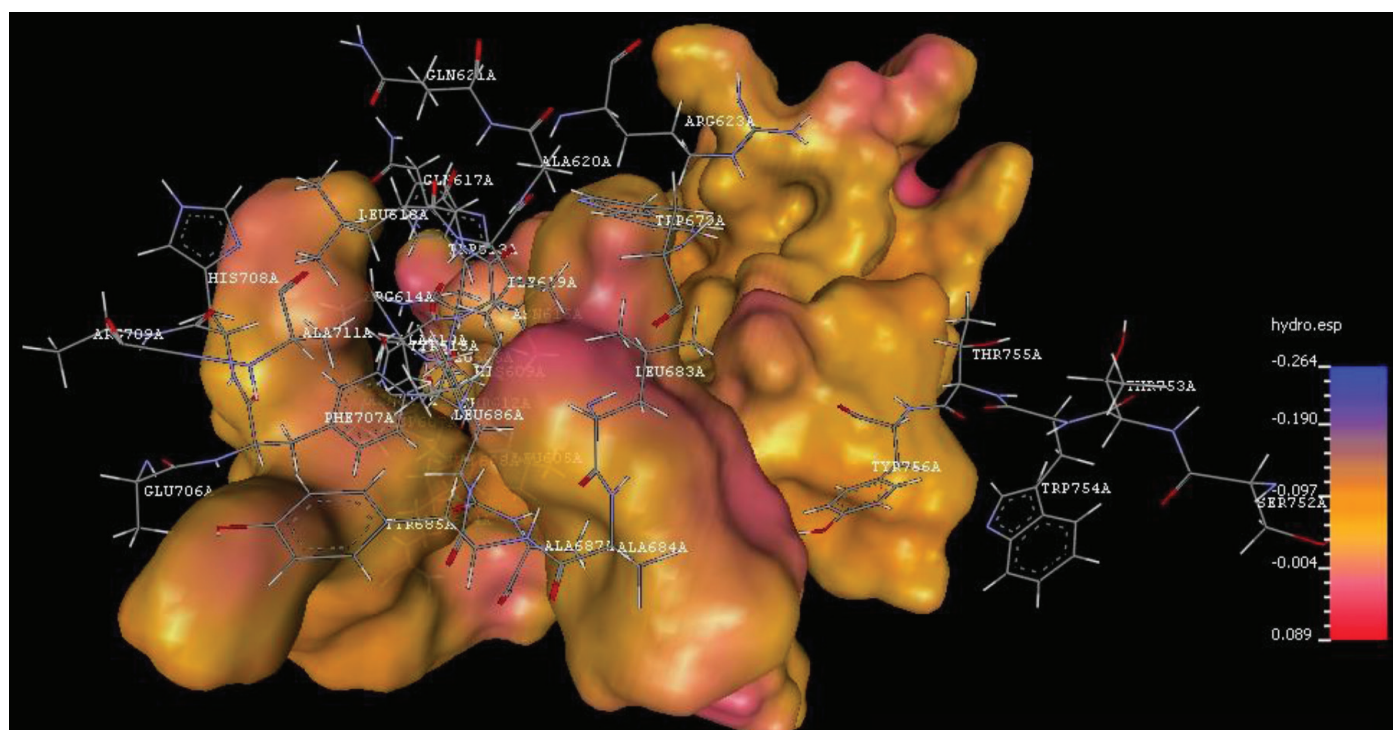


**Figure 2.** Hydrophobic map of active site of secondary translocase pathway of *Mycobacterium tuberculosis*

## RESULTS AND DISCUSSION

### Pocket modeling of SEC of *M. tuberculosis*

Binding pocket analysis was performed on the X-ray structure of the SEC from *M. tuberculosis* downloaded from free protein database www.rcsb.org. The ProViz module of Vlife MDS 4.4 was utilized to perform the pocket analysis. An electrostatic and hydrophobic map of the binding pocket of the SEC was generated to identify the relative orientation of critical amino acids. Pocket modeling of the SEC revealed its binding pocket is highly hydrophobic and ASP224, HIS534, and LYS115 are the three important amino acids required for ATP binding. Figure 2 shows the hydrophobic map of the active site of the SEC of *M. tuberculosis*. The SEC runs protein export, which is driven by ATP as the energy source, and inhibition of this ATP binding or blocking three amino acids will inhibit the SEC and ultimately protein export. The binding pocket of the SEC was found to be highly hydrophobic and U-shaped. Molecules were designed with the intent that they will retain necessary hydrophobicity and

relative conformation with respect to the SEC of *M. tuberculosis*. Molecules were developed keeping thiazole as the template. Thiazole derivatives due the presence of two heteroatoms that will act as an anchor and two aromatic rings that will act as wings to the nucleus are capable of achieving the bioactive U- or V-shaped conformation, which is complementary to the binding site of the SEC. Aromatic benzaldehydes are utilized to manipulate the required hydrophobic characters from aromatic interaction with Histidine 534.

### Screening based on the drug-like properties

Pharmacokinetic properties of the molecules are an important factor in the conversion of any New Chemical Entity to the drug. Pre-assessment of these drug-like properties plays a vital role in the selection of potential drug-like candidates from the designed data set of the molecules. All the molecules in the designed set of thiazole derivatives were assessed for Lipinski parameters like molecular weight, H-bond acceptor, H-bond donor, rotatable bond logp, and predicted oral absorption. In all,

**Table 3.** Table showing the molecules having the desired drug-like properties

Sr. no.	Compound code	Mole. wt.	H-acce	H-donor count	RBC	logP	TPSA (Å)	Pre. % oral abs.
1	A10	476.988	4	0	4	4.738	44.81	93.54
2	A11	476.988	4	0	4	4.738	81.4	80.91
3	B3	476.442	1	0	3	4.939	35.57	96.72
4	C1	431.99	1	0	3	4.83	35.57	96.72
5	C13	431.99	1	0	3	4.83	35.57	96.72
6	F1	492.043	3	0	7	4.847	54.04	90.35
7	H25	405.498	2	0	3	3.908	46.57	85.26
8	L13	475.059	2	0	6	4.896	41.37	94.72
9	M9	447.99	2	1	4	4.535	58.63	88.77
10	M26	438.019	1	0	3	4.891	35.57	96.72
11	O13	447.99	2	1	4	4.535	58.63	88.77
12	O17	447.99	2	1	4	4.535	58.63	88.77
13	Q21	447.56	3	1	7	3.873	81	81.05
14	Q22	417.534	2	0	5	3.778	57.95	89.00
15	Q24	433.533	3	1	6	3.483	81	81.05
16	Q30	431.517	1	0	3	3.498	67.18	85.82
17	R6	492.043	3	0	7	4.847	54.04	90.35
18	R25	421.952	1	0	3	4.423	48.71	92.19505
19	R26	438.019	1	0	3	4.891	35.57	96.72
20	U8	491.588	5	1	8	4.038	77.1	82.40
21	V3	457.598	3	1	7	4.28	67.86	85.58
22	W8	445.562	3	0	5	4.324	44.81	93.54
23	W13	462.017	2	0	5	4.838	44.81	93.54

TPSA: Total polar surface area, RBC: Red blood cell

**Table 4. Binding interactions and energy of docked molecules**

Sr. no.	Compound code	Binding energy	H-bond	Pi-stacking
1.	A10	-33.43	HIS534	HIS534
2.	A11	-0.12	HIS534	HIS534
3.	B3	-35.40	HIS534	HIS534
4.	C1	-7.41	ASP224	HIS534
5.	C13	-2.31	HIS534 HIS534	HIS534
6.	F1	-33.32	HIS534	HIS534
7.	L13	-8.74	HIS534	HIS534
8.	M9	-37.54	ASP219	HIS534
9.	M26	-38.54	ASP224	HIS534
10.	O13	-11.91	GLN498	HIS534
11.	O17	-9.81	HIS534	HIS534
12.	Q21	23.92	ASP219	HIS534
13.	Q22	-11.97	HIS534	HIS534
14.	Q24	-11.03	HIS534	HIS534
15.	Q30	-3.89	HIS534	HIS534
16.	R25	-2.51	HIS534	HIS534
17.	R26	-4.66	ASP224	HIS534
18.	R6	-11.74	HIS534	HIS534
19.	U8	-0.21	HIS534	HIS534
20.	V3	-36.40	HIS534	HIS534
21.	H25	-8.37	HIS534	HIS534
22.	W8	-33.40	ASP224	HIS534
23.	W13	-31.56	HIS534	HIS534

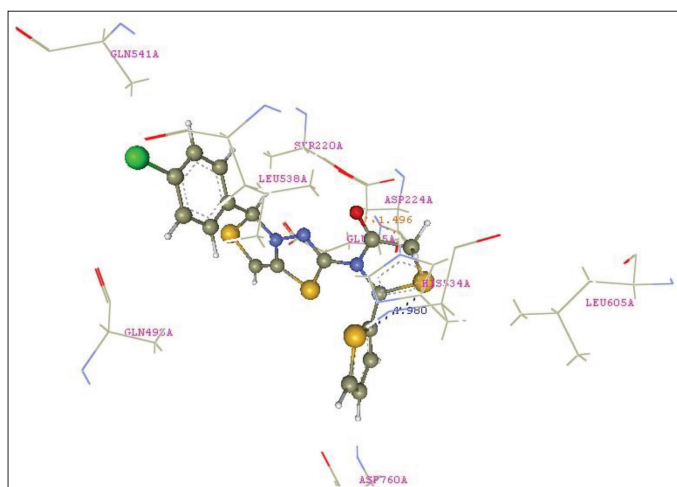


**Figure 3.** Figure showing posed molecule M26 (Ball and Stick) with PDB ID 4UAQ with hydrogen bond interaction (red color) and Pi-Stacking Interaction (blue colour)

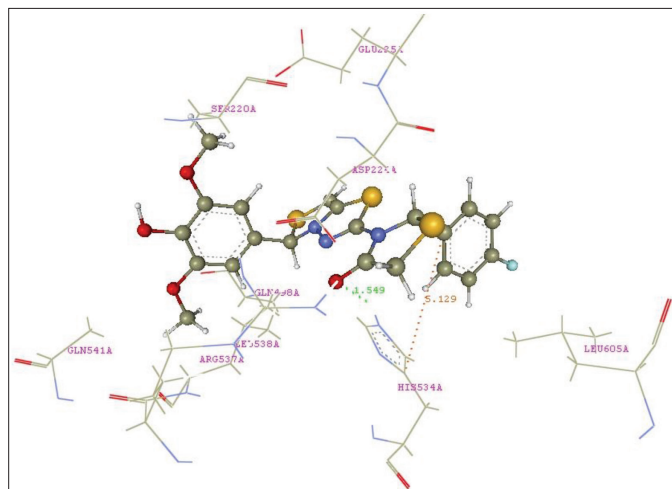


**Figure 4.** Showing the posed molecule U8 (Ball and Stick) with PDB ID 4UAQ with hydrogen bond interaction (red color)

23 derivatives were found to have the desired pharmacokinetic properties and predicted oral absorption <70%. The selected 23 derivatives with the drug-like properties are given in Table 3.

#### Molecular docking

Molecular docking was utilized to predict the potential active inhibitors from the designed set of ligands. Grip-based docking analysis was performed maintaining the SEC in rigid conformation and ligands in flexible conformation. All the design set of molecules were found to be binding to the same binding site to that of ATP in the SEC. The designed set of molecules was found to be interacting with HIS 534 and ASP224 via formation with hydrogen bond interaction and pi-stacking interaction. Binding interactions of the 23 selected molecules are summarized in Table 4, while Figures 3, 4, 5, and 6 show the most active conformation of molecules M26, U8, R26, and A10 (Ball and Stick) with PDB ID 4UAQ, respectively.

#### Biological activity

The antimycobacterial activity of the synthesized derivatives was determined against the standard *M. smegmatis* (NCIM No: 5138). *M. smegmatis* is an organism belonging to the family Mycobacterium having nearly 80% genome similarity with *M. tuberculosis*. Isoniazid was utilized as the positive standard for the antimycobacterial activity. MICs of all 23 derivatives are summarized in Figure 7. All the compounds showed good to moderate activity against the tested strain. Compounds R26, Q30, and M9 showed maximum antitubercular activity (MIC: 62.5 µg/mL). The excellent activity of M9 and R26 indicates halogens have a positive effect on antitubercular activity, and the activity of Q30 is an interesting finding that indicates substitution of the heterocyclic nucleus will also potentiate the activity. Derivative L13 showed good activity (MIC: 125 µg/mL), which justifies the substitution of halogen in the aromatic ring. A10, C13, F1, O13, O17, Q21, Q22, Q24, R25, R6, U8, and W13 are moderately active compounds with MIC: 500 µg/mL.



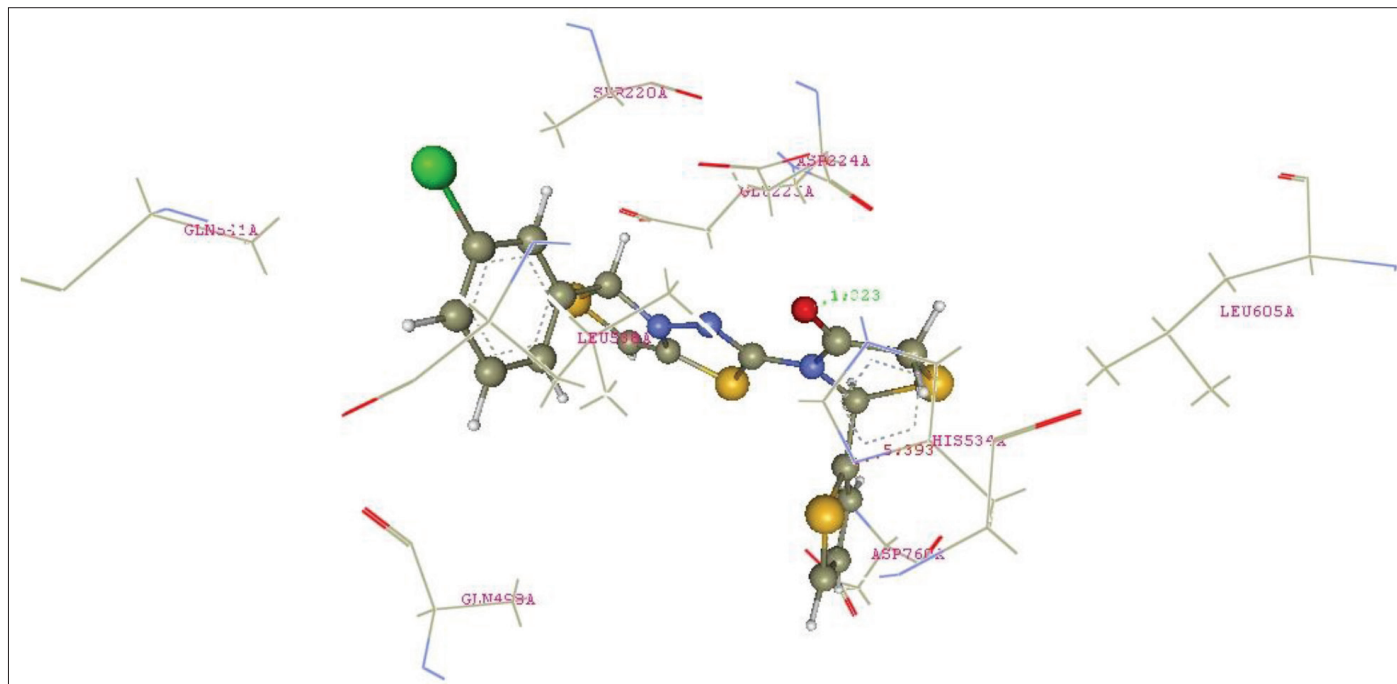


Figure 5. Showing the posed molecule R26 (Ball and Stick) with PDB ID 4UAQ with hydrogen bond interaction (red color)

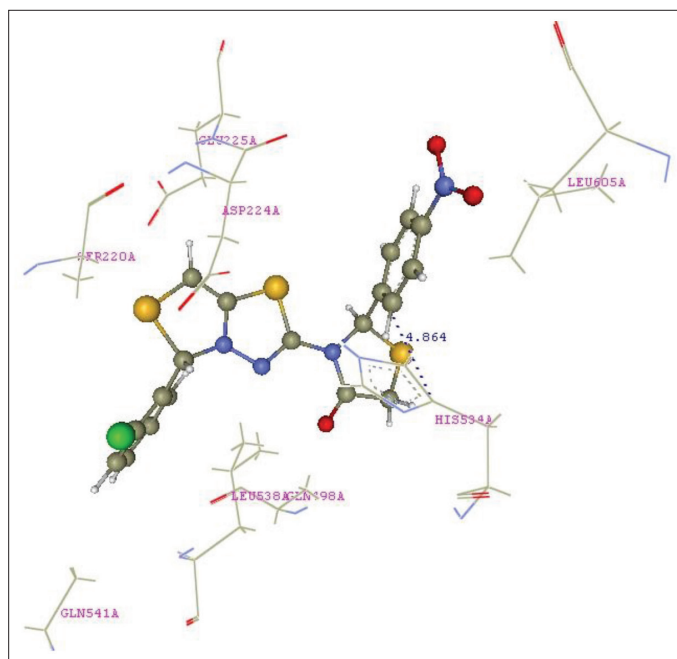


Figure 6. Showing the posed molecule A10 (Ball and Stick) with PDB ID 4UAQ

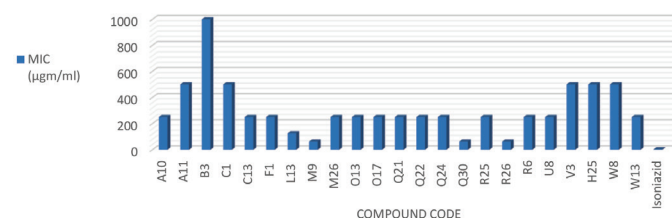


Figure 7. Designed compounds with minimum inhibitory concentration

## CONCLUSIONS

Attempts to design and develop molecules targeting secretory systems of *M. tuberculosis* yielded the following significant findings. Identification and validation of secretory systems as targets for antitubercular drug design and discovery were successfully carried out. Out of the three protein export systems associated with *M. tuberculosis* the SEC protein export system was utilized successfully for the development of antitubercular agents that are selective and can be utilized against all resistant forms of tuberculosis. Protein export systems are conserved systems and they have no isoform in humans and so targeting protein export systems will be the potential route for the development of selective and active antitubercular agents. Pocket modeling of the active site or binding site of the SEC revealed an interesting fact about the size and shape of the binding pocket of the SEC and signified the development of hydrophobic ligands for binding with the SEC of *M. tuberculosis*. Based on the pocket modeling data and literature survey in total 5184 molecules were designed around the thiazole scaffold via the change in the different aromatic benzaldehyde structures. Moreover, 5625 designed molecules were further scrutinized via Lipinski drug-like properties and toxicity profile using OCHEM and for binding efficiency using molecular docking analysis. The results of all three analyses yielded 23 potent, selective molecules successfully synthesized via reaction of an aromatic aldehyde, thiosemicarbazide, and thioglycolic acid. All the molecules were successfully synthesized using microwave-assisted synthesis, which improved the yield and reduced the time of reaction compared to the procedures reported in the literature. All 23 derivatives synthesized were characterized via all physicochemical methods, melting point, and IR and NMR spectroscopy. Halogen-substituted derivatives

showed significant activity, which indicates substitution of an electron-withdrawing group in the aryl ring will potentiate antimycobacterial activity. M26, U8, and R26 molecules have significant desirable biological activity and specific interactions with the SEC. Further optimization of these leads is necessary for the development of potential antitubercular drug-like candidates. These potential drug candidates with specific SEC inhibitory properties resulted from the utilization of integration of pocket modeling and virtual screening.

*Conflict of Interest:* No conflict of interest was declared by the authors.

## REFERENCES

1. Abagyan R, Totrov M, High-throughput Docking for Lead Generation. *Curr Opin Chem Biol.* 2001;5:375-382.
2. Alam S, Khan F. QSAR and Docking studies on Xanthone Derivatives for Anticancer Activity Targeting DNA topoisomerase II $\alpha$ . *Drug Des Devel Ther.* 2014;8:183-195.
3. Bermudez LE, Goodman J. *Mycobacterium tuberculosis* invades and replicates within Type II alveolar cells. *Infect Immun.* 1996;64: 1400-1406.
4. Bhatia MS, Ingale KB, Choudhari PB, Bhatia NM, Sawant RL. Application quantum and physicochemical molecular descriptors utilizing principal components to study the mode of anticoagulant activity of pyridyl chromen-2-one derivatives. *Bioorg Med Chem.* 2009;17:1654-1662.
5. Borrell S, Gagneux S. Infectiousness, reproductive fitness, and evolution of drug-resistant *Mycobacterium tuberculosis*. *Int J Tuberc Lung Dis.* 2009;13:1456-1466.
6. Brodin P, Majlessi L, Marsollier L, de Jonge MI, Bottai D, Demangel C, Hinds J, Neyrolles O, Butcher PD, Leclerc C, Cole ST, Brosch R. Dissection of ESAT-6 system of *Mycobacterium tuberculosis* and impact on immunogenicity and virulence. *Infect Immun.* 2006;74:88-98.
7. Choudhari PB, Bhatia MS, Bhatia NM. Application of Pocket Modeling and k-nearest Neighbor Molecular Field Analysis (kNN-MFA) for Designing of some Anticoagulants: Potential Factor IXa Inhibitors. *Medicinal Chemistry Research.* 2012;19:3-5.
8. Choure R, Pitre KS. Structural modification of coumarin for its increased anticoagulation potency. *Canadian J Chem Engineering Technology.* 2010;1:7-15.
9. Derrick SC, Morris SL. The ESAT6 protein of *Mycobacterium tuberculosis* induces apoptosis of macrophages by activating caspase expression. *Cell Microbiol.* 2007;9:1547-1555.
10. Ducati RG, Ruffino-Netto A, Basso LA, Santos DS. The Resumption of Consumption - A Review on Tuberculosis. *Mem Inst Oswaldo Cruz.* 2006;101:697-714.
11. Feltcher ME, Sullivan JT, Braunstein M. Protein Export Systems of *Mycobacterium tuberculosis*: novel target for drug development. *Future Microbiol.* 2010;5:1581-1597.
12. Fenton MJ, Vermeulen MW. Immunopathology of tuberculosis: roles of macrophages and monocytes. *Infect Immun.* 1996;64:683-690.
13. Finlay BB, Falkow S. Common themes in microbial pathogenicity revisited. *Microbiol Mol Biol Rev.* 1997;61:136-169.
14. Fortune SM, Jaeger A, Sarracino DA, Chase MR, Sasseti CM, Sherman DR, Bloom BR, Rubin EJ. Mutually dependent secretion of proteins required for mycobacterial virulence. *Proc Natl Acad Sci USA.* 2005;102:10676-10681.
15. Ginsberg AM. Tuberculosis drug development: Progress challenges and the road ahead. *Tuberculosis (Edinb).* 2010;90:162-167.
16. Jain A, Mondal R. Extensively drug-resistant tuberculosis: current challenges and threats. *FEMS Immunol Med Microbiol.* 2008;53:145-150.
17. Keane J, Balcewicz-Sablinska MK, Remold HG, Chupp GL, Meek BB, Fenton MJ, Kornfeld H. Infection by *Mycobacterium tuberculosis* promotes human alveolar macrophages apoptosis. *Infect Immun.* 1997;65:298-304.
18. Leung AN. Pulmonary Tuberculosis: The Essentials. *Radiology.* 1999;210:307-322.
19. Sugie Y, Inagaki S, Kato Y, Nishida H, Pang CH, Saito T, Sakemi S, Dib-Hajj F, Mueller JP, Sutcliffe J, Kojima Y. CJ-21,058, a new SecA inhibitor isolated from a fungus. *J Antibiot (Tokyo).* 2002;55:25-29.
20. Jang MY, De Jonghe S, Segers K, Anné J, Herdewijn P. Synthesis of novel 5-amino-thiazolo[4,5-d]pyrimidines as *E. coli* and *S. aureus* SecA inhibitors. *Bioorg Med Chem.* 2011;19:702-714.
21. Tripathi L, Kumar P, Singh R, Stables JP. Design, synthesis and anticonvulsant evaluation of novel N-(4-substituted phenyl)-2-[4-(substituted) benzylidene]-hydrazinecarbothioamides. *Eur J Med Chem.* 2012;47:153-166.
22. Malipeddi H, Karigar AA, Malipeddi VR, Sikarwar MS. Synthesis and Antitubercular Activity of Some Novel Thiazolidinone Derivatives. *TroJ of Pharm Res.* 2012;11:611-620.



# Optimization of Immobilized Aldose Reductase Isolated from Bovine Liver

## Sığır Karaciğerinden İzole Edilen İmmobilize Aldoz Redüktazın Optimizasyonu

© Marya Vakıl NASLIYAN, © Sidar BERKETOĞLU, © Özlem YILDIRIM\*

Ankara University, Faculty of Science, Department of Biology, Ankara, Turkey

### ABSTRACT

**Objectives:** Isolation of enzymes and experiments on them require great effort and cost and are time-consuming. Therefore, it is important to extend the usability of the enzymes by immobilizing them. In this study our purpose was to immobilize the enzyme aldose reductase (AR) and to optimize the experimental conditions of the immobilized AR and compare them to those of free AR.

**Materials and Methods:** AR was isolated from bovine liver and the enzyme immobilized in photographic gelatin by cross-linking with glutaraldehyde. Then the optimum conditions for free and immobilized AR in terms of pH, temperature, and storage were characterized by determining the enzyme activity.

**Results:** Following immobilization, the optimum pH and temperature levels for free AR, which were pH 7.0 and 60°C, slightly altered to pH 7.5 and 50°C. The enzyme activity of the immobilized AR was maintained at about 65% after reusing 15 times. Moreover, immobilized AR maintained 95% of its original activity after 20 days of storage at 4°C, while the retained activity of the free AR was 85% of the original.

**Conclusion:** Our experiments indicated that the conditions that affect enzyme activity might alter following immobilization. Once the optimum experimental conditions are fixed, the immobilized AR can be stored and reused with efficiency higher than that of free AR. Moreover, this study provides an insight into the advantages of using immobilized AR in enzyme assays rather than free AR.

**Key words:** Aldose reductase, isolation, immobilization

### ÖZ

**Amaç:** Enzim izolasyonu ve enzimler üzerinde yapılan deneyler, büyük çaba, maliyet ve zaman gerektirir. Bu yüzden, enzimlerin kullanılabilirliğinin immobilizasyon ile uzatılması önemlidir. Bu çalışmadaki amacımız, aldoz redüktaz (AR) enzimini immobilize etmek ve serbest AR'ninkiler ile karşılaştırarak immobilize AR'nin deney şartlarını optimize etmektir.

**Gereç ve Yöntemler:** AR, sığır karaciğer ve böbreğinden izole edildi ve glutaraldehid ile fotografik jelatine çapraz bağlanarak immobilize edildi. Daha sonra, enzim aktivitesi belirlenerek serbest ve immobilize AR'nin optimum pH, sıcaklık ve depolama koşulları tespit edildi.

**Bulgular:** Serbest AR için pH 7.0 ve 60°C olan optimum pH ve sıcaklık seviyeleri, immobilizasyondan sonra pH 7.5 ve 50°C olarak belirlendi. İmmobilize AR'nin enzim aktivitesinin, 15 kez kullanımdan sonra %65 oranında korunduğu tespit edildi. Bununla birlikte, +4°C'de 20 gün boyunca saklanan serbest AR'nin aktivitesi %85 oranında korunurken immobilize AR'nin aktivitesinin %95 oranında korunduğu bulunmuştur.

**Sonuç:** Deneylerimiz, immobilizasyonu takiben enzim aktivitesini etkileyen koşulların değişebileceğini göstermektedir. Ayrıca, immobilize AR, serbest AR'ye göre daha yüksek aktiviteyle korunup tekrar tekrar kullanılabilir. Ayrıca, immobilize AR, serbest AR'ye göre daha yüksek aktiviteyle korunup tekrar tekrar kullanılabilir.

**Anahtar kelimeler:** Aldoz redüktaz, izolasyon, immobilizasyon

\*Correspondence: E-mail: ozlem.e.yildirim@science.ankara.edu.tr, Phone: +90 532 471 60 46 ORCID-ID: orcid.org/0000-0002-7529-9786

Received: 28.02.2018, Accepted: 29.03.2018

©Turk J Pharm Sci, Published by Galenos Publishing House.

## INTRODUCTION

Aldose reductase (AR) (EC 1.1.1.21) is expressed by the AKR1B1 gene in humans. It is located on the 7q35 chromosome, consists of 315 amino acids, and its molecular weight is 36 kD. AR is a cytosolic monomeric protein.<sup>1</sup> It specifically catalyzes the polyol pathway, which includes the conversion of glucose-bound nicotinamide adenine dinucleotide phosphate (NADPH) cofactor to sorbitol.<sup>2,3</sup> Moreover, it reduces the activity of aldehydes such as glutathione complexes.<sup>4</sup> Indeed, AR is crucial in the detoxification of lipid aldehydes produced by oxidative stress.<sup>5</sup>

Under optimum conditions, enzymes are able to display their activities outside of their natural environment. Using this feature, they can be employed on a large scale in health science, such as in the diagnosis and treatment of diseases and drug design. However, their structure tends to alter during the experimental process. Therefore, studies aim to improve the conformational stability of enzymes.<sup>6</sup> Immobilization is a method reducing disruption of the enzyme structure. Enzyme immobilization avoids the majority of the instability and loss of enzyme activity. This provides a longer time and flexibility to work on enzymes. Immobilization is not only useful to maintain the stability of biomolecules but also it reduces the cost of enzyme studies.

In the present study for the first time AR was isolated from bovine liver, immobilized, and characterized with respect to several kinetic properties. In addition, AR derived from bovine kidney was used as a side control and simultaneously applied to identical experiments. The AR enzymes from both sources were immobilized in gelatin by glutaraldehyde and washed to remove the free enzyme. We compared the behavior of the free and the immobilized AR under different conditions of pH, temperature, reusing, and storage. The difference in optimum conditions of the free and the immobilized enzyme may be due to alterations in the structure caused by several factors such as carrier material, immobilization method, and activation method.<sup>7</sup> Indeed it was previously indicated that immobilization significantly changes the conformation of enzymes and thus their activity.<sup>8</sup>

## MATERIALS AND METHODS

### *Chemical materials*

In this research, ethylenediaminetetraacetic acid (EDTA), NADPH, and lithium sulfate ( $\text{Li}_2\text{SO}_4$ ) were purchased from Gerbu, Germany. Ammonium sulfate was supplied by Merck. Phenylmethylsulfonyl fluoride (PMSF), DL-glyceraldehyde, and all other materials used were analytically graded and obtained from Sigma Aldrich, Germany.

### *Isolation of AR enzyme from bovine liver*

The bovine liver was provided by a slaughterhouse in Kazan, Ankara, Turkey. Small pieces of liver samples were washed with 1.0 mM EDTA. Then they were measured and homogenized with threefold 1.0 mM EDTA and 50  $\mu\text{M}$  PMSF and spun at +4°C and 10,000 rpm for 30 min. To acquire 40% saturation, 22.6 g of ammonium sulfate was added to each 100 mL of supernatant

followed by rotation at 10,000 rpm at +4°C for 25 min. To gain 50% and 75% saturations, the same method was carried out by adding 5.8 g and 15.9 g of ammonium sulfate to the 100 mL of supernatant solution, respectively. The pellets were dissolved with 50 mM sodium chloride and stored in a freezer at -80°C.

### *Determining the protein amount*

Following isolation, the amount of protein was detected by Bradford assay.<sup>9</sup> The bovine serum albumin (BSA) standards were used at the concentrations of 0.4, 0.6, 0.8, 1.0, 1.2, and 1.4 mg/mL. BIO-RAD reagent was added to the BSA standards and the sample. Then each solution was measured using a spectrophotometer at 595 nm wavelength. Finally, protein amount was calculated using the standard graph generated with optical densities of the standards.

### *Assay of AR enzyme activity*

AR activity was detected against DL-glyceraldehyde, by monitoring the NADPH oxidation to  $\text{NADP}^+$  at 340 nm.<sup>10</sup> The reaction mixture consisted of AR enzyme (4.54 mg/mL), NADPH ( $9 \times 10^{-5}$  M),  $\text{Li}_2\text{SO}_4$  (320 mM-400 mM), DL-glyceraldehyde ( $6 \times 10^{-4}$  M), and KP buffer (50 mM, pH 6.2).  $\text{NADP}^+$  oxidation was followed in 0.25 mL of reaction mixture using a multimode microplate reader at 340 nm for 4 min. Initial and final rates of enzymatic reactions were measured and recorded as nmol/min/mg protein.

### *Immobilization of AR enzyme*

The immobilization gel consisted of 0.025 g of photographic gelatin and 0.125 M glutaraldehyde in 0.067 M phosphate tampon solution (pH 7.4). The photographic gelatin was prepared at 50°C and then cooled to 30-35°C. Different units of AR enzyme were added to the gelatin and then vortexed. Cross-linking glutaraldehyde was included at the concentration of  $5 \times 10^{-5}$  M. Then 100  $\mu\text{L}$  of the mixture was placed onto cellulose triacetate. Enzyme and gelatin complexes were dried for 24 h at room temperature.

The film strips carrying the immobilized AR were assayed for enzyme activity. The reaction mixture consisted of 2.7 mL of potassium phosphate, 0.1 mL of NADPH, and 0.1 mL DL-glyceraldehyde. Absorbance of this reaction mixture was measured at 340 nm before and after 20 min incubation with the film strips to detect enzyme activity.

## RESULTS AND DISCUSSION

AR isolated from bovine liver was immobilized by cross-linking with glutaraldehyde in photographic gelatin. To detect the amount of AR protein we used the Bradford assay and spectrophotometric measurements. The results indicated that the protein amount was  $18.39 \pm 0.09$  mg/mL. In the standard group, the activity values for only AR were  $4.172 \times 10^{-4}$  U/L in liver. These values are accepted as 100% enzyme activity.

Following immobilization, the free enzyme was removed by washing the film strips three times with phosphate buffer (0.067 M, pH 6.2) at 25°C for 5 min and spectrophotometry was used to detect the amount of free enzyme. Using the washed

film strips, the effect of enzyme concentration on immobilized enzyme activity was tested to detect the immobilized enzyme leakage. Our results showed that AR leakage from the film strips increased with enzyme concentration while the enzyme activity was reduced after each wash. On the other hand, three washes were sufficient to remove the leakage completely (Table 1).

We demonstrated that enzyme leakage increased depending on the increasing enzyme unit. This is because of the constant concentrations of the gelatin and glutaraldehyde. In other words, when there was insufficient gelatin, which is the immobilization medium, and/or glutaraldehyde, which is the cross-linker in the immobilization reaction, there was more unbound AR released from the film strips at high enzyme concentrations.

#### Characterization of the free and immobilized AR

Conditions of pH, temperature, and storage were optimized to characterize the free and the immobilized AR. Moreover, the effects of storage stability and continual use on the activity of the immobilized strips were tested.

#### pH

To evaluate the optimum pH for the free ( $1.46 \times 10^{-8}$  U) and the cross-linked ( $1.56 \times 10^{-8}$  U) AR, we measured the levels of enzyme activity in a pH gradient between pH 4 and 9 at 25°C for 5 min. It was demonstrated that the optimal pH values for the free and the immobilized AR from liver were respectively 7.0 and 7.5 (Figure 1).

**Table 1.** Effect of the enzyme concentration on the immobilized AR from liver

Enzyme volume ( $\times 10^{-8}$ U)	Activity (Enzyme unit/ $\mu$ mol/min/L)		
	Number of washes		
	1	2	3
1.04	0.017	0.007	0.000
1.46	0.130	0.015	0.000
2.08	0.347	0.024	0.000

AR: Aldose reductase

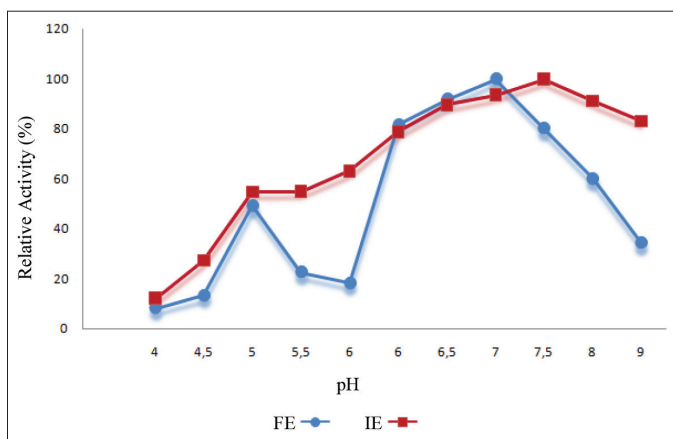


**Figure 1.** The enzyme activity levels of the free (FE) and the immobilized (IE) AR enzyme from liver according to pH

AR: Aldose reductase

We observed that the optimum pH for AR shifted to 7.5 from 7.0 upon immobilization. This alteration should be because of the  $H^+$  and the  $OH^-$  ions that are released into the microenvironment during the reaction. Indeed, this result about the optimum pH alteration was expected because of the context of the environments of free and immobilized enzymes as previously indicated.<sup>11</sup> Moreover, previous studies showed that the optimum pH of the enzyme was changed by the polar groups of gelatin during the immobilization.<sup>12</sup> There are possible interactions such as hydrogen bonds that are generated between enzyme and polymer carrier.<sup>13</sup> However, the immobilization might not significantly affect the stability of optimum pH for enzymes in some cases. For instance, NADH-cytochrome b5 reductase enzyme was isolated from rabbit liver microsomes and it was immobilized in photographic gelatin by chemical cross-linking using chromium (III) acetate. The experiments showed that the optimum pH for the free and the immobilized enzyme was in the range from 6.1 to 7.5.<sup>14</sup> Similarly, the free and the immobilized  $\beta$ -galactosidase on the gelatin carboxymethylcellulose carrier were assayed for the optimum pH. It was observed that immobilization of  $\beta$ -galactosidase did not have any significant effect on pH stability.<sup>15</sup> Consequently, it can be foreseen that the values of optimum pH for free and immobilized enzyme can change; however, this might not be the case for all enzymes and immobilization methods.

#### Temperature

We aimed to uncover the difference between optimum temperatures for the free and the immobilized AR, which is important for enzyme activity. To detect the optimum temperatures, activity of the enzyme was tested at different levels ranging from 5°C to 70°C. The highest enzyme activity was observed at 60°C for the free AR from liver and this shifted to 50°C after the cross-link immobilization (Figure 2).

These results suggested that the immobilization of AR from liver reduces the optimum temperature. However, in our experiments we also showed that immobilization increased the thermal stability of the enzyme between 60°C and 70°C (Figure

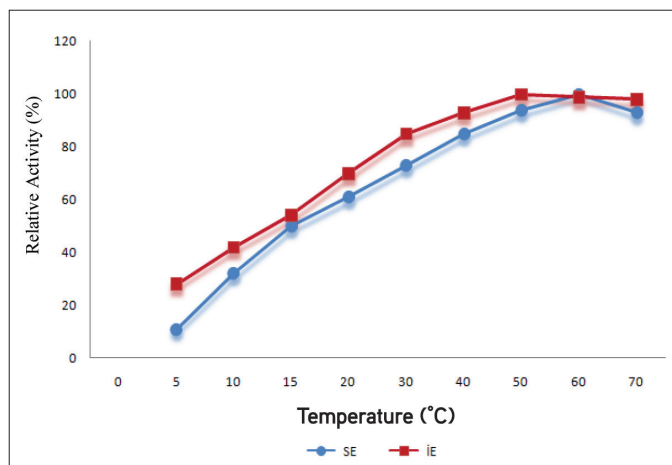


**Figure 2.** The enzyme activity levels of the free and the immobilized AR from liver according to temperature

AR: Aldose reductase

2). These results indicated that immobilization generated an optimum temperature range from 50°C to 70°C, while free enzyme showed the highest activity only at 60°C. In other words, immobilization maintained enzyme stability against increasing temperature. It was previously demonstrated that the optimum temperature of NADH-cytochrome b5 reductase enzyme from rabbit was 30°C, while it decreased to 25°C upon cross-link immobilization of the enzyme.<sup>14</sup> Conversely, free  $\beta$ -galactosidase showed the highest enzyme activity at 47°C, while it was at 57°C after the enzyme was cross-linked to the gelatin carboxymethylcellulose carrier.<sup>15</sup> This might suggest that the carrier system protects the immobilized enzyme from thermal denaturing.

**Reusing**

To test the activity of the reused AR, it was immobilized in photographic gelatin with glutaraldehyde at  $5 \times 10^{-8}$  M concentration. Upon reusing the immobilized AR from liver ( $1.46 \times 10^{-8}$  U) 15 times a day at 25°C, 65% of its original activity was recovered (Figure 3a). Similarly, we applied the same

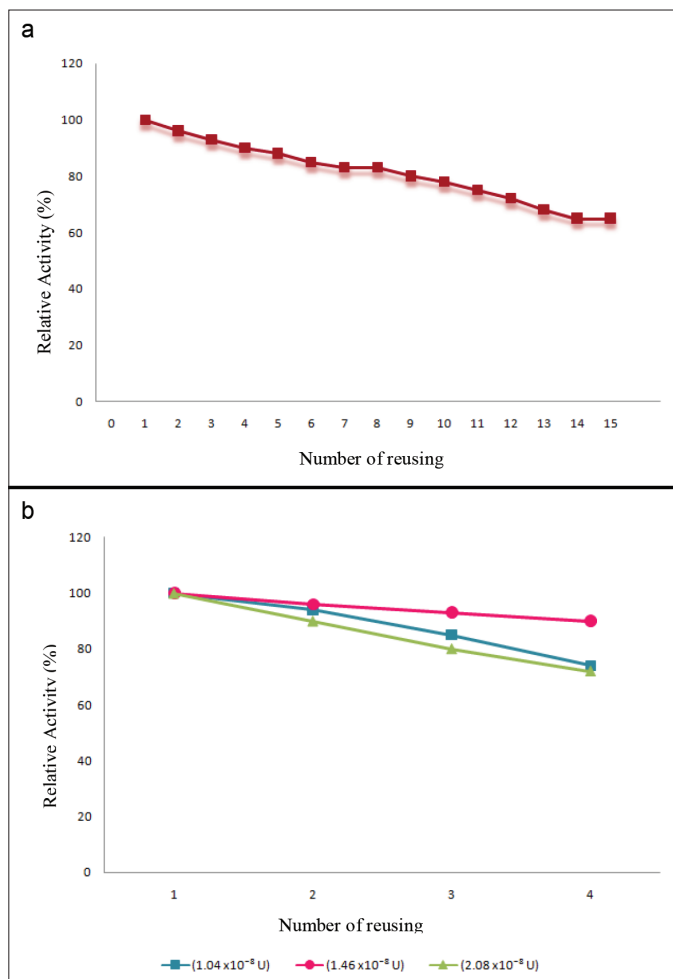


**Figure 3.** a) The enzyme activity levels of the immobilized AR from liver ( $1.46 \times 10^{-8}$  U) according to reusing stability. b) The enzyme activity levels of the immobilized AR from liver ( $1.04 \times 10^{-8}$  U) and ( $1.46 \times 10^{-8}$  U) ( $2.08 \times 10^{-8}$  U) according to reusing stability

AR: Aldose reductase

approach to different concentrations of the immobilized AR in different conditions. For instance, the immobilized AR from liver at the concentration of  $2.08 \times 10^{-8}$  U conserved 35% of the beginning enzyme activity after being used 10 times at 25°C (data not shown). We also tested the immobilized AR from liver for concentrations at  $1.04 \times 10^{-8}$  U,  $1.46 \times 10^{-8}$  U, and  $2.08 \times 10^{-8}$  U after being reused 4 times and reported that its activity was conserved about 74%, 90%, and 72%, respectively (Figure 3b).

**Storage**

To evaluate the effect of storage period on enzyme activity, we stored the free and immobilized AR at 4°C for 20 days and at 25°C for 10 days. After 20 days of storage at 4°C, activity of the immobilized AR was 95% of its original activity from liver (Figure 4a). Moreover, the free and the immobilized liver AR preserved 54% and 78% of their enzyme activity capacities following storage at 25°C for 10 days (Figure 4b).

Enzyme stability during storage is an important parameter for enzyme studies. Although it is expected that enzyme activity will be lower than at the beginning, the decrease should be minimized. This impairment in activity is most probably because of the denaturation of the enzyme structure.<sup>16</sup> In Yildirim et al.<sup>14</sup>

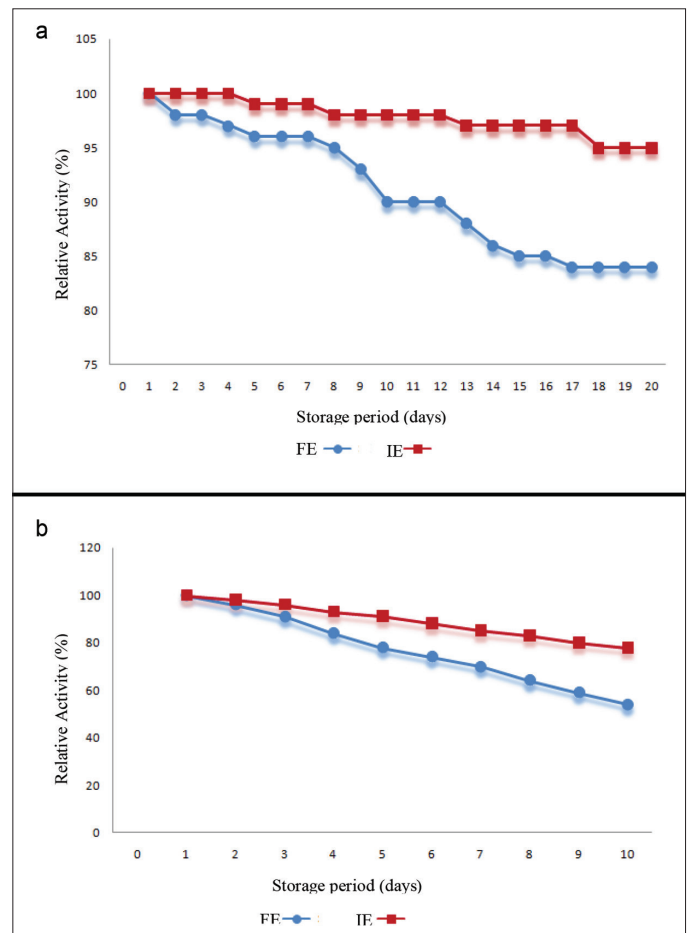


**Figure 4.** a) The enzyme activity levels of the immobilized AR from liver according to storage stability at 4°C. b) The enzyme activity levels of the immobilized AR from liver according to storage stability at 25°C

AR: Aldose reductase

research the free and the immobilized NADH-cytochrome b5 reductase enzymes were compared for their activities after 60 days of storage at  $-7^{\circ}\text{C}$ ,  $+4^{\circ}\text{C}$ , and  $+25^{\circ}\text{C}$ . They recorded that immobilization protects activity of the stored enzyme with higher efficiency at high temperature ( $+25^{\circ}\text{C}$ ) than at lower temperatures ( $-7^{\circ}\text{C}$  and  $+4^{\circ}\text{C}$ ).<sup>14</sup> Similarly, Kim et al.<sup>6</sup> showed that immobilized lipase enzyme maintained 82% of its activity after 30 days at room temperature, while the free lipase lost its activity completely. These results suggested that immobilization is a good tool to protect enzyme activity against temperature increases during storage. The efficiency of immobilization can be increased by carrying out the immobilization in a specific manner. For instance, it was demonstrated that the aldo/keto reductase AKR1A1 was immobilized as specific-oriented and so it was surface-bound. On the other hand, the unspecific immobilization was adsorptive; therefore, it showed less activity relative to the specifically immobilized aldo/keto reductase AKR1A1.<sup>17</sup>

The present study showed that immobilized AR enzyme can be preferable to work with than the free one. Our results showed that enzyme activity is retainable following immobilization as long as the experimental conditions are specifically fixed according to the immobilized AR.

## CONCLUSIONS

Consequently, we indicated that immobilization is a convenient method to utilize the enzyme AR in multiple experiments. While free enzymes can be used only once in experiments, immobilized enzymes can be used several times due to the protective features of glutaraldehyde cross-linking. In this case, optimal conditions for the immobilized AR should be indicated and applied to the experiments since these conditions might be different from those of the free AR.

*Conflict of Interest: No conflict of interest was declared by the authors.*

## REFERENCES

- Ramana KV, Srivastava SK. Aldose reductase: A novel therapeutic target for inflammatory pathologies. *Int J Biochem Cell Biol.* 2009;42:17-20.
- Petrash JM. All in the family: Aldose reductase and closely related aldo-keto reductases. *Cell Mol Life Sci.* 2009;61:737-749.
- Reddy GB, Satyanarayana A, Balakrishna N, Ayyagari R, Padma M, Viswanath K, Petrash JM. Erythrocyte aldose reductase activity and sorbitol levels in diabetic retinopathy. *Mol Vis.* 2008;14:593-601.
- Srivastava S, Chandra A, Bhatnagar A, Srivastava SK, Ansari NH. Lipid peroxidation product, 4-hydroxynonenal and its conjugate with GSH are excellent substrates of bovine lens aldose reductase. *Biochem Biophys Res Commun.* 1995;217:741-746.
- Srivastava SK, Ramana KV, Bhatnagar A. Role of aldose reductase and oxidative damage in diabetes and the consequent potential for therapeutic options. *Endocr Rev.* 2005;26:380-392.
- Kim M, Park JM, Um HJ, Lee DH, Lee KH, Kobayashi F, Iwasaka Y, Hong CS, Min J, Kim YH. Immobilization of cross-linked lipase aggregates onto magnetic beads for enzymatic degradation of polycaprolactone. *J Basic Microbiol.* 2010;50:218-226.
- Yemul O, Imae T. Covalent-bonded immobilization of lipase on poly (phenylene sulfide) dendrimers and their hydrolysis ability. *Biomacromolecules.* 2005;6:2809-2814.
- Atia KS, Ismail SA, Dessouki AM. Immobilization of  $\beta$ -amylase using polyacrylamide polymer derivatives. *J Chem Technol Biotechnol.* 2003;78:891-898.
- Bradford MM. A rapid and sensitive method for the quantitation of microgram quantities of protein utilizing the principle of protein-dye binding. *Anal Biochem.* 1976;72:248-254.
- Hayman S, Kinoshita JH. Isolation and properties of lens aldose reductase. *J Biol Chem.* 1965;2:240.
- Hasirci N, Aksoy S and Tümtürk H. Activation of poly(dimer acid-co alkylpolyamine) particles for covalent immobilization of  $\alpha$ -amylase. *React Funct Polym.* 2006;66:1546-1551.
- Emregül E, Sungur S, Akbulut U. Immobilization of glucose oxidase onto gelatin for biosensor construction. *J Biomater Sci Polym Ed.* 2009;16:505-519.
- Chen KC, Wu JY. Substrate protection of immobilized glucose isomerase. *Biotechnol Bioeng.* 1987;30:817-824.
- Yıldırım Ö, Akbulut U, Arınç E, Sungur S. Immobilization of NADH-cytochrome b5 reductase into gelatin by crosslinking. *Macromolecular Reports.* 1994;31:19-28.
- Sungur S, Yıldırım Ö. Batch and continuous hydrolysis of lactose using  $\beta$ -galactosidase immobilized on gelatin-CMC. *Polym Plast Technol Eng.* 1999;38:821-829.
- Chellapadian M. Preparation and characterization of alkaline protease immobilized on vermiculite. *Process Biochem.* 1997;33:169-173.
- Holland-Nell K, Beck-Sickingler AG. Specifically immobilized aldo/keto reductase AKR1A1 shows a dramatic increase in activity relative to the randomly immobilized enzyme. *ChemBiochem.* 2007;8:1071-1076.



# Screening of Sacrificial Excipients for Arresting Devitrification of Itraconazole from Solid Dispersion

## İtrakonazolün Katı Dispersiyondan Devitrifikasyonunu Önlemek için Amaca Yönelik Yardımcı Maddelerin Taranması

© Bhargavi M. PATEL, © Mukesh C. GOHEL, © Vaishali T. THAKKAR\*, © Lalji H. BALDANIYA, © Ruby R. CHRISTIAN, © Tejal R. GANDHI

Gujarat Technological University, Anand Pharmacy College, Anand, Gujarat, India

### ABSTRACT

**Objectives:** The aim of the present investigation was to develop a solid dispersion of itraconazole (ITR) using sacrificial excipients like pregelatinized starch and spray-dried lactose alongside hydroxypropyl methylcellulose and Poloxamer 188, thereby arresting the conversion of the amorphous form of ITR to crystalline form, and to assess the dissolution stability of an amorphous form of the drug during short-term storage.

**Materials and Methods:** ITR-loaded solid dispersions were prepared by kneading. Formulation optimization was achieved by using a 2<sup>4</sup> full factorial design on the basis of cumulative percent drug released at t<sub>30'</sub>, t<sub>60'</sub> and t<sub>120'</sub> min. An artificial neural network (ANN) was also applied as a statistical tool for obtaining better predictive ability and the outcomes of the ANN were compared with that of Design-Expert software.

**Results:** The spectral data revealed no drug-carrier interactions. The P-X-ray diffraction study of the optimized batch showed a decrease in the crystallinity of drug as compared to the untreated drug. The *in vitro* dissolution studies of the optimized batch showed higher dissolution (92% at 120 min) in comparison to the other formulations. The dissolution stability study was performed at 40°C and 75% relative humidity for 90 days for the optimized formulation. The results of the optimized batch showed insignificant changes in cumulative percentage drug release during storage.

**Conclusion:** Dissolution stability could be attributed to the presence of sacrificial excipients as they tend to absorb moisture during storage and possibly get converted into crystalline form, thereby minimizing the recrystallization of ITR.

**Key words:** Solid dispersion, itraconazole, ANN, sacrificial excipients, devitrification

### ÖZ

**Amaç:** Mevcut araştırma, prejelatinize nişasta, püskürterek kurutulmuş laktoz yanısıra hidroksipropil metilselüloz ve Poloxamer 188 gibi amaca yönelik yardımcı maddeler kullanılarak itrakonazolün (ITR) katı dispersiyonunu geliştirmeyi ve böylece ITR'nin amorf formunun kristal formuna dönüştürülmesini durdurmaya ve kısa süreli depolamada etkin maddenin amorf formunun çözülme stabilitesini değerlendirmeyi amaçlamıştır.

**Gereç ve Yöntemler:** ITR yüklü katı dispersiyonlar hamur etme metoduyla hazırlandı. Formülasyon optimizasyonu, t<sub>30'</sub>, t<sub>60'</sub> ve t<sub>120'</sub> dakikada salınan kümülatif yüzde etkin maddeyi baz alarak 2<sup>4</sup> tam faktörlü tasarım kullanılarak elde edilmiştir. Yapay sinir ağı (YSA), daha iyi bir tahmin yeteneği elde etmek için istatistiksel bir araç olarak uygulanmış ve YSA'nın sonuçları, design expert yazılımınıninkilerle karşılaştırılmıştır.

**Bulgular:** Spektral veri ilaç taşıyıcı etkileşimi göstermemiştir. Optimize edilmiş partinin P-X-ışını difraksiyon çalışması, işlem görmemiş etkin maddeye kıyasla etkin maddenin kristalliğinde azalma göstermiştir. Optimize edilmiş partinin *in vitro* çözünme çalışmaları, diğer formülasyonlara kıyasla en yüksek çözünme (120 dakikada %92) göstermiştir. Çözünme stabilitesi çalışması, optimize edilmiş formülasyon için 90 gün boyunca 40°C'de ve %75 bağıl nem yapılmıştır. Optimize edilmiş partinin sonuçları, depoda kümülatif yüzde etkin madde salımında önemsiz değişiklikler göstermiştir.

**Sonuç:** Çözünme stabilitesi, amaca yönelik yardımcı maddelerin varlığında depolamadaki nemi absorbe etme eğiliminde olduklarından ve muhtemelen bu nem ile kendilerinin kristalli bir forma dönüşmesine ve ITR'nin yeniden kristalleşmesine en aza indirmesine bağlanabilir.

**Anahtar kelimeler:** Katı dispersiyon, itrakonazol, YSA, amaca yönelik madde, devitrifikasyon

\*Correspondence: E-mail: vtthakkar@rediffmail.com, Phone: 9724431131 ORCID-ID: orcid.org/0000-0000-6332-7703

Received: 10.01.2018, Accepted: 05.04.2018

©Turk J Pharm Sci, Published by Galenos Publishing House.



## INTRODUCTION

More than 40% of newly discovered active pharmaceutical ingredients (APIs) fail to enter the market due to low aqueous solubility.<sup>1</sup> Micronization, pH modification, hydrotropy, and solid dispersion have been examined for improvement of apparent drug solubility in aqueous medium, API release rate, and possibility of bioavailability. Solid dispersions can be incorporated into tablets, capsules, bioadhesive film, implants, and dry powder inhalers.<sup>2</sup> The other merits of solid dispersion include generation of fine particles of APIs without excessive use of energy and availability of a variety of formulation options.

The main limitation of a solid dispersion is, as reported in the literature, its physical stability and recrystallization of APIs on standing, due to absorption of moisture by the carrier and particle growth. The phenomenon of reverse crystallization of APIs results in retarded API dissolution.<sup>3</sup> Maintenance of the amorphous state of the drug in a dosage form is always a challenge to the formulators. This is one of the reasons for the availability of a limited number of formulations on the market.

We hypothesized that if amorphous excipients are added to a solid dispersion containing amorphous APIs then the probability of recrystallization of APIs will be arrested to a certain extent due to competition between the APIs and excipient. Such excipients are referred to as sacrificial excipients in the present investigation. This term is coined from the widely used term sacrificial antioxidants (ascorbic acid and others), which are added to formulations containing oxygen-sensitive APIs.

The example amorphous excipients are spray-dried lactose, pregelatinized starch, low-substituted hydroxypropyl ether of cellulose, and Neusilin. The sacrificial excipient will preferentially absorb moisture on standing and preferentially get converted in crystalline form and afford protection to the amorphous physical state of the API. In the present investigation, the use of quality by design is also demonstrated to speed up the formulation development work at the plant. Comparison is also done between the use of design of experiments (DoE) and artificial neural network (ANN).

The main objectives of the present study were to improve the apparent solubility of itraconazole (ITR) and to test the proposed hypothesis of using sacrificial amorphous excipients for imparting dissolution stability to APIs during storage.

## MATERIALS AND METHODS

### Materials

ITR was received as a gratis sample from Alembic Pharmaceuticals (Baroda, India). The samples of hydroxypropyl methylcellulose (HPMC E5) and pregelatinized starch were procured from Colorcon Asia Pvt. Ltd. (Goa, India). Spray-dried lactose was procured from Signet Chemicals (Mumbai, India). Poloxamer 188 was purchased from BASF (Mumbai, India) and the solvents used were obtained from Astron Chemicals Pvt. Ltd., (Ahmedabad, India)

### Preparation of solid dispersion by kneading method

Solid dispersions of ITR were prepared by kneading. Accurately weighed quantities of HPMC E5, Poloxamer 188, and sacrificial

excipients (spray-dried lactose or pregelatinized starch) were mixed with a sufficient quantity of water to obtain a smooth and homogeneous paste; after that a weighed quantity of ITR was added to the paste and kneaded for 30 min. Finally the paste was dried in an oven at 45°C for 3 h and then passed through sieve #100. The samples were stored in a screw-capped glass vial until use.<sup>4</sup>

### Experimental design

The concentrations of spray-dried lactose ( $X_1$ ), pregelatinized starch ( $X_2$ ), HPMC E5 ( $X_3$ ), and Poloxamer 188 ( $X_4$ ) were selected as independent variables in a  $2^4$  full factorial design. All the other formulation factors were kept constant throughout the experiment. The percentages of drug dissolved at 30 ( $Y_1$ ), 60 ( $Y_2$ ), and 120 ( $Y_3$ ) min in 0.1 N HCl were selected as dependent variables. Design-expert software (version 9.0.0.7) was used for creating the mathematical models.<sup>5</sup> The design layout with the results is shown in Table 1. Polynomial models including interaction terms were generated for all the response variables. The full polynomial equation is shown below (Equation 1).

$$Y = b_0 + b_1X_1 + b_2X_2 + b_3X_3 + b_4X_4 + b_{12}X_1X_2 + b_{13}X_1X_3 + b_{14}X_1X_4 + b_{23}X_2X_3 + b_{24}X_2X_4 + b_{34}X_3X_4 + b_{1234}X_1X_2X_3X_4$$

Here  $b_0$  is the intercept representing the arithmetic average of all quantitative outcomes of factorial runs;  $b_1$  to  $b_4$  are the main effects. The terms  $b_{12}$ ,  $b_{13}$ ,  $b_{14}$ ,  $b_{23}$ ,  $b_{24}$ , and  $b_{34}$  represent the interaction terms. The statistical validity of the model was established on the basis of analysis of variance. Subsequently, feasibility and grid searches were performed to locate the composition of the optimum formulation. Contour plots were also constructed in MS-Excel environment using the output files generated by the design-expert software.

### Artificial neural network

ANN is a machine-based computational technique that attempts to simulate some of the neurological processing ability of the human brain. Fundamentally, ANNs are interconnected networks of processing units termed as 'neurons', which are responsible for the completion of the decision-making process. They have the ability to discern complex and latent patterns in the information presented to them. This feature of ANNs proves they are a powerful tool for modeling and predictive purposes and offers great potential for application in a variety of disciplines. ANNs have attracted the attention of many computer scientists and have been successfully applied to solve a multitude of problems in diverse areas of science, engineering, and business.<sup>6</sup>

A three-layer network with a different activation function was applied in this study. NeuroSolutions version 7.0.0 evaluation software was downloaded from NeuroDimension, Inc (www.nd.com). The independent variables  $X_1$ ,  $X_2$ ,  $X_3$ , and  $X_4$  were used as inputs and the responses recorded were cumulative drug release at 30, 60, and 120 min. Generally, the neural network methodology has several empirically determined parameters. These include the number of iterations or epochs, the processing

element, learning rate, and momentum terms. The optimum values for ANN parameters were evaluated by obtaining those values that yielded the lowest prediction error. The multilinear perceptron network model was selected from the customized new network. Different functions like TanhAxon, SigmoidAxon, LinearTanAxon, LinearSigmoidAxon, BiasAxon, LinearAxon, and Axon were used to predict the output response.<sup>7</sup>

#### Evaluation parameters

##### Drug content

Solid dispersions equivalent to 10 mg of ITR were weighed accurately and dissolved in a suitable quantity of methanol. The drug content was analyzed at 260 nm by ultraviolet spectrophotometer (Shimadzu, Japan). Each sample was analyzed in triplicate.

##### *In vitro drug release study*

Dissolution experiments were conducted on the untreated drug and solid dispersion. The *in vitro* release test was performed using a USP type-I (basket type) dissolution apparatus (Electrolab TDT 08L, India). The dissolution medium was 0.1 N HCl (pH 1.2) maintained at a temperature of  $37\pm 1^\circ\text{C}$  with a paddle speed of 100 rpm. The powdered samples (sieved through a 100- $\mu\text{m}$  sieve) of pure drug and solid dispersion batches, equivalent to 100 mg of ITR, were separately added to the dissolution vessels while stirring. Samples (5 mL) were drawn at 30, 60, and 120 min and fresh dissolution medium (5 mL) was added after sampling to maintain sink condition. The samples were immediately filtered through 0.45- $\mu\text{m}$  filters. The first 2 mL of the filtrate was discarded and the samples were assayed for drug content after appropriate dilution with

**Table 1. Variables, their levels, and responses in 2<sup>4</sup> full factorial design**

Batch	Independent variables				Responses % CDR $\pm$ SD			Drug content
	X <sub>1</sub> (mg)	X <sub>2</sub> (mg)	X <sub>3</sub> (mg)	X <sub>4</sub> (mg)	t <sub>30</sub> (Y <sub>1</sub> )	t <sub>60</sub> (Y <sub>2</sub> )	t <sub>120</sub> (Y <sub>3</sub> )	
SD1	100	0	50	100	19.03 $\pm$ 0.13	38.11 $\pm$ 0.23	57.34 $\pm$ 0.25	98.7 $\pm$ 0.08
SD2	0	100	100	100	23.09 $\pm$ 0.20	47.23 $\pm$ 0.15	70.45 $\pm$ 0.06	100.5 $\pm$ 0.12
SD3	0	0	50	50	18.30 $\pm$ 0.01	36.35 $\pm$ 0.13	55.12 $\pm$ 0.05	99.5 $\pm$ 0.13
SD4	100	100	50	50	18.51 $\pm$ 0.12	37.48 $\pm$ 0.05	55.13 $\pm$ 0.05	99.7 $\pm$ 0.05
SD5	0	0	50	100	18.00 $\pm$ 0.01	36.35 $\pm$ 0.03	54.11 $\pm$ 0.08	98.8 $\pm$ 0.104
SD6	0	0	100	50	21.60 $\pm$ 0.14	42.28 $\pm$ 0.03	63.12 $\pm$ 0.11	100.9 $\pm$ 0.40
SD7	0	100	50	100	16.24 $\pm$ 0.02	36.67 $\pm$ 0.23	52.56 $\pm$ 0.23	99.6 $\pm$ 0.80
SD8	100	100	50	100	17.05 $\pm$ 0.16	34.18 $\pm$ 0.03	51.33 $\pm$ 0.05	99.5 $\pm$ 0.78
SD9	0	100	100	50	11.09 $\pm$ 0.03	22.31 $\pm$ 0.08	33.45 $\pm$ 0.05	98.9 $\pm$ 0.63
SD10	100	100	100	100	26.41 $\pm$ 0.08	53.24 $\pm$ 0.11	92.19 $\pm$ 0.11	100.6 $\pm$ 0.03
SD11	100	0	100	50	24.09 $\pm$ 0.01	48.19 $\pm$ 0.06	72.13 $\pm$ 0.06	101 $\pm$ 0.12
SD12	0	0	100	100	27.05 $\pm$ 0.02	54.10 $\pm$ 0.03	80.17 $\pm$ 0.06	98.8 $\pm$ 0.72
SD13	0	100	50	50	16.24 $\pm$ 0.07	32.08 $\pm$ 0.05	48.29 $\pm$ 0.17	99.6 $\pm$ 0.13
SD14	100	0	100	100	24.13 $\pm$ 0.06	49.12 $\pm$ 0.06	85.28 $\pm$ 0.11	99.3 $\pm$ 0.06
SD15	100	100	100	50	14.09 $\pm$ 0.03	28.46 $\pm$ 0.05	42.22 $\pm$ 0.11	99.9 $\pm$ 0.18
SD16	100	0	50	50	23.53 $\pm$ 0.35	46.06 $\pm$ 0.05	69.07 $\pm$ 0.06	101 $\pm$ 0.53

Where

Independent variables	Levels	
	Low (mg)	High (mg)
X <sub>1</sub> = Concentration of spray-dried lactose	0	100
X <sub>2</sub> = Concentration of pregelatinized starch	0	100
X <sub>3</sub> = Concentration of HPMC E5	50	100
X <sub>4</sub> = Concentration of Poloxamer 188	50	100
Dependent variables	Y <sub>1</sub> = %CDR at t <sub>30</sub> min Y <sub>2</sub> = %CDR at t <sub>60</sub> min Y <sub>3</sub> = %CDR at t <sub>120</sub> min	

SD: Standard deviation

the dissolution medium. The cumulative amounts of the drug dissolved (expressed as % of the total drug added) were plotted as a function of time to produce the dissolution profiles.<sup>8</sup>

#### Fourier transform infrared spectroscopy

Spectroscopy was conducted using an Fourier transform infrared (FTIR) spectrophotometer (Spectrum GX-FT-IR, PerkinElmer, USA) for the untreated ITR and optimized batch of ITR solid dispersion. The spectrum was recorded in the range of 4000–400  $\text{cm}^{-1}$ . The procedure consisted of dispersing a sample in KBr followed by gentle mixing. The spectrum was scanned at a resolution of 0.15  $\text{cm}^{-1}$  and scan speed was 20 scan/s.

#### Differential scanning calorimetry

A differential scanning calorimeter (DSC) (DSC-PYRIS-1, Phillips, Netherlands) was used to study the thermal behavior of the untreated ITR and optimized batch of ITR solid dispersion. The experiments were performed in a dry nitrogen atmosphere. The samples (2–4 mg) were heated in hermetically sealed flat-bottomed aluminum pans under nitrogen flow (20 mL/min) at a scanning rate of 10°C/min from 25°C to 200°C. Empty aluminum pans were used as the reference standard.

#### X-ray diffraction

The X-ray diffraction (XRD) study was carried out to characterize the physical form of ITR in samples of untreated ITR and optimized batch of ITR solid dispersion. Vacuum grease was applied onto the glass slide to stick the sample. The sample was allowed to spread on the glass slide in approximately 0.5 mm thickness. The slide was then placed vertically at 0° angle in the X-ray diffractometer (X'Pert Model, Phillips, Netherlands) so that the X-ray beam fell on it properly. The results were recorded over a range of 0–90° (2 $\theta$ ) using the Cu-target X-ray tube and Xe-filled detector. The operating conditions were as follows: voltage 40 kV, current 20 mA, scanning speed 1/min, temperature of acquisition: room temperature, detector: scintillation counter detector, and sample holder: nonrotating holder.

#### Moisture uptake study

Accurately weighed amounts of optimized solid dispersion (ITR + HPMC E5 + Poloxamer 188), solid dispersion with sacrificial excipient (ITR + HPMC E5 + Poloxamer 188 + PGS + spray-dried lactose), and also amorphous excipients PGS and spray-dried lactose were exposed to 75% RH for a fixed period of time.

The stated humidity was obtained using saturated aqueous solution of sodium chloride in a sealed desiccator at 40±1°C. The samples were observed in two different conditions, i.e., with a packaging system (samples sealed with aluminum foil) and without a packaging system.

#### Stability study

Short-term dissolution stability was studied under accelerated stability condition. The optimized batch with and without sacrificial excipient was stored at ambient conditions in capped amber vials (40°C/75% RH). Samples were evaluated at an interval of 30, 60, and 90 days for drug content and *in vitro* release characteristics study. In addition, further confirmation of stability was obtained by performing an XRD study so as to confirm the amorphous property of the drug during storage.<sup>9</sup>

## RESULTS AND DISCUSSION

#### Drug content

The drug contents of the solid dispersions were found to be in the range of 98.7%–101.3% (Table 1), which is acceptable according to the United States Pharmacopeia.<sup>10</sup>

#### *In vitro* release study

The cumulative drug release for the batches (SD1 to SD16) at  $t_{120}$  showed a wide variation of 33% to 98% (Table 1, Figure 1a). The fitted polynomial equations (full and reduced model) relating the response at  $t_{30}$ ,  $t_{60}$ , and  $t_{120}$  to the transformed factors are shown in Table 2. The polynomial equations can be used to draw conclusions after considering the magnitude of coefficient and the mathematical sign it carries, i.e., positive or negative. The significance level of coefficients, which was found to be >0.05, was omitted from the full model equation to generate the reduced model equation for all three responses. The coefficients found to be significant at p value less than 0.05 were retained in the reduced model. Table 2 shows the results of the regression analysis. The high values of correlation coefficients of %CDR at  $t_{30}$ ,  $t_{60}$ , and  $t_{120}$  indicate a good fit. Table 3 shows the results of ANOVA. The p value is less than 0.05 for all three responses. It can, therefore, be concluded that at least one of the independent variables influences the release of the drug from the solid dispersion.

The change in %CDR at  $t_{30}$ ,  $t_{60}$ , and  $t_{120}$  as a function of  $X_3$  and  $X_4$  is depicted in the form of a response surface plot (Figure 1b) based on the full factorial design. Low level of  $X_3$  and high

**Table 2. Results of regression analysis**

Response	$b_0$	$b_1$	$b_2$	$b_3$	$b_4$	$b_1b_2$	$b_1b_3$	$b_1b_4$	$b_2b_3$	$b_2b_4$	$b_3b_4$
Full model for $t_{30}$	20.01	1.55	1.58	-2.02	0.91	2.26	-0.74	-0.16	1.43	-0.72	0.15
Reduced model for $t_{30}$	20.01	1.55	1.58	-2.02	-	2.26	-	-	1.43	-	-
Full model for $t_{60}$	40.03	3.07	3.31	-3.84	1.81	4.48	-1.45	-0.19	2.79	-1.52	0.34
Reduced model for $t_{60}$	40.03	3.07	3.31	-3.84	1.81	4.48	-	-	2.79	-	-
Full model for $t_{120}$	59.96	4.59	5.09	-5.62	2.84	6.73	-2.06	-0.10	4.39	2.02	0.41
Reduced model for $t_{120}$	59.96	4.59	5.09	-5.62	-	6.73	-	-	4.39	-	-

level of  $X_1$ ,  $X_2$ , and  $X_4$  were found to be favorable conditions for obtaining faster dissolution. The multiple linear regression analysis (Table 2) revealed that coefficients  $X_1$ ,  $X_2$ , and  $X_4$  are positive and  $X_3$  is negative. This indicates that on increasing factor  $X_1$ ,  $X_2$ , and  $X_4$ , the drug release rate at each time point increases. A higher amount of HPMC may lead to gelation.<sup>11</sup> This is due to the tendency of HPMC E5 to form a hydrogel that slowly erodes in water, which probably explains the delayed dissolution. In contrast, poloxamer is a water-soluble nonionic surface-active agent and has been used in solid dispersions to improve the apparent solubility of APIs. It is proposed that the amorphous state of ITR in Poloxamer 188 solid dispersions and the solubilizing effect of poloxamer are attributable to the high dissolution rate.<sup>12</sup> Pregelatinized starch and spray-dried lactose improved the dissolution of ITR by virtue of its ability to arrest the devitrification process, thereby keeping the drug in amorphous state. Checkpoint batches C1, C2, and C3 were prepared as per the composition given in Table 4a. The theoretical % cumulative drug release at  $t_{120}$  of batches C1, C2, and C3 was 92.30%, 92.17%, and 92.38%, respectively. The experimental values were 92.22%, 92.00%, and 92.16%,

respectively, for the three batches (Table 4b), which are in good agreement with theoretical values. This confirms the validity of the model. The optimized batch obtained from the solutions of DoE was 99.21 mg of HPMC E5, 98.90 mg of Poloxamer 188, 100 mg of pregelatinized starch, and 100 mg of spray-dried lactose, which met the set dissolution criterion, i.e. more than 75% drug release at 120 min. The dissolution profile comparison of pure ITR with the optimized formulation clearly indicated enhanced solubility of the drug in solid dispersion form rather than in pure form as seen in Figure 1c.

*Overlay plot*

The US Food and Drug Administration (FDA) insists that while submitting the ANDA application the design space shall be submitted. Hence, the design space was generated by overlapping the three contour plots (Figure 2). The area in the right top corner indicates the design space. It is the space within which if variations occur then the FDA should not be approached for SUPAC, i.e., scale-up and postapproval changes.

*Artificial neural network*

In the ANN, the training data set (a couple of data points are picked from the experimental runs) was used to develop a mathematical model and thereafter the test data (the data points not included in training) were uploaded for prediction. Then the observed value of response and computed values of the selected responses were compared. The difference between the two responses is expressed as root mean square of error (RMSE). If the model is perfect, the value of RMSE is zero. A low value of RMSE is an indication of better fit. The data collected were entered into the Neurosolutions software and for each response ANN was run to get the values of RMSE.<sup>6,7</sup> The number of epochs needed by the various options and the MSE values for all responses are summarized in Table 5. The TanhAxon function showed the lowest RMSE value for all the responses. Moreover, 18, 18, and 15 epochs were required by the software to arrive at the minimum mean square of error of

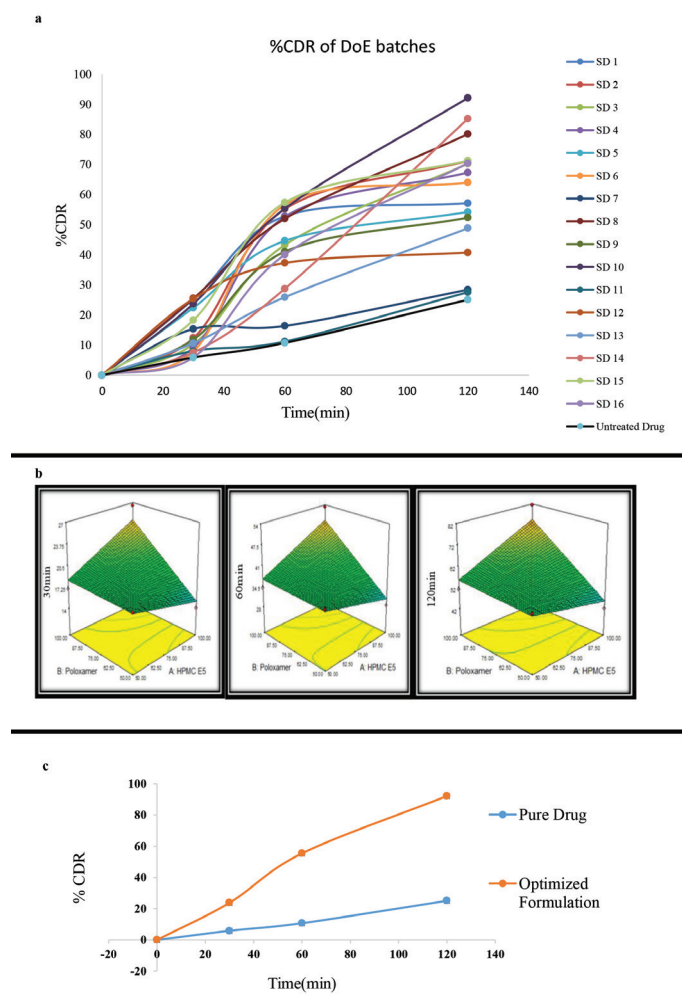


Figure 1. a) %CDR of design of experiments batches, b) response surface plot of %CDR at 30, 60, and 120 min, c) dissolution profile of pure drug itraconazole and optimized formulation

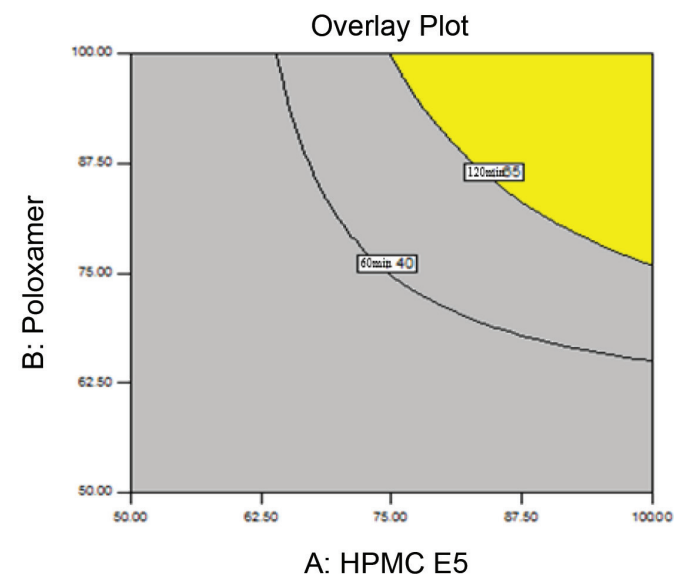
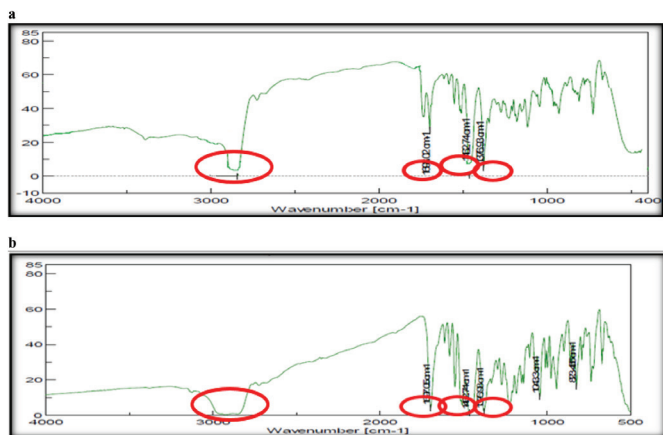


Figure 2. Overlay plot

0.07,  $1.972 \times 10^{-25}$ , and 0.017 for all three responses, respectively, when the TanhAxon option was selected in the software. The value of MSE is very close to zero. When the observed value of a response and a calculated value of response are exactly identical MSE is equal to zero. It means that the fit is perfect (the predicted value is very close to the observed value). The software generally achieves this by an iteration technique. Comparison of RMSE in the DoE and the ANN showed that the ANN serves as a better predictive tool as shown in Table 6.

**FTIR study**

The FTIR spectrum of pure ITR and that of optimized solid dispersions are shown in Figures 3a and 3b, respectively. The



**Figure 3.** a, b) Fourier transform infrared spectra of itraconazole and itraconazole solid dispersion

**Table 3.** The results of ANOVA\*

Response	Df	SS	MS	F	P value	R <sup>2</sup>	Model
t <sub>30</sub>	10	288.49	28.85	5.99	0.030	0.922	
t <sub>60</sub>	10	1134.14	113.41	6.44	0.02	0.928	Significant
t <sub>120</sub>	10	2554.98	255.50	5.85	0.03	0.921	

\*ANOVA indicates analysis of variance, Df: Degrees of freedom, SS: Sum of squares, MS: Mean of squares, F: Fisher’s ratio, R<sup>2</sup>: Regression coefficient, FM: Full model, RM: Reduced model

**Table 4a.** Check point batches composition

Batch	X <sub>1</sub> (mg)	X <sub>2</sub> (mg)	X <sub>3</sub> (mg)	X <sub>4</sub> (mg)
C1	100	100	99.21	98.90
C2	100	100	98.83	98.90
C3	100	100	98.83	99.28

**Table 4b.** Check point batches response

Batch	t <sub>30</sub> (% CDR)			t <sub>60</sub> (% CDR)			t <sub>120</sub> (% CDR)		
	Predicted	Cal.	Error%	Predicted	Cal.	Error%	Predicted	Cal.	Error%
C1	23.94	23.75	0.22	48.26	48.00	0.53	92.30	92.22	0.46
C2	23.89	23.73	0.46	48.17	47.95	0.45	92.17	92.00	0.23
C3	23.96	23.85	0.45	48.31	48.15	0.33	92.38	92.16	0.29

spectrum of ITR showed characteristic bands at 2935 and 2833 cm<sup>-1</sup> (O-H stretching), 3320 cm<sup>-1</sup> (N-H stretching), 1697 cm<sup>-1</sup> (C=O stretching), 1375 and 1465 cm<sup>-1</sup> (O-H in plane bending), 1040 cm<sup>-1</sup> (O-H out of plane bending), and 722 and 749 cm<sup>-1</sup> (out of plane bending for N-H). If we focus on the spectra of the solid dispersions, then prominent peaks of the drug are seen at 2935 cm<sup>-1</sup> for O-H stretching, which is shifted to lower frequency of 2922 cm<sup>-1</sup> in its kneaded particles with the same ratio. The reason for this observation might be interpreted as a consequence of O-H stretching, which was found to be very weak in its kneaded particles. These suggest that there must be strong hydrogen bonding of the drug with HPMC E-5. It can be inferred that ITR molecules were entrapped in the matrix structure of HPMC E-5 and its physical movement in the matrix was minimum and so re-aggregation and recrystallization chances were minimum with the HPMC E-5.<sup>13</sup>

**DSC thermogram**

The DSC curves obtained for untreated ITR and solid dispersions are shown in Figures 4a and 4b. Pure ITR showed a sharp endotherm at 167.38°C corresponding to its melting point. The DSC thermogram of ITR solid dispersion (Figure 4b) shows characteristic peaks at 50.17°C and 216.42°C corresponding to melting point of Poloxamer 188 and HPMC E5, respectively. Absence of a characteristic peak of the drug was noted in solid dispersions. These suggest that the physical state of the drug has been changed from crystalline to amorphous form. It is well known that transforming the physical state of the drug to amorphous or partially amorphous state leads to a high energy

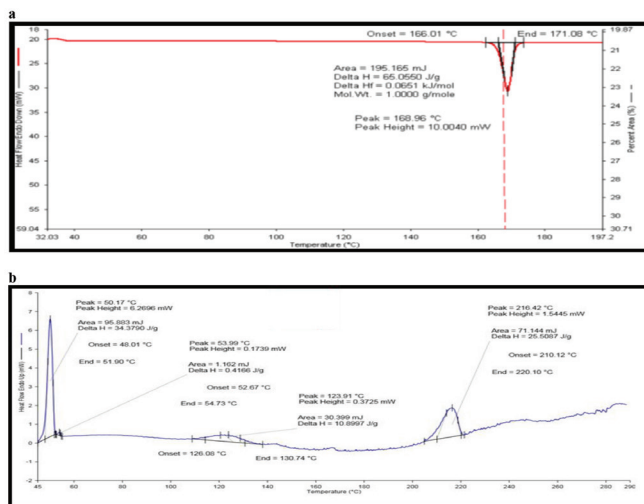


**Figure 4.** Differential scanning calorimeter thermographs of a) itraconazole, b) itraconazole physical mixture

state and high disorder, resulting in enhanced solubility and faster dissolution.<sup>14</sup>

### XRD

The XRD pattern of untreated ITR, solid dispersions, and solid dispersion after the stability study of 90 days are shown in Figures 5a, 5b, and 5c, respectively. The XRD scan of pure ITR showed intense peaks of crystallinity, whereas the XRD pattern of prepared solid dispersion and solid dispersion after stability exhibited a reduction in both number and intensity of peaks compared to the plain ITR, indicating a decrease in crystallinity or partial amorphization of the drug in its kneaded form. Untreated ITR drug powder showed sharp intense peaks

at diffraction angles of  $2\theta$ , 7.62, 10.33, 14.23, 15.41, 18.66, 19.73, 20.70, 21.86, 22.73, 23.61, 25.03, 27.61, and 28.62. These sharp peaks were present in the diffractograms of all the samples. The number of peaks and peak height in the diffractograms of solid dispersion decreased compared to that of untreated ITR crystalline powder. Relative crystallinity at  $2\theta$  angle 20.70 was found to be 0.675. This indicates a decrease in crystallinity or amorphization of the drug. After 90 days of stability study at  $40^\circ\text{C}\pm 75\% \text{RH}$ , the same XRD pattern was obtained, indicating that the solid dispersion was stable and the drug was in amorphous state.

### Moisture uptake study

It is well understood that amorphous drugs formulated in a solid dispersion tend to undergo devitrification upon storage at high temperature and humidity.<sup>4</sup> The optimized solid dispersion, without sacrificial excipients, was found to be highly hygroscopic ( $>30\%$  water uptake) in nature at 75% RH. As the exposure time to the humidity was increased, the moisture content also increased. The plasticizing effect of absorbed moisture can reduce the  $T_g$  of an amorphous substance and lead to further instability. Hence, a decrease in dissolution rate is expected on long-term storage. The samples of SD containing PGS and spray-dried lactose picked up less moisture. The results of the moisture uptake study of SD with and without sacrificial excipients and amorphous excipients (PGS and spray-dried lactose) are shown in Table 7. The data reveal that presence of sacrificial excipients absorbs the moisture in preference to the amorphous drug, thereby stabilizing the solid dispersion during storage. The improved stability of amorphous ITR in the presence of sacrificial excipient could be explained on the basis of a combination of several effects: (a) elevation of  $T_g$ ;

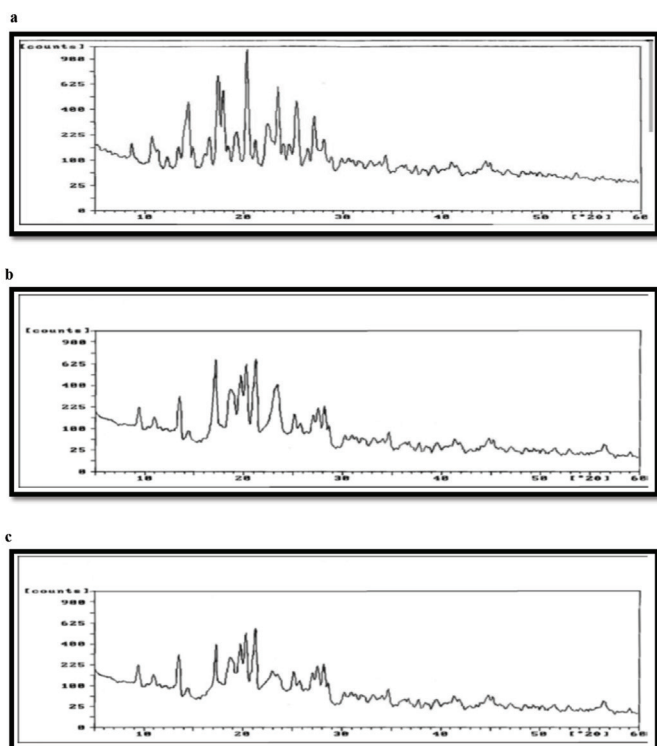


**Figure 5.** X-ray diffraction patterns of a) untreated itraconazole, b) itraconazole solid dispersion, c) itraconazole solid dispersion after 90-day stability study

**Table 6.** RMSE of DoE and ANN

Response	RMSE (DoE)-EXCEL	RMSE (ANN)
1 ( $t_{30}$ )	5.084	0.070
2 ( $t_{60}$ )	10.649	$1.972 \times 10^{-25}$
3 ( $t_{120}$ )	15.984	0.017

RMSE: Root mean square of error, DoE: Design of experiments, ANN: Artificial neural network

**Table 5.** RMSE values and number of epochs for each response variable

Function/parameter	$Y_1$ response		$Y_2$ response		$Y_3$ response	
	RMSE	No. of epochs	RMSE	No. of epochs	RMSE	No. of epochs
TanhAxon	0.070	18	$1.972 \times 10^{-25}$	18	0.017	15
SigmoidAxon	0.695	311	0.713	155	0.725	285
LinearTanAxon	0.0707	19	0.070	25	0.031	19
LinearSigmoidAxon	0.827	57	0.828	1000	0.759	896
BiasAxon	0.262	6	0.244	7	0.223	5
LinearAxon	0.262	4	0.244	5	0.223	6
Axon	0.275	4	0.256	4	0.225	6

RMSE: Root mean square of error

**Table 7. Water uptake study at 75% RH**

Formulation	With packaging system	Without packaging system	Conclusion
SD without sacrificial excipients	30±0.23	36±0.12	Expected conversion of amorphous to crystalline material is more
SD + sacrificial excipients (PGS and spray-dried lactose)	8±0.25	17±0.34	Expected conversion of amorphous to crystalline material is less
PGS	15±0.15	18±0.32	Higher % of moisture uptake
Spray-dried lactose	6±0.35	10±0.25	Higher % of moisture uptake

**Table 8. Stability study in presence and absence of sacrificial excipient**

Formulations	Time (days)	Parameter at (40±2°C/75±5% RH)	
		Drug content	% CDR
Absence of sacrificial excipient	0	101.6±0.23	92.88±0.11
	30	100.4±0.11	92.22±0.21
	60	98.48±0.23	90.86±0.13
	90	98.08±0.39	80.32±0.22
Presence of sacrificial excipient	0	101.91±0.12	92.96±0.06
	30	100.2±0.17	92.12±0.11
	60	99.81±0.13	92.16±0.16
	90	99.15±0.23	91.96±0.11

(b) hydrogen bonding between the drug and the polymer; (c) antiplasticizing effect of the polymers.<sup>15</sup> Therefore, it can be concluded that the sacrificial excipients could be useful to prevent devitrification of an amorphous drug by decreasing the plasticizing effect of adsorbed water.

#### Stability studies

The effect of aging on the performance of amorphous ITR was investigated by performing an accelerated dissolution stability study of the optimized formulation over 3 months (40°C/75% RH). The results of the evaluation are shown in Table 8.

The solid dispersion containing only plasticizer, i.e., HPMC E5 and Poloxamer 188, showed less drug release (80.32% after 3 months), whereas the solid dispersion with sacrificial excipients, i.e., PGS and spray-dried lactose, showed 91% drug release after 3 months, which is comparable to its dissolution profile at the time of its manufacture. From the study, it can be inferred that if the formulation is exposed to high humidity the spray-dried lactose and PGS may absorb moisture and therefore less moisture (or no moisture) will be available to the drug. Therefore, the possibility of conversion of drug from amorphous form to crystalline form may be reduced. Thus, it can be concluded that sacrificial excipients play a major role in keeping the drug in amorphous form.<sup>16,17</sup>

## CONCLUSIONS

The results of the present study indicate that the dissolution rate of ITR can be significantly enhanced from its solid dispersion with HPMC E5 and pregelatinized starch. ITR solid dispersion

prepared by kneading method showed higher dissolution than the untreated drug. Moreover, the presence of sacrificial excipients like pregelatinized starch and spray-dried lactose in the solid dispersion aided in maintaining the amorphous state of the drug and preventing devitrification during storage, by self-absorption of moisture in place of the drug. As moisture is one of the main reasons for conversion of an amorphous form to crystalline form of a drug during storage, a smart choice of excipients can help in maintaining the drug in amorphous state during long-term storage. The innovative use of pregelatinized starch and spray-dried lactose as sacrificial excipients has not been reported in the literature.

*Conflict of Interest:* No conflict of interest was declared by the authors.

## REFERENCES

- Kansara H, Panola R, Mishra A. Techniques used to Enhance Bioavailability of BCS Class II Drugs: A Review. *Int J Drug Dev Res.* 2015;7:82-93.
- Vemula VR, Lagishetty V, Lingala S. Solubility enhancement techniques. *Int J Pharm Sci Rev Res.* 2010;5:41-51.
- Hart ML, Do DP, Ansari RA, Rizvi AA. Brief Overview of Various Approaches to Enhance Drug Solubility. *J Dev Drugs.* 2013;2:1-7.
- Ambike AA, Mahadik KR, Paradkar A. Stability study of amorphous valdecoxib. *Int J Pharm.* 2014;282:151-162.
- Shirakura T. Fractional factorial designs of two and three levels. *Discrete Math.* 1993;116:99-135.

6. Priyanka W, Sonali BM. Research Paper on Basic of Artificial Neural Network. IJRITCC. 2014;2:96-100.
7. Patel B, Suhagia B, Patel D. Artificial neural network as a tool for Quality by Design in formulation development of solid. Bull Pharm Res. 2015;5:2249-2255.
8. Segale L, Giovannelli L, Mannina P. Formulation and characterization study of itraconazole-loaded microparticles. Pharm Dev Technol. 2015;20:153-158.
9. Meng F, Gala U, Chauhan H. Classification of solid dispersions: correlation to (i) stability and solubility (ii) preparation and characterization techniques. Drug Dev Ind Pharm. 2015;41:1401-1415.
10. United States Pharmacopeia and National Formulary USP 30-NF 25. The United States Pharmacopeial Convention, Inc.: Rockville, MD, 2007:3179-3180.
11. Zhang L, Chai G, Zeng X, He H, Xu H, Tang X. Preparation of fenofibrate immediate-release tablets involving wet grinding for improved bioavailability. Drug Dev Ind Pharm. 2010;36:1054-1063.
12. Zhang L, Chai G, Zeng X, He H, Xu H, Tang X. Preparation of a solid dispersion of felodipine using a solvent wetting method. Eur J Pharm Biopharm. 2010;36:1054-1063.
13. Furquan A, Sonali J. Improvement of dissolution rate of aceclofenac by solid dispersion technique. Powder Technol. 2011; 207:47-54.
14. Mahesh K, Kataria AB. Solubility and dissolution rate enhancement of itraconazole by solid dispersion technique. Indo Am J Pharm Res. 2014;4:849-863.
15. Jondhale S, Bhise S, Pore Y. Physicochemical Investigations and Stability Studies of Amorphous Gliclazide. AAPS PharmSciTech. 2012;13:448-459.
16. Bronlund J, Paterson T. Moisture sorption isotherms for crystalline, amorphous and predominantly crystalline lactose powders. Int Dairy J. 2004;14:247-254.
17. Dalton CR, Hancock BC. Processing and storage effects on water vapor sorption by some model pharmaceutical solid dosage formulations. Int J Pharm. 1977;156:143-151.





# Essential Oil and Fatty Acid Composition of Endemic *Gypsophila laricina* Schreb. from Turkey

## Türkiye’de Yetişen Endemik *Gypsophila laricina* Schreb. Türünün Uçucu Yağ ve Yağ Asidi Bileşimi

© Hüseyin SERVİ<sup>1\*</sup>, © Betül EREN KESKİN<sup>2</sup>, © Sezgin ÇELİK<sup>3</sup>, © Ümit BUDAK<sup>4</sup>, © Büşra KABABIYIK<sup>3</sup>

<sup>1</sup>Altınbaş University, Faculty of Pharmacy, Department of Pharmaceutical Botany, İstanbul, Turkey

<sup>2</sup>Üsküdar University, Faculty of Engineering and Natural Sciences, Department of Molecular Biology and Genetics, İstanbul, Turkey

<sup>3</sup>Yıldız Technical University, Faculty of Arts and Science, Department of Molecular Biology and Genetics, İstanbul, Turkey

<sup>4</sup>Bozok University, Faculty of Arts and Science, Department of Biology, Yozgat, Turkey

### ABSTRACT

**Objectives:** *Gypsophila* species have very high medicinal and commercial importance and contain interesting natural substances. However, there is no report on the essential oil or fatty acid composition of any *Gypsophila* species. This prompted us to investigate the essential oil and fatty acid composition of *Gypsophila laricina* Schreb.

**Materials and Methods:** Plant materials were collected during the flowering period. The essential oil composition of the aerial parts of *G. laricina* Schreb. was analyzed by gas chromatography and gas chromatography-mass spectrometry. The fatty acid compositions were analyzed by gas chromatography-mass spectrometry.

**Results:** Sixty-six and ten compounds were identified in the essential oil and fatty acid of *G. laricina* Schreb., respectively. The major components of the essential oil were hexadecanoic acid (27.03%) and hentriacontane (12.63%). The main compounds of the fatty acid were (Z,Z)-9,12-octadecadienoic acid methyl ester (18:2) 40.4%, (Z)-9-octadecenoic acid methyl ester (18:1) 35.0%, and hexadecanoic acid methyl ester (16:0) 13.0%.

**Conclusion:** The results showed that the fatty acid composition is rich in polyunsaturated fatty acids. The essential oils of *G. laricina* Schreb. were dominated by fatty acid derivatives and *n*-alkanes. We think the results obtained from this research will stimulate further research on the chemistry of *Gypsophila* species.

**Key words:** *Gypsophila laricina*, essential oil, fatty acid

### ÖZ

**Amaç:** *Gypsophila* türleri, tıbbi ve ticari açıdan çok önemlidirler ve ilginç doğal maddeler içerirler. Bununla birlikte, literatürde *Gypsophila* türlerinin uçucu yağ ve yağ asidi bileşimi hakkında herhangi bir çalışma bulunmamaktadır. Bu nedenle *Gypsophila laricina* Schreb.’nin uçucu yağ ve yağ asidi bileşiminin araştırılmasına karar verilmiştir.

**Gereç ve Yöntemler:** Bitki materyali çiçeklenme döneminde toplanılmıştır. *G. laricina* Schreb. türünün toprak üstü kısmının uçucu yağ bileşimleri gaz kromatografi ve gaz kromatografi-kütle spektrometresi aracılığıyla analiz edilmiştir. Yağ asit bileşimleri gaz kromatografi-kütle spektrometresi aracılığıyla analiz edilmiştir.

**Bulgular:** *G. laricina* Schreb. uçucu yağlarında altmış altı bileşik ve yağ asitlerinde on bileşik tespit edilmiştir. Uçucu yağın ana bileşenleri heksadekanoik asit (%27.03) ve hentriakontan (%12.63) olarak belirlenmiştir. Yağ asidinin ana bileşenleri ise (Z,Z)-9,12-oktadekadienoik asit metil ester (18:2) %40.4, (Z)-9-oktadesenoik asit metil ester (18:1) %35.0 ve heksadekanoik asit metil ester (16:0) %13.0 olarak tespit edilmiştir.

**Sonuç:** Bitki yağ asidi bileşiminin çoklu doymamış yağ asitleri bakımından zengin olduğu saptanmıştır. Bitki uçucu yağının yüksek oranda *n*-alkan ve yağ aside türevleri içerdiği belirlenmiştir. Bu araştırmadan elde edilen sonuçların, *Gypsophila* türlerinin kimyası üzerine yapılacak daha ileri araştırmalara katkı sağlayacağı düşünülmektedir.

**Anahtar kelimeler:** *Gypsophila laricina*, uçucu yağ, yağ asidi

\*Correspondence: E-mail: huseyin.servi@altinbas.edu.tr, Phone: +90 543 649 54 13 ORCID-ID: orcid.org/0000-0002-4683-855X

Received: 30.01.2018, Accepted: 19.04.2018

©Turk J Pharm Sci, Published by Galenos Publishing House.

## INTRODUCTION

The family Caryophyllaceae has about 85 genera and 2630 species worldwide and is distributed mainly in Mediterranean and Irano-Turanian areas.<sup>1</sup> *Gypsophila* is the third biggest genus in the family Caryophyllaceae in Turkey. *Gypsophila* species are annual, biennial, or perennial herbaceous plants. Stem length of the plant is about 1 m and its flowering time is June and July.<sup>2</sup>

Some *Gypsophila* species are used in folk medicine as remedies for coughs, colds, and ailments of the upper respiratory tract<sup>3</sup> and also used for medical treatment such as an expectorant and diuretic, and for hepatitis, gastritis, and bronchitis.<sup>4</sup> The underground parts of the genus *Gypsophila* have triterpenoid saponins as a main component. *Gypsophila* species are used in industrial, medicinal, and decorative applications.<sup>5</sup> The commercial Merck saponin, which has been widely utilized as a standard for hemolytic tests, was obtained from the roots of several *Gypsophila* species.<sup>3</sup> The genus was reported to have cytotoxic activity,  $\alpha$ -glucosidase activity, an immunomodulating effect, and cause normalization of carcinogen-induced cell proliferation.<sup>4,6</sup> The saponins obtained from the genus *Gypsophila* are interesting in terms of their applications in vaccines.<sup>7</sup> The biological activities of the genus seem to be associated with triterpene saponins. Due to the various beneficial biological activities, *Gypsophila* was the focus of studies that described the phytochemistry of the genus extensively.

Previously, antioxidant and antibacterial activities of chloroform extracts of the underground parts of *Gypsophila eriocalyx* and *Gypsophila sphaerocephala* var. *sphaerocephala* were investigated. The chloroform extracts of both species had high antioxidant properties but showed low antibacterial activity.<sup>8</sup>

Additionally, the toxic boron levels of some plant species (*G. sphaerocephala* var. *sphaerocephala*, *Gypsophila perfoliata*, *Puccinellia distans* subsp. *distans*, and *Elymus elongates*) were reported. Among these plant species, *G. sphaerocephala* contained considerably higher boron concentrations in its above-ground parts compared to the roots and organs of the other species. That study shows that *G. sphaerocephala* was not only able to grow on heavily boron contaminated soils, but was also able to accumulate extraordinarily high concentrations of boron.<sup>9</sup>

In a study from Iran, the antimicrobial activity and chemical constituents of the essential oils from the flower, leaf, and stem of *Gypsophila bicolor* were investigated. The main components of the essential oil from the flower were germacrene-D (21.2%), *p*-cymene (20.6%), bicyclogermacrene (17.6%),  $\gamma$ -dodecadienolactone (13.7%), and terpinolene (9.4%). The main components of the essential oil from the leaf were germacrene-D (23.4%), terpinolene (14.5%), bicyclogermacrene (7.5%),  $\gamma$ -dodecadienolactone (6.8%), *p*-cymene (6.7%), and *cis*- $\beta$ -ocimene (6.3%). The main components of the essential oil from the stem were  $\gamma$ -dodecadienolactone (28.5%), bicyclogermacrene (14.8%), germacrene-D (12.6%), *p*-cymene (12.5%), terpinolene (11.6%), and *trans*- $\beta$ -ocimene (4.2%). The essential oils had a moderate effect on gram-positive and gram-negative bacteria, but had a significant effect on fungi.<sup>10</sup>

In another study from Turkey, the essential oil composition and fatty acid profile of *Gypsophila tuberculosa* and *G. eriocalyx* were reported. The main components of the essential oils were hexadecanoic acid (25.3%) and hentriacontane (13.0%) for *G. tuberculosa* and octacosane (6.83%), eicosanal (6.19%), triacontane (6.03%), and heneicosane (5.78%) for *G. eriocalyx*. The major compounds of the fatty acids of *G. tuberculosa* and *G. eriocalyx* were (*Z*)-9-octadecenoic acid methyl ester (42.0% and 36.0% respectively), (*Z,Z*)-9,12-octadecadienoic acid methyl ester (19.6% and 10.5% respectively), and hexadecanoic acid methyl ester (17.7% and 25.2% respectively).<sup>11</sup>

As summarized above, *Gypsophila* species have very high medicinal and commercial importance and contain interesting natural substances. However, during our literature survey we did not encounter any reports on the essential oil or fatty acid composition of *Gypsophila laricina* Schreb. This prompted us to investigate the essential oil and fatty acid composition of this species. Here we report for the first time on the essential oil composition and fatty acid profile of *G. laricina* Schreb.

## EXPERIMENTAL

### Plant materials

The plant materials were collected during the flowering period; *G. laricina* Schreb. was collected from 1740-1800 m altitude in Üçpınar, Şarkışla, Sivas, Turkey, in July 2015 by Çelik and Budak. The voucher specimen has been deposited in the Herbarium of Bozok University (Voucher no. Bozok HB 3302).

### Fatty acid analyses

The aerial parts of the collected specimen were dried separately in the shade and ground with an electric mill (Retsch SM 100). The aerial parts of the plant (400 g) were extracted with hexane for 3 days at room temperature. After filtration through filter paper, the extract was concentrated by rotary evaporator and 4 g of crude hexane extract was obtained from the aerial parts. The crude extract was stored at 4°C. In the present study we used hexane extract for fatty acid compositions. Methyl-ester derivatives of fatty acids found in the hexane extract were obtained by transesterification.<sup>12</sup> In this method 1 g of dried extract was dissolved in 5 mL of hexane and then extracted with 2 M methanolic KOH at room temperature. The mixture was shaken for 2 min and left to stand for 10 min. The upper phases were removed. *G. laricina* Schreb. afforded fixed oil from the hexane extract in 0.07% (v/w) yields. The fixed oil was analyzed by gas chromatography-mass spectrometry (GC-MS).

### Essential oil analyses

The aerial parts (200 g) of the air-dried plants were subjected to hydrodistillation for 3 h using a Clevenger-type apparatus to produce essential oils. The condenser of the apparatus was attached to a microchiller set to 4°C. *G. laricina* Schreb. afforded oils from the aerial parts in 0.01% (v/w) yields. The oils were recovered with 1 mL of *n*-hexane and preserved in amber vials at -20°C until the day they were analyzed.

### GC-MS for fatty acids

The fatty acid compositions of the hexane extracts were investigated by means of GC-MS. The fatty acid methyl esters were analyzed using an Agilent 5975C GC-MSD system with an Innowax FSC polar column (30 m×0.25 mm, 0.25 μm). The inlet temperature was set at 250°C. Helium was the carrier gas at a constant flow rate of 1 mL/min. Split ratio was set to 50:1. The oven temperature was programmed from 40°C to 210°C at the rate of 5°C/min and kept constant at 210°C for 10 min. EI/MS was taken at 70 eV ionization energy. Mass range was  $m/z$  35–450 atomic mass unit. Relative percentage amounts of the separated compounds were calculated from integration of the peaks in the MS chromatograms. The identification of fatty acid components was carried out by comparison of their retention indices obtained by a series of *n*-alkanes (C5 to C30) to the literature and with mass spectra comparison.<sup>13–19</sup> The mass spectra comparison was done by computer matching with the commercial Wiley 8<sup>th</sup> Ed./NIST 05 Mass Spectra library. The analysis was completed in 50 min.

### GC-MS for essential oils

The GC-MS analysis was performed with an Agilent 5975C GC-MSD system operating in EI mode. Essential oil samples were diluted 1/100 (v/v) with *n*-hexane. Injector and MS transfer line temperatures were set at 250°C. An Innowax FSC column (60 m×0.25 mm, 0.25 μm film thickness) and helium as carrier gas (1 mL/min) were used in both GC/MS analyses. Splitless injection was employed. The oven temperature was programmed to 60°C for 10 min and raised to 220°C at the rate of 4°C/min. The temperature was kept constant at 220°C for 10 min and then raised to 240°C at the rate of 1°C/min. The mass spectra were recorded at 70 eV with the mass range  $m/z$  35 to 425.

### GC for essential oils

The GC analyses were done with an Agilent 6890N GC system. FID detector temperature was set to 300°C and the same operational conditions were applied to a duplicate of the same column used in the GC-MS analyses. Simultaneous autoinjection was used to obtain the same retention times. The relative percentage amounts of the separated compounds were calculated from integration of the peaks in the FID chromatograms. The identification of the essential oil components was carried out by comparison of their relative retention indices obtained by series of *n*-alkanes (C5 to C30) to the literature and with mass spectra comparison.<sup>20–40</sup> The mass spectra comparison was done by computer matching with the commercial Wiley 8<sup>th</sup> Ed./NIST 05 Mass Spectra library, Adams Essential Oil Mass Spectral Library, and Pallsade 600K Complete Mass Spectra Library.

## RESULTS AND DISCUSSION

The fatty acid composition of *G. laricina* Schreb. was analyzed by GC-MS. Ten compounds were identified in the fatty acid, making up 98.9% of the fatty acid. The extract consisted of six saturated fatty acids (21.8%) and four unsaturated fatty acids (77.2%). The major components of the fatty acid were (Z,Z)-9,12-octadecadienoic acid methyl ester (linoleic acid) (18:2)

40.4%, (Z)-9-octadecenoic acid methyl ester (oleic acid) (18:1) 35.0%, and hexadecanoic acid methyl ester (palmitic acid) (16:0) 13.0%. The fatty acid composition of *G. laricina* Schreb. is represented in Table 1.

The essential oil composition of *G. laricina* Schreb. was analyzed by GC and GC-MS. The essential oils of the aerial parts of *G. laricina* Schreb. afforded very low oil yields (0.03% (v/w) yield). Sixty-six compounds were identified in the essential oil of *G. laricina* Schreb. by GC, representing 76.0% of the oil. The major components of the oil were hexadecanoic acid (27.03%) and hentriacontane (12.63%). The essential oil composition of *G. laricina* Schreb. is given in Table 2.

The essential oil composition of *G. laricina* showed similar chemical behavior to *G. tuberculosa*.<sup>11</sup> Both species had hexadecanoic acid and hentriacontane as major components in their essential oils. However, hexadecanoic acid was contained at 4.64% levels in *G. eriocalyx* and nearly six times that amount in *G. tuberculosa* and *G. laricina*. Moreover, hentriacontane

**Table 1. The fatty acid composition of *Gypsophila laricina* Schreb.**

RI	Compound	Mean (%)**	Identification method***
1299	Dodecanoic Acid ME (Lauric acid)	0.3	RI, MS
1499	Tetradecanoic Acid ME (Myristic acid)	1.2	RI, MS
1678	(Z)-9-Hexadecenoic Acid ME* (Palmitoleic acid)	0.6	RI, MS
1699	Hexadecanoic Acid ME (Palmitic acid)	13.0	RI, MS
1867	(Z,Z)-9,12-Octadecadienoic Acid ME* (Linoleic acid)	40.4	RI, MS
1873	(Z)-9-Octadecenoic Acid ME* (Oleic acid)	35.0	RI, MS
1899	Octadecanoic Acid ME (Stearic acid)	2.3	RI, MS
1984	(Z)-11-Eicosenoic Acid ME (Gondoic acid)	1.2	RI, MS
1999	Eicosanoic Acid ME (Arachidic acid)	3.4	RI, MS
2299	Docosanoic Acid ME (Behenic acid)	1.5	RI, MS
<b>Total saturated acid</b>		<b>21.8</b>	
<b>Total unsaturated acid</b>		<b>77.2</b>	
<b>Total</b>		<b>98.9</b>	
<b>Unsaturated/saturated</b>		<b>3.6</b>	

ME: Methyl ester, MS: Mass spectrometry, RI: Retention index

\*Fatty acids with cis (Z) configuration, \*\*The results of the analysis,

\*\*\*Identification method: RI: identification based on the retention times of genuine compounds on the HP Innowax column and the literature data; MS: identification based on MS comparison with the database or the literature data.

Table 2. The essential oil composition of *Gypsophila laricina* Schreb.

No	RRI'	RRI literature''	Compound	Mean (%)****	Identification method****	Literature
1	1233	1244	2-pentyl furan	0.27	RI, MS	20
2	1397	1399	Nonanal	0.29	RI, MS	20
3	1400	1400	Tetradecane	0.16	RI, MS, Ac	
4	1442	1443	Dimethyl-tetradecane	0.06	RI, MS	27
5	1499	1505	Dihydroedulan II	0.15	RI, MS	27
6	1502	1500	Pentadecane	0.15	RI, MS, Ac	
7	1504	1505	Decanal	0.47	RI, MS	28
8	1510	1516	Theaspirane B	0.7	RI, MS	28
9	1525	1532	Camphor	0.04	RI, MS	22
10	1529	1535	Dihydroedulan I	0.14	RI, MS	28
11	1543	1548	( <i>E</i> )-2-nonenal	0.12	RI, MS	28
12	1549	1553	Theaspirane A	0.64	RI, MS	27
13	1558	1549	1-Tetradecene	0.08	RI, MS	28
14	1602	1600	Hexadecane	0.29	RI, MS, Ac	
15	1632	1638	$\beta$ -cyclocitral	0.13	RI, MS	28
16	1635	1644	Thujopsene	0.04	RI, MS	32
17	1652	1655	( <i>E</i> )-2-decanal	0.25	RI, MS	28
18	1660	1664	Nonanol	0.1	RI, MS	28
19	1693	1685	6,10-dimethyl-2-undecanone	0.1	RI, MS	39
20	1702	1700	Heptadecane	0.28	RI, MS, Ac	
21	1717	1722	Dodecanal	0.29	RI, MS	28
22	1761	1763	Naphthalene	0.32	RI, MS	28
23	1775	1779	( <i>E,Z</i> )-2,4-Decadienal	0.13	RI, MS	28
24	1804	1779	Octadecane	0.21	RI, MS, Ac	
25	1824	1827	( <i>E,E</i> )-2,4-decadienal	0.4	RI, MS	28
26	1831	1823	( <i>E</i> )- $\alpha$ -Damascenone	0.2	RI, MS	20
27	1836	1838	( <i>E</i> )- $\beta$ -Damascenone	0.36	RI, MS	28
28	1865	1864	( <i>E</i> )-Geranyl acetone	1.12	RI, MS	28
29	1879	1871	Undecanol	0.17	RI, MS	33
30	1886	1864	<i>p</i> -Cymene-8-ol	0.08	RI, MS	28
31	1931	1933	Tetradecanal	0.38	RI, MS	28
32	1953	1958	( <i>E</i> )- $\beta$ -Ionone	1.03	RI, MS	28
33	1968	1973	Dodecanol	0.63	RI, MS	28
34	2002	2000	Eicosane	0.29	RI, MS, Ac	
35	2005	2007	Caryophyllene oxide	0.29	RI, MS	23
36	2037	2036	Pentadecanal	0.26	RI, MS	21
37	2043	2050	( <i>E</i> )-Nerolidol	0.05	RI, MS	24
38	2051	2056	13-Tetradecanolide	0.35	RI, MS	37

Table 2. Continued

No	RRI*	RRI literature**	Compound	Mean (%)****	Identification method*****	Literature
39	2135	2131	Hexahydro farnesyl acetone	1.65	RI, MS	21
40	2138	2142	Spathulenol	0.05	RI, MS	20
41	2145	2136	Hexadecanal	0.3	RI, MS	27
42	2170	2192	Nonanoic acid	0.5	RI, MS	22
43	2276	2282	Decanoic acid	1.03	RI, MS	20
44	2304	2300	Tricosane	0.55	RI, MS, Ac	
45	2315	2315	2,4-bis( <i>tert</i> -butyl)phenol	0.35	RI, MS	40
46	2354	2353	Octadecanal	0.28	RI, MS	36
47	2382	2384	Farnesyl acetone	1.41	RI, MS	20
48	2407	2400	Tetracosane	0.31	RI, MS, Ac	
49	2448	2471	Nonadecanal	0.2	RI, MS	30
50	2488	2492	Dodecanoic acid	3.51	RI, MS	20
51	2508	2500	Pentacosane	1.4	RI, MS, Ac	
52	2585	2582	Eicosanal	2.07	RI, MS	30
53	2590	2617	Tridecanoic acid	0.23	RI, MS	28
54	2606	2600	Hexacosane	0.31	RI, MS, Ac	
55	2615	2614	Phytol	1.76	RI, MS	20
56	2671	2676	Heneicosanal	1.97	RI, MS	30
57	2701	2704	Tetradecanoic acid	4.7	RI, MS	21
58	2708	2700	Heptacosane	0.7	RI, MS, Ac	
59	2775	2783	1-Docosanol	0.31	RI, MS	30
60	2795	2800	Octacosane	0.25	RI, MS, Ac	
61	2803	2809	Pentadecanoic acid	1.4	RI, MS	20
62	2838	2857	Palmito- $\gamma$ -lactone	0.21	RI, MS	37
63	2921	2931	Hexadecanoic acid	27.03	RI, MS	25
64	2982	2990	Docosanal	0.22	RI, MS	30
65	3108	3100	Hentriacontane	12.63	RI, MS, Ac	
<b>Total</b>				<b>76.0</b>		

MS: Mass spectrometry, RRI: Relative retention index, FID: Flame ionization detector, Ac: According

In addition to the above data, diisobutyl phthalate is a common plasticizer contaminant and it was detected as a considerable component (2.15%) for *G. laricina* Schreb. \*RRI (FID): Relative retention time indices calculated against n-alkanes (C5-C30) in FID chromatograms, \*\*RRI literature: Relative retention time given in the literature for the compound in similar columns and analysis conditions, \*\*\*The result of the analysis in FID chromatograms, \*\*\*\*Identification method: RI: identification based on the RRI of genuine compounds on the HP Innowax column and the literature data; MS: identification based on MS comparison with the database or the literature data, Ac: Identification is done according to RRI and MS values of the authentic compounds

was contained in very low amounts in *G. eriocalyx*.<sup>11</sup> The three *Gypsophila* species had linoleic acid, oleic acid, and palmitic acid as the main components in different percentages.

According to a study from Iran, *G. bicolor* contained germacrene-D, *p*-cymene, bicyclogermacrene,  $\gamma$ -dodecadienolactone, terpinolene, *cis*- $\beta$ -ocimene, and *trans*- $\beta$ -ocimene;<sup>10</sup> however, these compounds were not detected in the oil of *G. laricina* Schreb. *G. laricina* Schreb. showed very different chemical behavior from *G. bicolor*. These differences in the previous

literature and the present data could be related to different collection times, climatic and soil conditions, ecological factors, methods and instruments employed in the analysis, or different genotypes. There are very few reports on the essential oil or volatile composition of *Gypsophila* species and therefore it is difficult to comment on the chemo-systematic position of this species according to the current findings and the existing reports.

## CONCLUSIONS

The essential oil composition and fatty acid profile of *G. laricina* Schreb. were investigated for the first time. The major fatty acid components were oleic acid, linoleic acid, and palmitic acid. The unsaturated fatty acids were higher in content than the saturated fatty acids. The essential oils of *G. laricina* Schreb. were dominated by fatty acid derivatives and *n*-alkanes. Hexadecanoic acid and hentriacontane were the major essential oil components. The high hexadecanoic acid content might be explained by the collection time of the plant materials in the late flowering period. *G. laricina* exhibited important differences from *G. bicolor* and *G. eriocalyx*, highlighting the existence of different main chemical constituents. Thus, the results of this study certainly contributed to the taxonomy of the genus *Gypsophila* via essential oil chemistry. We think the results obtained from this research will stimulate further research on the chemistry of *Gypsophila* species.

## ACKNOWLEDGEMENTS

We are indebted to YTÜ BAP 2015-01-07-KAP05 and TÜBİTAK (project no. TBAG-111T820) for the financial support.

*Conflict of Interest: No conflict of interest was declared by the authors.*

## REFERENCES

- Mabberley DJ. Mabberley's plant-book: a portable dictionary of plants, their classifications, and uses (3th ed). Cambridge; Cambridge University Press; 2008:1-50.
- Davis PH, Mill RR, Tan K, Edmondson JR. Flora of Turkey and the East Aegean Islands (2nd ed). Edinburgh; University Press; 1982:2:149-180.
- Elbandy M, Miyamoto T, Lacaille-Dubois MA. Sulfated lupane triterpene derivatives and a flavone C-glycoside from *Gypsophila repens*. Chem Pharm Bull. 2007;55:808-811.
- Yücekutlu AN, Bildacı I. Determination of Plant Saponins and Some of *Gypsophila* Species: A review of the literature. Hacettepe J Biol Chem. 2008;36:129-135.
- Krasteva IN, Popov IS, Balabanova VI, Nikolov SD, Pencheva IP. Phytochemical study of *Gypsophila trichotoma* wend (Caryophyllaceae). Quim Nova. 2008;31:1125-1126
- Xie LX, Zhang HC, Wang HY, Wang Y, Wang FL, Sun JY. Two new triterpenoids from *Gypsophila oldhamiana*. Nat Prod Res. 2016;30:1068-1074.
- Gevrenova R, Stancheva T, Voynikov Y, Laurain-Mattar D, Henry M. Root *in vitro* cultures of six *Gypsophila* species and their saponin contents. Enzyme Microb Tech. 2010;47:97-104.
- Çona IG. *Gypsophila eriocalyx* Boiss. ve *G. sphaerocephala* Fenzl ex tchihat var. sphaerocephala taksonlarının antioksidan ve antibakteriyel aktivitelerinin belirlenmesi. Master thesis. Pamukkale University. 2012.
- Babaoglu M, Gezgin S, Topal A, Sade B, Dural H. *Gypsophila sphaerocephala* Fenzl ex Tchihat.: a boron hyperaccumulator plant species that may phytoremediate soils with toxic B levels. Turk J Bot. 2004;28:273-278.
- Shafagha A, Shafaghatlonbar M. Antimicrobial activity and chemical constituents of the essential oils from flower, leaf and stem of *Gypsophila bicolor* from Iran. Nat Prod Commun. 2011;6:275-276.
- Servi H, Keskin BE, Celik S, Budak U, Kirmızıtaş FC, Bektas EB. Essential oil composition and fatty acid profile of two endemic *Gypsophila* species from Turkey. Am J Essent Oil Nat Prod. 2017;5:16-20
- Paquo TC. Standard Methods for the Analysis of Oils, Fats and Derivatives (6th ed). Oxford;Pergamon Press; 2013;16:1-188.
- Eyol PC, Sarikahya NB, Karakoc OC, Gokce A, Demirci F, Kirmizigul S, Goren N. Fatty Acid Composition and Biological Activities of *Tanacetum zahlbruckneri* (Náb.) Grierson Growing in Turkey. Rec Nat Prod. 2017;11:401-405.
- Kirmizigul S, Sarikahya NB, Sümbül H, Arda N. Essential fatty acid components and antioxidant activities of eight *Cephalaria* species from southwestern Anatolia. Pure Appl Chem. 2007;79:2297-2304.
- Maltas E, Vural CH, Yildiz S. Antioxidant activity and fatty acid composition of *Ginkgo biloba* from Turkey. Pure Appl Chem. 2011;35:803-818.
- Laribi B, Kouki K, Mougou A, Marzouk B. Fatty acid and essential oil composition of three *Tunisian caraway* (*Carum carvi* L.) seed ecotypes. J Sci Food Agr. 2010;90:391-396.
- Denis C, Wielgosz-Collin G, Bretéché A, Ruiz N, Rabesaotra V, Boury-Esnault N, Kornprobst JM, Barnathan G. New 17-Methyl-13-Octadecenoic and 3,16-Docosadienoic Acids from the Sponge *Polymastia penicillus*. Lipids. 2009;44:655-663.
- Tsevegsuren N, Fujimoto K, Christie WW, Endo Y. Occurrence of a Novel *cis,cis,cis*-Octadeca-3,9,12-trienoic (*Z,Z,Z*-octadeca-3,9,12,trienoic) Acid in *Chrysanthemum* (*Tanacetum*) *zawadskii* Herb. (*Compositae*) Seed Oil Lipids. 2003;38:573-578.
- Nickavar B, Mojab F, Javidnia K, Amoli MA. Chemical Composition of the Fixed and Volatile Oils of *Nigella sativa* L. from Iran Z Naturforsch C. 2003;58:629-631.
- Polatoğlu K, Şen A, Bulut G, Bitiş L, Gören N. Essential Oil Composition of *Centaurea stenolepis* Kerner. from Turkey. J Essent Oil Bear Pl. 2014;17:1268-1278.
- Polatoğlu K, Arsal S, Demirci B, Başer KH. DPPH Scavenging, PRAP Activities and Essential Oil Composition of Edible *Lathyrus ochrus* L. (Cyprus Vetch, Luvana) from Cyprus. J Oleo Sci. 2015;64:309-314.
- Polatoğlu K, Demirci F, Demirci B, Gören N, Başer KHC. Antibacterial Activity and the Variation of *Tanacetum parthenium* (L.) Schultz Bip. Essential Oils from Turkey. J Oleo Sci. 2010;59:177-184.
- Polatoğlu K, Demirci B, Gören N, Başer KHC. Essential oil composition of *Tanacetum kotschyi* from Turkey. Chem Nat Compd. 2011;47:297-299.
- Polatoğlu K, Gören N, Karakoç ÖC. Phytotoxic, DPPH scavenging, insecticidal activities and essential oil composition of *Achillea vermicularis*, *A. teretifolia* and proposed chemotypes of *A. biebersteinii* (Asteraceae). Ind Crop Prod. 2013;51:35-45.
- Polatoğlu K, Karakoç ÖC, Yücel YY, Demirci B, Gören N, Başer KH. Composition, insecticidal activity and other biological activities of *Tanacetum abrotanifolium* Druce. essential oil. Ind Crop Prod. 2015;71:7-14.
- Polatoğlu K, Demirci B, Demirci F, Gören N, Başer KH. Biological activity and essential oil composition of two new *Tanacetum chiliophyllum* (Fisch. & Mey.) Schultz Bip. var. *chiliophyllum* chemotypes from Turkey. Ind Crop Prod. 2012;39:97-105.
- Sura BE, Demirci B, Demir S, Karaalp C, Başer KH. Composition of the essential oils of *Centaurea aphrodisaea*, *C. polyclada*, *C. athoa*, *C. hyalolepis* and *C. iberica*. J Essent Oil Res. 2013;25:79-84.
- Karamenderes C, Demirci B, Başer KH. Composition of Essential Oils of Ten *Centaurea* L. Taxa from Turkey. J Essent Oil Res. 2008;20:342-349.

29. Demirci B, Başer KH, Yıldız B, Bahçecioglu Z. Composition of the essential oils of six endemic *Salvia* spp. from Turkey. *Flavour Frag J*. 2003;18:116-121.
30. Moronkola DO, Ogunwande IA, Başer KHC, Ozek T Ozek G. Essential Oil Composition of *Gmelina arborea* Roxb., Verbenaceae from Nigeria. *J Essent Oil Res*. 2009;21:264-266.
31. Bassole IHN, Ouattara AS, Nebie R, Ouattara CAT, Kabore ZI, Traore SA. Chemical composition and antibacterial activities of the essential oil of *Lippia chevalieri* and *Lippia multiflora* from Burkina Faso. *Phytochemistry*. 2003;62:209-212.
32. Kose YB, Altintas A, Tugay O, Uysal T, Demirci B, Ertugrul K, Baser KHC. Composition of the Essential Oils of *Centaurea sericeae* Wagenitz and *Centaurea ensiformis* P.H. Davis from Turkey. *Asian J Chem*. 2010;22:7159-7163.
33. Kirimer N, Tabanca N, Özek T, Tümen G, Baser KHC. Essential oils of Annual *Sideritis* Species Growing in Turkey. *Pharm Biol*. 2000;38:106-111.
34. Saidana D, Mahjoub MA, Boussaada O, Chriaa J, Cheraif I, Daami M, Mighri Z, Helal AN. Chemical composition and antimicrobial activity of volatile compounds of *Tamarix boveana* (Tamaricaceae). *Microbiol Res*. 2008;163:445-455.
35. Bardakcı H, Demirci B, Yesilada E, Kirmizipekmez H, Baser KHC. Chemical Composition of the Essential Oil of the Subterranean Parts of *Valeriana alliariifolia*. *Rec Nat Prod*. 2012;6:89-92.
36. Tabanca N, Demirci B, Ozek T, Kirimer N, Baser KHC, Bedir E, Khan IA, Wedge DE. Gas chromatographic-mass spectrometric analysis of essential oils from *Pimpinella* species gathered from Central and Northern Turkey. *J Chromatogr A*. 2006;1117:194-205.
37. Polatoglu K, Demirci F, Demirci B, Gören N, Baser KHC. Antimicrobial activity and Essential oil composition of a new *T. argyrophyllum* (C. Koch) Tuzel. var. *argyrophyllum* chemotype. *J Oleo Sci*. 2010;59:307-313.
38. Dregus M, Engel KH. Volatile constituents of uncooked rhubarb *Rheum rhabarbarum* L. stalks. *J Agric Food Chem*. 2003;51:6530-6536.
39. Miyazawa M, Nagai S, Oshima T. Volatile Components of the Straw of *Oryza sativa* L. *J Oleo Sci*. 2008;57:139-143.
40. Viegas MC, Bassoli DG. Utilização do índice de retenção linear para caracterização de compostos voláteis em café solúvel utilizando GC-MS e coluna HP-Innowax. *Quím Nova*. 2007;30:2031-2034.



# Simultaneous Estimation of Saxagliptin and Dapagliflozin in Human Plasma by Validated High Performance Liquid Chromatography - Ultraviolet Method

## Saksagliptin ve Dapagliflozin Tarafından Doğrulanmış Yüksek Performanslı Sıvı Kromatografi - Ultraviyole Yöntemi İnsan Plazma Eş Zamanlı Tahmin

Sharmila DONEPUDI<sup>1</sup>, Suneetha ACHANTA<sup>2\*</sup>

<sup>1</sup>V.V. Institute of Pharmaceutical Sciences, Department of Pharmaceutical Analysis, Andhra Pradesh, India

<sup>2</sup>Hindu College of Pharmacy, Department of Pharmaceutical Analysis, Andhra Pradesh, India

### ABSTRACT

**Objectives:** The fixed dose combination of saxagliptin and dapagliflozin is a recently approved antidiabetic medication. It is marketed under the brand name Qtern. The aim of this study was to develop a simple, rapid, sensitive, and validated isocratic reversed phase-high performance liquid chromatography (RP-HPLC) method for the simultaneous estimation of saxagliptin and dapagliflozin in human plasma using linagliptin as internal standard as per US-Food and Drug Administration guidelines.

**Materials and Methods:** The method was performed on a Waters 2695 HPLC equipped with a quaternary pump. The analyte separation was achieved using an Eclipse XDB C18 (150 × 4.6 mm × 5 µm) column with a mobile phase consisting of 0.1% ortho phosphoric acid and acetonitrile (50:50) with pH adjusted to 5.0 at 1 mL/min flow rate.

**Results:** The analyte was detected at 254 nm. The retention time of the internal standard, saxagliptin, and dapagliflozin was 2.746, 5.173, and 7.218 min, respectively. The peaks were found to be free of interference. The method was validated over a dynamic linear range of 0.01 to 0.5 µg/mL and 0.05 to 2 µg/mL for saxagliptin and dapagliflozin, respectively, with a correlation coefficient of 0.998. The precision and accuracy of samples of six replicate measurements at lower limits of quantification level were within the limits. The analytes were found to be stable in human plasma at -28°C for 37 days.

**Conclusion:** The stability, sensitivity, specificity, and reproducibility of this method make it appropriate for the determination of saxagliptin and dapagliflozin in human plasma.

**Key words:** Saxagliptin, dapagliflozin, linagliptin, human plasma, isocratic

### ÖZ

**Amaç:** Saksagliptin ve dapagliflozinin sabit doz kombinasyonu antidiyabetik ilaç tedavisi için onaylanmıştır ve Qtern markası ile pazarda yer almaktadır. Bu çalışmada amaç, insan plazmasındaki saksagliptin ve dapagliflozinin eş zamanlı tayini için Avrupa Gıda ve İlaç İdaresi kılavuzlarına uygun şekilde linagliptin iç standardı kullanarak ve basit, hızlı, hassas ve validasyonu yapılmış izokratik ters faz-yüksek performanslı sıvı kromatografi (RP-HPLC) yöntemi geliştirmektir.

**Gereç ve Yöntemler:** Method 4'lü akış pompasına sahip Waters 2695 marka HPLC cihazı ile gerçekleştirilmiştir. Analitin ayrılmasında Eclipse XDB C18 kolon (150 × 4.6 mm × 5 µm) kullanılmıştır. Kullanılan mobil fazın bileşimi ise pH 5.0 ayarlanmış %0.1 orto fosforik asit ve asetonitril (50:50) şeklinde olup akış hızı analiz süresince 1 mL/dk'dır.

**Bulgular:** Analit 254 nm'de tayin edilmiştir. İç standart, saksagliptin ve dapagliflozinin alıkonma zamanları sırasıyla 2.746, 5.173 ve 7.218 dk olarak tespit edilmiştir. Pikler interferanslar gözlenmeden elde edilmiştir. Metot validasyonu saksagliptin ve dapagliflozin için sırasıyla 0.01 ile 0.5 µg/mL ve 0.05 ile 2 µg/mL doğrusal derişim aralığında 0.998 korelasyon katsayısı ile gerçekleştirilmiştir. Numunlere ait 6 ölçüme ait kesinlik ve doğruluk tayin sınırları içerisinde bulunmuştur. Analitlerin insan plazması içinde -28°C sıcaklıkta 37 gün boyunca kararlı halde kaldığı belirlenmiştir.

\*Correspondence: E-mail: drasuneetha@gmail.com, ORCID-ID: orcid.org/0000-0002-9793-7937

Received: 01.04.2018, Accepted: 25.04.2018

©Turk J Pharm Sci, Published by Galenos Publishing House.



**Sonuç:** Bu yöntemle elde edilen kararlılık, duyarlılık, özgüllük ve tekrarlanabilirlik sonuçları, geliştirilen bu yöntemin insan plazmasında saxagliptin ve dapagliflozinin belirlenmesi için uygun olduğunu ortaya koymuştur.

**Anahtar kelimeler:** Saksagliptin, dapagliflozin, linagliptin, insan plazma, izokratik

## INTRODUCTION

The combination of saxagliptin and dapagliflozin has the potential to confer significant benefits in glycaemic control without the risk of weight gain and hypoglycemia, which may be associated with other medications used to treat type 2 diabetes.<sup>1</sup> The fixed dose combination containing 10 mg of dapagliflozin and 5 mg of saxagliptin was recently approved by the US-Food and Drug Administration (FDA) for adults with type-2 diabetes. The combination was available under the brand name Qtern.<sup>2</sup> Dapagliflozin belongs to the sodium glucose co-transporter-2 inhibitors with the chemical name (2*S*,3*R*,4*R*,5*S*,6*R*)-2-[4-chloro-3-(4-ethoxybenzyl)phenyl]-6-(hydroxymethyl) tetrahydro-2*H*-pyran-3,4,5-triol (Figure 1a).<sup>3-6</sup>

Saxagliptin belongs to the class of drugs inhibiting the enzyme dipeptidyl-peptidase-4. This class of compound works by stimulating glucose-dependent insulin release. Chemically, it is (1*S*,3*S*,5*S*)-2-((2*S*)-amino(3-hydroxytricyclo(3.3.1.1<sup>3,7</sup>)dec-1-yl)acetyl)-2-azabicyclo(3.1.0) hexane-3-carbonitrile (Figure 1b) and has the molecular formula C<sub>18</sub>H<sub>25</sub>N<sub>3</sub>O<sub>2</sub>.<sup>7-9</sup> A review of the literature revealed that a few analytical methods like LC-Mass spectrometry,<sup>10,11</sup> HPLC,<sup>12-19</sup> and spectroscopic methods<sup>20,21</sup> are available for the estimation of these drugs, either individually or in combination with other diabetic drugs like metformin.<sup>22-26</sup> The present work aimed to develop a simple, rapid, and accurate method for the estimation of dapagliflozin and saxagliptin in human plasma, as per US-FDA guidelines.<sup>27</sup> Moreover, the present method is the first for the estimation of this combination in a biological matrix.

## MATERIALS AND METHODS

### Reagents and chemicals

The pure drug samples of saxagliptin and dapagliflozin were purchased from Selleckchem.com LLC, supplied by Pro Lab Marketing. HPLC grade acetonitrile, HPLC grade methanol, and all other chemicals were obtained from Merck Chemical Division, Mumbai. HPLC grade water obtained from the Milli-Q water purification system was used throughout the study.

### Instrumentation

Chromatography was performed with a Waters 2695 HPLC provided with a quaternary pump, auto-sampler, column oven, degasser, and 2996 PDA detector and with Empower-2 software.

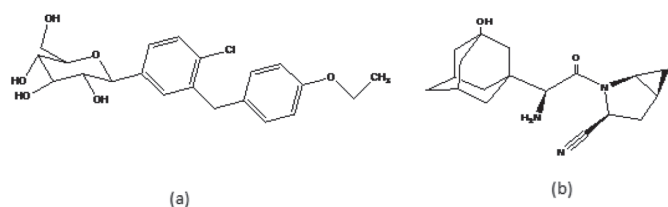


**Figure 1.** Chemical structure of a) dapagliflozin and b) saxagliptin

### Chromatographic conditions

The separation was achieved by isocratic elution using an Eclipse XDB C18 column (150 × 4.6 mm × 5 μm) with a mobile phase consisting of 0.1% orthophosphoric acid and acetonitrile (50:50) with pH adjusted to 4.5. The separation was achieved within 10 min at 254 nm using a 1 mL/min flow rate. The sample dilution was carried out using water:acetonitrile (50:50 ratio) as diluent.

### Preparation of internal standard

The working internal standard was prepared by transferring 10 mg of linagliptin to a 10 mL volumetric flask; the final volume was completed using the diluent. From the resulting stock, 10 μg/mL solution was prepared by further dilutions.

### Preparation of calibration and quality control solutions

The stock solutions of saxagliptin and dapagliflozin were prepared individually by dissolving 10 mg of the drug in 10 mL of diluent to obtain a 1 mg/mL concentration of each analyte. The stock solution was further diluted to prepare working standards. The calibration and quality control samples were obtained by spiking 10 μL of the above-prepared solutions of each analyte into 250 μL of plasma containing 50 μL of the internal standard. This resulted in final concentrations of saxagliptin and dapagliflozin of 0.01 μg/mL to 0.50 μg/mL and 0.05 μg/mL to 2.00 μg/mL, respectively, after spiking them into the plasma.

### Sample preparation and extraction

The standard plasma samples, containing 10 μL of each analyte and 50 μL of internal standard (10 μg/mL), were mixed with 2 mL of acetonitrile. The sample tubes were vortexed for 2 min and were then centrifuged at 3200 rpm for 3 min. The resultant organic layer was used for analysis.

### Method validation

A thorough and complete method validation was performed following the US-FDA guidelines. The method was validated for system suitability, auto-sampler carryover, specificity and screening of the biological matrix, sensitivity, matrix effect, linearity, precision and accuracy, recovery of the analyte and internal standard, ruggedness, reinjection reproducibility, and stability. The stability studies included bench top, freeze-thaw, and long-term stability at -28°C and -80°C.

### Specificity

Specificity of the biological matrix was assessed and screening was performed using six blank standards and lower limit of quantification (LLOQ) level samples. All of the samples were checked to determine the extent of interference by the plasma components with the analyte and internal standard.

### Calibration curve

The linearity of the method was determined by analysis of the standard plots associated with an eight-point standard

calibration curve. Eight concentrations of saxagliptin and dapagliflozin ranging from 0.01 to 0.50  $\mu\text{g/mL}$  and 0.05 to 2.00  $\mu\text{g/mL}$ , respectively, were used, which included the LLOQ, low quality control (LQC), medium quality control (MQC), high quality control (HQC), and upper limit of quantification (ULOQ). The calibration curve was constructed by plotting the peak area ratio of the analytes to the internal standard against standard concentrations. The percentage difference of back-calculated concentrations to the nominal concentration (distribution of the residuals) was determined to validate the correlation. The acceptance criterion for the calibration model applied if residuals were within 15% for all calibration levels except LLOQ. Correlation coefficient, slope, and intercept were determined to evaluate the calibration curve.

#### Accuracy and precision

Intraday precision and accuracy were assessed at the lower, middle, high, and lower limit of quantification quality control samples LQC, MQC, HQC, and LLOQ in six replicates for both of the analytes, while interday precision and accuracy were assessed for three consecutive days by using quality control samples. Mean values were obtained for calculated drug concentration over these batches. The accuracy of the analytical method describes the closeness of the mean test results obtained by the method to the actual value of the analyte and was determined by replicate analysis of the analyte. The accuracy and precision were calculated and expressed in terms of % mean accuracy and coefficient of variation (% CV), respectively.

#### Recovery

Recovery of the analytes from the extraction procedure was performed at LQC, MQC, and HQC levels. It was assessed by comparing the peak area of the extracted samples (spiked before extraction) to the peak area of the unextracted samples (quality control working solutions spiked in extracted plasma).

#### Ruggedness

Ruggedness refers to the ability of an analytical method to remain unaffected by small variations. Parameters were used to evaluate the constancy of the results when external factors such as analyst, laboratory, instrument, reagents, and

days were varied. The ruggedness of the method assessed was determined using different analysts and on different instruments of the same make.

#### Sensitivity

Sensitivity is defined as the lowest analyte concentration that can be measured with acceptable accuracy and precision. Sensitivity experiments were carried out by using six replicates of the LLOQ level sample to determine the lowest limit of detection, the % mean accuracy, and the % CV.

#### Stability

Stability studies were performed by keeping replicates of plasma samples at room temperature for 24 h. The freeze-thaw stability of the drugs in plasma samples was studied over three freeze-thaw cycles, by thawing at room temperature for 2-3 h and refreezing for 12-24 h. The stability of the drugs in plasma was also tested after storage at  $-80^{\circ}\text{C}$ . The concentration of the drugs after each storage period was related to the initial analyte concentrations of freshly prepared samples. Samples were considered stable if the assay values were within the acceptable limits of accuracy and precision.

## RESULTS

#### Method optimization

To obtain the best results, different mobile phase compositions containing phosphate buffer systems with varied pH and organic solvents like methanol and acetonitrile were used to provide adequate sensitivity and selectivity in a short separation time. The best results were obtained with the mobile phase consisting of 0.1% phosphoric acid (pH 4.5) and acetonitrile (50:50) with a flow rate of 1 mL/min. The detection was monitored at 254 nm. With these conditions, the retention times of linagliptin, saxagliptin, and dapagliflozin were found to be 2.784, 5.295, and 7.204 min, respectively.

#### Method validation

##### System suitability and auto-sampler carryover

System suitability was assessed using the MQC level sample as six homogenous injections. The % CV for retention time and response was calculated. The results are presented in Table 1. The values obtained were lower than 1%, which shows

**Table 1. Statistical analysis of system suitability parameters**

Parameter	Internal standard	Saxagliptin	Dapagliflozin	Acceptance
Retention time ( $t_R$ )	0.50	1.07	0.49	% RSD $\leq 2$
Area under the peak	0.88	0.35	0.98	% RSD $\leq 5$
Resolution ( $R_s = 2[t_{R2} - t_{R1}] / [W_1 - W_2]$ )	-	10.95	7.11	$R_s > 2$
Number of theoretical plates ( $n = 16 \times [t_r/W]^2$ )	7238	9817	9758	Increases with efficiency of the separation
Tailing factor (T)	1.13	1.12	1.08	$T \leq 2$
HETP ( $H = L/N$ cm/plate)	0.005	0.015	0.0038	Smaller the value, higher the column efficacy
Capacity factor ( $K' = [t_R - t_M]/t_M$ )	1.11	2.98	4.55	1-10

RSD: Relative standard deviation, HETP: Height equivalent of a theoretical

the suitability of the system for the analysis of the selected combination in human plasma.

Auto-sample carryover was assessed by ULOQ and LLOQ levels to ensure that it did not affect the accuracy and precision. No carryover was observed.

#### Linearity

The ratio of peak area of analyte to internal standard was used for construction of the calibration curve. The linearity of saxagliptin and dapagliflozin was established by an eight-point calibration curve. The most variable regression equation of the calibration curve for saxagliptin and dapagliflozin was  $y=0.126(\pm 0.02)x + 0.003$  and  $y=0.53(\pm 0.02)x - 0.002$ , respectively. The linearity of the calibration graph was validated by the high value of the correlation coefficient with an average value of 0.996 and 0.998 for saxagliptin and dapagliflozin, respectively. The standard curves of saxagliptin and dapagliflozin are presented in Figure 2.

#### Precision and accuracy

The precision and accuracy of the methods were assessed by analyzing six replicates of LLOQ, LQC, MQC, and HQC levels. The accuracy of the method was determined by calculating the % mean accuracy and the precision by calculating relative standard deviation. The data regarding precision and accuracy

are summarized in Table 2. The chromatogram of quality control samples is shown in Figure 3. The % mean accuracy of saxagliptin and dapagliflozin ranged from 98.33 to 101.29 and from 98.43 to 103.28, respectively.

#### Recovery

Recovery of saxagliptin and dapagliflozin was determined by comparing the mean peak areas of six replicates of three quality control samples (HQC, MQC, and LQC) with the mean peak areas of unextracted quality control samples at the same level. The results of the recovery study are given in Table 3. The results are within the acceptance limits.

#### Ruggedness

The present method showed good ruggedness when it was performed using different analysts and on different instruments

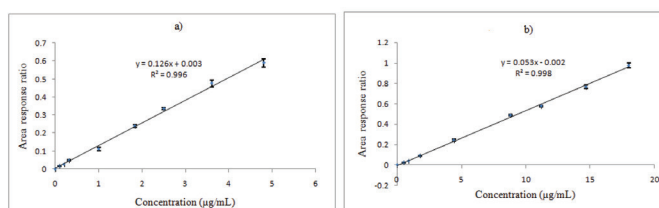
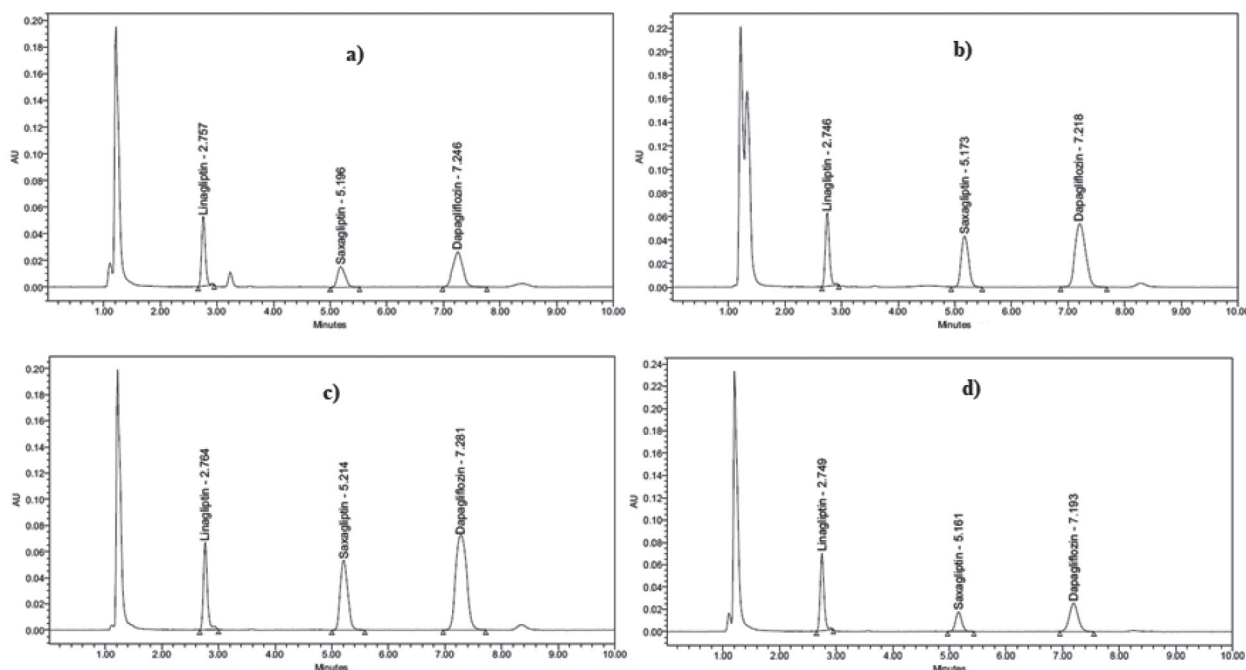


Figure 2. Standard curves of a) saxagliptin and b) dapagliflozin

Table 2. Intra- and interday precision and accuracy summary \*n=18

Added concentration (µg/mL)	Saxagliptin					Dapagliflozin		
	0.40	0.02	0.040	0.010	1.60	1.00	0.2	0.050
<b>Between-batch (n=18)</b>								
Mean	0.4038	0.0199	0.0394	0.0098	1.6127	1.0017	0.2019	0.0496
SD	0.0196	0.0015	0.0021	0.0008	0.0743	0.0763	0.0103	0.0037
% RSD	4.85	7.29	5.31	7.99	4.61	7.62	5.12	6.97
% CV	100.94	99.44	98.61	98.33	100.79	100.17	100.95	99.26
<b>Day 1 (n=6)</b>								
Mean	0.4030	0.0197	0.0395	0.0098	1.6128	1.0085	0.2018	0.0493
SD	0.0217	0.0012	0.0016	0.0008	0.1138	0.0915	0.0097	0.0037
% RSD	5.40	6.16	4.16	7.66	7.05	9.08	4.83	7.44
% CV	100.75	98.33	98.75	98.33	100.80	100.85	100.92	98.67
<b>Day 2 (n=6)</b>								
Mean	0.4052	0.0200	0.0395	0.0098	1.6117	1.0328	0.2062	0.0492
SD	0.0107	0.0017	0.0027	0.0008	0.0534	0.0525	0.0114	0.0029
% RSD	2.65	8.37	6.93	7.66	3.31	5.08	5.52	5.90
% CV	101.29	100.00	98.75	98.33	100.73	103.28	103.10	98.43
<b>Day 3 (n=6)</b>								
Mean	0.4032	0.0200	0.0393	0.0098	1.6135	0.9637	0.1977	0.0503
SD	0.0267	0.0017	0.0022	0.0010	0.0545	0.0755	0.0098	0.0042
% RSD	6.61	8.37	5.49	10.00	3.38	7.83	4.94	8.40
% CV	100.79	100.00	98.33	98.33	100.84	96.37	98.83	100.67

SD: Standard deviation, RSD: Relative standard deviation, CV: Coefficient of variation



**Figure 3.** Chromatograms of a) low quality control sample, b) middle quality control sample, c) high quality control sample, and d) lower limit quality control sample

Analyte	Nominal concentration (µg/mL)	% Recovery	% RSD*
Saxagliptin	0.04 (LQC)	76.40	1.58
	0.20 (MQC)	88.07	0.21
	0.4 (HQC)	71.60	2.08
	Across mean	78.689	8.469
Dapagliflozin	0.2 (LQC)	82.82	0.17
	1.0 (MQC)	78.76	0.93
	1.6 (HQC)	82.79	0.96
	Across mean	81.458	2.86
Internal standard	0.1	82.22	0.46

LQC: Low quality control, MQC: Medium quality control, HQC: High quality control, RSD: Relative standard deviation

of the same make. The results of the ruggedness study were found to be within acceptable limits, proving no significant analyst-to-analyst and instrument-to-instrument variation and hence the ruggedness of the method. The results are presented in Table 4.

**Stability**

The stability of the analytes in human plasma was assessed by analysis of six replicates of quality control samples at low and high concentration levels at room temperature over 24 h (bench-top stability). The measured concentrations were compared with those of freshly prepared and processed samples. The results obtained indicated that the two drugs saxagliptin and

Parameter	Saxagliptin				Dapagliflozin			
	HQC	MQC	LQC	LLOQ	HQC	MQC	LQC	LLOQ
<b>Different column</b>								
Mean	0.401	0.195	0.039	0.010	1.597	1.008	0.198	0.050
SD	0.027	0.011	0.001	0.008	0.119	0.052	0.011	0.004
% CV	6.66	5.38	2.98	7.66	7.47	5.12	5.31	7.90
% Mean accuracy	100.17	97.50	97.92	98.33	99.79	100.77	98.83	100.00
<b>Different analyst</b>								
Mean	0.404	0.195	0.040	0.010	1.614	1.006	0.201	0.049
SD	0.018	0.0164	0.002	0.001	0.070	0.071	0.009	0.002
% CV	4.39	8.43	3.84	8.94	4.35	7.02	4.45	4.71
% Mean accuracy	101.08	97.50	98.75	100.00	100.86	100.63	100.33	98.33

LQC: Low quality control, MQC: Medium quality control, HQC: High quality control, SD: Standard deviation, CV: Coefficient of variation, LLOQ: Lower limit of quantification

dapagliflozin were stable for at least 24 h in human plasma when retained at room temperature. On the other hand, the results obtained for quality control samples subjected to long-term storage at -28°C for 37 days and at -80°C indicate the stability of analytes in human plasma. In contrast, the freeze-thaw stability determined by using LLOQ, LQC, MQC, and HQC level of samples also indicated the stability of analytes in human plasma. The results obtained are compiled in Table 5.

Table 5. Stability data of saxagliptin and dapagliflozin in human plasma

Storage conditions	Saxagliptin		Dapagliflozin	
	LQC	HQC	LQC	HQC
<b>Bench-top stability</b>				
Mean calculated concentration ( $\mu\text{g/mL}$ ) $\pm$ SD	0.0402 $\pm$ 0.0017	0.4033 $\pm$ 0.0175	0.1952 $\pm$ 0.0111	1.5783 $\pm$ 0.0686
% CV	4.29	4.34	5.67	4.35
% Mean accuracy	100.42	100.83	97.58	98.65
<b>Freeze-thaw stability (after 3 cycles)</b>				
Mean calculated concentration ( $\mu\text{g/mL}$ ) $\pm$ SD	0.0379 $\pm$ 0.0023	0.3998 $\pm$ 0.0188	0.1903 $\pm$ 0.0273	1.5639 $\pm$ 0.0904
% CV	3.76	8.56	7.34	4.35
% Mean accuracy	98.78	99.47	97.89	99.90
<b>Stability at <math>-28^\circ\text{C}</math> (long-term stability)</b>				
Mean calculated concentration ( $\mu\text{g/mL}$ ) $\pm$ SD	0.0398 $\pm$ 0.0012	0.4013 $\pm$ 0.01328	0.1920 $\pm$ 0.01279	1.6110 $\pm$ 0.0718
% CV	2.93	3.31	6.66	4.46
% Mean accuracy	99.58	100.33	96.00	100.69
<b>Stability at <math>-80^\circ\text{C}</math> (long-term stability)</b>				
Mean calculated concentration ( $\mu\text{g/mL}$ ) $\pm$ SD	0.0400 $\pm$ 0.0015	0.4018 $\pm$ 0.0098	0.1968 $\pm$ 0.01347	1.6120 $\pm$ 0.0830
% CV	3.87	2.43	6.84	5.15
% Mean accuracy	100.00	100.46	98.42	100.80

LQC: Low quality control, HQC: High quality control, SD: Standard deviation, CV: Coefficient of variation

## DISCUSSION

Since there is no reported sensitive method for the estimation of saxagliptin and dapagliflozin in combination, the validated LC-UV method was developed for routine analysis in a biological matrix. Moreover, the available methods were developed to assess drugs either individually or in combination. Therefore, there is a need to develop an analytical method for the estimation of this combination. The current method aims to develop a simple, accurate, and reliable method for the simultaneous estimation of saxagliptin and dapagliflozin in human plasma. Good resolution and minimum tailing were achieved using this method. The method used simple single-step protein precipitation with acetonitrile and provided good selectivity when tested for peak interference from endogenous sources by comparing the blank chromatogram with quality control samples. The retention times of the internal standard, saxagliptin, and dapagliflozin were found to be 2.746, 5.173, and 7.218 min, respectively. The developed method proved to be rugged and had adequate recovery and no matrix effect. The recovery was determined by comparing the extracted sample with the unextracted samples at three quality control sample levels, i.e., LQC, MQC, and LLOQ. The results were found to be within acceptable limits. The linearity of the method was tested by developing an eight-point calibration curve that included all quality control sample concentrations. The linear range for saxagliptin and dapagliflozin was found to be 0.01 to 0.50  $\mu\text{g/mL}$  and 0.05 to 2.00  $\mu\text{g/mL}$ , respectively. The regression coefficient for saxagliptin and dapagliflozin was 0.996 and 0.998, respectively. The linear range and statistical

parameters prove that the developed method is more sensitive than the reported LC coupled with a PDA detector. Using the stability studies, it was found that the analytes were stable in plasma throughout the analysis period. The stability data were built by comparing the stability samples with freshly prepared samples. On the other hand, long-term stability was established by subjecting quality control samples to  $-28^\circ\text{C}$  for 37 days and to  $-80^\circ\text{C}$ . The results obtained indicate that the method is sensitive, reliable, and cost-effective. Furthermore, the method can be made applicable to pharmacokinetic estimation.

## CONCLUSIONS

The proposed method for the estimation of a saxagliptin and dapagliflozin binary mixture in human plasma is simple, accurate, and reliable. The single-step protein precipitation, short runtime of 10 min, and isocratic elution make the method economical and suitable for the analysis of a large number of samples. The method has been validated as per the requirements of the US-FDA. It can therefore be concluded that the method is suitable for the routine quantification of saxagliptin and dapagliflozin in human plasma.

## ACKNOWLEDGEMENT

The authors are grateful to V.V. Institute of Pharmaceutical Sciences, Gudlavalleru, for providing the facilities to carry out this work.

*Conflict of Interest: No conflict of interest was declared by the authors.*

## REFERENCES

1. Williams DM, Stephens JW. Combination Therapy with Saxagliptin and Dapagliflozin for the Treatment of Type 2 diabetes. *Expert Opin Pharmacother*. 2015;16:2373-2379.
2. FDA Approves Once-Daily Qtern (dapagliflozin and saxagliptin) Tablets for Adults with Type-2 Diabetes [Internet]. *Drugs.com*. Available from: <https://www.drugs.com/newdrugs/fda-approves-once-daily-qtern-dapagliflozin-saxagliptin-adults-type-2-diabetes-4493.html>.
3. Manasa S, Dhanalakshmi K, Nagarjunareddy G, Sreenivasa S. Development and Validation of a RP-HPLC Method for the Estimation of Dapagliflozin in API. *Int J Pharm Sci*. 2014;5:5394-5397.
4. Shyamala M, Nidhi B, Kavitha M, Pooja Sharma JV. Validated RP-HPLC Method for Simultaneous Estimation of Metformin Hydrochloride and Dapagliflozin in Tablet Dosage Form. *AJBPR*. 2015;2:109-113.
5. Dapagliflozin [Internet]. National Center for Biotechnology Information. PubChem Compound Database. U.S. National Library of Medicine; Available from: <https://pubchem.ncbi.nlm.nih.gov/compound/Dapagliflozin> (accessed May 23, 2017).
6. Dave DJ. Saxagliptin: A dipeptidyl peptidase-4 inhibitor in the treatment of type 2 diabetes mellitus. *J Pharmacol Pharmacother*. 2011;2:230-235.
7. Saxagliptin [Internet]. National Center for Biotechnology Information. PubChem Compound Database; U.S. National Library of Medicine; Available from: <https://pubchem.ncbi.nlm.nih.gov/compound/Saxagliptin> (accessed May 23, 2017).
8. Gumieniczek A, Berecka A. Analytical tools for determination of new oral antidiabetic drugs, glitazones, gliptins, gliflozins and glinides, in bulk materials, pharmaceuticals and biological samples. *Open Chem*. 2016;14:215-242.
9. El-Bagary RI, Elkady EF, Ayoub BM. Spectrophotometric Methods Based on Charge Transfer Complexation Reactions for the Determination of Saxagliptin in Bulk and Pharmaceutical Preparation. *Int J Biomed Sci*. 2012;8:204-208.
10. Aubry AF, Gu H, Magnier R, Morgan L, Xu X, Tirmenstein M, Wang B, Deng Y, Cai J, Couerbe P, Arnold M. Validated LC-MS/MS Methods for the Determination of Dapagliflozin, a Sodium-Glucose Co-Transporter 2 Inhibitor in Normal and ZDF Rat Plasma. *Bioanalysis*. 2010;2:2001-2009.
11. Batta N, Pilli N, Derangula V, Vurimindi H, Damaramadugu R, Yejella R. A Rapid and Sensitive LC-MS/MS Assay for the Determination of Saxagliptin and its Active Metabolite 5-Hydroxy Saxagliptin in Human Plasma and its application to a pharmacokinetic study. *Drug Res*. 2014;65:133-140.
12. Pawanjeet JC, Balaji M, Srinivasarao V, Ramakrishna K, Apparao KM. Development and validation of simple stability indicating RP-HPLC method for analysis of saxagliptin and its forced degradation impurities in bulk drug and pharmaceutical dosage form. *Int J Res Dev Pharm Sci*. 2014;3:993-1003.
13. Scheeren LE, Marcolino AIP, Adams AIH, Rolim CMB. Stability indicating RP-LC-PDA method for the quantitative analysis of saxagliptin in pharmaceutical dosage form. *Braz J Pharm Sci*. 2015;51:461-466.
14. Islam S, Hossain T, Kundu SK, Halim A, Rafiquzzaman. Development and validation of RP-HPLC method for determination of saxagliptin hydrochloride in bulk and tablet dosage form. *World Journal of Pharmaceutical Research*. 2016;5:107-119.
15. Daswadkar SC, Roy MA, Walode SG, Mahendra Kumar CB. Quality by design approach for the development and validation of saxagliptin by RP-HPLC with application to formulated forms. *Int J Pharm Sci*. 2016;7:1670-1677.
16. Andac SC, Alp AR. A Validated High Performance Liquid Chromatography Method for the Determination of Saxagliptin and Metformin in Bulk, a Stability Indicating Study. *J Anal Bioanal Tech*. 2014;12:1-5.
17. Sanagapati M, Dhanalakshmi K, Nagarjunareddy G, Sreenivasa S. Development and validation of a RP-HPLC method for the estimation of dapagliflozin in API. *Int J Pharm Sci*. 2014;5:5394-5397.
18. Debata J, Kumar S, Jha SK, Khan A. A New RP-HPLC method development and validation of dapagliflozin in bulk and tablet dosage form. *Int J Drug Dev Res*. 2017;9:48-51.
19. Jeyabaskaran M, Rambabu C, Dhanalakshmi B. RP-HPLC method development and validation of dapagliflozin in bulk and tablet formulation. *IJPAP*. 2013;2:221-226.
20. Kalaichelvi R, Jayachandran E. Validated spectroscopic method for estimation of saxagliptin in pure and from tablet formulation. *Int J Pharm Pharm Sci*. 2011;3:179-180.
21. Moneeb SM. Spectrophotometric and spectrofluorimetric methods for the determination of saxagliptin and vildagliptin in bulk and pharmaceutical preparations. *Bulletin of Faculty of Pharmacy Cairo University*. 2013;51:139-150.
22. Prasad PBN, Satyanaryana K, Krishnamohan G. Development and Validation of a Method for Simultaneous Determination of Metformin and Saxagliptin in a Formulation by RP-HPLC. *Am J of Anal Chem*. 2015;6:841-850.
23. Merey HA, Ramadan NK, Diab SS, Moustafa AA. Chromatographic methods for the simultaneous determination of binary mixture of Saxagliptin HCl and Metformin HCl. *Bulletin of Faculty Pharmacy Cairo University*. 2017;55:311-317.
24. Thangabalan B, Srisowmya P, Manohar Babu S. Method development and validation for simultaneous estimation of saxagliptin and metformin in tablet dosage form by RP-HPLC method. *IJPAP*. 2014;3:363-369.
25. Yunoos M, Gowri SD. Stability indicating quantitative RP-HPLC method development and validation for simultaneous determination of metformin hydrochloride and saxagliptin in bulk and combined tablet dosage form. *J Chem Pharm Res*. 2015;7:346-355.
26. Yunoos M, Gowrisankar D. A validated stability indicating high-performance liquid chromatographic method for simultaneous determination of metformin hcl and dapagliflozin in bulk drug and tablet dosage form. *Asian J Pharm Clin Res*. 2015;8:320-326.
27. Guidance for Industry. Bioanalytical Method Validation for human studies. U. S. Department of Health and Human Services Food and Drug Administration, Center for Drug Evaluation and Research (CDER); 2013:1-23.



# Identification, Quantification, and Antioxidant Activity of Hydroalcoholic Extract of *Artemisia campestris* from Algeria

## Cezayir’de Yetişen *Artemisia campestris*’in Sulu Alkollü Ekstresinin Tanımlanması, Kantitasyonu ve Antioksidan Aktivitesi

✉ Boulanouar BAKCHICHE<sup>1\*</sup>, ✉ Abdelaziz GHERIB<sup>1</sup>, ✉ Maria Rosário BRONZE<sup>2</sup>, ✉ Mosad A. GHAREEB<sup>3</sup>

<sup>1</sup>Amar Telidji University, Faculty of Technology, Laboratory of Process Engineering, Laghouat, Algeria

<sup>2</sup>University of Lisbon, Faculty of Pharmacy, Lisboa, Portugal

<sup>3</sup>Medicinal Chemistry Department, Theodor Bilharz Research Institute, Kornaish El-Nile, Warrak El-Hadar, Imbaba, Giza, Egypt

### ABSTRACT

**Objectives:** Our study aimed to investigate the chemical profile of hydroalcoholic extract of Algerian *Artemisia campestris* and its antioxidant activity.

**Materials and Methods:** The hydroalcoholic extract of Algerian *A. campestris* was investigated for its phenolic constituents using high performance liquid chromatography (HPLC)-diode array detection (DAD)-electrospray ionization (ESI)-mass spectrometer (MS)/MS. The *in vitro* antioxidant activity and total phenolic content were also evaluated via oxygen radical absorbance capacity and Folin-Ciocalteu assays, respectively.

**Results:** HPLC-DAD-ESI-MS/MS analysis revealed that the main tentatively identified compounds were caffeoylquinic acid isomers, flavonoids, and benzoic acid derivatives. Additionally, the hydroalcoholic extract exhibited a promising antioxidant activity value of  $120.5 \pm 10.4$   $\mu\text{mol}$  Trolox equivalent antioxidant capacity/g dry weight (DW), and a strong correlation exists between this activity and the total phenolic content value of  $102.09 \pm 1.65$  mg/g gallic acid equivalents DW.

**Conclusion:** The hydroalcoholic extract of *A. campestris* is a promising candidate for the production of naturally occurring antioxidant agents.

**Key words:** *Artemisia campestris*, polyphenols, flavonoids, chlorogenic acid, antioxidant

### ÖZ

**Amaç:** Bu çalışmada, Cezayir’de yetişen *Artemisia campestris*’in sulu alkollü ekstresinin kimyasal profilinin ve antioksidan etkisinin araştırılması amaçlanmıştır.

**Gereç ve Yöntemler:** Cezayir’de yetişen *A. campestris*’in sulu alkollü ekstresinin fenolik bileşenleri yüksek performanslı sıvı kromatografisi (HPLC) diyot dizinli dedektör-(DAD)-elektrosprey iyonizasyonu (ESI)-mass spektrometresi (MS)/MS kullanılarak incelenmiştir. *In vitro* antioksidan aktivite ve toplam fenolik içerik de sırasıyla oksijen radikal absorban kapasitesi ve Folin-Ciocalteu analizleri ile değerlendirilmiştir.

**Bulgular:** HPLC-DAD-ESI-MS/MS analizi, esas olarak saptanan ana bileşiklerin, kafeoilkuinik asit izomerleri, flavonoidler ve benzoik asit türevleri olduğunu ortaya koymuştur. Bununla birlikte, sulu alkollü ekstre  $120.5 \pm 10.4$   $\mu\text{mol}$  Trolox eşdeğeri antioksidan kapasitesi/g kuru ağırlık (KA) değeri ile önemli derecede antioksidan aktivite göstermiş ve bu aktivite ile  $102.09 \pm 1.65$  mg/g gallik asit eş değeri KA olduğu belirlenen toplam fenolik içerik değeri arasında güçlü bir korelasyon saptanmıştır.

**Sonuç:** Sonuç olarak, *A. campestris*’in sulu alkollü ekstresinin, doğal antioksidan ajanların üretimi için umut verici bir aday olduğu belirtilmiştir.

**Anahtar kelimeler:** *Artemisia campestris*, polifenoller, flavonoidler, klorojenik asit, antioksidan

\*Correspondence: E-mail: b.bakchiche@lagh-univ.dz, Phone: 00213662174441 ORCID-ID: orcid.org/0000-0002-3124-5153

Received: 01.02.2018, Accepted: 25.04.2018

©Turk J Pharm Sci, Published by Galenos Publishing House.

## INTRODUCTION

The genus *Artemisia* is one of the largest and most widely distributed genera of the family *Asteraceae* in Europe and North Africa, and its species have been characterized for their pronounced biological activities and are considered to produce most medicinally important secondary metabolites. Eleven species of *Artemisia* can be found in the Algerian flora.<sup>1,2</sup> *Artemisia campestris* is a perennial faintly aromatic herb widespread in the south of Algeria, commonly known as “dgouft”. The aerial parts of the plant have been used in traditional medicine as a febrifuge, vermifuge, and anticancer agent and to treat digestive troubles, gastric ulcer, and menstrual pain.<sup>3-5</sup> *A. campestris* extract was reported to be a potent free radical scavenger of 2,2'-diphenyl-1-picryl hydrazyl, 2,2'-azinobis(3-ethylbenzthiazoline-6-sulfonic acid (ABTS<sup>•+</sup>), and superoxide anion radicals (O<sub>2</sub><sup>•-</sup>) but there is a lack of knowledge regarding the phenolic composition of this plant and its relation with its antioxidant properties, since only a few studies have identified a small number of phenolic compounds.<sup>5-8</sup>

However, the phenolic profile of *A. campestris* is quite complex. Flavonoids present in this species consist of flavones, flavonols, flavanones, dihydroflavonols, and their methyl ethers, whereas the isolation of coumarins and phloracetophenones is also reported.<sup>9,10</sup> Chlorogenic acid is a natural product occurring in a large number of different plants or parts of the plant; for example, in *A. campestris* chemically it is the ester of caffeic acid and quinic acid, 3-*O*-caffeoylquinic acid. Other isomers are derivative chlorogenic acid 4-*O*-caffeoylquinic acid and 5-*O*-caffeoylquinic acid. Additionally, there are other isomers, called iso-chlorogenic acids, with two caffeic acid moieties such as 3,4-dicaffeoylquinic acid, 4,5-dicaffeoylquinic acid, and 1,5-dicaffeoylquinic acid.

The objective of the present work was to contribute to the identification of the major phenolic compounds in the hydroalcoholic extract of *A. campestris* by high-performance liquid chromatographic/diode array detector (HPLC-DAD) coupled with electrospray ionization/mass spectrometry (ESI-MS). In addition, HPLC-DAD-electrochemical detector quantification of phenolic and flavonoid contents and hydroxycinnamic acid was carried out. Finally, the antioxidant capacity of the extract was also evaluated by oxygen radical absorbance capacity (ORAC) assay.

## EXPERIMENTS

### Chemicals

Chlorogenic acid was purchased from Extrasynthese (Genay, France). Methanol for HPLC-GOLD-Ultra gradient was purchased from Carlo Erba Reagents (Val de Reuil, France). Phosphoric acid (85%) and formic acid (98%) were purchased from Panreac Química (Barcelona, Spain) Acetonitrile HPLC gradient grade was purchased from VWR® (Leuven, Belgium). Milli-Q® water (18.2 MΩ.cm) was obtained in a Millipore-Direct Q3 ultraviolet (UV) System (Molsheim, France).

### Plant material

Aerial parts of *A. campestris* were collected from the Laghouat region in the northern Algerian Sahara in summer 2015. The identification and authentication of the plant were carried out by Dr. Mohamed Kouidri, botanist (Department of Agronomy, Faculty of Sciences, University of Laghouat, Algeria) and the voucher specimens were deposited at the Laboratory of Process Engineering, University of Laghouat (number LGP Ac/08/15).

### Preparation of the hydroalcoholic extract

One gram of dried powder was mixed with ethanol:water (8:2; v/v, 10 mL) and macerated under sonication, (water bath, room temperature, 30 min). The material was filtered and the crude extract obtained was analyzed directly by HPLC. The procedure was performed in triplicate.

### Equipment and conditions of analysis

#### Liquid chromatography with diode array and electrochemical detection

The HPLC system used was a Thermo Finnigan (Surveyor, San Jose, CA, USA), equipped with an autosampler, pump, photodiode-array detector (PDA), and electrochemical detector (ED). Chromatographic separation of compounds was carried out on a Lichrocart RP-18 column (250×4 mm, particle size 5 μm, Merck). The Dionex® ED performed signal measurements by integrated voltammetry at potentials between -1.0 V and 1.0 V with a scan time of 1.00 s. The obtained results were acquired at a frequency of 50 Hz using an analogue/digital converter. The photodiode array detector was programmed for scanning between 192 and 798 nm at a speed of 1 Hz with a bandwidth of 5 nm. The detection was monitored using three individual channels, 280, 320, and 360 nm, at a speed of 10 Hz with a bandwidth of 11 nm. The injection volume was 20.00 μL and total time of analysis was 120 min. A binary gradient elution (Table 1) was used. The mobile phase was as follows: 0.5% formic acid in Milli-Q® Water 95% (eluent A) and 0.5% phosphoric acid in acetonitrile 90% and 9.5% Milli-Q® Water (eluent B). The flow rate was systematically controlled and set at 0.3 mL/min.

#### Liquid chromatography with mass spectrometry

The identification of compounds in the extracts was carried out by HPLC-MS/MS using Waters® Alliance 2695 HPLC equipment fitted with a DAD, Waters 2996 (PDA), and a triple quadrupole spectrometer (TQ) (Micromass® Quattro micro™, Waters) with an ESI source operating in negative mode. The capillary in the ESI source was placed at 3.0 kV and the cone at 30 V. The chromatographic separation was performed on a LiChroCART RP-18 column (250×4 mm, particularly from size 5 μm, Merck) at 35°C. The eluents used were A: formic acid (0.5% v/v) and B: acetonitrile (LC-MS grade). A gradient elution program was applied for chromatographic analysis (Table 1). Flow rate was maintained at 0.3 mL/min and the injection volume was 10 μL. Ultrapure nitrogen (N<sub>2</sub>) was used as nebulizer and drying gas and gas. Ultrapure argon was used as the collision gas at a



pressure of  $10^{-4}$  mbar. For data acquisition and treatment of data MassLynx® software version 4.1 was used.

#### Determination of phenolic chromatographic profile

Total phenolic content was determined using the 280 nm total peak area above 40 min. Calibration curves with gallic acid (0–25 ppm) were created and the final results were expressed in terms of gallic acid equivalents (GAE) per gram of dry weight (DW) (mg/g GAE DW).

Total flavonoids content was determined using the 360 nm total peak area above 40 min. Calibration curves with rutin (0–50 ppm) were created and the final results were expressed in terms of rutin equivalents (RE) per gram of DW (mg/g RE DW).

Total hydroxycinnamic acids content was determined using the 320 nm total peak area between 20 and 40 min. Calibration curves with caffeic acid (0–25 ppm) were created and the final results were expressed in terms of caffeic acid (CA) equivalents per gram of DW (mg/g CA DW). Additionally, the

content of total phenols was determined colorimetrically with Folin's reagent according to the method reported by Stamatakis et al.<sup>11</sup> The phenolic contents were expressed as mg of GAE per gram of DW (mg/g GAE DW).

#### ORAC

Peroxyl radical scavenging capacity was determined by the ORAC method. The assay was carried out by following the method reported by Huang et al.<sup>12</sup> modified for the FL800 microplate reader (BioTek Instruments, Winooski, VT, USA) as described by Feliciano et al.<sup>13</sup> All data were expressed as micromoles of Trolox equivalent antioxidant capacity (TEAC) per gram DW ( $\mu\text{mol TEAC/g DW}$ ).

## RESULTS

The HPLC method employed for the separation of phenolic components in the hydroalcoholic extract of *A. campestris* revealed a good separation of the majority of the compounds. Chromatograms at 280 nm are widely used to study phenolic compounds because absorption at this wavelength is suitable to detect a large number of such compounds. The maximum absorption wavelengths ( $\lambda_{\text{max}}$ ), and parent, aglycone, and fragment ion masses of the components detected in the aqueous extract of *A. campestris* are shown in Table 2, where the compounds are numbered according to their retention times ( $R_t$ ) in the obtained chromatograms.

Four compounds were unequivocally identified based on the analysis of standard compounds and comparing their HPLC retention time, UV spectra, and MS/MS fragmentation pattern. The remaining compounds were characterized and their structures proposed based mainly on the MS/MS fragmentation data conjugated with the UV-DAD spectra. Most of the peaks showed similar UV absorptions maxima with two bands at  $\lambda_{\text{max}}$  230–240 nm and 320–330 nm. These types of UV absorption bands are characteristic of hydroxycinnamic acids. Some peaks with characteristic UV absorptions bands for flavonoids were

**Table 1. Gradient eluents used for analysis by HPLC-DAD-ED**

Time (min)	Eluent A (%)	Eluent B (%)
0.10	98.90	1.10
15	91.00	9.00
20	87.80	12.20
30	87.80	12.20
55	86.50	13.50
95	73.00	27.00
105	37.00	63.00
110	37.00	63.00
125	98.90	1.10
130	98.90	1.10

HPLC: High performance liquid chromatography, DAD: Diode array detection, ED: Electrochemical detector

**Table 2. Phenolic compounds tentatively identified in hydroalcoholic extract of *Artemisia campestris***

Peak no.	$R_t$ (min)	Ultraviolet	[M-H] <sup>-</sup> $m/z$	Fragmentations	Compounds proposed	References
1	27.5	259	153	141, 109	Protocatechuic acid	19
2	29.45	325	353	191, 179, 173	5- <i>O</i> -Caffeoylquinic acid	28
3	31.6	266	205	143, 129, 114	Quinic acid methyl ester	20
4	40.26	224/326	353	191, 173, 85	3- <i>O</i> -Caffeoylquinic acid	28
5	44.9	325	179	135, 107, 89	Caffeic acid	21
6	58.6	328	367	191, 173, 134, 93, 87	4- <i>O</i> -Feruloylquinic acid	22
7	73.3	365	463	301, 179, 151	Quercetin- <i>O</i> -glucoside	23
8	76.8	256	609	301	Rutin	24
9	83.68	247/326	515	353, 235, 191, 179, 173, 135	3,4-Dicaffeoylquinic acid	28
10	89.18	244/326	515	353, 191, 179, 173, 135	4,5-Dicaffeoylquinic acid	28
11	114.0		313	298, 283, 255, 163, 117	4',7'-Dimethoxy luteolin	25

also detected.<sup>14</sup> The chromatogram of the hydroalcoholic extract of the aerial parts from *A. campestris* is presented in Figure 1. The most relevant components were caffeoylquinic acids. In general, in the MS spectrum the most intense peak corresponds to the deprotonated molecular ion  $[M-H]^-$ . The main fragments observed in the MS/MS experiments are given in Table 2. Chemical structures of some phenolic compounds tentatively identified in hydroalcoholic extract of *Artemisia campestris* are given in Figure 2.

#### Quantification of chlorogenic acid derivatives of *A. campestris*

The content of chlorogenic acid derivatives of *A. campestris* extract was determined. The amounts of the identified compounds are given in Table 3. 3,4-Dicaffeoylquinic acid was the major caffeoylquinic acid in the hydroalcoholic extract of *A. campestris* ( $274.76 \pm 9.50$  mg eq Trolox/L).

The data in Table 3 reveal the highest quantities of the three isomers of the caffeoylquinic acid (3-*O*-caffeoylquinic acid  $191.92 \pm 5.4$  mg eq Trolox/L, 4,5-dicaffeoylquinic acid  $117.61 \pm 3.52$  mg eq Trolox/L, and 5-*O*-caffeoylquinic acid  $6.48 \pm 0.25$  mg eq Trolox/L).

#### Antioxidant activity and total phenolic content

The antioxidant and total phenolic content of the *A. campestris* extract were measured by ORAC assay and the results are shown in Table 4.

**Table 3. Quantification of chlorogenic acid derivatives by electrochemical detector**

Peak no.	$R_t$	$m/z$	Compounds proposed	mg eq Trolox/L
2	29.45	353	5- <i>O</i> -Caffeoylquinic acid	$6.48 \pm 0.25$
4	40.26	353	Chlorogenic acid (3- <i>O</i> -Caffeoylquinic acid)	$191.92 \pm 5.4$
9	83.68	515	3,4-Dicaffeoylquinic acid	$274.76 \pm 9.50$
10	89.18	515	4,5-Dicaffeoylquinic acid	$117.61 \pm 3.52$

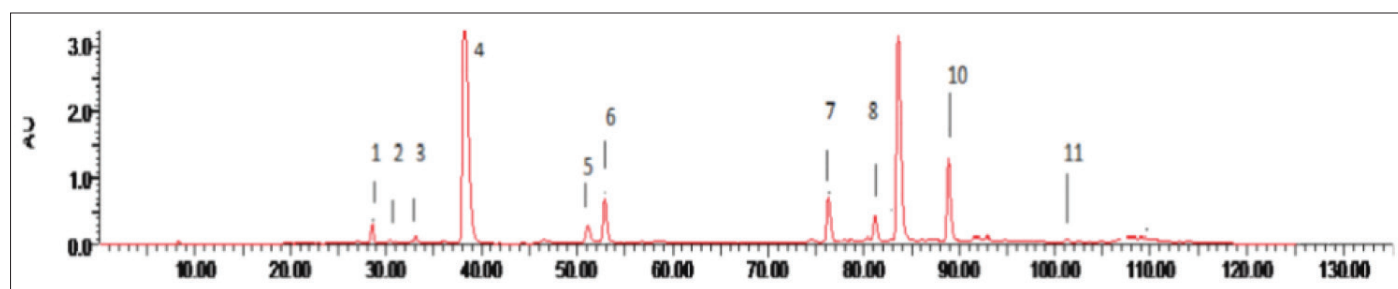


**Figure 1.** Chromatographic profile of *Artemisia campestris* obtained by HPLC-DAD at 280 nm  
HPLC: High performance liquid chromatography, DAD: Diode array detection

**Table 4. Phenolic, hydroxycinnamic acid, and flavonoids contents and value of ORAC assay of *Artemisia campestris* extract**

Sample	TPC (280 nm) mg/g DW	HAC (320 nm) mg/g CA DW	TFC (360 nm) mg/g RE DW	TPC (Folin method) (mg/g EGA DW)	ORAC $\mu$ mol TEAC/ g DW)
<i>Artemisia campestris</i> extract	$61.42 \pm 2.13$	$37.26 \pm 0.88$	$17.94 \pm 1.26$	$102.09 \pm 1.65$	$120.5 \pm 10.4$

TPC: Total phenolic content, HAC: Hydroxycinnamic acid content, TFC: Total flavonoids content, CA: Caffeic acid, DW: Dry weight, RE: Rutin equivalents, EGA: Equivalents of gallic acid, TEAC: Trolox equivalent antioxidant capacity, ORAC: Oxygen radical absorbance capacity

## DISCUSSION

### Characterization of caffeoylquinic acids ( $M=354$ ) and dicaffeoylquinic acids ( $M=516$ )

Two peaks were detected at  $m/z$  353 and assigned using the hierarchical keys previously developed<sup>15-18</sup> as well-known chlorogenic acid (3-*O*-caffeoylquinic acid) and 5-*O*-caffeoylquinic acid. Two dicaffeoylquinic acid isomers were identified by their parent ion  $m/z$  515 and were assigned as 3,4-dicaffeoylquinic acid and 4,5-dicaffeoylquinic acid.<sup>8,18</sup>

### Characterization of other nuclei

A peak was detected at  $R_t=27.5$  min with  $[M-H]^-$  at  $m/z$  153 with a characteristic MS<sup>2</sup> fragment at  $m/z$  109  $[M-H-44]^-$  due to loss of CO<sub>2</sub> moiety; it was identified as 3,4-dihydroxybenzoic acid (protocatechuic acid).<sup>19</sup> Another peak at  $R_t=31.6$  min showed a deprotonated molecule  $[M-H]^-$  at  $m/z$  205 with MS<sup>2</sup> fragments of 143, 129, and 114; it was assigned to quinic acid methyl ester.<sup>20</sup> A molecular ion was seen at  $R_t=44.9$  with a deprotonated ion  $[M-H]^-$  at  $m/z$  179 with daughter ions at  $m/z$  135  $[M-H-44]^-$  due to the neutral loss of CO<sub>2</sub> moiety and 107  $[M-H-44-28]^-$  due to further neutral loss of CO moiety; it was identified as 3,4-dihydroxy-cinnamic acid (caffeic acid) as previously described.<sup>21</sup> A peak at  $R_t=58.6$  showed a deprotonated ion  $[M-H]^-$  at  $m/z$  367 and MS<sup>n</sup> ions at  $m/z$  191 equivalent to quinic acid moiety, and another fragment at  $m/z$  173 due to loss of H<sub>2</sub>O molecule; it was identified as 4-*O*-feruloylquinic acid.<sup>22</sup> Moreover, a peak at  $R_t=73.3$  showed a deprotonated ion  $[M-H]^-$  at  $m/z$  463 and MS<sup>n</sup> ions at  $m/z$  301 due to loss of glucose moiety ( $-m/z$  162) and equivalent to quercetin aglycone moiety. In addition, characteristic fragments of aglycone appeared at  $m/z$  179 and 151; it was identified as quercetin-*O*-glucoside.<sup>23</sup> A peak at  $R_t=76.8$  showed a deprotonated ion  $[M-H]^-$  at  $m/z$  609 and a characteristic MS<sup>n</sup> ion at  $m/z$  301 due to loss of rutinoyl moiety ( $-m/z$  308) and equivalent to quercetin aglycone moiety; it was identified as quercetin-3-*O*-rutinoside (rutin).<sup>24</sup> Finally,

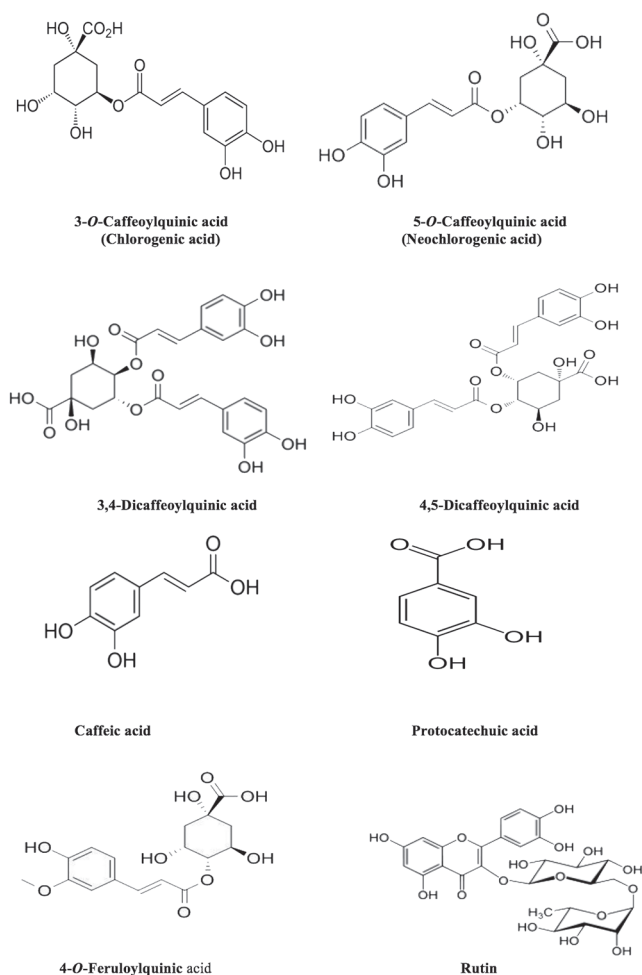


**Figure 2.** Chemical structures of some phenolic compounds tentatively identified in hydroalcoholic extract of *Artemisia campestris*

a peak at  $R_f=114.0$  showed a deprotonated ion  $[M-H]^-$  at  $m/z$  313 and characteristic  $MS^n$  ions at  $m/z$  298 due to the loss of methyl moiety  $[M-H-CH_3]^-$  and 283 due to further loss of another methyl moiety  $[M-H-2CH_3]^-$ ; it was identified as 4',7'-dimethoxy luteolin.<sup>25</sup>

#### Antioxidant activity and total phenolic content

In the current study, the ORAC (Trolox equivalents, TE) value ( $120.5 \pm 10.4 \mu\text{mol TEAC/g DW}$ ) was below the results ( $263.65 \pm 39.7 \mu\text{mol TEAC/g DW}$ ) found by Bakchiche et al.<sup>7</sup> and higher than the values of different *Artemisia* species harvested in Korea reported by Lee.<sup>26</sup> This can be due to several reasons such as the method of extraction and the date and place of harvest (seasonal variations).

The reagent Folin-Ciocalteu is used in the quantification of total phenols; it is not only specific for phenols but also has the ability to react with sugar, protein, etc. For this reason our result was very high. We found a value greater than the values of the total phenols with the same species reported by Djeridane et al.<sup>27</sup> ( $20.38 \text{ mg/g GAE DW}$ ) and Bakchiche et al.<sup>7</sup> ( $53.84 \text{ mg/g GAE DW}$ ).

Bakchiche et al.<sup>7</sup> previously stated that the hydroalcoholic extract from aerial parts of *A. campestris* possessed high antioxidant activity coupled to high phenolic content. Further investigation of known phenolic compounds in this extract, quantified by HPLC-MS/MS, revealed that chlorogenic acid was in high abundance ( $161.92 \pm 5.4 \text{ mg/g DW}$ ) and was most likely responsible for the majority of the observed antioxidant activity.<sup>7</sup> In the current study, *A. campestris* extract, which demonstrated high antioxidant activity and phenolic content, was further analyzed for the presence of a number of mono (3-O-caffeoylquinic, 5-O-caffeoylquinic acids) and di (3,4-dicaffeoylquinic acid, 4,5-dicaffeoylquinic acid) substituted chlorogenic acid derivatives using HPLC-MS/MS. Numerous previous reports revealed the antioxidant activity of medicinal plants based on the presence of certain polyphenolic compounds including phenolic acids, flavonoids, tannins, and their derivatives.<sup>28-30</sup>

## CONCLUSIONS

The aim of the present study was to contribute to the identification of the major phenolic compounds in the hydroalcoholic extract of *A. campestris*; quantification of phenolic and flavonoid contents and hydroxycinnamic acid was carried out, and the antioxidant capacity of the extract was evaluated by ORAC assay. According to the data obtained, 11 phenolic compounds in the hydroalcoholic extract were tentatively identified using HPLC-DAD-ESI-MS/MS. The identified compounds contained phenolic acid derivatives and flavonoids. Moreover, the hydroalcoholic extract showed a noticeable antioxidant potential; this high activity may be due to the presence of phenolic compounds. In conclusion, the aerial parts of *A. campestris* are considered a promising source of naturally occurring antioxidant agents, and its polyphenol profile may be regarded as a model for caffeoylquinic acid distribution in the plant *A. campestris* and can help to distinguish chlorogenic acid isomers.

*Conflict of Interest:* No conflict of interest was declared by the authors.

## REFERENCES

1. Quézel P, Santa S. New flora of Algeria and the meridional desert regions (In French). Paris; CNRS;2013:2.
2. Abad MJ, Bedoya LM, Apaza L, Bermejo P. The *Artemisia* L. Genus: a review of bioactive essential oils. *Molecules*. 2012;17:2542-2566.
3. Dob T, Dahmane D, Berramdane T, Chelghoum C. Chemical composition of the essential oil of *Artemisia campestris* L. from Algeria. *Pharm Biol*. 2005;43:512-514.
4. Akrouf A, Gonzalez LA, El Jani H, Madrid PC. Antioxidant and antitumor activities of *Artemisia campestris* and *Thymelaea hirsuta* from southern Tunisia. *Food Chem. Toxicol*. 2011;49:342-349.
5. Djeridane A, Yousfi M, Nadjemi B, Vidal N, Lesgards JF, Stocker P. Screening of some Algerian medicinal plants for the phenolic compounds and their antioxidant activity. *Eur Food Res Technol*. 2007;224:801-809.

6. Karabegovic I, Nikolova M, Velickovic D, Stojicevic S, Veljkovic, V, Lazic M. Comparison of antioxidant and antimicrobial activities of methanolic extracts of the *Artemisia* sp. recovered by different extraction techniques. *Chin J Chem Eng.* 2011;19:504-511.
7. Bakchiche B, Gherib A, Aazza, S, Gago C, Miguel MG. Antioxidant activities of eight Algerian plant extracts and two essential oils. *Ind Crops Prod.* 2013;46:85-96.
8. Megdiche-Ksouri W, Trabelsi N, Mkadmini K, Bourgoua S, Noumi A. *Artemisia campestris* phenolic compounds have antioxidant and antimicrobial activity. *Ind Crops Prod.* 2014;63:104-113.
9. Valant-Vetschera K, Fischer R, Wollenweber E. Exudate flavonoids in species of *Artemisia* (Asteraceae-Anthemideae): new results and chemosystematic interpretation. *Biochem Syst Ecol.* 2003;31:487-498.
10. Ferchichi L, Merza J, Landreau A, Ray AML, Legseir B, Seraphin D, Richomme P. Occurrence of isocoumarinic and phenolic derivatives in *Artemisia campestris* L. subsp. *campestris*. *Biochem Syst Ecol.* 2006;34:829-832.
11. Stamatakis G, Tsantila N, Samiotaki M, Panayotou GN, Dimopoulos AC, Halvadakis CP, Demopoulos CA. Detection and isolation of antiatherogenic and antioxidant substances present in olive mill wastes by a novel filtration system. *J Agric Food Chem.* 2009;57:10554-10564.
12. Huang D, Ou B, Hampsch WM, Flanagan JA, Prior RL. High throughput assay of oxygen radical absorbance capacity (ORAC) using a multichannel liquid handling system coupled with a microplate fluorescence reader in 96-well format. *J Agric Food Chem.* 2002;50:4437-4444.
13. Feliciano RP, Bravo MN, Pires MM, Serra AT, Duarte CM, Boas LV, Bronze MR. Phenolic Content and Antioxidant Activity of Moscatel Dessert Wines from the Setubal Region in Portugal. *Food Analy Meth.* 2009;2:149-161.
14. Mabry TJ, Markham KR, Thomas M. *The Systematic Identification of Flavonoids.* New York; Springer Verlag Publication; 1970;294:261-266.
15. Riedel H, Cai Z, Kutuk O, Smetanska I. Obtaining phenolic acids from cell cultures of various *Artemisia* species. *Afric J Biotech.* 2010;9:8805-8809.
16. Carvalho M, Silva BM, Silva R, Valentão P, Andrade PB, Bastos ML. First report on *Cydonia oblonga* Miller anticancer potential: Differential antiproliferative effect against human kidney and colon cancer cells. *J Agric Food Chem.* 2010;58:3366-3370.
17. Dagnon S, Ivanov I, Bojilov D, Docheva M, Statkova S. Evaluation of the Main Polyphenolic Compounds in Aromatic Plants of Asteraceae and Solanaceae Families of Bulgarian Origin. *J Pharma and Phytoch.* 2013;76-84.
18. Sebai H, Jabri MA, Souli A, Hosni K, Selmi S, Tounsi H, Tebourbi O, Boubaker S, El-Benna J, Sakly M. Protective effect of *Artemisia campestris* extract against aspirin-induced gastric lesions and oxidative stress in rat. *RSC Adv.* 2014;4:49831-49841.
19. Charrouf Z, Hilali M, Jauregui O, Soufiaoui M, Guillaume D. Separation and characterization of phenolic compounds in arganfruit pulp using liquid chromatography-negative electrospray ionization tandem mass spectroscopy. *Food Chem.* 2007;100:1398-1401.
20. Al-Rawahi AS, Edwards G, Al-Sibani M, Al-Thani G, Al-Harrasi AS, Rahman MS. Phenolic constituents of pomegranate peels (*Punica granatum* L.) cultivated in Oman. *Euro J Med Plants.* 2014;4:315-331.
21. Biesaga M, Pyszynska K. Liquid chromatography/tandem mass spectrometry studies of the phenolic compounds in honey. *J Chrom A.* 2009;1216:6620-6626.
22. Ghareeb MA, Mohamed T, Saad AM, Refahy LA, Sobeh M, Wink M. HPLC-DAD-ESI-MS/MS analysis of fruits from *Firmiana simplex* (L.) and evaluation of their antioxidant and antigenotoxic properties. *J Pharm Pharm.* 2018;70:133-142.
23. Sobeh M, Hassan SA, El Raey MA, Khalil WA, Hassan MAE, Wink M. Polyphenolics from *Albizia harveyi* exhibit antioxidant activities and counteract oxidative damage and ultra-structural changes of cryopreserved bull semen. *Mol.* 2017;22:1993.
24. Abu-Reidah IM, Ali-Shtayeh MS, Jamous RM, David Arráez-Román D, Segura-Carretero A. HPLC-DAD-ESI-MS/MS screening of bioactive components from *Rhus coriaria* L. (Sumac) fruits. *Food Chem.* 2015;166:179-191.
25. Simirgiotis MJ, Benites J, Areche C, Sepúlveda B. Antioxidant capacities and analysis of phenolic compounds in three endemic *Nolana* species by HPLC-PDA-ESI-MS. *Mol.* 2015;20:11490-11507.
26. Lee JH. Evaluation for Antioxidant Activity of *Artemisia* sp. *Plants. Research J Med Plant.* 2014;8:258-268.
27. Djeridane A, Yousfi M, Nadjemi B, Boutassouna D, Stocker P, Vidal N. Antioxidant activity of some Algerian medicinal plants extracts containing phenolic compounds. *Food Chem.* 2006;97:654-660.
28. Ghareeb M, Saad A, Ahmed W, Refahy L, Nasr S. HPLC DAD ESI MS/MS characterization of bioactive secondary metabolites from *Strelitzia nicolai* leaf extracts and their antioxidant and anticancer activities *in vitro*. *Pharmacogn Res.* 2018;10:368-378.
29. Ghareeb MA, Sobeh M, Rezaq S, El-Shazly AM, Mahmoud MF, Wink M. HPLC-ESI-MS/MS profiling of polyphenolics of a leaf extract from *Alpinia zerumbet* (Zingiberaceae) and its anti-inflammatory, anti-nociceptive, and antipyretic activities *in vivo*. *Molecules.* 2018;23:3238.
30. Sobeh M, Mahmoud MF, Hasan RA, Abdelfattah MA, Sabry OM, Ghareeb MA, El-Shazly AM, Wink M. Tannin rich extracts from *Lannea stuhlmannii* and *Lannea humilis* (Anacardiaceae) exhibit hepatoprotective activities *in vivo* via enhancement of the anti apoptotic protein bcl 2. *Sci Rep.* 2018;8:9343.



# Antimicrobial and Anti-Inflammatory Activity of Some *Lathyrus* L. (Fabaceae) Species Growing in Turkey

## Türkiye'de Yetişen Bazı *Lathyrus* L. (Fabaceae) Türlerinin Antimikrobiyal ve Antienflamatuvar Aktivite Değerlendirilmesi

© Hajar HEYDARI<sup>1</sup>, © Gülçin SALTAN İŞCAN<sup>1\*</sup>, © Müjde ERYILMAZ<sup>2</sup>, © Özlem BAHADIR ACIKARA<sup>1</sup>, © Sezen YILMAZ SARIALTIN<sup>3</sup>, © Mehmet TEKİN<sup>4</sup>, © Tülay ÇOBAN<sup>3</sup>

<sup>1</sup>Ankara University, Faculty of Pharmacy, Department of Pharmacognosy, Ankara, Turkey

<sup>2</sup>Ankara University, Faculty of Pharmacy, Department of Pharmaceutical Microbiology, Ankara, Turkey

<sup>3</sup>Ankara University, Faculty of Pharmacy, Department of Pharmaceutical Toxicology, Ankara, Turkey

<sup>4</sup>Cumhuriyet University, Faculty of Pharmacy, Department of Pharmaceutical Botany, Sivas, Turkey

### ABSTRACT

**Objectives:** The present study aimed to evaluate the antimicrobial and anti-inflammatory activities of methanol extracts and n-hexane, ethyl acetate, chloroform, and water fractions of five *Lathyrus* species, namely *Lathyrus armenus*, *Lathyrus aureus*, *Lathyrus cilicicus*, *Lathyrus laxiflorus* subsp. *laxiflorus*, and *Lathyrus pratensis*, growing in Turkey.

**Materials and Methods:** The antimicrobial activities were screened against *Staphylococcus aureus* ATCC 29213, *Bacillus subtilis* ATCC 6633, *Escherichia coli* ATCC 25922, *Pseudomonas aeruginosa* ATCC 27853, and *Candida albicans* ATCC 10231. Broth dilution was used to determine the antimicrobial activities of extracts and fractions. *In vitro* anti-inflammatory activity of these extracts and fractions was determined using human red blood cell membrane stabilization.

**Results:** The results demonstrated that ethyl acetate fractions of the tested species exhibited higher antimicrobial activity than the other extracts. Among all of the tested extracts and fractions, the highest anti-inflammatory activity was detected in water fractions. Furthermore, water fractions of *L. pratensis* showed better anti-inflammatory activity than acetylsalicylic acid and diclofenac sodium, which were used as standard drugs in this assay.

**Conclusion:** The results indicate the membrane stabilizing effect of the various extracts and fractions of the *Lathyrus* species and could constitute preliminary work for *in vivo* anti-inflammatory activity experiments.

**Key words:** Anti-inflammatory activity, antimicrobial activity, human red blood cell membrane, *Lathyrus*

### ÖZ

**Amaç:** Bu çalışmada Türkiye yetişen beş *Lathyrus* türü, *Lathyrus armenus*, *Lathyrus aureus*, *Lathyrus cilicicus*, *Lathyrus laxiflorus* subsp. *laxiflorus* ve *Lathyrus pratensis* türlerinin metanollü ekstraları ve hekzan, etil asetat, kloroform ve su fraksiyonlarının antimikrobiyal ve anti-enflamatuvar aktivitesi değerlendirilmiştir.

**Gereç ve Yöntemler:** Ekstrelerin ve fraksiyonların antimikrobiyal aktivitesi *Staphylococcus aureus* ATCC 29213, *Bacillus subtilis* ATCC 6633, *Escherichia coli* ATCC 25922, *Pseudomonas aeruginosa* ATCC 27853 ve *Candida albicans* ATCC 10231 suşlarına karşı değerlendirilmiştir. *In vitro* anti-enflamatuvar etki ise insan kırmızı kan hücresi kullanarak membran stabilizasyon yöntemi ile değerlendirilmiştir.

**Bulgular:** Etil asetatlı fraksiyonlar diğer ekstre ve fraksiyonlara göre daha yüksek antimikrobiyal aktivite, sulu fraksiyonlar ise diğer ekstre ve fraksiyonlara göre daha yüksek anti-enflamatuvar aktivite göstermiştir. Ayrıca, *L. pratensis*'in su fraksiyonu, standart olarak kullanılan asetilsalisilik asit ve diklofenak sodyumdan daha yüksek anti-enflamatuvar aktivite göstermiştir.

**Sonuç:** Elde edilen sonuçlara göre *Lathyrus* türlerinin ekstraları ve fraksiyonlarının membran stabilizasyon aktiviteye sahip olup, ve *in vivo* anti-enflamatuvar aktivite deneyleri için bir ön çalışma olabileceğini belirtmiştir.

**Anahtar kelimeler:** Anti-enflamatuvar aktivite, antimikrobiyal aktivite, insan kırmızı kan hücresi membran, *Lathyrus*

\*Correspondence: E-mail: gulcin.saltan@pharmacy.ankara.edu.tr, Phone: +90 312 203 30 88

Received: 13.02.2018, Accepted: 03.05.2018

©Turk J Pharm Sci, Published by Galenos Publishing House.

## INTRODUCTION

*Lathyrus* L. is one of the largest genera in the family Fabaceae, with about 160 species distributed worldwide.<sup>1</sup> Turkey has a rich diversity of the genus *Lathyrus*, with 65 species and 75 taxa.<sup>2</sup>

Secondary metabolites that have been found in plants, such as tannins, terpenoids, alkaloids, and flavonoids, have extensively different bioactive properties. Antibiotics are commonly used in fighting against bacterial infections and have been profoundly effective in terms of human health and quality of life since their invention.<sup>3</sup> However, because of the appearance of resistance to antibiotics and some toxic products that resulted due to their consumption in recent decades antibiotics have become less effective against certain illnesses. Therefore, antibacterial agents derived from natural sources have started to play a significant role in the prevention and treatment of infection diseases.<sup>4</sup> Plant extracts have become established as a source of many applications, including raw and processed food preservation, pharmaceuticals, alternative medicine, and natural therapies.<sup>5</sup>

Inflammation is a protective mechanism of living organisms against abnormal stimulation. It is a complex series of biochemical activities performed by the body in response to injury or abnormal stimulation caused by a physical, chemical, or biological agent. In general, generation of cytokines is considered to play a major role in inducing inflammatory process, and free radicals can propagate inflammation by stimulating release of proinflammatory cytokines such as interleukin-1 $\beta$ , interleukin-6, and tumor necrosis factor- $\alpha$ .<sup>6</sup> Drugs that are currently used for treatment of inflammatory conditions are nonsteroidal anti-inflammatory drugs (NSAIDs) and corticosteroids. NSAIDs inhibit the synthesis of prostaglandins and thromboxane inflammatory mediators by deactivating cyclooxygenase (COX), COX-1 and COX-2 enzymes. Some of these drugs such as aspirin, diclofenac, ketorolac, naproxen, and piroxicam have toxic effects such as risk of gastrointestinal bleeding.<sup>7,8</sup>

Moreover, the generation of oxygen free radicals is known to be involved in the development of the inflammatory process. These radicals are highly reactive molecules with an unpaired electron that can initiate radical chain reactions, leading to damage or destruction of the normal function of a living cell, and consequently causing many different diseases such as neurodegenerative disorders, cancer, cardiovascular diseases, atherosclerosis, diabetes, cataracts, and inflammation.<sup>9,10</sup> In addition, inflammation caused by oxidative stress is the origin of many human diseases.

The potential harmful effects of free radicals are usually controlled by endogenous antioxidant mechanisms present in the cells. These mechanisms include cellular enzymes such as superoxide dismutase, catalase, glutathione peroxidase, and other defensive mechanisms, involving antioxidants, such as ascorbic acid,  $\alpha$ -tocopherol, and glutathione. In biological systems antioxidant agents show their effects by different mechanisms including electron donation, metal ion chelation,

co-antioxidants, or by gene expression regulation.<sup>11,12</sup> Reactive oxygen species such as hydroxyl radicals, superoxide anions, and peroxy radicals cause cellular damage by destroying cellular biomolecules such as nucleic acids, proteins, carbohydrates, and lipids, which results in inflammation. Therefore, compounds with radical scavenging activities may be expected to have anti-inflammatory properties.<sup>13</sup> Current anti-inflammatory drugs essentially have become ineffective for long-term protection since they have unexpected side effects. Hence, new plants and herbal compounds with anti-inflammatory properties are investigated in order to discover more effective compounds and avoid the toxic effects of anti-inflammatory drugs.

Radical scavenging activities of phenolic and polyphenolic compounds, which are secondary metabolites in plants, were shown in previous studies. There are many studies on the anti-inflammatory activity of plant extracts and secondary metabolites such as flavonoids.<sup>14,15</sup>

The aim of the present study was to evaluate the total flavonoid contents and the antimicrobial and anti-inflammatory activities of methanol extracts and *n*-hexane, chloroform, ethyl acetate, and water fractions of the aerial parts of *Lathyrus armenus* (Boiss&Huet) Sirj, *Lathyrus aureus* (Stev.) Brandza, *Lathyrus cilicicus* Hayek&Siehe, *Lathyrus laxiflorus* (Desf.) O. Kuntze subsp. *laxiflorus*, and *Lathyrus pratensis* L. growing in Turkey. Among these species, *L. armenus* and *L. cilicicus* are endemic for Turkey. There are no previous reports dealing with the anti-inflammatory activities of the five examined *Lathyrus* species.

The study protocol was approved by the ethics committees of the Faculty of Medicine of Ankara University, Ankara, Turkey (26.10.2015/16-695-15).

## MATERIALS AND METHODS

### *Chemical material*

The solutions, acetylsalicylic acid, sodium chloride, and Mueller Hinton Broth were purchased from Merck (Germany), Sigma-Aldrich (USA), Riedel-de Haën (Germany), and Difco Laboratories (USA), respectively.

### *Instruments*

Absorbance was measured by SpectraMax 190 Microplate Reader (SpectraMax Molecular Devices Inc, USA); the centrifugation was carried out by Sigma 4K15 10740 and vortexing by Labinco L46 (Netherlands).

### *Plant material*

The aerial parts of *L. armenus*, *L. aureus*, *L. cilicicus*, *L. laxiflorus* subsp. *laxiflorus*, and *L. pratensis* were collected and identified by Dr. M. Tekin. Voucher specimens were deposited in Ankara University, Faculty of Pharmacy, Kamil Karamanoğlu Herbarium (AEF). Data for the collected species are given in Table 1.

### *Preparation of extracts*

The obtained plants were dried and powdered. Then 20 g of plant material was extracted separately with methanol using a Soxhlet apparatus over 24 h. The solvent was evaporated

under reduced pressure and dissolved in water and partitioned with *n*-hexane, chloroform, and ethyl acetate, in that order. All extracts were dried and stored at 4°C.

#### *In vitro* antibacterial and antifungal activity of *Lathyrus* species

Methanol extracts and *n*-hexane, chloroform, ethyl acetate, and water fractions from the aerial parts of five *Lathyrus* species were investigated for their potential *in vitro* antibacterial activities against *Staphylococcus aureus* ATCC 29213, *Bacillus subtilis* ATCC 6633, *Escherichia coli* ATCC 25922, and *Pseudomonas aeruginosa* ATCC 27853 and antifungal activity against *Candida albicans* ATCC 10231. Stock solution was prepared by dissolving 4 mg of the methanol crude extract and water fraction in 70% (*v/v*) methanol and in water, respectively, and chloroform, ethyl acetate, and *n*-hexane fractions in 20% (*v/v*) dimethyl sulfoxide. A broth dilution assay was used for determination of the minimum inhibitory concentration (MIC). The cultures were obtained in Mueller Hinton Broth; serial two-fold dilutions ranging from 1.000 to 0.0625 mg/mL were prepared in the medium. A series of tubes containing only inoculated broth were used as controls. After incubation for 18–24 h at 37±1°C for bacteria and 48 h for fungi, the last tube with no microbial growth was recorded to represent MIC value (mg/mL).<sup>16,17</sup>

#### Total flavonoid content

The extracts and fractions (2 mg/mL) were placed in a 3 mL test tube. Then distilled water was added to the test tube to make it up to 1.5 mL and then it was vortexed. After that, 0.075 mL of NaNO<sub>2</sub> 5% (*w/v*) was added, it was vortexed again, and then left for 5 min. Next, 0.15 mL of AlCl<sub>3</sub> 10% (*w/v*) was added to the tube. After 6 min, 0.5 mL of 1 M NaOH was added to the mixture. Then the final volume was made up to 3 mL with distilled water. This mixture was vortexed and the absorbance was measured against a blank at 510 nm. Quercetin was used as standard for the calibration curve. The flavonoid content was calculated by using the quercetin calibration equation.<sup>18</sup>

$$A=0.0245C-0.0417, r^2=0.9834$$

A: Absorbance

C: Flavonoid content (µg/mg)

#### Anti-inflammatory assay

##### Preparation of the human red blood cell suspension

Fresh whole blood was collected from healthy volunteers

**Table 1. Collection data of the examined *Lathyrus* species**

Species	Collection location	AEF no.
<i>Lathyrus armenus</i>	Sivas (M. Tekin 1278)	26680
<i>Lathyrus aureus</i>	Sivas (M. Tekin 1277)	26684
<i>Lathyrus cilicicus</i>	Karaman (M. Tekin 1210)	26681
<i>Lathyrus laxiflorus</i> subsp. <i>laxiflorus</i>	Sivas (M. Tekin 1274)	26682
<i>Lathyrus pratensis</i>	Sivas (M. Tekin 1273)	26683

who had not taken any anti-inflammatory or steroidal drug for 2 weeks before the experiment and it was transferred to centrifuge tubes. The tubes were subjected to centrifugation at 3000 rpm for 10 min. The supernatant part of the tubes was decanted and the precipitated part was washed three times with an equal volume of isosaline (0.85%, pH 7.2). The volume of the blood was measured and reconstituted as 10% *v/v* suspension with isosaline.

#### Heat-induced hemolysis

The reaction mixture (2 mL) consisted of 1 mL of test sample (methanol extract, water, ethyl acetate, chloroform, and *n*-hexane fractions) and 1 mL of 10% RBC suspension; instead of test sample only saline was added to the control test tube. Acetylsalicylic acid and diclofenac sodium were used as standard drugs. All the centrifuge tubes containing reaction mixture were incubated in a water bath at 56°C for 30 min. At the end of the incubation the tubes were cooled under running tap water. The reaction mixture was centrifuged at 2500 rpm for 5 min and the absorbance of the supernatants was measured at 560 nm. The experiment was performed in triplicate for all the test samples.<sup>19,20</sup>

The percentages of hemolysis and protection were calculated according to the following formula:

$$\text{Hemolysis\%} = (\text{Optical density of test sample} / \text{Optical density of control}) \times 100$$

$$\text{Protection\%} = 100 - [(\text{Optical density of test sample} / \text{Optical density of control}) \times 100]$$

## RESULTS

The antimicrobial activity of the methanol extracts and *n*-hexane, chloroform, ethyl acetate, and water fractions of *Lathyrus* species is shown in Table 2. The results indicated that the water and *n*-hexane fractions of *L. cilicicus* showed no activity against the tested microorganisms. Methanol extract was effective against *C. albicans* and the chloroform fraction was effective against *C. albicans* and *P. aeruginosa*. While the water fraction of *L. armenus* showed no activity, the methanol extract and *n*-hexane and chloroform fractions showed activity against *C. albicans*. The methanol extract and *n*-hexane and chloroform fractions of *L. laxiflorus* showed activity against *C. albicans*, and the water fraction of *L. laxiflorus* was found effective against *B. subtilis*. The methanol extract and *n*-hexane and chloroform fractions of *L. aureus* showed activity against *C. albicans*; additionally the water fraction of *L. aureus* was found effective against *B. subtilis*. The methanol extract of *L. pratensis* was effective against *C. albicans* and the chloroform fraction was effective against *C. albicans* and *P. aeruginosa*; additionally the water fraction of *L. pratensis* was found effective against *B. subtilis*. Ethyl acetate fractions of all studied *Lathyrus* species were effective against all tested microorganisms. The antimicrobial effect of the plant extracts against the microorganisms may have been due to the secondary metabolites content of these extracts, like phenolic compounds and saponin, which are reported to be antimicrobial.<sup>3</sup> There are

not many reports of research on the antibacterial screening of *Lathyrus* species. According to the literature, from butanolic extracts of *L. aphaca* seeds two triterpenoid saponins were isolated that showed antifungal activity against *Colletotrichum dematium* and *Alternaria alternata*.<sup>21</sup> Inhibition of growth of *Xanthomonas campestris* pv. citri by *L. odoratus* L. and *L. sativus* L. seed extracts was studied. While *L. odoratus* showed no

antibacterial activity, the mean inhibition zone of *L. sativus* seed extract was 1.16 mm.<sup>22</sup> The antifungal activity of ethanolic extract and dichloromethane and water fractions of *L. pratensis* was expressed as MICs against *C. albicans*, *Aspergillus fumigatus*, and *Aspergillus niger*.<sup>23</sup> Methanol and ethanol extracts of the leaf and body of *L. karsianus* showed antibacterial activity against *Klebsiella pneumoniae*, *P. aeruginosa*, *S. aureus*, *Staphylococcus epidermidis*, *Bacillus cereus*, *Salmonella enteritidis*, *Proteus mirabilis*, *E. coli*, and *Enterococcus faecalis*.<sup>24</sup> Butanolic extract of the seeds of *L. ratan* and *L. aphaca* was investigated for antibacterial screening. The maximum inhibition was shown by *L. ratan* against *S. aureus*. As reported *L. ratan* extract was more active than *L. aphaca*.<sup>25</sup> The antimicrobial activity of isolated anthocyanins and the ethanolic extract of *L. odoratus* were tested by disc diffusion assay against *S. aureus*, *E. coli*, *Bacillus subtilis*, *Aspergillus niger*, and *C. albicans*.<sup>26</sup>

In the study by Heydari et al.,<sup>27</sup> the antioxidant activities of these species were investigated by DPPH radical scavenging. In that study, different extracts of *Lathyrus* species exhibited significant free radical scavenging activity. The highest antioxidant activity was seen in *L. laxiflorus* subsp. *laxiflorus*. As seen in Table 3, *L. laxiflorus* subsp. *laxiflorus* and *L. pratensis* have the highest contents of flavonoids. Recent studies showed that flavonoids possess antioxidant, anti-inflammatory, antinociceptive, and cytostatic properties due to their effects on the prostaglandin pathway.<sup>28</sup> Therefore, they are effective in reducing oxidative stress and acute inflammation. The human red blood cell (HRBC) membrane is analogous to the lysosomal membrane. Therefore, HRBC membrane stabilization has been used as a method to study *in vitro* anti-inflammatory effects.<sup>29</sup> During inflammation neutrophils and monocytes are impaired or destroyed, resulting in release of lysosomal enzymes.<sup>30</sup> Stabilization of the membrane suggests that the extracts might stabilize lysosomal membranes. Most anti-inflammatory drugs show their effects either by stabilizing the lysosomal membranes or inhibiting lysosomal enzymes. Moreover, several studies indicate that herbal products and plants could be effective in stabilizing the red blood cell membrane against hypotonicity, heat, or chemicals.<sup>31</sup> Therefore, stabilization of the HRBC membrane was studied for further establishing the mechanism of the anti-inflammatory action of different extracts and fractions of *Lathyrus* species. The anti-inflammatory activity of the methanol extracts and *n*-hexane, chloroform, ethyl acetate, and water

**Table 2. MIC values (mg/mL) of the examined *Lathyrus* species against the tested microorganisms**

Extracts	MIC (mg/mL)	Microorganisms				
		<i>Staphylococcus aureus</i> ATCC 29213	<i>Bacillus subtilis</i> ATCC 6633	<i>Escherichia coli</i> ATCC 25922	<i>Pseudomonas aeruginosa</i> ATCC 27853	<i>Candida albicans</i> ATCC 10231
<i>Lathyrus armenus</i>	Chloroform	-	-	-	-	0.5
	<i>n</i> -Hexane	-	-	-	-	1
	Water	-	-	-	-	-
	Ethyl acetate	0.5	0.5	0.5	0.5	0.5
	Methanol	-	-	-	-	1
<i>Lathyrus aureus</i>	Chloroform	-	-	-	-	0.5
	<i>n</i> -Hexane	-	-	-	-	1
	Water	-	1	-	-	-
	Ethyl acetate	1	0.5	0.5	0.5	0.5
	Methanol	-	-	-	-	1
<i>Lathyrus cilicicus</i>	Chloroform	-	-	-	1	0.5
	<i>n</i> -Hexane	-	-	-	-	-
	Water	-	-	-	-	-
	Ethyl acetate	1	0.5	0.5	0.5	0.5
	Methanol	-	-	-	-	1
<i>Lathyrus laxiflorus</i> subsp. <i>laxiflorus</i>	Chloroform	-	-	-	-	0.5
	<i>n</i> -Hexane	-	-	-	-	1
	Water	-	1	-	-	-
	Ethyl acetate	1	0.5	0.5	1	0.25
	Methanol	-	-	-	-	1
<i>Lathyrus pratensis</i>	Chloroform	-	-	-	1	0.5
	<i>n</i> -Hexane	-	-	-	-	1
	Water	-	1	-	-	-
	Ethyl acetate	0.5	0.5	0.5	0.5	0.5
	Methanol	-	-	-	-	1

-: No activity, MIC: Minimum inhibitory concentration

**Table 3. Total flavonoid contents of methanolic extracts of the examined *Lathyrus* species**

Species	$\mu\text{g}_{\text{Quercetin}}/\text{mg}_{\text{extracts}} \pm$ standard deviation
<i>Lathyrus armenus</i>	55.6±0.75
<i>Lathyrus aureus</i>	90.9±0.84
<i>Lathyrus cilicicus</i>	36.2±1.32
<i>Lathyrus laxiflorus</i> subsp. <i>laxiflorus</i>	105.4±2.38
<i>Lathyrus pratensis</i>	105.3±2.68

Each value represents mean ± standard deviation



fractions of *Lathyrus* species was investigated using HRBC membrane stabilization. Most of the extracts and fractions at a concentration of 2 mg/mL showed protective effects on human erythrocyte membranes against lysis induced by heat as shown in Table 4. In comparison to the other fractions and extracts, water fractions showed higher activity. Furthermore, the maximum membrane stabilization effect was observed for

the water fraction of *L. pratensis* (88%) among all the extracts, followed by *L. laxiflorus* (86%), methanol extract of *L. laxiflorus*, *L. armenus* (83%), and *L. aureus* (81%). Methanol extract of *L. laxiflorus* showed the maximum membrane stabilization effect (82%) among the methanol extracts. Acetylsalicylic acid and diclofenac sodium were used as standard drugs and showed almost 87% protection at a concentration of 2 mg/mL.

**Table 4. Protection and hemolysis percentage of the examined *Lathyrus* species on the human red blood cell (HRBC) membrane stability method**

Extracts	Human red blood cell		
	Hemolysis %	Protection %	
	Concentration (2 mg/mL)		
Control (distilled water)	100	-	
Control (isosaline)	100	-	
<i>Lathyrus armenus</i>	Chloroform	87.85±0.004*	12.14*
	<i>n</i> -Hexane	99.85±0.005	0.14
	Water	17.20±0.006*	82.79*
	Ethyl acetate	24.65±0.004*	75.34*
	Methanol	43.23±0.001*	56.76*
<i>Lathyrus aureus</i>	Chloroform	74.47±0.017*	25.52*
	<i>n</i> -Hexane	86.84±0.002*	13.15*
	Water	19.16±0.002*	80.83*
	Ethyl acetate	23.86±0.009*	76.13*
	Methanol	38.03±0.005*	61.96*
<i>Lathyrus cilicicus</i>	Chloroform	62.40±0.003*	37.59*
	<i>n</i> -Hexane	97.90±0.022	2.09
	Water	18.72±0.004*	81.27*
	Ethyl acetate	22.41±0.005*	77.58*
	Methanol	27.62±0.003*	72.37*
<i>Lathyrus laxiflorus</i> subsp. <i>laxiflorus</i>	Chloroform	75.05±0.003*	24.94*
	<i>n</i> -Hexane	91.03±0.003*	8.96*
	Water	14.09±0.004*	85.90*
	Ethyl acetate	21.25±0.006*	78.74*
	Methanol	17.64±0.003*	82.35*
<i>Lathyrus pratensis</i>	Chloroform	97.68±0.014	2.313
	<i>n</i> -Hexane	99.78±0.001	0.216
	Water	12.07±0.004*	87.92*
	Ethyl acetate	18.72±0.004*	81.27*
	Methanol	30.22±0.003*	69.77*
Acetylsalicylic acid	12.74±0.37*	87.25±0.37*	
Diclofenac sodium	12.14±0.02*	87.85±0.02*	

Each value represents mean ± standard deviation

\*Statistically significant as compared to controls, p<0.05 (one-way ANOVA).

## DISCUSSION

Most *Lathyrus* species are consumed as a food by animals and humans. In spite of this, there is not enough biological activity research on *Lathyrus* taxa. The aim of our study was to investigate the antimicrobial and anti-inflammatory activities of *L. armenus*, *L. aureus*, *L. cilicicus*, *L. laxiflorus* subsp. *laxiflorus*, and *L. pratensis*. According to the results, ethyl acetate fractions were more effective than the other extracts and fractions against the test microorganisms. Our results also revealed that different extracts and fractions of the examined *Lathyrus* species possessed anti-inflammatory properties. The methanol extracts and water fractions exhibited membrane stabilization by inhibiting heat-induced lysis of the erythrocyte membrane more than the others. The water fraction of *L. pratensis* showed the maximum activity (almost equal to the standard drugs) among all of the fractions of the examined *Lathyrus* species.

## CONCLUSIONS

*Lathyrus* species are consumed as a food by animals and humans, but there is not enough biological activity research about *Lathyrus*. Thus the aim of this study was to investigate the antimicrobial and anti-inflammatory activities of *Lathyrus* species, two of which are endemic for Turkey. According to the results ethyl acetate fractions were more effective than the other extracts and fractions against gram-positive and gram-negative bacteria and fungi. Our results also revealed that different extracts and fractions of *Lathyrus* species possessed anti-inflammatory properties. The methanol extracts and water fractions exhibited membrane stabilization by inhibiting heat-induced lysis of the erythrocyte membrane more than the others. The water fraction of *L. pratensis* showed the maximum activity (almost equal to the standard drugs) among all of the fractions. In conclusion, these experimental results indicate that the membrane stabilizing effect of the various extracts and fractions of the *Lathyrus* species is primarily due to the active phytoconstituents (i.e., flavonoids) in the plant, which seems to support the use of this plant in traditional medicine. In this regard, isolation from *Lathyrus* species is proceeding simultaneously in our laboratory. To the best of our knowledge, this is the first study evaluating the membrane stabilizing activity of *Lathyrus* species growing in Sivas, Turkey. However, further studies are needed to evaluate the exact mechanism and responsible substances of these activities.

*Conflict of Interest:* No conflict of interest was declared by the authors.

## REFERENCES

1. Lewis GP, Schrire B, Mackinder B, Lock M. Legumes of the World. Edinb J Bot. 2005;3:195-196.
2. Davis PH. Flora of Turkey and the East Aegean Islands. Edinburgh University Press; Edinburgh;1970:325-354.
3. Cowan MM. Plant products as antimicrobial agents. Clin Microbiol Rev. 1999;12:564-582.
4. Bhalodia NR, Shukla V. Antibacterial and antifungal activities from leaf extracts of *Cassia fistula* L.: An ethnomedicinal plant. J Adv Pharm Technol Res. 2011;2:104-109.
5. Hammer KA, Carson C, Riley T: Antimicrobial activity of essential oils and other plant extracts. J Appl Microbiol. 1999;86:985-990.
6. Libby P. Inflammatory mechanisms: the molecular basis of inflammation and disease. Nutr Rev. 2007;65:140-146.
7. Dinarello CA. Anti-inflammatory agents: present and future. Cell. 2010;140:935-950
8. Singh R, Patil S, Pal G and Ahmad M. Evaluation of *in vivo* and *in vitro* anti-inflammatory activity of *Ajuga bracteosa* Wall ex Benth. Asian Pac J Trop Dis. 2012;2:404-407.
9. Aruoma OI. Free radicals, oxidative stress and antioxidants in human health and disease. J Am Oil Chem Soc. 1998;75:199-212.
10. Kris-etherton PM, Lefevre M, Beecher GR. Bioactive compounds in nutrition and health-research methodologies for establishing biological function. the antioxidant and anti-inflammatory effects of flavonoids on atherosclerosis. Annu Rev Nutr. 2004;24:511-538.
11. Choei HR, Choi JS, Han YN, Bae SJ, Chung HY. Peroxynitrite scavenging activity of herb extracts. Phytother Res. 2002;16:364-367.
12. Lobo V, Patil A, Phatak A, Chandra N. Free radicals, antioxidants and functional foods: Impact on human health. Pharmacogn Rev. 2010;4:118-126.
13. Cui XY, Kim JH, Zhao X, Chen BQ, Lee BC, Pyo HB, Yun YP, Zhang YH. Antioxidative and acute anti-inflammatory effects of *Campsis grandiflora* flower. J Ethnopharmacol. 2006;103:223-228.
14. Kim SH, Song YS, Kim SK, Kim BC, Lim CJ, Park EH. Anti-inflammatory and related pharmacological activities of the n-BuOH subfraction of mushroom *Phellinus linteus*. J Ethnopharmacol. 2004;93:141-146.
15. Nagaharika Y, Rasheed S. Anti-inflammatory activity of leaves of *Jatropha gossypifolia* L. by HRBC membrane stabilization method. J Acute Dis. 2013;2:156-158
16. Ferraro MJ, Swenson JM. Methods for dilution antimicrobial susceptibility tests for bacteria that grow aerobically, Approved standard, (8th ed). Clinical and Laboratory Standards Institute. 2009;29:15-18.
17. Karunai Raj M, Balachandran C, Duralpandiyan V, Agastian P, Ignacimuthu S. Antimicrobial activity of Ulopterol isolated from *Toddalia asiatica* (L.) Lam: A traditional medicinal plant. J Ethnopharmacol. 2012;140:161-165
18. Bag GC, Grihanjali P, Bhaigyabati TH. Assessment of total flavonoid content and antioxidant activity of methanolic rhizome extract of three *Hedychium* species of manipur valley. Int J Pharm Sci Rev Res. 2015;30:154-159.
19. Sakat S, Juvekar AR, Gambhire MN. *In vitro* antioxidant and anti-inflammatory activity of methanol extract of *Oxalis corniculata* Linn. Int J Pharm Pharm Sci. 2010;2:146-155.
20. Shinde U, Phadke A, Nair A, Mungantiwar A, Dikshit V, Saraf M. Membrane stabilizing activity a possible mechanism of action for the anti-inflammatory activity of *Cedrus deodara* wood oil. Fitoterapia. 1999;70:251-257.
21. Khan NA. Two antifungal active triterpenoid saponins from the seeds of *Lathyrus plants*. Nat Prod Res. 2011;25:1687-1694.
22. Aktar MA, Rahber-Bhatti M, Aslam M. Antibacterial activity of plant diffusate against *Xanthomonas campestris* pv. citri. Int Pest Manage. 1997;43:149-153.
23. Arabi Z, Sardari S. An investigation into the antifungal property of *Fabaceae* using bioinformatics tools. Avicenna J Med Biotechnol. 2010;2:93-100.
24. Özkan OA, Adıgüzel MC, Erdağ D, Bağcıgil AF and Aydın H. *In Vitro* comparison of the antibacterial activity of extracts from endemic plants species. J Ayu Med Sci. 2014;4:1608-1614.
25. Khan NA, Quereshi S, Pandey A and Srivastava A. Antibacterial Activity of Seed Extracts of Commercial and Wild *Lathyrus* Species. Turkish J Biol. 2009;33:165-169.
26. Mohamed S. Anthocyanins and fatty acids from the flowers of *Lathyrus odoratus* L. and their antimicrobial activity. Planta Med. 2009;75:175.
27. Heydari H, Saltan GS, Acikara ÖB, Yilmaz S, Çoban T, Tekin M. Antioxidant Activity of five *Lathyrus* species growing in Turkey. Turk J Pharm Sci. 2015;12:369-376.
28. Diniz TC, Silva JC, De Lima-Saraiva SR, Ribeiro FP, Pacheco AG, De Freitas RM, Quintans-Junior LJ, Quintans JDES, Mendes RL, Almeida JR. The role of flavonoids on oxidative stress in epilepsy. Oxid Med Cell Longev. 2015;2015:1-9.
29. Anosike CA, Obidoa O, Ezeanyika LU. Membrane stabilization as a mechanism of the anti-inflammatory activity of methanol extract of garden egg. DARU. 2012;20:76-83.
30. Barkley JR, Myers CM. Practice Guidelines for acute Care Nurse Practitioners, (2nd ed). USA; Saunders Elsevier Health Sciences; 2007:50.
31. Mariappan G, Saha BP, Sutharson L, Singh A, Garg S, Pandey L, and Kumar D. Analgesic, anti-inflammatory, antipyretic and toxicological evaluation of some newer 3-methyl pyrazolone derivatives. Saudi Pharm J. 2011;19:115-122.



# Phytotherapy as a Complementary Medicine for Multiple Sclerosis

## Multipl Sklerozda Tamamlayıcı Tedavi Olarak Fitoterapi

© Zahra RABIEI\*

Shahrekord University of Medical Sciences, Basic Health Sciences Institute, Medical Plants Research Center, Shahrekord, Iran

### ABSTRACT

Multiple sclerosis (MS) is the most common cause of neurologic disability in adults worldwide. Two main issues have caused MS patients to face several problems. One issue is that the definite cause of MS has not yet been determined and the other issue is the lack of a definite treatment for this disease. The people with MS, therefore, seek out complementary and alternative medications to manage the symptoms of this disease. Meanwhile, medicinal plants have been demonstrated to have possible positive pharmacological effects in treating MS in different models. The reliable articles indexed in the databases *Web of Science*, *Scopus*, *PubMed Central*, *PubMed*, *Scientific Information Database*, and *Institute for Scientific Information* were retrieved and analyzed to conduct this review. Medicinal plants and plant compounds caused decreases in the neurologic deficits due to MS. Clinical evidence has demonstrated the clinical potential of *Cannabis sativa* extract, cannabinoids, *Ginkgo biloba*, beta-phytosterol, and *Lippia citriodora* extract to improve MS symptoms. These plants and compounds can also improve spasticity, muscle spasm, neuropathic pain, and urinary tract complications in at least some of these patients. Nanocurcumins and *Punica granatum* L. peel extract have exhibited positive effects in animal models and can decrease neurologic deficits by reducing inflammation. Medicinal plants and their compounds can serve as new sources of MS drugs because they can improve MS symptoms.

**Key words:** Multiple sclerosis, phytotherapy, medicinal plants

### ÖZ

Multipl skleroz (MS), dünya çapında yetişkinlerde en sık görülen nörolojik problemdir. MS hastalarının pek çok sorunla karşı karşıya kalmasına neden olan iki ana sorun bulunmaktadır. İlk sorun, MS'in kesin nedeninin henüz belirlenmemiş olmasıdır. Diğer problem ise bu hastalık için kesin bir tedavinin olmayışıdır. Bu nedenle, MS'li hastalar, bu hastalığın semptomlarını giderebilmek için tamamlayıcı ve alternatif tedavi arayışındadırlar. Aynı zamanda, tıbbi bitkilerin, MS'in farklı modellerde tedavisinde olası olumlu farmakolojik etkilere sahip olduğu gösterilmiştir. Bu derlemenin hazırlanmasında, *Web of Science*, *Scopus*, *PubMed Central*, *PubMed*, *Scientific Information Database* ve *Institute for Scientific Information* gibi veri tabanlarında indekslenen güvenilir makalelere başvurulmuş ve değerlendirilmiştir. Tıbbi bitkiler ve bitkisel bileşikler, MS kaynaklı nörolojik problemlerin azalmasını sağlamıştır. Klinik çalışmalar, MS semptomlarını iyileştirmek için *Cannabis sativa* ekstresi, kannabinoidler, *Ginkgo biloba*, beta-fitosterol ve *Lippia citriodora* ekstresinin klinik potansiyelini ortaya koymuştur. Bu bitkiler ve bileşikler, bu hastaların en azından bazılarında spastisite, kas spazmı, nöropatik ağrı ve idrar yolu komplikasyonlarını iyileştirebilmektedir. Nanokurkuminler ve *Punica granatum* L. kabuğu ekstresi, hayvan modelleri üzerinde olumlu etkiler göstermiş ve inflamasyonu azaltarak nörolojik bozuklukları azaltmıştır. Tıbbi bitkiler ve bunların bileşikleri, MS semptomlarını iyileştirebildikleri için yeni MS ilaç kaynakları olarak kullanılabilir.

**Anahtar kelimeler:** Multipl skleroz, fitoterapi, tıbbi bitkiler

### INTRODUCTION

Multiple sclerosis (MS) is an inflammatory, central nervous system (CNS)-demyelinating disease that is characterized by autoimmune presentations. In MS, the immune system is stimulated for unknown reasons and specific lymphocytes against myelin are activated.<sup>1</sup> The entry of these cells into the brain plays a role in the immunopathology of MS and the exacerbation of the inflammatory responses in the brain. MS is 2-3 times more prevalent in women than in men and often occurs in the age range of 20 to 40 years.<sup>1</sup> The most important

symptoms of MS include motor paralysis, sensory degeneration, visual impairment, and cognitive impairment. No definite treatment for MS has yet been offered and certain drugs are available only to improve disease symptoms and slow down its progression.<sup>2</sup>

Although people with MS have life spans similar to those of others, they experience major changes due to changes in the quality of their lives.<sup>3</sup> The treatments of choice for MS include conventional treatments such as beta-interferon and complementary and alternative therapies. Alternative therapies

\*Correspondence: E-mail: zahrarabiei@gmail.com, Phone: +989132815431 ORCID-ID: orcid.org/0000-0003-0129-3581

Received: 10.04.2018, Accepted: 06.09.2018

©Turk J Pharm Sci, Published by Galenos Publishing House.

are increasingly being welcome day by day such that one out of every three people is projected to use these treatments during his/her lifespan for common diseases such as back pain, headache, anxiety, and depression.<sup>4</sup> The use of complementary and alternative medicine to treat chronic diseases such as Parkinson disease, epilepsy, and cancer has raised the potential of these therapies to treat MS. Although the conventional treatment for MS can help to decrease the frequencies of relapses and the severity of the disease and also slow down its progression,<sup>5</sup> it is only partly effective to treat symptoms and improve functioning and quality of life. Patients, therefore, often seek out various other ways to treat MS.

Alternative medicine or complementary medicine refers to different approaches to treat or prevent diseases whose protocols or efficacies are different from those of conventional or biological approaches. These approaches include exercise, meditation, medical nutrition therapy and phytotherapy, energy therapy and relaxation, acupuncture, and pressure medicine.<sup>6</sup>

Recent studies have shown promising results regarding the effects of medicinal plants to treat or prevent different diseases including Alzheimer disease,<sup>7,8</sup> stroke,<sup>9,10</sup> depression,<sup>11,12</sup> and drug abuse.<sup>13</sup>

In the study by Giveon et al.<sup>14</sup> with 150 physicians, 68% of the physicians reported that 15% of their patients used complementary medicine and 40% conjectured that 10% of patients used medicinal plants in treating diseases.

### *Pathogenesis of MS*

In MS, acute inflammation, which is accompanied by demyelination, acts as a strong stimulus to mobilize the oligodendrocyte precursor cells. Suppressing inflammatory responses can lead to defective repair. Perhaps one reason for the impairment of remyelination in patients is that they are treated with anti-inflammatory drugs such as corticosteroids. When inflammation is suppressed, remyelination remains incomplete and demyelination becomes chronic.<sup>1</sup>

The etiology of MS is still unknown and it is argued that a combination of genetics and environmental factors may lead to the onset of MS. Genetically, MS is most associated with the human leukocyte antigen located on chromosome 6.<sup>15</sup>

MS is an autoimmune disease of the CNS. The most important protein components of the myelin that target the immune system include myelin basic protein, myelin-associated glycoprotein, protein proteolipid protein, and myelin oligodendrocyte glycoprotein.<sup>16</sup>

The roles of different components of the immune system in the occurrence of MS have been studied. The resident microglia and macrophages of the CNS are involved in exerting phagocytotic activities, donating antigen, and producing cytokines. The macrophages and microglia contribute to demyelinating nerves and phagocytosing myelin by producing inflammatory cytokines and myeloperoxidase.<sup>17</sup>

The number of mast cells in the CNS is low in normal conditions but increases in the platelets and inflammatory lesions in MS. Regulated on activation, normal T cell expressed

and secreted is a potential absorbent of the mast cells that increases in the cerebrospinal fluid (CSF) of MS patients. Mast cell proteases such as tryptase and chymase activate matrix metalloproteinases (MMPs) and mast cells can produce MMP9 and MMP2. The MMPs can contribute to degenerating tissues such as the blood-brain barrier (BBB).<sup>16</sup>

The number of dendritic cells that act as antigen-donating cells is very low in the CNS in normal conditions but increases in the peripheral blood and CSF in patients with MS.<sup>17</sup>

Certain subgroups of natural killer (NK) cells contribute to regulating the immune system in MS. It has been reported that NK cells in patients with relapse-remitting MS express greater amounts of Fas (CD95) and also secrete the cytokines of T helper 2 (Th2) cells such as interleukin 5 (IL-5) and IL-13. In the immune system, the Th cells are classified into different subgroups depending on the pattern of the produced cytokines, including Th2, Th1, Th17, Th9, and Th22. The other subgroup of T cells, known as regulatory T cells (Tregs), are also essential to maintain self-tolerance.<sup>18</sup>

Th1 lymphocytes produce certain cytokines such as IL-2 tumor necrosis factor (TNF)- $\alpha$ , TNF- $\delta$ , and granulocyte-macrophage colony-stimulating factor (GM-CSF) and play important roles in increasing delayed sensitivity and defense against intracellular pathogens. The differentiation of Th1 cells from naïve T cells depends on interferon (IFN) and IL-12 that express the T-bet factor, which is indeed the specific patterning factor of Th1 cells, by activating the signal transducers STAT-1 and then STAT-4. The T-bet factor leads to production of Th1 cytokines, especially IFN- $\delta$ , and therefore strengthens the differentiation of Th cells via developing a positive feedback ring. Meanwhile, the T-bet factor also leads to suppression of differentiation of other Th cell subgroups. IFN- $\delta$  is the most important cytokine of Th1 cells and leads to an increase in toll-like receptor expression, induction of immunoglobulin production, increase in phagocytosis, major histocompatibility complex classes I and II molecules, and alienation as well as activation of macrophages.<sup>19</sup>

Th17 cells produce a variety of cytokines, such as IL-17a, IL-17F, IL-6, IL-9, IL-21, IL-22, IL-23, TNF- $\alpha$ , GM-CSF, and IL-26. However, IL-17A is a specific cytokine of these cells. In humans, the effects of IL-17 in demyelinating nerve cells in MS patients have been demonstrated, and MS exacerbation is associated with an increase in the number of Th17 cells in the patients' blood. During the development of experimental autoimmune encephalomyelitis (EAE), Th17 cell infiltration occurs in the brain before the onset of clinical symptoms, while a significant Th1 cell infiltration occurs after the development of EAE.<sup>20</sup> The purpose of this article is to review the findings of the studies with animal models as well as clinical trials on the effects of medicinal plants and their compounds on MS (Table 1).

## **DISCUSSION**

The use of medicinal plants has long been on the rise and the evidence indicates that this trend will predictably persist. The use of medicinal plants is more common in patients at risk

Table 1. Medicinal herbs and plant compounds affecting MS

The name of plant or compound	Concentration	Study design and subjects	Properties	Reference
<i>Cannabis sativa</i>	Oral use of <i>Cannabis sativa</i> extract 5-25 mg daily for 10 weeks	Double-blind, placebo-controlled clinical trial	Relaxation of stiff muscles after 4, 8, and 12 weeks of treatment compared to the placebo group	21
Delta-9 THC and CBD	Oral use of THC with CBD spray at 2.5 mg/spray for 8 weeks	Clinical trial Open-label pilot study	Reducing urinary urgency, urination frequency and urine volume, urinary incontinence and night time urination frequency after treatment; Decreasing daily total body weight, reducing catheterization and urinary incontinence; Relieving pain and improving muscle stiffness and the quality of sleep	22
<i>Cannabis sativa</i>	Aerial parts, ethanol extract, intraperitoneal administration of $\Delta$ THC-rich9 extract at 50 mg/kg and CBD-rich extract at 50 mg/kg	Experimental study with mouse model of autoimmune encephalomyelitis (acute and chronic phase)	Reducing neurologic deficits after administration with $\Delta$ THC-rich9 extract	23
<i>Cannabis sativa</i>	Capsule containing 2.5 mg THC and 0.9 mg CBD	Clinical trial; Double-blind, randomized design placebo controlled crossover; 57 patients, administration for 14 days	Improving spasm frequency, movement	24
Sativex	Sativex used as inhaled containing 2.7 mg THC and 2.5 mg CBD/spray puff	Double-blind, placebo-controlled clinical trial	160 patients Decreasing muscle spasm	25
$\beta$ -SIT	1, 4, 16, 32 $\mu$ M	Clinical trial, 11 female patients and 7 controls aged 18-65 years	$\beta$ -sitosterol at 4 $\mu$ M causes decrease in the release of TNF- $\alpha$ and at 4 and 16 $\mu$ M causes decrease in the release of IL-12 in the PBMCs of multiple sclerosis patients	26
Curcumin (polymerized nano-curcumin)	Intraperitoneal administration of polymerized nano-curcumin at 12.5 mg/kg	Animal model of EAE, Female Lewis rats	Decreasing neurologic deficits, demyelination, inflammation, blood-brain barrier permeability, oxidative stress; Improving remyelination Increasing the precursor of cell marker	27
<i>Lipia citriadora</i> (lemon verbena)	Extract at 600 mg/day PLX capsules containing 10% verbascoside w/w administered for 28 days	Clinical trial; Double-blind, placebo-controlled 30 patients	Decreasing C-reactive protein, IFN- $\gamma$ levels, IL-12 levels, IL-4 and IL-10 levels	28
<i>Capparis ovata</i>	Butanol fraction of hydroalcoholic extract	<i>In vitro</i> study with SH-SY5Y cell line	Inhibiting the expression of the genes below in cell lines: TNF- $\alpha$ , NF- $\kappa$ B1; GFAP, CXCL10, PTPN11	29
Pomegranate peel extract	Ethanol extract, intraperitoneal administration at 100 mg/kg for 8 days	<i>In vitro</i> study with female DA rat model of EAE	Inhibiting the production of IL-17 in the GALT cell line; Decreasing the production of IL-17 in the activated T cell of an animal model of EAE	30
<i>Ginkgo biloba</i>	120 mg/day for 8 weeks	Open study, 30 patients; Wechsler Memory Scale Beck Depression Inventory and the MSIS-29	Improving the scores on Wechsler Memory Scale and MSIS-29	31

Table 1. Continued

The name of plant or compound	Concentration	Study design and subjects	Properties	Reference
<i>Boswellia papyrifera</i>	Receiving two <i>Boswellia papyrifera</i> capsules (300 g) per day for 2 months	Randomized, double-blind clinical trial with 80 patients using Brief International Cognitive Assessment for MS	Improving spatial memory; Not influencing verbal memory and information processing speed	32
<i>Crocus sativus</i> L.	Receiving ethanol extract (500 mg/kg) by gavage for 21 days	Experimental study with C57BL/6 mouse model of EAE	Inhibiting leukocyte infiltration into the CNS and oxidative stress	33
<i>Pterodon emarginatus</i> seeds	Oral use of essential oil (50 and 100 mg/kg)	Mouse model of EAE	Decreasing neurologic deficits Inhibiting immune response by Th1 cell, axonal demyelination and neuronal death; Regulating Treg response <i>in vitro</i> Activating microglia and expressing iNOS	34
Oleanolic acid	Intraperitoneal administration at 50 mg/kg for 21-24 days	C57BL/J6 mice model of EAE	Improving the symptoms of neurologic deficits Decreasing blood-brain barrier permeability; Low inflammatory cell infiltration into the CNS; Playing a molecular role in Th1/Th2 polarization Inhibiting anti-inflammatory and chemical cytokines; Stimulating its anti-inflammatory effect	35

THC: Tetrahydrocannabinol, CBD: Cannabidiol, SIT:  $\beta$ -sitosterol, TNF: Tumor nuclear factor, IL: Interleukin, PBMC: Peripheral blood mononuclear cell, EAE: Experimental autoimmune encephalomyelitis, IFN: Interferon, NF- $\kappa$ B: Nuclear factor kappa B, GFAP: Glial fibrillary acidic protein, CXCL10: C-X-C motif chemokine 10, PTPN11: Tyrosine-protein phosphatase nonreceptor type 11, GALT: Gut-associated lymphoid tissue, MSIS-29: Multiple sclerosis impact scale-29, MS: Multiple sclerosis, CNS: Central nervous system, iNOS: Inducible nitric oxide synthase

than in healthy people. Due to the lack of strong evidence to support the effectiveness of the available treatments, the use of medicinal plants continues to increase in frequency. Despite the lack of controlled studies, there is a partial yet confirmed association between the dosage and the efficacy of medicinal plants.<sup>36</sup>

We conducted the current review to investigate the results of studies with animals and humans regarding the effects of medicinal plants and plant compounds on treatment of MS.

Most studies have been conducted with *Cannabis sativa* and its compounds. *C. sativa* has been used for several pharmaceutical purposes for 4000 years, but the structure and the properties of its compounds, such as cannabinoid, have been identified only in the last few years. To date, two cannabinoid receptors, CB1 and CB2, have been cloned. Endocannabinoids are metabolized by an amino acid called fatty acid amide hydrolase and mono-glyceride lipase.<sup>37</sup>

The endocannabinoid system is currently the therapeutic target for treating many diseases, including MS. Clinical evidence confirms the therapeutic potential of cannabinoids to treat MS symptoms.<sup>25</sup> Numerous studies have been conducted to investigate the effects of cannabinoids in MS treatment, suggesting that they may yield improvements in spasticity, muscle spasm, neuropathic pain, and urinary tract complications in at least some patients. These studies are not longitudinal, with treatments of over 10 to 15 weeks.<sup>22,38,39</sup>

It is estimated that over 80% of MS patients suffer from spasticity. Oral antispasmodics such as baclofen and benzodiazepines often

fail to control these symptoms and therefore new, effective, and safe drugs are required.<sup>40,41</sup> Nabiximols is a cannabinoid-based oral drug that is composed of tetrahydrocannabinol (THC) and cannabidiol (CBD) at a ratio of approximately 1:1 (2.7 mg THC and 2.5 mg CBD/100 mL).<sup>42</sup> Several randomized clinical trials have shown the efficacy of this drug in reducing limb spasticity and pain in MS patients.<sup>25,43-46</sup>

Studies showed that  $\beta$ -sitosterol and lemon verbena reduced the secretion of IL-12 and TNF- $\alpha$  in the peripheral blood mononuclear cells of MS patients.<sup>26,28</sup> Phytosterols and lemon verbena can affect the signaling pathways in tumor cells, including the stimulation of apoptotic pathways and the sphingomyelin cycle as well as the inhibition of prostaglandin release from macrophages in the culture medium. Therefore, a possible mechanism of these can be influencing certain signaling pathways that regulate the synthesis and release of cytokines.<sup>26,28</sup>

Based on preliminary research on cell cultures and animal models, pilot and clinical studies suggest that curcumin may be a therapeutic agent in several inflammatory diseases associated with Th17 cells such as MS, Alzheimer disease, Parkinson disease, inflammatory bowel disease, and rheumatoid arthritis. Curcumin, as an inhibitor of nuclear factor kappa B, is effective in preventing BBB breakdown caused by Th17 cells by influencing ZO-1 expression, inhibiting myosin light chain phosphorylation, and eliminating reactive oxygen species.<sup>47</sup>

Cognitive changes represent a major problem among MS patients that can simultaneously be more influential than the physical disabilities due to this disease. Ginkgo treatment for

8 weeks caused a significant improvement according to the Wechsler Intelligence Test.<sup>31</sup>

*Punica granatum* peel extract exerts significant immune effects that lead to prevention or treatment of EAE or streptozotocin-induced type 1 diabetes. This extract effectively inhibits the production of IL-17 in certain lymphatic tissues and also Th17 in the immune system.<sup>30</sup>

Cognitive impairments represent one of the most important disorders among MS patients, with a 43-70% prevalence rate.<sup>48</sup> *Boswellia papyrifera* can significantly improve the spatial memory of MS patients. Two studies have separately attributed the improving effects of *B. papyrifera* and *Crocus sativus* L. to their antioxidant properties.<sup>32,33</sup>

## CONCLUSIONS

Taken together, phytotherapy is a useful approach to decrease MS symptoms and leads to reduction of fatigue, pain, and stress in MS patients. However, physicians and neurologists are recommended to gain certain information about complementary and alternative therapies and to assess the patients' experiences by discussing this area with them.

## ACKNOWLEDGEMENT

This study was funded by the Research and Technology Deputy of Shahrekord University of Medical Sciences.

*Conflicts of Interest: No conflict of interest was declared by the authors.*

## REFERENCES

- Franklin RJ. Why does remyelination fail in multiple sclerosis? *Nat Rev Neurosci.* 2002;3:705-714.
- McQualter JL, Bernard CC. Multiple sclerosis: a battle between destruction and repair. *J Neurochem* 2007;100:295-306.
- Olsen SA. A review of complementary and alternative medicine (CAM) by people with multiple sclerosis. *Occup Ther Int.* 2009;16:57-70.
- Mirzai V, Saiadi AR, Heydarinasab M. Knowledge and attitude of Rafsanjan physicians about complementary and alternative medicine. *Zahedan J Res Med Sci.* 2011;13:20-24.
- Goodin DS, Frohman EM, Garmany GP Jr, Halper J, Likosky WH, Lublin FD, Silberberg DH, Stuart WH, van den Noort S; Therapeutics and Technology Assessment Subcommittee of the American Academy of Neurology and the MS Council for Clinical Practice Guidelines. Disease modifying therapies in multiple sclerosis: report of the Therapeutics and Technology Assessment Subcommittee of the American Academy of Neurology and the MS Council for Clinical Practice Guidelines. *Neurology.* 2002;58:169-178.
- Yadav V, Bever C Jr, Bowen J, Bowling A, Weinstock-Guttman B, Cameron M, Bourdette D, Gronseth GS, Narayanaswami P. Summary of evidence-based guideline: Complementary and alternative medicine in multiple sclerosis Report of the Guideline Development Subcommittee of the American Academy of Neurology. *Neurology.* 2014;82:1083-1092.
- Rabiei Z, Rafieian-kopaei M, Heidarian E, Saghaei E, Mokhtari S. Effects of *Zizyphus jujube* extract on memory and learning impairment induced by bilateral electric lesions of the nucleus Basalis of Meynert in rat. *Neurochem Res.* 2014;39:353-360.
- Rabiei Z, Mokhtari S, Asgharzade S, Gholami M, Rahnama S, Rafieian-kopaei M. Inhibitory effect of *Thymus vulgaris* extract on memory impairment induced by scopolamine in rat. *Asian Pac J Trop Biomed.* 2015;5:845-851.
- Rabiei Z, Rafieian-Kopaei M. Neuroprotective effect of pretreatment with *Lavandula officinalis* ethanolic extract on blood-brain barrier permeability in a rat stroke model. *Asian Pac J Trop Med.* 2014;7:421-426.
- Rabiei Z, Bigdeli MR, Rasouljan B, Ghassempour A, Mirzajani F. The neuroprotection effect of pretreatment with olive leaf extract on brain lipidomics in rat stroke model. *Phytomedicine.* 2012;19:940-946.
- Rabiei Z, Gholami M, Rafieian-Kopaei M. Antidepressant effects of *Mentha pulegium* in mice. *Bangladesh J Pharmacol.* 2016;11:711-715.
- Rabiei Z, Naderi S, Rafieian-Kopaei M. Study of antidepressant effects of grape seed oil in male mice using tail suspension and forced swim tests. *Bangladesh J Pharmacol.* 2017;12:397-402.
- Rabiei Z, Lorigooini Z, Kopaei MR. Effects of hydroalcoholic extract of *Borago officinalis* on naloxone-precipitated withdrawal syndrome in morphine-dependent mice. *Bangladesh J Pharmacol.* 2016;11:824-829.
- Giveon S, Liberman N, Klang S, Kahan E. A survey of primary care physicians' perceptions of their patients' use of complementary medicine. *Complement Ther Med.* 2003;11:254-260.
- Hollenbach JA, Oksenberg JR. The immunogenetics of multiple sclerosis: a comprehensive review. *J Autoimmun.* 2015;64:13-25.
- Conti P, Kempuraj D. Important role of mast cells in multiple sclerosis. *Mult Scler Relat Disord.* 2016;5:77-80.
- Zrzavy T, Hametner S, Wimmer I, Butovsky O, Weiner HL, Lassmann H. Loss of 'homeostatic' microglia and patterns of their activation in active multiple sclerosis. *Brain.* 2017;140:1900-1913.
- Raphael I, Nalawade S, Eagar TN, Forsthuber TG. T cell subsets and their signature cytokines in autoimmune and inflammatory diseases. *Cytokine.* 2015;74:5-17.
- Zhu J, Jankovic D, Oler AJ, Wei G, Sharma S, Hu G. The transcription factor T-bet is induced by multiple pathways and prevents an endogenous Th2 cell program during Th1 cell responses. *Immunity.* 2012;37:660-673.
- Jadidi-Niaragh F, Mirshafiey A. Th17 cell, the new player of neuroinflammatory process in multiple sclerosis. *Scand J Immunol.* 2011;74:1-13.
- Zajicek JP, Hobart JC, Slade A, Barnes D, Mattison PG; MUSEC Research Group. Multiple Sclerosis and Extract of Cannabis: results of the MUSEC trial. *J Neurol Neurosurg Psychiatry.* 2012;83:1125-1132.
- Brady CM, DasGupta R, Dalton C, Wiseman OJ, Berkley KJ, Fowler CJ. An open-label pilot study of cannabis-based extracts for bladder dysfunction in advanced multiple sclerosis. *Mult Scler J.* 2004;10:425-433.
- Buccellato E, Carretta D, Utan A, Cavina C, Speroni E, Grassi G, Candeletti S, Romualdi P. Acute and chronic cannabinoid extracts administration affects motor function in a CREAE model of multiple sclerosis. *J Ethnopharmacol.* 2011;133:1033-1038.
- Vaney C, Heinzl-Gutenbrunner M, Jobin P, Tschopp F, Gattlen B, Hagen U, Schnelle M, Reif M. Efficacy, safety and tolerability of an orally administered cannabis extract in the treatment of spasticity in patients

- with multiple sclerosis: a randomized, double-blind, placebo-controlled, crossover study. *Mult Scler*. 2004;10:417-424.
25. Wade DT, Makela P, Robson P, House H, Bateman C. Do cannabis-based medicinal extracts have general or specific effects on symptoms in multiple sclerosis? A double-blind, randomized, placebo-controlled study on 160 patients. *Mult Scler*. 2004;10:434-441.
  26. Desai F, Ramanathan M, Fink CS, Wilding GE, Weinstock-Guttman B, Awad AB. Comparison of the immunomodulatory effects of the plant sterol beta-sitosterol to simvastatin in peripheral blood cells from multiple sclerosis patients. *Int J Immunopharmacol*. 2009;9:153-157.
  27. Mohajeri M, Sadeghizadeh M, Najafi F, Javan M. Polymerized nano-curcumin attenuates neurological symptoms in EAE model of multiple sclerosis through down regulation of inflammatory and oxidative processes and enhancing neuroprotection and myelin repair. *Neuropharmacology*. 2015;99:156-167.
  28. Mauriz E, Vallejo D, Tunon MJ, Rodriguez-Lopez JM, Rodriguez-Perez R, Sanz-Gomez J, García-Fernández Mdel C. Effects of dietary supplementation with lemon verbena extracts on serum inflammatory markers of multiple sclerosis patients. *Nutr Hosp*. 2015;31:764-771.
  29. Sen A, Topcu G, Ozgun O, Kolak U, Hacibekiroglu I, Celik G, Arslan S. Anti-neuroinflammatory effect of butanolic subextract of *Capparis ovata* water extract used as an alternative and complementary treatment for multiple sclerosis. *J Neuroimmunol*. 2014;275:172-173.
  30. Stojanovic I, Savikin K, Dedovic N, Zivkovic J, Saksida T, Momcilovic M, Koprivica I, Vujicic M, Stanisavljevic S, Miljkovic D, Menkovic N. Pomegranate peel extract ameliorates autoimmunity in animal models of multiple sclerosis and type 1 diabetes. *J Funct Foods*. 2017;35:522-530.
  31. Noroozian M, Mohebbi-Rasa S, Tasviechi A, Sahraian M, Karamghadiri N, Akhondzadeh S. Ginkgo biloba for Improvement of Memory and Quality of Life in Multiple Sclerosis: an Open Trial. *J Med Plant Res*. 2011;3:33-49.
  32. Sedighi B, Pardakhty A, Kamali H, Shafiee K, Hasani BN. Effect of *Boswellia papyrifera* on cognitive impairment in multiple sclerosis. *Iranian J Neurol*. 2014;13:149.
  33. Ghazavi A, Mosayebi G, Salehi H, Abtahi H. Effect of ethanol extract of saffron (*Crocus sativus* L.) on the inhibition of experimental autoimmune encephalomyelitis in C57bl/6 mice. *PJBS*. 2009;12:690-695.
  34. Alberti TB, Marcon R, Bicca MA, Raposo NR, Calixto JB, Dutra RC. Essential oil from *Pterodon emarginatus* seeds ameliorates experimental autoimmune encephalomyelitis by modulating Th1/Treg cell balance. *J Ethnopharmacol*. 2014;155:485-494.
  35. Martín R, Carvalho-Tavares J, Hernández M, Arnes M, Ruiz-Gutierrez V, Nieto ML. Beneficial actions of oleanolic acid in an experimental model of multiple sclerosis: a potential therapeutic role. *Biochemical Pharmacology*. 2010;79:198-208.
  36. Clafin SB, van der Mei IA, Taylor BV. Complementary and alternative treatments of multiple sclerosis: a review of the evidence from 2001 to 2016. *J Neurol Neurosurg Psychiatry*. 2017;1:1-8.
  37. Matsuda LA, Lolait SJ, Brownstein MJ, Young AC, Bonner TI. Structure of a cannabinoid receptor and functional expression of the cloned cDNA. *Nature*. 1990;346:561-564.
  38. Lakhan SE, Rowland M. Whole plant cannabis extracts in the treatment of spasticity in multiple sclerosis: a systematic review. *BMC Neurol*. 2009;9:59.
  39. Brady CM, DasGupta R, Wiseman OJ, Dalton CM, Berkley KJ, Fowler CJ. The effect of cannabis based medicinal extract on lower urinary tract dysfunction in advanced multiple sclerosis: Preliminary results. *J Neurol Neurosurg Psychiatry*. 2002;72:139.
  40. Beard S, Hunn A, Wight J. Treatments for spasticity and pain in multiple sclerosis: a systematic review. *Health Technol Assess*. 2003;7.
  41. Shakespeare DT, Young CA, Boggild M. Anti-spasticity agents for multiple sclerosis. *Cochrane Database Syst Rev*. 2000:CD001332.
  42. Syed YY, McKeage K, Scott LJ. Delta-9-tetrahydrocannabinol/cannabidiol (Sativex®): a review of its use in patients with moderate to severe spasticity due to multiple sclerosis. *Drugs*. 2014;74:563-578.
  43. Collin C, Davies P, Mutiboko I, Ratcliffe S. Randomized controlled trial of cannabis-based medicine in spasticity caused by multiple sclerosis. *Eur J Neurol*. 2007;14:290-296.
  44. Collin C, Ehler E, Waberzinek G, Alsindi Z, Davies P, Powell K, Notcutt W, O'Leary C, Ratcliffe S, Nováková I, Zapletalova O, Píková J, Ambler Z. A double-blind, randomized, placebo-controlled, parallel-group study of Sativex, in subjects with symptoms of spasticity due to multiple sclerosis. *Neurol Res*. 2010;32:451-459.
  45. Novotna A, Mares J, Ratcliffe S, Novakova I, Vachova M, Zapletalova O, et al. A randomized, double-blind, placebo-controlled, parallel-group, enriched-design study of nabiximols (Sativex®), as add-on therapy, in subjects with refractory spasticity caused by multiple sclerosis. *Eur J Neurol*. 2011;18:1122-1131.
  46. Notcutt W, Langford R, Davies P, Ratcliffe S, Potts R. A placebo-controlled, parallel-group, randomized withdrawal study of subjects with symptoms of spasticity due to multiple sclerosis who are receiving long-term Sativex® (nabiximols). *Mult Scler J*. 2012;18:219-222.
  47. Xie L, Li XK, Takahara S. Curcumin has bright prospects for the treatment of multiple sclerosis. *Int J Immunopharmacol*. 2011;11:323-330.
  48. Bobholz JA, Rao SM. Cognitive dysfunction in multiple sclerosis: a review of recent developments. *Curr Opin Neurol*. 2003;16:283-288.